Structure-Property Relationships In Extruded Plastics Foams.

By

Mohammad Reza Shishesaz B.Sc. and M.Sc.

A Dissertation Submitted To Brunel, The University Of West London For The Degree Of Doctor Of Philosophy.

Department Of Materials Technology
Brunel, West London University
Uxbridge Middlesex

March 1989

Brunel, The West London University
Materials Technology Department
Uxbrdige, Middlesex,

Mohammad Reza Shishesaz

Structure-Properties Relationships in Extruded Plastics Foams.

Ph. D. Degree

March 1989

Abstract

Physical properties and morphology of extruded semi-crystalline polymers can be significantly affected by modification and change in die design and melt viscosity of the molten polymer. Further modifications to physical properties (i.e. density and open cell fraction) of foamed material occur, following the modification of melt viscosity by melt blending of polypropylene and high density polyethylene).

The main object of this research project was to carry out a systematic examination of rheological properties of polymer/gas mixture, affect of die design, polymer molecular weight (melt viscosity), and processing conditions on density, open cell fraction, cell morphology (i.e. cell size and cell size distribution) and micromorphology of polyolefin foams. Also attention was given to method of stabilisation of extruded foam, where, it was found support of the extrudated foam (by adding a specially designed die adapter to the end of the die) prior to entering the cooling tank could result not only to a specimen with uniform cross section, but also due to drop in melt temperature, the cell walls are to some extent rigidized, hence, the collapse of bubbles are limited. From commercial point of view control of cell collapse, density and open cell fraction, will make these foamed materials valuable for their filtration characteristics.

Microstructural analysis of polypropylene (unfoamed state) by X-ray diffraction and Differential Scanning Calorimetry revealed β-spherulites are only formed in skin layer, and beneath the thickness of 500 μm from the surface, the crystal structure of this polymer is only consist of β-spherulites. On the other hand, the chemical blowing agent (Hydrocerol CF-20), was found to have nucleating affect on microstructure of polypropylene, where, it has resulted in reduction of size of spherulites together with a drop in recrystallisation temperature and formation of β and α spherulites through the thickness of extrudated foam. The foregoing chemical blowing agent was found to have no significant affect on the crystal structure of the high density polyethylene.

Acknowledgements

I would like to thank Dr. P.R. Hornsby, my supervisor, for his valuable comments, suggestions, and guidance through this project.

Thanks are also due to staff members of Material Department of Brunel University, namely, Mr. K. Johns, L. Mellett and R. Andrew. Also I would to thank my brother Dr. A. Shishesaz for his help in typing this thesis.

Finally I would like to thank my parents for their love, support and encouragement through these past few years.

DEDICATED TO MY PARENTS

Table of Contents

CHAPTER 1

INTRODUCTION

1. Introduction

The polymer foam extrusion process has been used commercially for the past two decades. The most commonly used extruded polymer foams in the market today are polystyrene and low density polyethylene. Polystyrene foam sheets are widely used in food packaging applications (e.g. meat and fruit trays and fast food containers), and polyethylene foamed products are used in packaging applications (e.g. protecting fragile electronic equipments and dishwares).

Because of their complex nature, polymer foams have been classified in variety of ways (1). The most usual are; the cellular morphology, the mechanical behaviour and the composition. Structurally the material system can be described as open cell or closed cell. With closed cell polymer foam, the gas is dispersed in the form of discrete gas bubbles and polymer matrix forms a continuous phase. In open cell forms the voids coalesce so that both the solid and the fluid phases are continuous. Schematic representations of the different physical forms of cellular polymers are given in Figure 1.1.

These materials are also classified according to their stiffness, the two extremes being rigid and flexible. Skochdopole and Rubens (2) have defined a rigid foam as

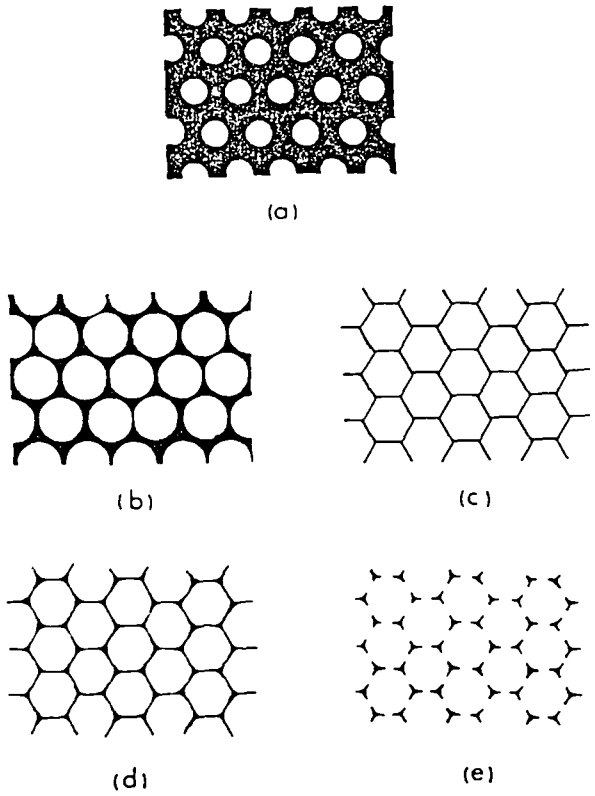

Figure 1.1. Two dimensional representation of idealised cellular structures at different stages of bubble expansion. (a) and (b) closed packed structure, (c) and (d) cell drainage morphology, (e) open cell structure (after 1).

one in which the polymer matrix exists in the crystalline state, or if amorphous, is below its glass transition temperature. Following from this, a flexible foam is a system in which the matrix polymer is above the crystalline melting point or above its glass transition temperature. According to this classification most polyolefin foams are rigid, whereas rubber foams, elastomeric polyurethanes are flexible.

However, the published literature has very little fundamental information on the processing-property-cell morphology relationships in foam extrusion. Most of the publications deal with the type and choice of process equipment (3-7), the properties and choice of blowing agents (8-10), and relationships among foam density and mechanical properties (11-13).

A systematic study was therefore initiated to improve current knowledge on the effect of processing conditions and polymer molecular weight on the rheological properties, foam density and macro and micro-morphology of polyolefin foams. The effect of gas on polymer melt viscosity has been studied in detail and it has been shown, in order to improve the polymer foam quality (lower density with higher open cell fraction), the melt viscosity of polymer should be modified. This has been achieved by melt blending of polypropylene and high density polyethylene. It was therefore intended to

establish the role of melt viscosity on the foam density, porosity and macromorphology of the extruded polyolefin foamed rod.

This dissertation is divided into nine chapters(as introduction presented in chapter 1).

Chapter 2 deals with a comprehensive review of the existing literature concerned with rheological properties of polymer containing gas, technological approaches to polyolefin foam extrusion, and the effect of gas on the crystalline structure of injection moulded semi-crystalline polymers. Within this literature review aspects such as affect of processing conditions on morphology of low density polyethylene and polystyrene have been discussed.

Chapter 3 is concerned with the selection and preparation of materials, instrumentation and control of extruder and methods involve in characterisation techniques employed to study the macro and micro-morphology of extruded foam rods of polyolefin.

Chapter 4 present the affect of processing conditions on rheological properties of polypropylene and high density polyethylene in foamed and unfoamed states. In this chapter it has been shown the reduction of melt viscosity (with increasing gas content of polymer) can

severely affect the foam density. Also it has been shown, how the addition of gas in polymer melt can affect the melt fracture of extruded polymer.

Chapter 5 presents preliminary investigation of extrusion of polyolefin foam. In this chapter the effect of melt flow index, processing conditions and blowing agent concentration on foam density in both melt and solid states and porosity of the extruded polyolefin foam has been discussed in detail. This study revealed, the melt viscosity and melt strength are strongly affect the quality of extruded foam, mainly the solid state density and open cell fraction content. It has been shown when the melt viscosity was modified (by melt blending polypropylene and high density polyethylene), greater reduction in solid state density was achieved with higher open cell fraction.

Chapter 6 and 7 present the study of macro and micro-morphology of extruded polyolefin foam rod respectively. The foamed specimens were characterised and cell geometry, cell size, and cell size distribution have been studied in chapter 6. In chapter 7 micro-morphology of these specimens are characterised by means of optical microscopy, transmission electron microscopy (TEM), scanning electron microscopy (SEM), differential scanning calorimeter (DSC), and X-ray diffraction. It has been shown that the crystalline structure of polypropylene and

high density polyethylene has been changed by introducing gas in molten polymer. This study also revealed interesting points in size and distribution of the two polymorphs (in the case of polypropylene) through the cross section of extruded foam rod. X-ray diffraction revealed notable affect of blowing agent on the α-phase nucleation in polypropylene foam.

The gained quantitative informations from the foregoing chapters are presented in last chapter. The industrial importance of this work and possibly further investigation of this project has also been highlighted in the last chapter (recommendations).

CHAPTER 2

LITERATURE REVIEW

2. Literature Review
2.1. Literature Review of Polymer Foam
2.1.1. Rheological Review of Polymer Foam

Although work on foam morphology and stability has been on going for a long time, it is only recently that studies on its rheology have been undertaken. David (14) was one of the first researchers to do a systematic study on polymeric foams. He used a capillary viscometer for his studies and observed considerable wall slippage in foam flow. He determined the viscosity of the foam and found it to be shear thinning (pseudoplastic). Wenzel and co-workers and Patton et al.(15,16) reported the same finding. These authors used tube flow experiments, and also showed that tube diameter affected viscosity. In addition, Patton found that viscosity is inversely proportional to tube length. This finding clearly indicates that Patton's experiments did not involve fully developed flow. Another problem with these experiments was that tube diameter was almost commensurate with the bubble diameter. Further, the small diameter led to a considerable pressure drop and hence, to bubble collapse. Conflicting reports exist on the dependence of viscosity on gas volume fraction (Φ). Wenzel (15,17), using cone and plate geometry, and David (4) found no influence of gas volume fraction on viscosity. Beyer et al.(18) and Khan (19) worked on highly expanded foam, (gas volume fraction greater than 95%)

and found viscosity to increase with gas volume fraction. However, some investigators (20-22) measured apparent viscosity of molten polymer containing gaseous component (e.g. nitrogen and carbon dioxide), using a plunger type viscometer and reported that apparent viscosity decreases as the gas volume fraction increases. However, these findings are subject to some criticism, since plunger type viscometers (e.g. an Instron viscometer) cannot guarantee foaming does not occur in the capillary as the mixture approaches the exit of the die. Han et al.(23-25), by using a cone and plate rheometer and introducing up to 15 percent physical blowing agent into molten polymer were able to measure the viscosity and first normal stress difference for different temperatures and gas volume fractions. They also reported that as the gas volume fraction increased, the viscosity reduction factor (VRF), decreased.

Princen (26) developed a structural model for highly concentrated emulsion(oil and water) and foam. He used a two dimensional hexagonal cell geometry for foam and derived a stress-strain relationship for shear deformation up to the yield point. He extended his model to incorporate a finite liquid volume fraction, the lower limit being determined by a hexagonal closed packed sphere system(see Figure 2.1). His results

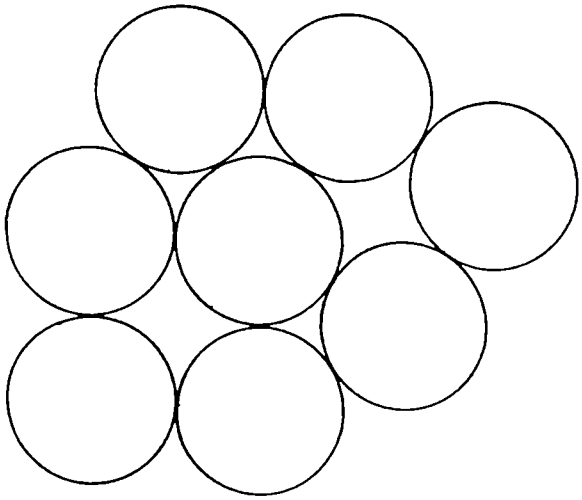

a) Closed-packed spheres

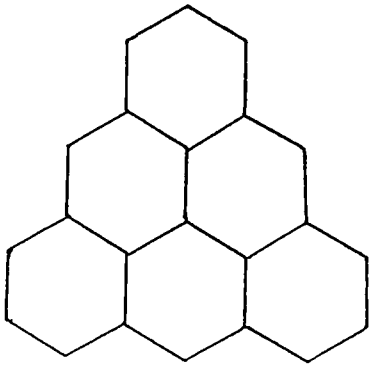

b) Hexagonal cells

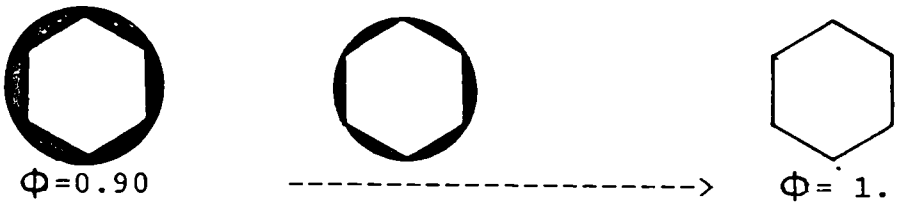

c) Increasing gas volume fraction

Figure 2.1. Two dimensional foam cell models. a) Hexagonal closed-packed spheres. b) Hexagonal cells having Φ=1. c)changing cell structure with increasing gas volume fraction (after 15).

show that the stress (and also yield stress) to be some function of gas volume fraction, directly proportional to surface tension (σ) and inversely proportional to hexagonal cell side length. This inverse dependency with cell size is in agreement with Wenzel's tube flow experiment (17).

In this model, Princen focused on only one specific initial cell orientation (Figure 2.1.b), namely that where the vertices pointed upward. Furthermore, he considered interfacial forces to be dominant, which were assumed to act along the liquid films. Thus the shear stress could be determined from the projection of all intersecting films on a horizontal shear plane. In order to get the orientation of the films as functions of strain, he used an iterative technique and found the stress response to be non-linear in strain.

To verify the theory, Princen (27) has recently focused on experiments with oil in water emulsion. The aims of this study were to evaluate the effect of gas volume fraction, surface tension, and cell diameter on the yield stress of the foam and look at boundary(wall slip) layer properties. He used Couette device for his experiments where the outer cylinder (radius R2) was rotated and the torque measured at inner one. He characterised the slip layer which

he defined as

$$\Phi w \times (Tw) = h/\mu \qquad 2.1$$

where Φw is gas volume fraction

Tw is shear stress at the wall

h is effective thickness of boundary layer

μ is viscosity of fluid

Here Φw is function of stress only. Thus, for flow where $T < Ty$, the emulsion moves like a plug with angular velocity(W). The stresses can be related by

$$T1 = \Phi w1 \times W \times R1 \qquad 2.2$$

$$T2 = \Phi w2 \times (W2-W) \qquad 2.3$$

if one neglects end effects then

$$T1 \times R1^2 = T2 \times R2^2 \qquad 2.4$$

Here 1 and 2 refer to inner and outer cylinders respectively. The angular velocity W was obtained by measuring the angular velocity of a pigmented radial line on the emulsion.

2.1.2. Theory

2.1.2.1. Characterisation of Rheology

The rheological properties of polymer melt may be measured in a number of ways. One of the easiest and widely used method is capillary rheometry, which is illustrated in Figure 2.2 By applying a specific pressure (which can be measured by means of pressure transducer) to the reservoir of a polymer melt, the volume flow rate (Q) can be determined by recording

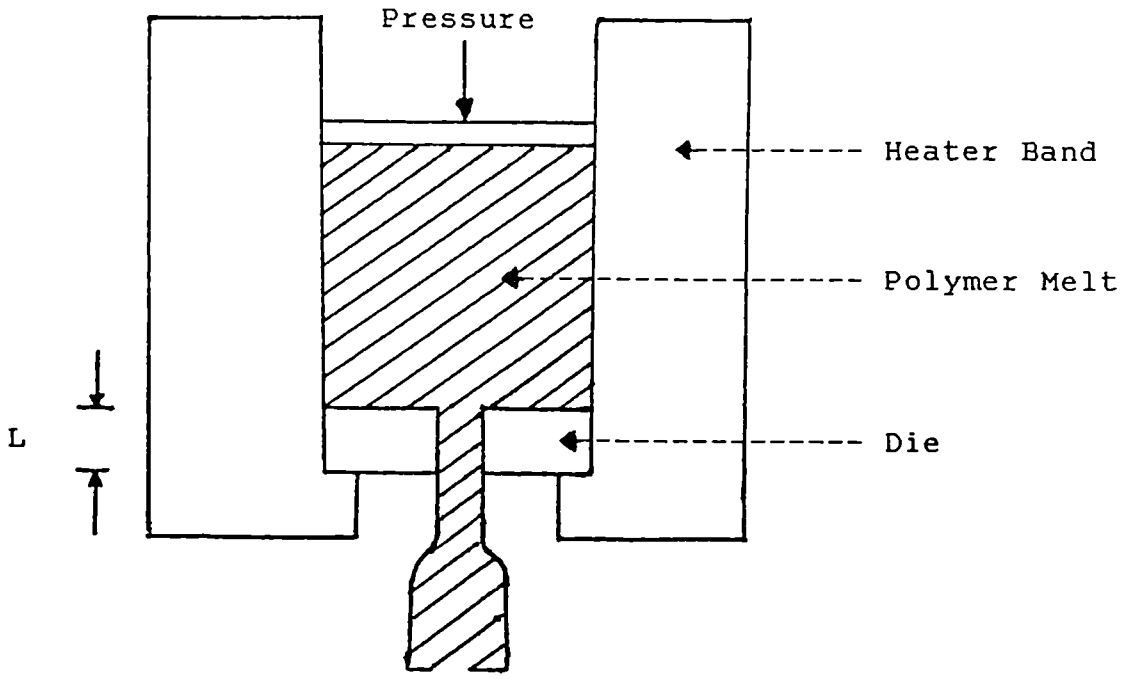

Figure 2.2. Schematic repersentation of capillary rheometer.

the speed of the piston, which is evaluated from

$$Q = \pi * R^2 * V \qquad 2.5$$

where R and V are the radius and velocity of piston respectively. In order to carry out rheological studies of a polymer containing dissolved gas, special rheological equipment is required to maintain pressure on the melt, in order to so to prevent premature expansion of the melt.

The density of polymer melt containing dissolved gas in the die is less than that of homopolymer (28). One way for the material in the die to have a lower density is if it were foamed. Han et al.(23) have shown that, since pressure continuously drops along the axial distance of the die, nucleation of bubbles will occur. These bubbles will start growing as they travel towards the die exit. Therefore, the material in the die appears to be foamed. In order to verify this finding, Throne (28) has suggested the following argument. The density of the material in the die head (P_{die}) can be given as

$$P_{die} = [(Mgas + Mmelt) / (Vgas + Vmelt)] \qquad 2.6$$

where M and V are mass and volume respectively.

or

$$(1/P_{die}) = [(Vgas/Mgas + Mmelt) + (Vmelt/Mgas + Mmelt)] \qquad 2.7$$

since the mass of the gas is much less than the mass of polymer melt therefore, one can assume

$$Mgas + Mmelt \equiv Mmelt$$

so Equation 2.7 becomes

$$(1/P_{die}) = [(Vgas/Mmelt) + (Vmelt/Mmelt)] \qquad 2.8$$

but

$$Vmelt/Mmelt = (1/P_{melt})$$

also assuming that the gas generated from blowing agent (BA) follows Boyle's law, then the volume of gas can be computed as follows:

$$Vgas = [Vg(stp) * MBA * (T/Tstp) * (Pstp/P)] + (1/Pmelt) \qquad 2.9$$

here Tstp = 273°K, Pstp = 1 atm., and MBA is weight of blowing agent. Substituting Equation 2.9 into Equation 2.8 gives,

$$(1/P_{die}) = A * B + (1/Pmelt) \qquad 2.10$$

where

$$A = Vg(stp) * (MBA/Mmelt)$$

$$B = (T/Tstp) * (Pstp/P)$$

also the Equation 2.10 can be further simplified by considering (MBA / Msolid) = (BA), the blowing agent concentration, so Equation 2.10 can be rewritten as:

$$(1/P_{die}) = C + (1/Pmelt) \qquad 2.11$$

where

$$C = Vg(stp) * (BA)* (T / 273*P) * (Msolid/Mmelt)$$

From Equation 2.11, it can be concluded that, for finite temperatures, pressures, and blowing agent concentrations, the density of the material in the die must be less than the density of polymer melt. This is

always the case regardless of whether the gas is generated from chemical blowing agent decomposition or added physically as a gas or volatile liquid.

The rheological data obtained from the capillary rheometer and extruder, namely the pressure drop ΔP and mass flow rate measurements, can be related to the wall shear stress (Tw) and to apparent shear rate ($\dot{\gamma}_{ap}$) as follow:

$$Tw = (r * \Delta P)/2L \qquad 2.12$$

$$\dot{\gamma}_{ap} = (4 * Q)/ \pi * r^3 \qquad 2.13$$

where

r is radius of capillary

L is length of capillary

Q is volumetric flow rate of polymer melt

The volumetric flow rate was obtained from

$$Q = m * 1/D \qquad 2.14$$

where m and D are are mass flow rate and density of melt extrudate.

In order to minimise the end effect, an end correction is applied by using two dies with same diameter (2mm) and different length (29-31). The length/diameter (L/D) ratio of these dies are 1 and 20 accordingly. The end correction is proportional to the intercept on the die length/diameter ratio axis (30). Therefore using the end correction the wall shear stress can be given as:

$$Tw = [r * (\Delta P1 - \Delta P2)] / 2(L1 - L2) \qquad 2.15$$

where P1 and P2 denote pressure drop along the die length of L1 and L2 respectively. The results of apparent shear were corrected for non-Newtonian flow effects, using the Rabinowitsch correction (31). Therefore, the true shear rate ($\dot{\gamma}_T$) can be computed from following equation;

$$\dot{\gamma}_T = 1/4 * (3 + 1/n) \qquad 2.16$$

where n is the slope of log Tw vs. log $\dot{\gamma}_{ap}$.
for a non-Newtonian fluid n is less than unity. However, the true viscosity according to Han (31) can be computed from

$$\mu = Tw / \dot{\gamma}_T \qquad 2.17$$

2.1.3. Characterisation of Melt Flow Instabilities

One of the common problems associated with extrusion of molten polymers is an instability in melt flow, which is due to the elasticity of flowing polymer melts. This phenomenon has been investigated for the past two decades. It has not yet been properly and fully explained and still presents an area of limited understanding in the polymer melts. During the extrusion of molten polymers through the die, it is frequently noticed that there is a critical shear stress, below which the polymer extrudate has smooth surface, but above which the surface and shape of the extrudate is

irregular distortion. This phenomenon has been explained as melt turbulence (32,33). Because the extrudate often gives an impression of being broken, the term "melt fracture" was proposed (23). However, this has the disadvantage of being used to described many rheological phenomena some of which are not caused by fracture, therefore, "extrusion defects" would be a preferable term (34).

With decreasing melt flow index (increasing melt viscosity) and increasing the molecular weight of the polymer melt the number of extrusion defects increases (32,35). It has been suggested, this is due to the fact that relaxation process takes longer with increasing molecular weight, so that surface irregularities remain visible for a longer period. A larger number of explanations for melt fracture have been proposed (36-47). It seems likely that in all cases elastic phenomena is the cause, but a more detailed investigation shows larger differences between different polymers. These authors also show that melt fracture starts at a well defined shear stress or shear rate and defects become more pronounced as the shear rate(or rate of output) increases. Spencer et al.(36) pointed out that the melt highly oriented in the capillary die must relax to a distorted state at the die exit and suggested that this causes the buckling of the extrudates.

The mechanism and severity of melt defects is strongly influenced by the structure of the polymer and die geometry, especially the shape of the entrance and the length of the capillary (34). Bagley et al.(47) and Tordella (48), have shown that the melt defect is closely associated with a disturbance in flow pattern at the die entry. In other words, it does not seem possible to maintain that these disturbances originate at the die exit, particularly in the case of a long capillary (L/D =100) as used by Metzer et al. (49).

Den Otter (35) has shown that the critical shear parameters recorded at the appearance of distortions in the extrudate shape are practically independent of die length (L), radius (R), and shape of the duct entrance and exit. However, the degree of disturbance is affected by the change in the angle of duct entrance and by length/diameter (L/D) ratio.

2.1.4. Review of Technological Approaches to Polyolefin Foam Extrusion

Cellular polymers are multiphase material systems that consist of polymer matrix and a fluid phase, the fluid usually being gas. Most polymers can be expanded into cellular product, but only a small

number have been exploited commercially (50). In terms of volume consumed, polyurethane, polystyrene, poly(vinyl chloride) and polyolefins have dominated the markets. However, over the last few years there has been increased utilisation of engineering structural foams for load bearing applications. The polymers used in this application include high density polyethylene, polypropylene, modified polyphenylene oxide, polycarbonate and acrylonitrile/butadiene/styrene (ABS). In some cases an additional solid phase may be present in the cellular system. Example may include fibre reinforced foams and syntactic foams, which are composite materials consisting of hollow glass, or plastic microspheres dispersed throughout a polymer matrix.

Several widely differing techniques have previously been developed for preparing porous polymer structures. Such techniques include:

(i) Expansion with chemical blowing agent

(ii) Expansion with physical blowing agent

(iii) Mechanical whipped emulsions

(iv) Leaching of soluble materials such as salt, starch etc.

With polyolefin foams, all but (iii) can be used. Today, however, most of polyolefin foams are produced by expansion with physical and chemical blowing agents (CBA). Chemical blowing agents are basically used in

conventional extrusion equipment and foamed products are made covering a range of different products e.g. cables, sheet, film etc. There is no published information on the production conditions necessary to produce very low density polyolefin foams using CBA.

Due to the complexity of producing polyolefin foam most of the information available for extrusion foaming these polymers, is available only under licence and little detailed information exists in journals. However, it is intended to cover these areas for production of closed and open cell polyolefins.

Several papers by Han and co-authors(25,51-53) consider an investigation on the effect of:

i) Processing conditions

ii) Chemical structure and concentration of blowing agent

iii) The geometry of the extrusion die on the density, open cell fraction and expansion ratio of the foam.

The main conclusion from their findings are listed below:

i) As the die temperature was increased the open cell fraction decreased, but too high temperature resulted in poor foam quality(i.e. high density foams and excessive cell collapse). This was attributed to the weak melt strength of resin at high

temperatures.

ii) As the pressure was increased (by increasing the throughput) the foam quality improved and foam density decreased. This is due to an increased solubility of gas in molten polymer and prevention of premature foaming in the die.

iii) As the die entry angle was increased the expansion ratio was also raised. This can be due to lower pressure drop for higher entry angle die, since as the entry angle increases the length of the die would decrease.

iv) The expansion ratio also increased as the L/D ratio decreased. Therefore with increase of L/D ratio one would expect an increase in foam density. A summary of their findings is listed in Table 2.1.

Schott and Weininger (54) carried out a paramatic study which also included processing as well as material effects on the foam extrusion quality. Their findings can be listed as follows:

i) The single screw extruder requires little or no equipment modification and produces good medium to high density foam (600-800 Kg m^{-3}) via chemical blowing agents. Better foam quality and improved temperature control can be achieved with a tandem system which couples two single screw extruders and uses mostly physical

Table 2.1. Tabulated results of investigation of Han et al. (after 53) on PE foam extrusion

L/D	Blowing agent type	Concentration of BA wt%	Pressure(PSI) Upstream	Pressure(PSI) Die	Die Temp. (°C)	Open Cell Frac. %	Density g cm^{-3}
8	FC(112)/143 *	15	-	-	100		.07 **
4	FC(114)/143	15	-	-	100	20	.06 **
2	FC(12)/143	15	-	-	100		.035 **
0	FC(12)/143	15			100	20	.1
-	FC(114)	3	1700	780	120		.15
-	FC(114)	4	1500	700	110		.128

* FC is dichlorotetraflouroethane blowing agent.

** The density also depends on the concentration of nucleating agent. In the above cases 0.25 wt% talc has been used.

blowing agents.

ii) **Effect of Pressure**

It was shown that an increase in pressure resulted in an increase in the number of cells and foam density.

iii) **Effect of Temperature**

In order to control the foam quality precise control of die temperature is essential. Increasing in die temperature could result in cell collapse due to lowering the melt strength of the polymer. Also a decrease in die temperature could result in only partial decomposition of blowing agent, which therefore, would increase the foam density.

iv) **Take off Speed**

Higher take off speeds moves expansion away from the die and is less likely to give a torn skin. Therefore, it was concluded that higher take off speeds would result in lowering foam density.

v) **Blowing Agent Concentration**

Reduction in density is proportional to blowing agent concentration up to a point where over foaming results in loss of gas through the extrudate wall.

There are only a few experimental studies published in the literature dealing with the solubility of gases in polymer melts (55-57). Durill and Griskey (55,56) report that the partial pressure of given gas

dissolved in a given polymer can be calculated using Henry's Law

$$X = H * P \qquad 2.18$$

where

- X is the concentration of gas in the melt (cm^3)
- H is the Henry's Law constant (cm^3 at STP, $(g\ atm)^{-1}$)
- P is the partial pressure of the dissolved gas (atm)

Therefore at any given temperature and pressure (T and P) the solubility of gas in the polymer melt may be expressed in terms of cm^3(STP)/g. Here STP refers to the standard temperature and pressure. Durill and Griskey (55) further report that for certain gas/ polymer combinations, the solubility parameter H follows the Arrhenius behaviour with temperature

$$H(T) = Ho\ Exp\ [\ -\ Es/\ R\ (T-To)] \qquad 2.19$$

Where

- Ho is the Henry's law constant at To (determined experimentally) (cm^3 at STP $(g\ atm)^{-1}$)
- Es is the heat of solution of gas in the melt $(KJ\ (g\ atm)^{-1})$
- R is the universal gas constant $(KJ\ (g\ mole\ ^oK)^{-1})$

Equations 2.18 and 2.19 permits calculation of the maximum amount of gas that can be dissolved in polymer melt at any given temperature and pressure. Figure 2.3 gives solubility information for nitrogen in polystyrene and high density polyethylene of selected melt temperature and pressure.

If we assume that the gas released by blowing agent is completely dissolved in a polymer melt, foaming

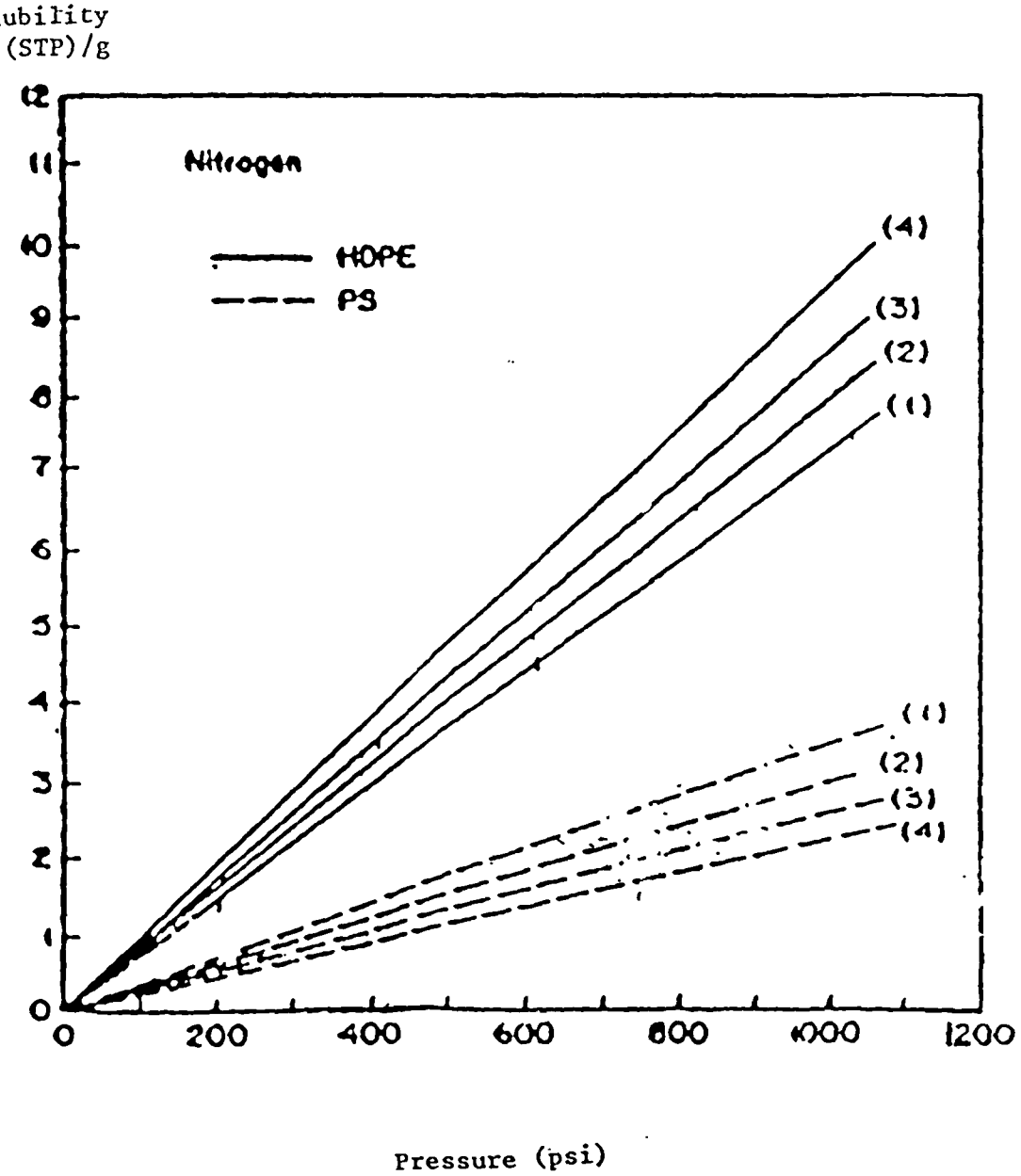

Figure 2.3. Solubility vs. pressure for nitrogen in high density polyethylene (solid lines) and polystyrene (doted lines) at various temperatures (1) 180°C, (2) 220°C, (3) 260°C, and (4) 320°C (after 23).

may not occur inside the die in foam extrusion as long as pressure anywhere in the die is kept above the vapour pressure of gas released from the chemical blowing agent. This vapour pressure will depend on the solubility of gas in the base polymer. However, when gas above the solubility limit is present in the melt as microbubbles, the growth of these microbubbles may depend on the magnitude of the external pressure applied to the melt. When nucleated bubbles (or microbubbles) have attained a certain minimum size, they will continue to grow until the pressure inside them, Pv, is in equilibrium with the apparent partial pressure of the gas dissolved in the polymer melt, P_L. That is at equilibrium the following force balance should hold

$$\Delta P = 2 * \gamma / r \qquad 2.20$$

where $\Delta P = Pv - P_L$, γ is the interfacial tension and r is the bubble radius. Note that value of γ is approximately 0.03-0.05 N m^{-1} for most gas/polymer melt systems (58). This equation indicates that the smaller the bubble radius r, the higher the pressure of gas in the bubble. In other words, application of the external pressure in excess of the pressure inside the bubble will suppress bubble growth because the pressure inside the bubble depends on the apparent partial pressure of the dissolved gas, which in turn is directly related to external pressure. It can then be said that the external pressure needed to suppress

bubble growth is referred to as the critical pressure for a gas/polymer system. Figure 2.4 gives plots of critical pressure against blowing agent concentration for different combinations of polymer and blowing agent (23). It is seen that at the same concentration of blowing agent, the polystyrene/celogen chemical blowing agent system has a critical pressure higher than the polystyrene/$NaHCO_3$ system. Upon decomposition celogen CBA releases nitrogen and $NaHCO_3$ releases carbon dioxide. It can be said therefore that the polystyrene melt containing nitrogen requires a higher external pressure than the polystyrene containing carbon dioxide in order to suppress the growth of gas bubbles. This may be attributed to the fact that the solubility of N_2 in polystyrene is lower than that of CO_2 in polystyrene.

From the previous discussion, one can see how important both the selection of blowing agent for a polymer and optimising melt pressure are, in order to achieve good quality foam during extrusion.

There is little information available in the literature concerning the morphology of polyolefin foams. Ahmadi (60) has shown the properties of polypropylene structural foam, such as impact strength, and flexural stiffness are dependent on skin to core ratio (hence, the density) and, to some

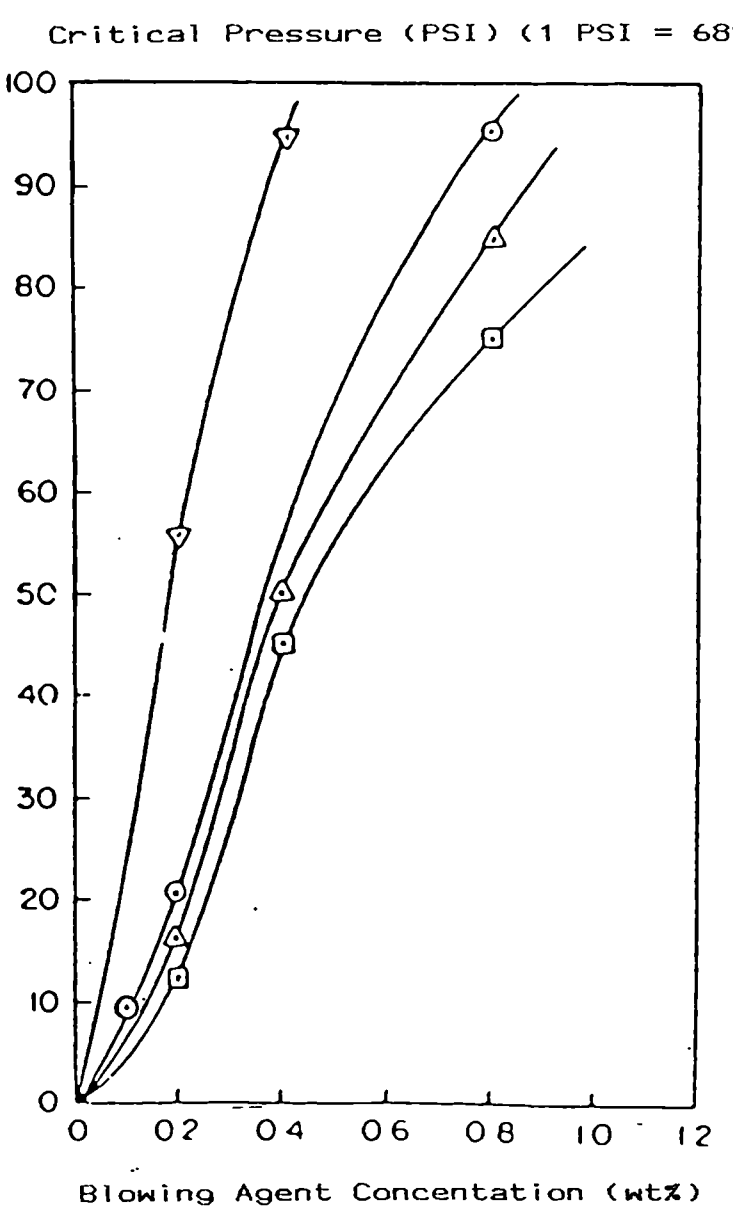

Figure **2.4.** Critical pressure vs. blowing agent concentration: (▽)Ps with Celogen CB at 200 °C, (⊙)PS with $NaHCO_3$ at 200 °C, (△) HDPE with Celogen CB at 220°C, (⊡)HDPE with Celogen CB at 260°C (after **23**).

extent, their surface texture. Also he has investigated the effects of processing conditions on structural foam density. In connection with this study, an examination of the internal structure of cells in the core of polypropylene structural foam mouldings has revealed a network of troughs and funnel shaped holes covering the cell walls and circumscribing what were identified as flattened spherulites (61). In another study Hornsby et al.(62) have proposed a model for the formation of these flat top spherulites. It has been suggested (see Figure 2.5) that the formation of polypropylene foam cell wall spherulites are formed in a series of stages. Firstly, the spherulites grow on cooling as the cells expand during foaming of the polymer. These growing spherulites are pushed ahead of the expanding melt-cell interface until they impinge on one another, so limiting their movement. If the cell continues to expand beyond the remaining spherulites it would leave flat topped structures protruding into the cell, a phenomenon which has been observed in higher density polypropylene foam variants. Further expansion would expose parts of any spherical spherulites, which were growing below the melt cell interface when the spherulitic movement was halted. When the melt is sufficiently solidified to prevent further expansion, shrinkage on crystallisation of remaining melt results in the formation of funnel-shaped holes in

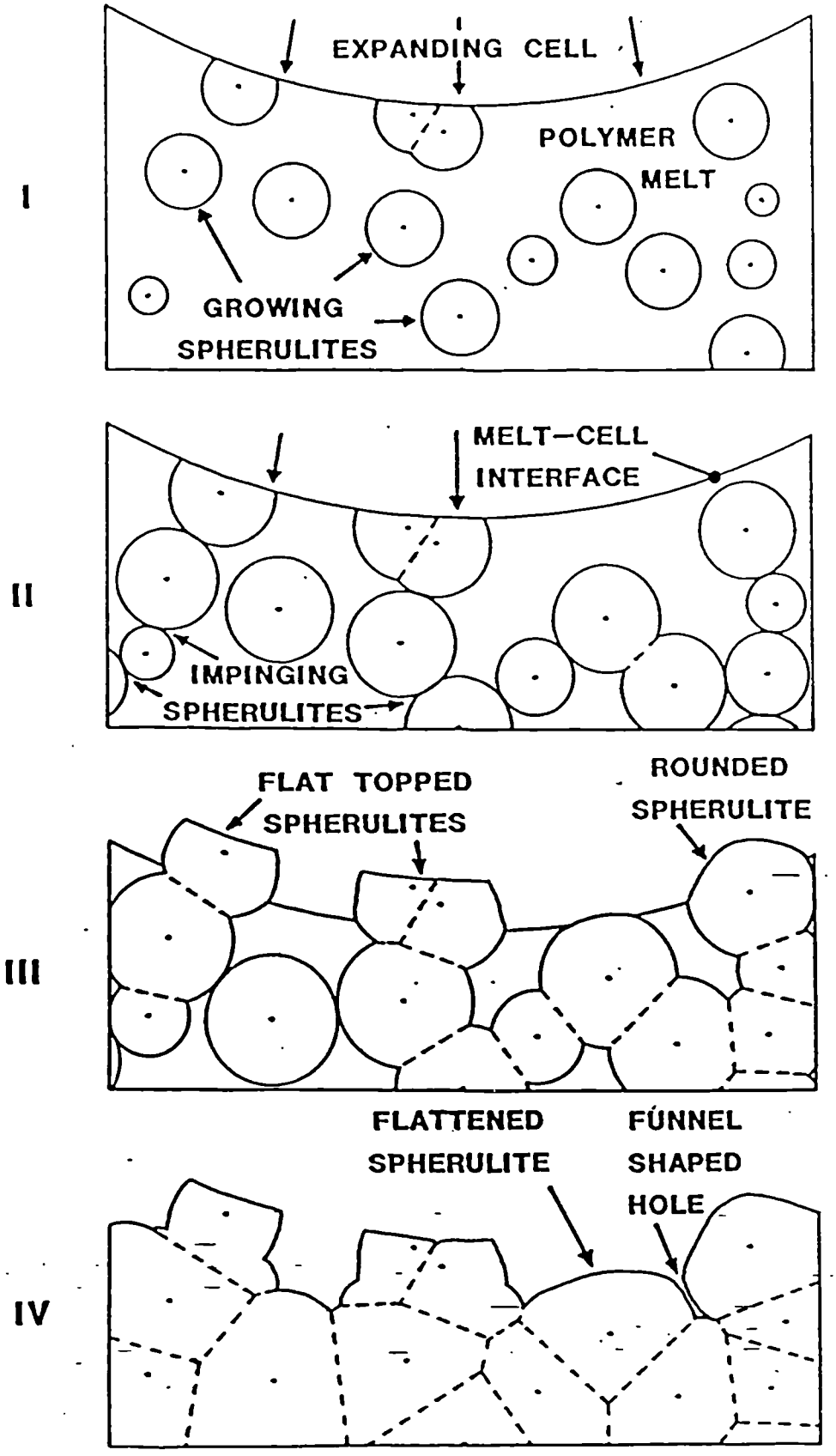

Figure 2.5. Suggested sequence of events in the formation of cell wall spherulites observed in polypropylene structural foam.

the inter-spherulite boundaries.

2.1.5. Mechanism of Bubble Formation

This subject has been described thoroughly in books by Frisch and Saunders(63), and by Benning (64), and also it has been reviewed by number of authors(65-68). Preparation of polymeric foam usually involves firstly the formation of gas bubbles in a liquid phase, and the growth and stabilisation of those bubbles as the liquid matrix increases in viscosity and finally solidifies as a continuous phase. Hence, the colloidal aspects of bubble formation, growth and stability are of prime importance.

A gas in a liquid can exist in two forms, in interstices between polymer chains or as discrete microbubbles. A microbubble, in order to resist collapse, must have an internal pressure greater than that of the surrounding melt. That is;

$$Pc > P + (2 * D/r) \qquad 2.21$$

where

Pc is pressure in the bubble

P is the hydrostatic pressure in the bubble

D is surface tension

r is bubble radius

At very high pressures, gas will be dissolved in the

polymer melt and it is likely that the amount of gas dissolved is linearly dependent upon imposed pressure at a given temperature(68).

Gas diffuses from the initial sites into the surrounding medium in order to achieve a uniform gas-liquid mixture. Rapid bubble growth implies high rates of gas diffusion to the bubble, and rapid dispersal of gas in the extrusion zone of the machine.

The formation of an internally blown foam proceeds through several stages (63,64). Firstly the blowing agent, in whatever form, generates a gas solution in a liquid phase, with the gas reaching its saturation limit in solution, then becoming supersaturated, and finally coming out of solution in the form of a bubble. A bubble of infinitesimal radius requires an infinite pressure difference between the gas in the bubble and that in the fluid surrounding it. Therefore, bubbles are undoutably nucleated at reactive sites on CBA surfaces, or deliberately introduced nucleants, or unmelted crystallites and/or debris present in the resin (64).

Highly supersaturated solutions of gases in polymers are extremely unstable and are relatively easy to nucleate. Finely divided particles well dispersed are

normally satisfactory. Materials less wetted by polymer melt are most effective.

Since the foam expansion is a dynamic process, therefore, it is influenced by such factors as degree of crystallinity, molecular orientation, and cross-linking. Viscoelastic character of the liquid can inhibit both bubble growth and bubble collapse. Diffusion of gas to the growing bubble (or away from collapsing bubble) is assumed to be very rapid when compared with bubble growth rate.

When the bubble is first formed, it is a sphere surrounded by a relatively liquid phase. As more gas is generated by the blowing agent the new gas may form additional bubbles if its concentration sufficiently exceeds the supersaturation at which the first bubbles were formed, or may diffuse from the liquid phase into existing bubbles, causing them to become larger. It may also diffuse to external surfaces. These three processes are competitive and depend on the number of bubbles generated, the amount and the rate at which the gas becomes available and the volume to surface relationships (65,66). As more bubbles form and as the bubbles grow the foam volume increases, with the result that the liquid phase becomes ever thinner and distance between bubbles diminishes. The bubbles eventually lose their spherical shape as the liquid

phase becomes less than 25% of the volume of the foam (64), with the bubbles finally assuming a structural bounded by several flat planes or membranes.

The initiation or nucleation, of cells is dependent on the formation of bubbles of such size that they are capable of growth under the given conditions of foam expansion. According to the Equation 2.20, the growth of a hole or cell in a fluid medium at equilibrium is controlled by the pressure difference P between the inside and the outside of a cell, the surface tension of liquid phase, and the radius r of the cell.

The pressure outside the cell is the pressure imposed on the fluid surface by its surroundings, the pressure inside the cell is the pressure generated by the blowing agent dispersed or dissolved in the fluid. If gas pressure is low, the radii of initiating cells must be large. The cell acts as an initiating site and can be filled with either a gas or a solid (chemical blowing agent residue) which breaks the fluid surface and thus enables blowing agent to surround it (65).

During the time of cell growth in a foam a number of properties of the system change greatly, therefore, cell growth can be treated only qualitatively. The following considerations are of particular importance.

i) The fluid viscosity changes considerably, which tends to influence both the cell growth rate and the flow of polymer from cell walls to intersections, leading to collapse.

ii) The pressure of the blowing agent decreases, falling off less rapidly than an inverse volume relationship, because new blowing agent diffuses into the cells as the pressure falls according to Equation 2.20.

iii) The rate of cell growth depends on the viscoelastic nature of the polymer phase, the blowing agent pressure, the external pressure on the foam, and the permeation rate of blowing agent through the polymer phase.

iv) As a consequence of Equation 2.20, the pressure in the cell of small radius r_2 is greater than that in cell of larger radius r_1. There will thus be a tendency to equalise these pressures either by breaking the wall separating the cells or by diffusion of the blowing agent from the small to large cells. The pressure difference ΔP between cells of radii r_1 and r_2 is shown as:

$$\Delta P = 2 * \gamma * [\ 1/r2 - 1/r1\ ] \qquad 2.22$$

To disperse a given volume of gas in a unit volume of liquid one must increase the free energy of the system such that;

$$E = \sigma * A \qquad 2.23$$

where

E is free energy

σ is surface tension

A is total interfacial area

Clearly one can see that greater free energy is necessary to produce fine rather than to produce large cells, and also the coalescence of cells and foam collapse is energetically favoured until the foam is solidified by cooling.

2.2. Literature Review of Polyolefin Homopolymer

2.2.1. Historical Background of Crystallisation of Polymer Melt

Historically the first knowledge of polymer morphology was that pertaining to crystal structure; i.e. using X-ray crystallographic techniques. But the reflections are found to be broad and diffuse and measurement of crystallinity were intermediate between those of a crystal and liquid. The observations are interpreted by means of the fringed micelle model(69), see Figure 2.6.

Another salient feature was the acknowledgement that chains were regarded as contributing to more than one crystallite, threading between each via the various disorder zones. This was a seemingly logical conclusion from the point of fact that of molecular

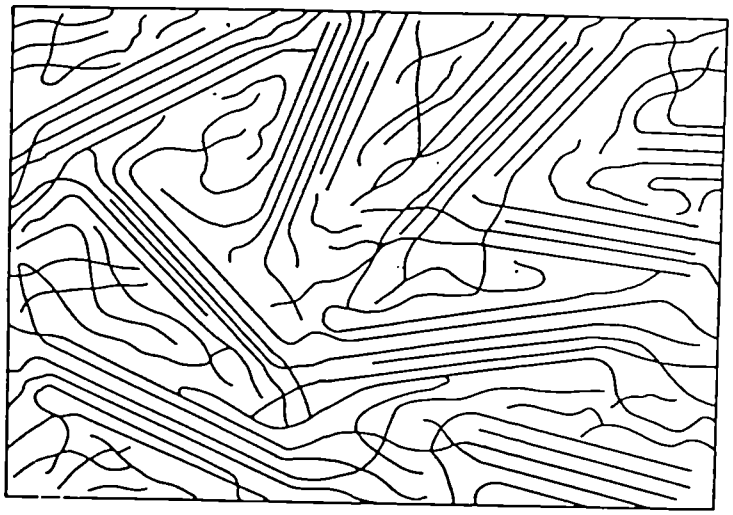

Figure 2.6. The fringed-micelle model of polymeric texture (after 69).

chain length(the contour length), being anything up to 10 μm is still the case today, scientific advance often parallels technical innovation, so that had these miceller structures existed they could not have been observed until later developments involving electron microscopy occurred.

By optical means, it was first appreciated that ordering also existed on macrotextural scale. The structure in question were so-called spherulites (see Figure 2.7), and were subsequently the focus of intensive studies proving the occurrence of crystalline units arranged in a spherically symmetrical fashion(70-72). These are now known to be a universal crystallisation product of the polymer quiescent melt.

The lamellar nature of the crystalline unit is now generally accepted even in the case of melt crystallised (involving spherulites) although acceptance of this phenomenon has been a gradual process. As distinct from solution grown aggregates, where the crystals are discrete entities, in a melt crystallised polymer the lamellae exist as contiguous structure which are interconnected to form familiar spherulites. Detail investigation of spherulitic microstructure (73-75) show that they are composed of readily thin platelets of lamellae ribbon-like crystals, which are very long in comparison to their thickness.

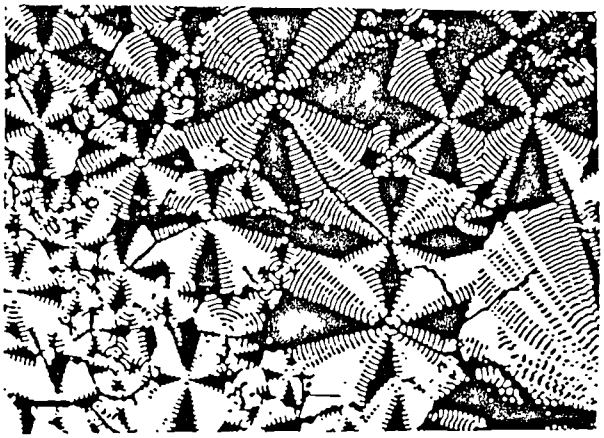

Figure 2.7. Spherulitic of polyhydrroxybutrate (PHB), a bacteria polyester (after 72).

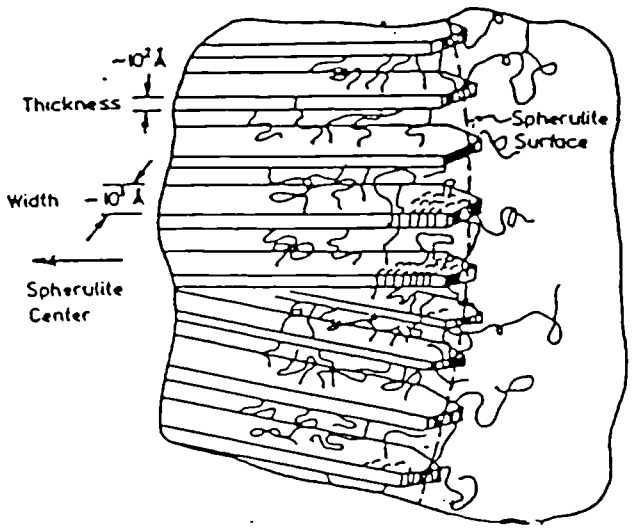

Figure 2.8. Schematic representation of sperulite.

The thickness of the crystal ribbon is in the order of 100-500 Å and since the thickness is only a fraction of the polymer chain length the polymer chain may enter a given ribbon many times (see Figure 2.8). The chains are oriented approximately parallel to the thin dimensions of the ribbon and 'tie chains' connect individual crystal ribbons. The inter-ribbon region is generally termed amorphous composed of tie chains, chain ends, loose loops or even totally unicorporated chains. The spherulite structure is often seen as a banded structure under polarised light and this is due to natural twisting of the ribbon like crystals about their molecular axis. For further study one should refer to the work of Keith and Padden (76,77), Price (78) and Keller (79).

The development of a spherulite depends upon how it is nucleated. A typical progression of spherulitic growth is presented in Figure 2.9, this starts with a fibre and evolving through sheaf-like embryos before attaining a spherical envelope. Upon further growth the spherulites impinge upon one another and they become polyhedral. Mature spherulites have the same crystallographic axis along their radius (80).

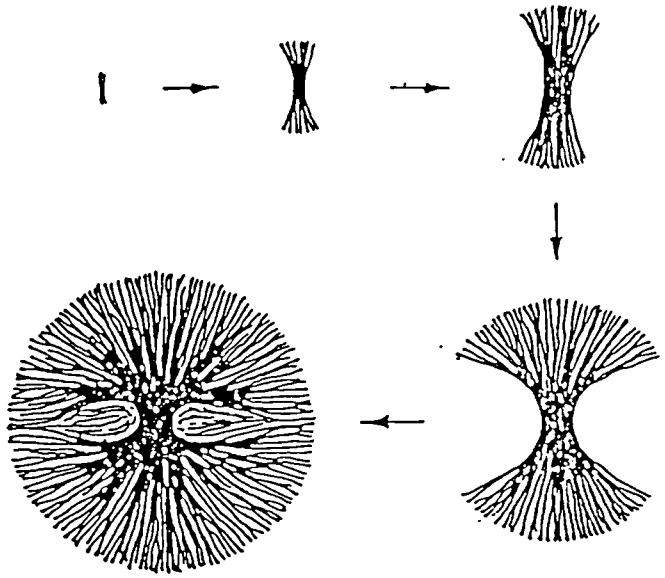

Figure 2.9. Progression of spherulite growth starting with fiber and leading to sheaf-like embryos.

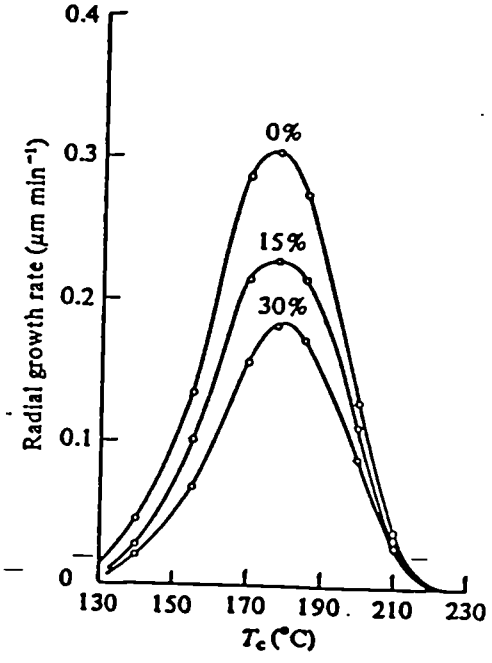

Figure 2.10. Relation of growth rates with crystallisation temperature in isotactic polystyrene and blends containing 15% and 30% of atactic polymer (after 81).

2.2.2. Nucleation and Growth

The polarising microscope has been used to study the growth rates of spherulites, i.e. the velocity of radical advance. All studies show that this quantity is remarkably linear with time at a given temperature, except when spherulites near impingement or when the viscosity of the melt is deliberately reduced (81). This is, in fact, a crucial point in the understanding of spherulitic growth. The variation with temperature typically takes the form of Figure 2.10. It has long been recognised, however, that the characteristic shape is a consequence of growth being slowed by increasing viscosity at lower temperatures and by a diminishing thermodynamic drive (i.e. supercooling) as the melting point is approached. For polyethylene, growth is so fast that only the higher end of this curve can be realised, while for other polymers such as isotactic polypropylene and isotactic polystyrene the whole range can be measured.

The extent to which growth rate can be measured depends on spherulite size and this in turns depends on the relation between nucleation rate and growth rate. Another words, if nucleation is slow and growth rate is fast by comparison, a few large spherulites

will result. On the other hand rapid extensive nucleation will lead to a profusion of spherulites, which may well be immature. Polyethylene often behaves in this way, resulting in a texture, recognisable as very many small embryos. Therefore, the control of spherulite size (for a desired form of end product), can be achieved if one varies the nucleation rate.

This phenomenon is possible, since, almost always, the nucleation in polymers is heterogeneous in origin, i.e. it is initiated on non-polymeric particles. Were it homogeneous, forming on the polymer itself, many fewer possibilities would present themselves. However, in a bulk sample when heterogeneous nucleation has started growth will proceed through the entire sample. Therefore, this is the reason why foreign particles are added to control the spherulites size development.

No matter whether the nucleation is homogeneous or heterogeneous it is still strongly affected by molecular weight, with longer molecules usually initiating crystallisation of the polymer. Presumably this is because the longer a molecules is, the greater the chance of being able to adapt a suitable conformation. For instance, as in the case of polyethylene, if large spherulites are desirable, one

has only to heat the polymer sufficiently to cause degradation, which then, the loss of longer molecules (also creation of additional very short ones) both will help to grow fewer and more open spherulite structure.

The growth of crystal is governed by diffusion, either of heat or matter, yet the solution of the diffusion equation for an expanding sphere is known to give a surface area increasing with time (82). If diffusion is a dominant process, therefore, the implication of constant growth rate is that local conditions are not changing with time.

Keith and Padden (82) propose a theory which considers a supercooled polymer melt within which the crystallisation is proceeding at finite rate. Although there must be a local temperature gradient to allow the heat of crystallisation to be dissipated, the uniform linear growth rate shows that this must be small and the system may be regarded as effectively isothermal. Let there be an equilibrium concentration C of effective impurities at points remote from growing crystals. The distribution of such impurities is dependent on the rate of advance of the crystal surface G and diffusion coefficient for 'impurities' D. The distance within which this concentration is enhanced by the length of $\delta=D/G$. The effect of this build up

of impurities on further crystallisation, is to depress the equilibrium melting temperature TL(liquid temperature) for melt with increasing concentration of impurities, below what it would otherwise be. The effective supercooling $\Delta T = TL-T$ is correspondingly decreased and the thermodynamic drive for crystallisation to proceed, is reduced.

2.2.3. Polypropylene Spherulite Morphology

The conventional and most widely occurring crystal structure of polypropylene is the one determined by Natta and Corradini (83), with a monoclinic lattice as illustrated in Figure 2.11, which later, when other polymorphs became apparent was refereed to as the 'α' structure.

Soon after, another polymorph with hexagonal lattice was recognised (84-87). The hexagonal lattice or 'β' structure is known to be favoured by high shear rates (88), fast cooling (89) and certain heterogeneous nucleants (90-93). The β crystals if present, are formed sporadically and in small quantities, 'admidst a sea' of α crystals. A third type of polymorph with triclinic lattice has been observed in samples of either fractionated or pressure crystallised polypropylene. The so called 'γ' structure was first identified by Addink et

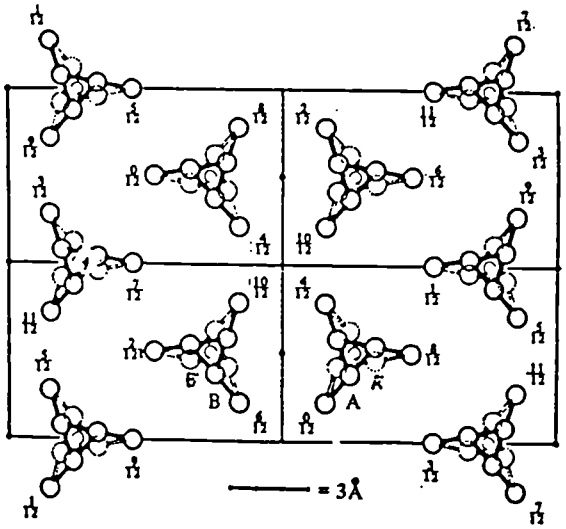

Figure 2.11. Shematic representation of structure of monoclinic polypropylene (after 83).

al. (94), from X-ray results concerning a low molecular weight fraction, while Tutner-Jones et al. (85) found the 'γ' structure in relatively high molecular weight. The γ-form in the latter case was virtually isolated and pure, formed by a carefully controlled cooling procedure following solvent extraction between 35-70°C in either petrol, ether or xylene. The cooled sample was obtained at 60°C hr^{-1} from a melt maintained at 190°C. The proportion of γ-form crystallising increases with increasing pressure (85,95). These authors hypothesise the stability of γ-form is due to decreased volume available for the packing of helical chains into a crystalline lattice at elevated pressure. Since the packing of the chains is very sensitive to the distance between CH_3 groups, this necessitates a modification of the unit cell in order to maintain the most favourable inter-methyl distances (85).

Samples that consisted entirely of γ-form, melt at 147°C (85), although by high temperature and pressure annealing this could ultimately reach about 160°C; which presumably is due to defect elimination.

At the level of resolution using a polarising microscope, there exist a variety of spherulite types classified by their appearance between cross-polars, and the sign and nature of birefringence. Four distinct

spherulite types and some mixed forms were identified by Keith et al. (96) and Fujiyama et al. (97). Types I and II, known as the α-modification are composed of monoclinic unit cells. Their birefringence is low, positive for the first and negative for the second. On the other hand spherulites of type III and IV are composed of hexagonal unit cells and were categorised as the β-form of spherulites. They are much more negative in birefringence and are easily distinguished by their luminous bright appearance in polarised light, surrounded by much less bright α-spherulites. The experiments carried out by these authors have shown that type I and II will grow at the same rate, whilst, spherulites of type III and IV will grow on the average about twenty percent faster. The properties of all the spherulites discussed are given in Table 2.2. In the bulk crystallised specimens, the spherulites are so called "mixed types ". These spherulites exhibit random distribution of positively and negatively birefringent regions where the birefringence is of a low and often not measurable value. The unit cell of the mixed category is the monoclinic 'α ' variety.

The lamellae morphology, resolved using the electron microscope, is also complex. The monoclinic polypropylene spherulites grown from solution , show a tightly 'cross-hatched' dendritic habit, incorporated

Table 2.2. Characteristics of iPP spherulite types.

Spherulite Type	1	Mixed	II	III	IV
	Monoclinic			Hexagonal	
Crystal Structure					
Magnitude of Birefringence	0.003	0.002	0.002	0.007	0.007
Sign of Birefringence	+ve	+ve/-ve	-ve	-ve	-ve
Concentric Banding	No	No	No	No	Yes
Isothermal Tc (°C)	<134	134-138	>138	<122	126-132

within the usual spherulitic structure (98). This unique morphology was noticed in melt grown specimens of α-polypropylene (99-101).

The study carried out by Khoury (98) on isotactic polypropylene(iPP) grown from solution, has shown the dendrites are comprise "twinned" crystals forming an acute angle of 80.67°. The consequence of such twinning provides an explanation for the change of birefringence of the spherulites of monoclinic iPP. The net birefringence depends on the relative proportions of twinned and untwinned components. The change noticed in birefringence of iPP spherulite from positive to negative with increasing crystallisation temperature may thus be interpreted in terms of a reduction in the degree of twinned component (99).

The cross-hatched texture is a unique feature intrinsic to polypropylene. Khoury (98) made a proposal that there is an epitaxial relationship between parent and twin. The basic structural unit is a lath-like chain folded lamellar crystal (revealed by the electron microscope). Three dimensional arrays of intercrossing laths are thus formed in solution which are a consequence of a particularly unusual mode of lamellar branching. Khoury's detailed analysis,

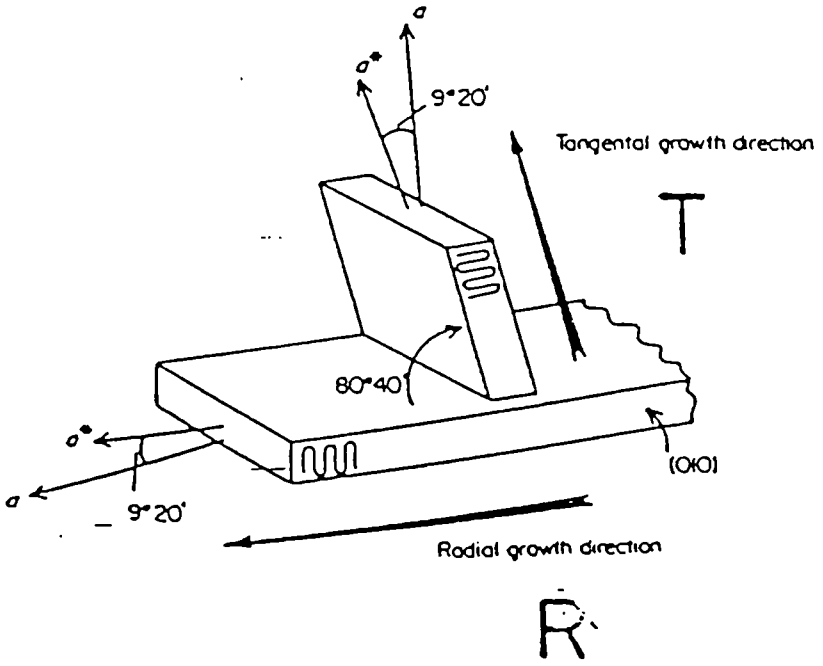

Figure 2.12. Schematic representation of cross hatching indicating epitaxial branch angle and fast growth direction.

incorporating the measurement of diffraction patterns, proposes that the branching angle of 80° 40' corresponds to parallelism of the a and c axis in one lattice with the -c and -a axis respectively of the other. Figure 2.12 exhibit a schematic representation of the cross-hatched morphology taken from Norton (102). On the above mentioned figure R represents the radial direction within the spherulite whilst the T represents, the branched tangential direction of a cross-hatched overgrowth.

Khoury's study concludes by discussing two points, the first concerns the degeneration of the regular 'dendrite' into spherulite, the second looks for mechanisms to induce branching. Instances where features such as curved lamellae being formed due to lattice distortions by the fold plane (103) and environmental factors such as cellation due to impurity segregation are thought to affect the first consideration. A form of epitaxial accretion is thought to be involved in the second.

2.2.4. Thermal Behaviour of Polypropylene

The different crystal structure of polypropylene discussed so far have different melting characteristics. If the specimen is only an α-form, the results of differential scanning calorimetry (DSC) shows only

one melting peak at about 441°K (168°C), while if both type of structures are present, then multiple peak will be observed (89,104-106). While the β type spherulites are usually scarce and occur under special conditions. However, a double melting peak of β-form crystals has been observed (105), particularly at slow heating rates. After the initial melting at about 145°C, still another structure showing a faint positive birefringence, which according to Fugiwara (105) the structure still has a hexagonal lattice. This recrystallised β , melt at about 152°C and is succeeded by a monoclinic α-form. β-spherulites are also favoured by presence of some nucleating agents or by crystallisation during melt shear (88-93).

2.2.5. X-ray Diffraction of Polypropylene

As described previously due to different cooling rates and different shear histories during processing, polypropylene specimens sectioned from skin to core layer may consist of different crystal structures. From the Bragg angles, at which diffraction from a crystal occurs, it is possible to obtain information concerning the crystal structure as well as the unit cell dimensions of the crystalline polymer. As stated previously the α-form structure was first determined by Natta and Corradini (83), comprising molecular chains ordered in a 3_1 helical conformation packed

monoclinically, the dimensions of the unit cell are

a= 6.65 ± .05 Å b= 20.96 ± .15 Å c=6.5 ± .04 Å

α= 90° β= 99° γ = 90°

the β-structure which was recognised by Keith and Padden (84) and later by Turner-Jones et al.(85), has the following dimensions;

a= 19.08 Å b= 19.08 Å c= 6.49 Å

α= 90° β= 90° γ= 120°

Table 2.3 gives the generally accepted Turner-Jones indexed reflections for these three polymorphs together with the observed intensities and calculated reciprocal spacings.

2.2.6. Polyethylene Morphology

The morphology of polyethylene is similar to the fine morphology of polypropylene previously described.

Heise and co-workers (107,108) presented detailed study of the morphology of linear and branched polyethylene. In these works they have studied the degree of orientation of molecular chains in injection moulded specimens. It is shown that the degree of orientation decreases as the thickness of the moulded specimen increases from 1mm to 4mm.

Table 2.3. Turner-Jones index of three polymorphs diffraction (after 85).

Line No.	Iobs *	dobs *	dcal *	Index (hkl)	Crystal phase
1	s	0.244	0.246	110	α
2	s	0.278	0.280	300	β
3	s	0.291	0.295	040	α
4	s	0.321	0.322	130	α
5	w	0.343	0.348	140	γ
6	s'	0.368	0.371	301	β
7	s	0.362	0.371	111	α
8	s	0.421	0.378	131	α
9	w	0.443	0.425	041	β
10	w	0.414	0.425	131	α
11	m	0.48	0.422	060	α
12	w	0.489	0.462	200	α
13	w	0.494	0.485	330	β
14	m	0.536	0.491	220	α
15	w	0.560	0.560	600	β

* s Strong

m Medium

W Weak

Kamal et al.(109,110) also have studied the morphological zones and orientation in injection moulded polyethylene. In this work a number of techniques were ,used including polarised light microscopy, infrared measurement and differential scanning calorimetry. These authors report that four distinct regions are present throughout the thickness of the specimen, a nonspherulitic skin zone with a certain degree of transcrystallinity, a second zone containing very fine asymmetric spherulites of almost uniform size nucleated at fast rates, a third zone containing asymmetric larger spherulites and fourth zone of randomly oriented and nucleated spherulites.

Heckmann and Johnsen (111) studied the orientation distribution with depth in the case of injection moulded polyethylene. It was noted, with the processing conditions used, the highest degree of orientation was found about 200 μm under the surface. They have also shown a strong maximum in modulus and in the melting temperature at the same depth. Although the photomicrographic evidence was not given, it was suggested that the surface showed a transcrystalline structure. That is, nucleation of fibrillar entities occurs in the most highly selected melt directly adjacent to the surface of the mould.

The rate of cooling from the melt state is an im-

portant criterion which governs the crystal structure of a polymer, and ultimately the properties of the final product. The crystallisation is a transformation that occurs by nucleation growth. In general, the rate of both nucleation and growth increases with undercooling (the difference between the melting point and instantaneous temperature). Thus, slowly cooled areas will have sufficient time to transform at higher temperatures while, during more rapid cooling, the major portion of the crystallisation occurs at lower temperatures. This is important, as the rate of transformation determines the degree of crystallinity and may also have a bearing on the orientation.

Chivers et al.(112) has studied the crystallisation of polyethylene from the melt at low degrees of supercooling. they have shown that the lamellar thickness 'l ' depends on the supercooling temperature at which the crystallisation occurs. Elsewhere, this is interpreted in terms of kinetic theories of crystallisation (113,114).

Also Hay et al. (115) have reported that there are three basic habits of dominant lamellae in crystallised polyethylene, which differing in the profiles, as they are viewed down the b axis. In addition to ridged sheets, there are planar, or slightly curved and S shaped sheets. The crystallography of all three

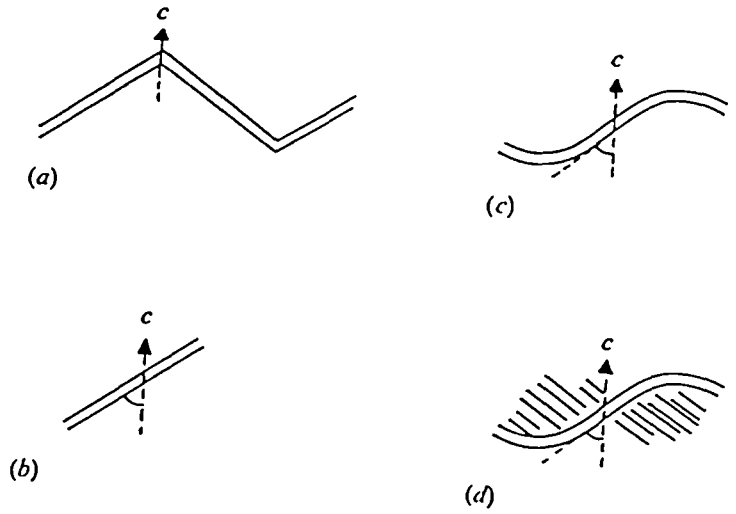

Figure 2.13. Crystallography of dominanat lamellae in PE viewed down b and c axis vertical: a) ridged, b) planar and c) S-shaped sheets. In (d) the pattern of subsidary platelets associate with an S is also drawn (after 80).

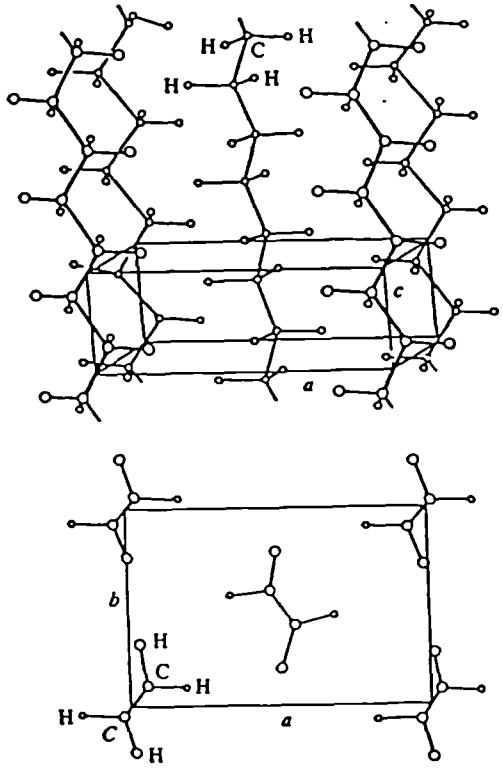

Figure 2.14. Schematic representation of the orthorhombic structure of polyethylene (after 80).

shapes is shown diagramatically in Figure 2.13. The sequence rigid, planar, and S shaped sheets occurs with increasing molecular length (and thus growth rate) at 130°C and again, but is shifted to a lesser length, at 128°C and slightly lower temperature (115). These authors do not give clear reasons for formation of these type of lamellae.

2.2.7. Thermal Analysis of Polyethylene

Processing of thermoplastics involves application of heat and stress. Thereby, resulting in deformation of the polymer, often at high shear rates. When the polymer being fabricated is capable of undergoing crystallisation, the removal of heat upon cooling to room temperature may be accompanied by crystallisation of the polymer, often during deformation of melt.

Haas et al. (116) have studied the effect of shear stress on the crystallisation kinetics of linear polyethylene. They have shown that the application of a sufficiently high shear stress to an initially super-cooled melt leads to a large increase in the number of crystalline structures formed and to the formation of oriented morphologies. In another study (117) they have suggested increasing the shear stress from 5.4×10^5 dyns cm^{-2} (5.42×10^4 N m^{-2}) to 43.6×10^5

dyns cm^{-2} (43.6×10^4 N m^{-2}) has changed the melting point of polyethylene from 132.2°C to 133.8°C.

The author has studied the thermal properties of low, medium and high density polyethylene and their blends, prepared by compression moulding (118). It has been shown the as moulded specimens of HDPE have higher melting point (137°C) than , when the same sample annealed at 90°C for 10 hours (melting peak appeared at 134°C).

Datta et al. (119) have studied the thermal properties of low and high density polyethylene and blends of LDPE/HDPE and LLDPE/HDPE by DSC technique. They have shown when HDPE specimens cooled at fast rate 10°C min^{-1}, the melting analysis showed two peaks at 111.75°C and 133.25°C, whereas when specimens cooled at slow rate (1°C min^{-1}), the thermal analysis shows 2 peaks at 120.0°C and 135.5°C. They have suggested slow cooling results in more perfect crystalline structure. the result of blend of LLDPE/HDPE has shown 1 melting peak, which suggest that , the blend of these two polymers are compatible in the crystalline phase and very similar to a single -compound system.

2.2.8. X-ray Diffraction Studies of Polyethylene

As has been stated earlier on, one of the important tools in studying the crystal structure of a crystalline material is the X-ray diffraction. Many investigators have attempted to study the crystalline structure of polyethylene prepared at different processing conditions (120-125).

From the Bragg angle at which diffraction from a crystal occurs it is possible to obtain information concerning the cell dimensions, crystal structure,and degree of orientation. In the crystalline state, polymer chains are aligned parallel to each other. Interchain distances correspond to bond distances at free energy minima. Figure 2.14 shows the unit cell structure of polyethylene. The chains are packed side by side so that their long axis are parallel, but zigzag planes are not all parallel. The whole arrangement has an orthorhombic structure.

Hay et al.(115) have studied the relation between molecular orientation and crystalline texture. A number of samples at different angles, respective to injection flow, were chosen in order to find the distribution of orientation in the specimen. The work was restricted to identification of the maximum distribution in each sample. Also it is stated that

owing to the large spread of orientation distributions, more than one of the three set of reflections 110,200,020 could be present simultaneously in a given photograph. Their relative intensities, however, are largely variable in photograph taken along x, y, or z direction.

Moy et al.(123) carried out an investigation on the orientation of molecular chain through an injection moulded specimen of polyethylene. X-ray diffraction results obtained, indicated that the crystallographic a-axis tends to orient in the flow direction, while the b and c axis vary symmetrically about that direction. Also with the aid of X-ray diffraction techniques, Woebcken and Heise (125), attempted to relate crystallite orientation in polyethylene injection moulding to mechanical properties and conditions. In their work, they observed significant interaction between microscopic structure, on one hand, and both processing conditions and the properties of the moulded articles on the other.

CHAPTER 3

EXPERIMENTAL PROCEDURE

3. Experimental Procedure
3.1. Introduction

The effect of processing conditions, die design and chemical blowing agent on the density and porosity of polyolefin foam were undertaken by selecting various grades of polypropylene and high density polyethylene with varying melt flow indices (MFI). Each grade was mixed with Hydrocerol (CF-20) blowing agent, then processed into foamed rod on a conventional single screw extruder.

The expansion ratio of foamed polymer emerging from the die was measured by using a cathetometer to measure its maximum diameter. The density of foamed samples produced in each run was measured and the cell size distribution analysed by image analysis. Further investigations were carried out to determine the effects of processing conditions and concentration of chemical blowing agent, on the percent of open cell fraction of the specimen. This was undertaken using a mercury intrusion porosimeter (Model 2000).

In addition, the microstructure of selective specimens was studied by optical microscopy, scanning electron microscopy and transmission electron microscopy.

Also the nature of the crystallinity was studied by

differential scanning calorimeter. More detailed information on the state of order of crystalline material was obtained from the analysis of specimens by X-ray diffraction.

3.2 Materials

In order to study the effect of melt viscosity on the cell morphology of polyolefin foam, six different grades of polypropylene and four grades of high density polyethylene with different melt flow indices were chosen for this study. All grades of polypropylene and two grades of high density polyethylene were supplied in granular form, whereas the other two grades of high density polyethylene were supplied in powder form. The average molecular weight and molecular weight distribution of these materials was determined at the Polymer Supply and Characterisation Centre at RAPRA by gel permeation chromatography(GPC). These results of are presented in Tables 3.1 and 3.2.

Throughout this study Hydrocerol CF-20 manufactured by Boehringer Ingelheim was used as the chemical blowing agent. This compound is a mixture of citric acid and carbonate components under normal storage conditions. The theoretical gas yield expressed as liberated carbon dioxide, is about 100 ml g^{-1} under normal conditions (126). Hydrocerol CF-20 decomposes

Table 3.1. Molecular Characteristics of Polypropylene* Homopolymer.

Polymer Grade	Wt. average Molecular Weight* 10^{-5}	No. Average Molecular Weight* 10^{-4}	polydis-persity	MFI g/10 min.
GSE-16	4.27	5.35	7.98	0.8
GWE-23	4.25	5.19	8.18	2
GWM-22	4.17	5.17	8.07	4
GXM-43	3.75	4.77	7.87	9
GYM-45	3.12	3.86	8.08	15
LXF-52	3.02	3.76	8.04	22

Table 3.2. Molecular Characteristics of high density Polyethylene**

Polymer Grade	Wt. Average Molecular Weight* 10^{-5}	No. Average Molecular Weight* 10^{-4}	Polydis-persity	MFI g/10 min.
HO20-54P	4.27	3.35	12.74	2
HO60-45P	3.00	2.12	14.19	6
H110-42	2.62	1.68	15.65	11
Natene 54-180	0.633	o.302	20.96	18

* All grades of PP were supplied by Imperial Chemical Industry (ICI) Co.

** All grades of HDPE were supplied by British Petroleum (BP) Co.

at temperatures between 180-220°C. Figure 3.1 exhibits the endothermic decomposition of this compound, as determined by DSC. As consequence of decomposition of this compound, two endothermic peaks appear at 460° and 492°K. It is believed these peaks are due to decomposition of citric acid and carbonate components. Hydrocerol CF-20 is a self nucleating blowing agent, and has been claimed by the manufacturer its residues are safe if the foam product comes in contact with human body.

Throughout the study various combinations of resin and blowing agent were used, as discussed below.

3.3. Preparation of Feedstocks

The ten different grades of polymer mentioned previously each were mixed with chemical blowing agent (Hydrocerol CF-20) for about 5 minutes using a Herschel high speed mixer.

In some experiments, polypropylene and high density polyethylene were blended in different proportion to modify the melt strength of the material, in order to achieve a more uniform cell and cross sectional structure in the final product. Melt mixing was undertaken in a specially modified twin screw extruder

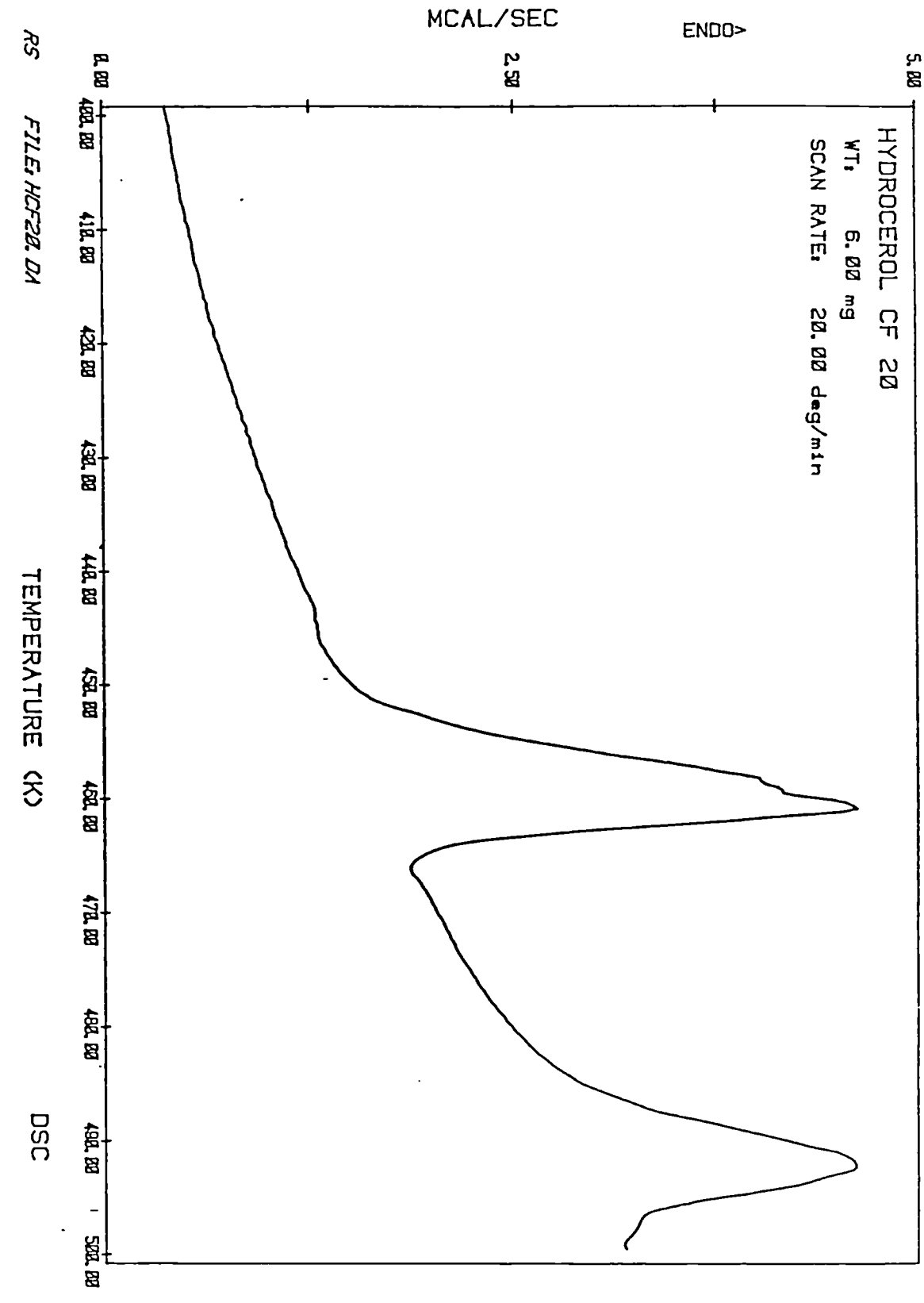

Figure 3.1. Schematic representation of endothermic analysis of chemical blowing agent (Hydrocerol CF-20).

(Betol TS 40-DV-L). The Betol TS-40 is a co-rotating intermeshing unit featuring modular screw and barrel sections enabling flexibility in screw configuration combined with twin barrel ports for devolatilizing and/ feeding additives. Table 3.3 shows the screw geometry together with optimised processing conditions used in this work.

3.4.1. Determination of Melt Rheology

In order to study the rheological characteristics of polymer containing gas, it should be bear in mind, to keep high pressure on the polymer-gas mixture to prevent phase separation. For this reason, a capillary rheometery was found unsuitable, instead a single screw extruder (Betol Model 2520 EX) with the following specification was used.

screw length	600 mm
screw diameter	25 mm
L/D ratio of screw	24:1
compression ratio of screw	3:1

screw type:

- constant pitch
- single stage with feed, compression and metering zone,a conventional polyolefin type screw.

Han et al. (25) have also applied similar method to study the rheological characteristics of low density polyethylene foam.

For the purpose of correcting for end effects, two

Table 3.3 TS40 Twin Screw Extrusion Conditions

Screw diameter		40 mm
Screw length		680 mm
L/D ratio of screw		17:1
Flight pitch		
	-feed	24 mm
	-compression	16 mm
	-metering	16 mm
Screw speed	speed control up to	180 rpm
Heater zone 1		160°C
Heater zone 2		170°C
Heater zone 3		190°C
Heater zone 4		210°C
Heater zone die adapter		200°C
Heater zone die		200°C

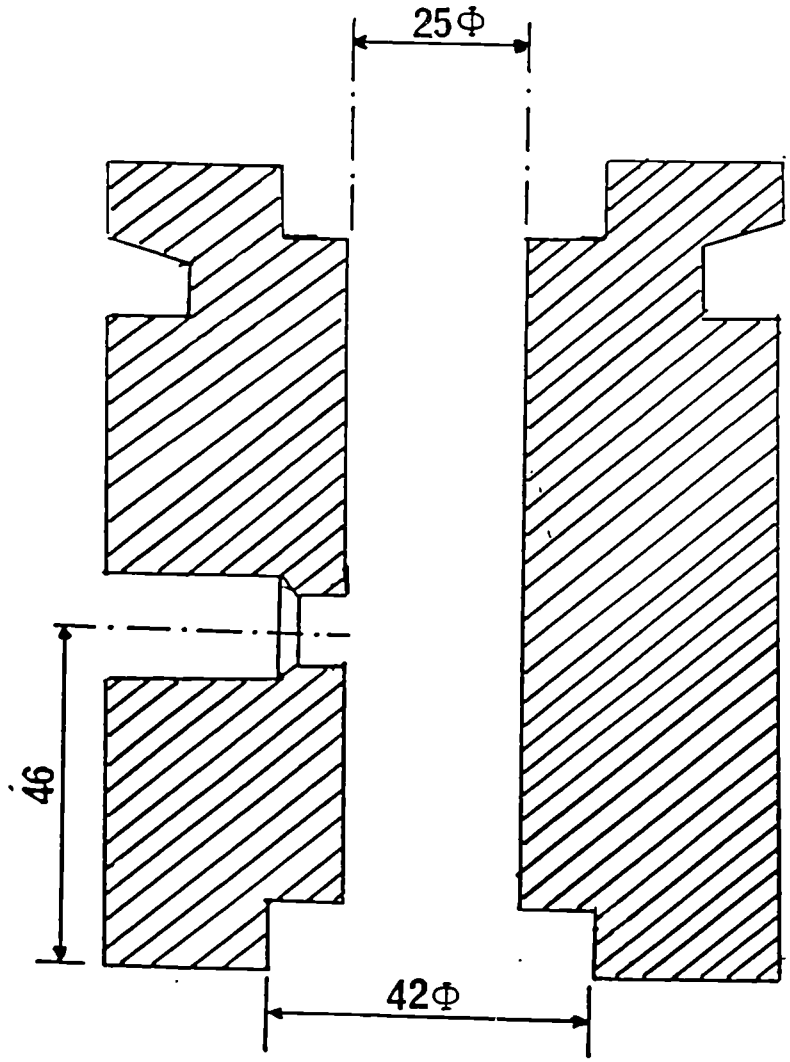

Figure 3.2. Schematic representation of dies used for rheological studies of polyolefin in foamed and unfoamed state. a) die adapter b)die insert. All sizes are in mm.

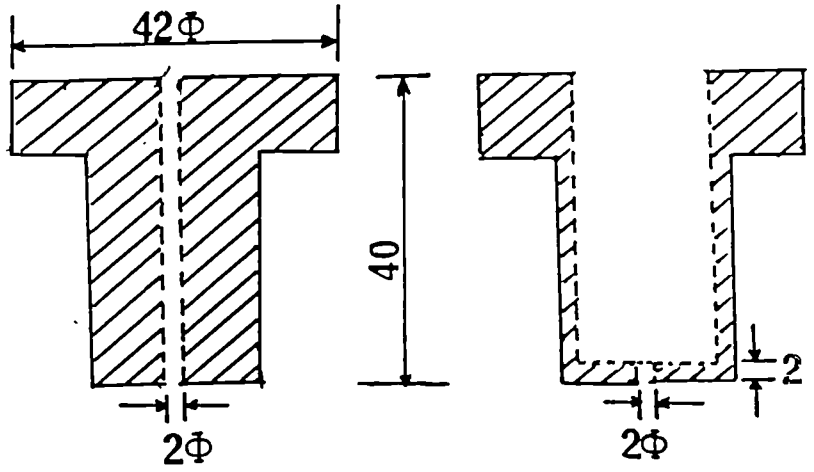

b

dies were designed, as shown in Figure 3.2. The melt temperature was monitored to an accuracy of ±2°C by manually inserting a temperature probe into melt emerging from the die exit. The melt pressure at the die entrance was also recorded by a Dynisco melt pressure transducer PT 422A.

In order to verify the accuracy of viscosity measurements obtained from the single screw extruder, rheological characteristics of polypropylene homopolymer in solid form was also studied on a Davenport capillary rheometer model ER 406. As it will be shown in chapter 4, the rheological results obtained from single screw extruder, are in a good agreement (± 5% difference) with those measured on Davonport rheometer. The main source of this difference is believed to be due to pressure fluctuation, which was found to be not greater than ±68.95 KPa (±10 PSI), together with melt slippage and melt temperature variation (±2°C).

3.4.2. Extrusion of Foamed Polyolefin Rod

Extruders are one of the most common industrial manufacturing processes for converting plastics materials. They are mainly used for melting compounding, mixing devolatizing, melt pressurising and pumping polymers prior to shaping through a die.

In order to investigate the effect of processing conditions on foaming characteristics of polypropylene and high density polyethylene, a conventional single screw extruder was used, with specification given in Table 3.4. It should be pointed out that the temperature of the extruder in zone 1 and 2 through the experiment, was kept constant, and only temperatures in zone 3 and 4 of the extruder and die zone varied in order to increase or decrease the melt temperature of the extrudate.

It should be emphasised that the foam emerging from the die exit has very low melt strength, therefore the set up for cooling the melt, should be exactly in line with the die exit, otherwise the cells readily will collapse prior to cooling. Figure 3.3 shows a typical set up which was used in this study.

3.5. Density Measurement of Polyolefin Foam

3.5.1. Density of Solid Foam

On selected samples from each run, five different sample were chosen and their density measured in the following manner:

i) the weight of each foam specimen was measured up to 0.10 of mg (W1). To minimise the error, the samples were chosen in a way so that their weight lie between 0.9-1.0 g.

Table 3.4. Betol Single Screw Extrusion Conditions

Model		Betol 5025	
Screw diameter		50 mm	
Screw length		125 mm	
L/D ratio of screw		25:1	
Screw type	-Constant pitch -Single stage with feed compression and metering zone		
Screw speed	speed control	5-100rpm	
Hopper capacity		22 Kg	
Heating capacity	-Extruder:barrel -Die	12 kw total 1.5 Kw	
	Set Temperature (°C)*		
		PP	HDPE
Heater zone 1		150	165
Heater zone 2		160	175
Heater zone 3		170	230
Heater zone 4		190	250
Heater zone adapter		185	245
Heater zone die 1		180	245
Heater zone die land adapter		170	230

* Make a note, the above mentioned temperatures are for the optimum processing conditions of PP and HDPE. The processing temperature of PP/HDPE blends, are similar to those of PP, except the temperature in last 5 zones was increased as much as of 5°C to 20°C, depending on the PP concentration in the blend.

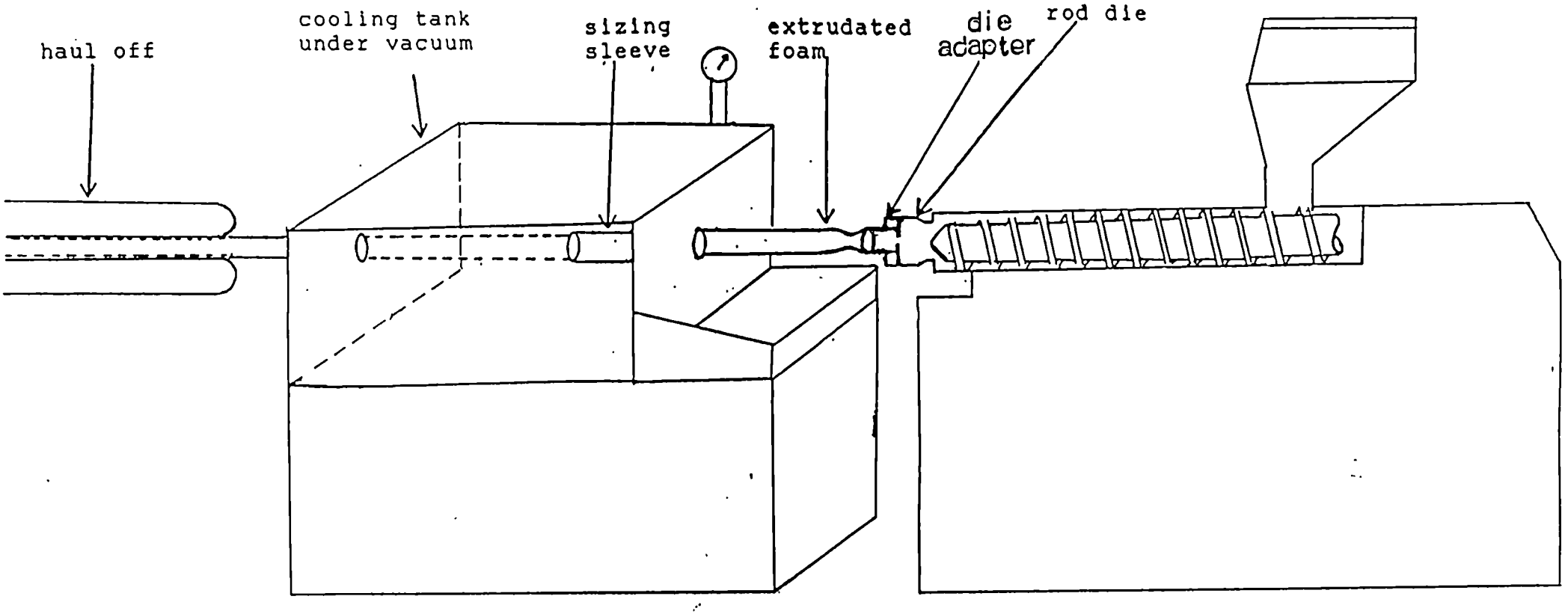

Fig. 3.3 Schematic representation of the foam extrusion line.

ii) the weight of the specimen was recorded while it was submerged in mercury with a help of a pin (W2).

From W2, which is the upthrust and it is equal to weight of mercury displaced, the volume of foam, hence,the density of foam specimen was calculated as:

$$Vf = \frac{W2}{\rho m} \qquad 3.1$$

and

$$\rho_f = \frac{W1.\rho m}{W2} \qquad 3.2$$

where:

Vf is volume of foam specimen
ρ_m is density of mercury at the test temperature
ρ_f density of foam specimen

It should be pointed out in order to prevent the mercury penetration inside the pores, after weighing the specimen a small amount of epoxy (approximately 15 mg) was applied on both ends of the foam specimen few hours prior to testing. This method enables one to measure the density to a high accuracy.

3.5.2. Density of Melt Foam

The density of foamed material in the melt condition was calculated from measurement of the diameter of the rod extrudate emerging from the die

$$D_f = [(d_p)/(d_f)]^2 * D_p \qquad 3.3$$

where

D_f is density of foamed polymer.
D_p is density of unfoamed polymer.
d_f is maximum measured diameter of foam extrudate prior to cooling.
d_p is maximum measured diameter of unfoamed extrudate prior to cooling.

It should be added that allowance was taken of the influence of die swell effects from polymer in the unfoamed state and drawdown effects due to the necessity applied tension to the rod during haul-off.

3.6. Determination of Open Cell Fraction

In order to measure the open cell fraction of foamed specimens, a Carlo Ebra Strumentazione Porosimeter 2000 was employed. In this technique, the volume of mercury, which penetrates the pores of the sample, is dilatometrically measured and automatically recorded as a function of applied pressure. The maximum reachable pressure is 2000 kg cm^{-2}(196.1 MPa). By applying Washburn equation which relates the pressure needed to force a nonwetting liquid into cylindrical pores, its diameter can be calculated as follow (127);

$$P = 4\,\delta \cos\theta / d \qquad 3.4$$

where;

P is the pressure
δ is the surface tension (surface tension of mercury= 0.480 N m^{-1})
θ is the contact angle of the advancing meniscus= 140°).
d is pore diameter

The instrument is designed to measure the pores up to

7.5 μm in diameter. Also the software is programmed, such that when mercury emerging from a small pore and entering a large one, the large pore will be considered as combination of both large and small pores, therefore, neither the cell size nor the cell distribution are correctly measured by this instrument. The only valuable information obtained by this machine is the percent of open cell fraction, which is taken as the volume fraction of mercury penetrating into the pores (this is done automatically by the instrument by pressurising the mercury to penetrate into the pores) to the total volume of the specimen (which is calculated from the weight and density of the foam specimen fed into the programme at the beginning of each run).

3.7. Quantitative Characterisation of Cell Morphology by Image Analysis

The cell size and cell size distribution of foamed samples produced under different processing conditions was determined by image analysis. The need to use an automatic cell sizing equipment resulted from the requirement for a large number of cells to be counted in order to reduce statistical errors. Quantitative image analysers have been designed and developed specifically to furnish various geometrical measurements of microscopic patterns or particles, and to present

these measurements in a meaningful form.

Several techniques can be use to measure the cell size and cell size distributions of foamed specimen. One method involves microtoming of the cross section, and measuring the cell size by means of light microscopy. Due to high porosity of the specimens, the resolution was found to be very poor and the results were not reproducible. Another technique involves, measuring the cell size with the help of image analyser, by transmitting light on the sample itself. Due to same reasons mentioned above, large error was found in the results. Best method (in terms of low percentage of error and reproducibility of the results) was found, when, the cross section of the specimens were scanned using SEM, and the pictures produced were used to measure the cell size and cell size distribution by image analysis. It should be pointed out that the experimental error was found to be less than $\pm$5% in most cases. The source error is believed to be due to the fact that in order to measure all the size of the cells over the whole cross section, it is necessary to vary the position of the specimen from left to right and/or top to bottom. Therefore, some of the cells could be counted more than one time.

The experimental procedure conducted on the image analyser given below, was based on scanning electron micrographs microtomed surfaces.

In order to measure the cell size and cell size distribution by image analysis , the programme on disk was loaded onto the computer. The central processing unit(CPU) processed the image produced from a picture of a microtomed surface (taken on a SEM). The raw data measured by the CPU was processed by the computer to the required form and this would be stored in the disk drive or printed out by printer.

In most microscopic imaging except stereomicroscopy, cells can only be measured in two dimensions and the shape of the two dimensional cell would depend on the location at which the cell is being sectioned.

For convenience the cell size was expressed in terms of the diameter of a sphere having the same surface area of cell measured or commonly known as equivalent area spherical diameter or surface diameter, so that irregular shaped cell sizes are comparable with regular shapes. This raw data is expressed in terms of the number of cells per unit area (Na) in the computer software.

In order to transfer the two dimensional data to

three dimensions, certain assumption and correction are required. The software programme written for this type of work is based on the Schwahz-Saltykov analysis (128) which account for the probability of cutting through cells at levels other than their mid-point(diameter), and transforms the data into a number of cells per unit volume (Nv). Here the assumption is taken so that the view in two dimensions is statistically repeated in the third dimension. The general equation for Schartz-Saltykov (diameter) analysis for number of cells of any size group per unit volume is:

$$(Nv)j=1/\Delta\ [(\alpha i(Na)i) - (\alpha i+1*(Na)i+1\ ) - (\alpha i+2\ * (Na)i+2\ ) ..... \alpha k(Na)k\ ] \qquad 3.5$$

where;

K	is equal to total number of class interval
i and j	are integer values from 1 to K
Δ	is the ratio of Dmax. (diameter of largest cell) to K
α	is a coefficient relating i and j (the values of are given in Schwartz-Saltykov Table presented in Table 5.3 of reference 128).

These data are expressed as a distribution of the volume of cells per unit volume (Nv) in each diameter size class from which the mean volume diameter is measured.

3.8. Preparation of Samples for Optical Microscopy

Due to simplicity of its use and informative results

obtained, the light microscopy has been used in microstructural characterisation of the unfoamed polymers produced in this study.

In this research selected areas were microtomed to provide thin layer (5-8 μm) which were examined in polarised transmission light using a Reichert Zetopan Nr 365467 light microscope. Best results were obtained when account was taken of the following points:

i) Blade quality;

It was necessary to make sure that the blade was in best condition to minimise damage on the surface of the specimen. A conventional mild steel Glen-Creston blade with a 37° facet angle was used for this work. Where the blade was sharpen by a Shandon and Southern Autosharp IV machine fitted with soft copper alloy lapping plates and 3 μm diamond pastes was used, which took approximately around 2 hours to sharpen the blade.

ii) The cutting Angle to the specimen;

This was set at 45° to the direction of flow, so that to distinguish the microstructure of the polymer from damages caused by the knife (if any).

iii) In order to minimise the distortion of the microtomed sample one should rigidize the specimen. A Mectron (Frigestor) microtomed cooling stage has been designed for the sledge microtome to

control the temperature of the specimen down to -24°C. The Frigestor microtome stage comprises: a Frigestor module mounted on a water cooled heat exchanger to which the adapter for the specific microtome is fitted. In addition harness water tubes and power leads run into the heat exchanger and module respectively.

3.9. Experimental Procedure of Preparation of Samples for Micromorphology

3.9.1 Preparation Specimens for Transmission Electron Microscopy (TEM)

In order to achieve best results in studying the microstructure of the extruded samples various etching procedures were utilised to enhance the polymer morphology. The steps which have been followed for preparing the specimens for TEM are similar to those described by Olley et al. (129). The procedure is as follow:

i) A mixture of 2:1 of orthophosphoric acid and Analar grade sulphuric acid (minimum assay 98 %) was made in a dry flask. The two acids were vigorously mixed by placing the mixture in an ultrasonic bath for one minute.

ii) 0.5 weight percent potassium permanganate was weighed and then carefully added to the mixture of acid. Care was taken when adding this strong

and potentially dangerous " cocktail " owing to the sporadic production of unstable and explosive component, manganese heptoxide. If at this stage the colour of solution turns blue it indicates contamination by water, and it should be discarded.

iii) After the surface of the sample was microtomed and polished, it was placed surface side downward into the etchant. From trial and error good results were achieved when etching time was arr-ound 20 hours and the temperature of etchant was at room temperature.

After the etching time was over, the following cleaning procedure was adopted:

i) The specimen was washed in a precooled(-20°C) solution of 2 parts sulphuric acid to 7 parts of distilled water for one minute in an ultrasonic bath. The above mentioned proportions of acid and water are believed to be those which gives lowest freezing point , which is helpful in pre-venting the heat of dilution of the original acid affecting the sample (129).

ii) The specimen was then transferred in a 30% solution of hydrogen peroxide for about 1 minute in an ultrasonic bath. This step is followed in order to remove manganese dioxide.

iii) The specimen was then transferred to a beaker containing distilled water and washed for 1 min.

in an ultrasonic bath.

iv) The sample was then rinsed in acetone for 1 minute and ,

v) Finally, it was dried in a vacuum oven for about 1 hour at temperature around 40°C.

3.9.2. Replication Procedure

Olley et al.(129) examined the microstructure of polypropylene using a two stage replication method, where the etched specimen is immediately shadowed with a very thin platinum/palladium (Pt/Pd) 80/20 alloy at angle of 20-40°C. Then followed by shadowing with a thicker and vertical backing of carbon film. The Pt/Pd-C layer is then covered by polyacrylic acid (PAA) and then allowed to dry for approximately 2 hours. Afterward the Pt/Pd-C layer which now adheres to PAA surface, can be easily removed by a razor blade. The PAA can be removed by placing the sandwich layer of Pt-Pd-C-PAA in distilled water with PAA side downward. Sufficient time should be given (approximately 2 hours) to allow PAA to dissolve, then the replica is floated onto copper grids for transmission electron microscopy.

The same procedures as those of Olley et al.(129) were also applied in this project, mainly for unfoamed specimens, since for foamed samples the PAA deposit was quite

impossible to separate due to high porosity of the surface. Therefore, it was decided to use the method devised by Norton (130), where samples were examined using a standard two stage replication process. First making an impression on cellulose acetate and then shadowing this with gold/Palladium (Au/Pd), then depositing a carbon film on the surface. The cellulose acetate-AU/Pd-C sandwich was then mounted onto copper grids and the cellulose acetate layer dissolved away using acetone vapour.

Examination of the replica produced in this way was performed using a Jeol 100CX transmission electron microscopy.

3.9.3. Preparation Samples for Scanning Electron Microscopy (SEM)

In contrast to TEM, SEM is used extensively for the study of polymer surfaces. It differs in that the electron beam, rather being fixed, is rastered across the sample. The image is produced by collecting secondary electrons emitted from the exited surface by means of a scintillator and then reproducing the scintillator image in a cathode ray tube(CRT) display, synchronised with the beam sweep. The beam size (100 Å) limits the resolution, but sample preparation is usually easier along with extremely

large depth of field. Images of higher contrast, albeit lower resolution, can be obtained by collecting higher energy back scattered electrons.

In order to study differences in crystalline morphology by SEM, specimens were prepared using a similar method to that used for producing the TEM replicas, namely by permanganatic etching. Hence microtomed sections were etched and cleaned. But the time consuming stage of replication was omitted. Instead, after the specimen was mounted on an aluminium disk with a double sided adhesive type, it was coated with gold vapour for 6 minutes (using Polaron Equipment SEM Coating Unit E-5000), then the edges of the specimen joined to the aluminium disk by coating with a solution of silver particles suspended in amylacetate, in order to minimise the risk of electron beam damage by SEM. Afterward, the sample was viewed directly in the SEM. In this study, the observations were performed on Cambridge Stereoscan 250 scanning electron microscopy.

3.10. Differential Scanning Calorimetry (DSC)

One of the most useful physical properties in characterisation of any polymer, is its thermal behaviour. The temperature dependent properties undergo major changes at one of two transition points. In crystal-

line polymers the one of greater importance is the crystalline melting point(Tm), while for amorphous polymers, it is the glass transition temperature(Tg) The property changes at Tm are more drastic, and are characteristic of a thermodynamic first-order transition. Associated with such a change is an uptake or emission of enthalpy-latent heat of fusion, which for crystallisation is an exothermic reaction and for melting is an endothermic one. Therefore, by careful consideration of the resulting endotherm or exotherms useful information can be derived concerning the phase change, i.e. in the case of polypropylene α and β-spherulites forms can be distinguished, in specimens from their different thermal response (see Chapter 7).

DSC is a technique designed to record the various heat requirements of small specimen (1-10 mg) during a heating or cooling experiment (at a constant rate), or under isothermal conditions.

The essential design of instrument consists of two calorimeters into which may be inserted small pans. One pan contains the sample whilst the other is left empty as a reference. Both the sample and reference are heated separately by individually controlled elements. The power to these heaters is adjusted continuously in response to any thermal effects in the sample, the point being to maintain sample and

reference at exactly same temperatures. The differential powers required to achieve this condition is recorded as the ordinate on an x-y recorder, with the programmed temperature of the system as the abscissa.

In the of case an isothermal experiment the abscissa equals time. In this work a Perkin-Elmer DSC II was used for qualitative melting and crystallisation analysis, where the instrument was calibrated by performing an experiment using indium a material with a known and sharp melting point.

Amongst others Lovinger and Samuels (89,131) have applied the technique of DSC to the investigation of polypropylene. The first study was primarily concerned with the melting of oriented isotactic polypropylene fibres. In this study the major point to note is that the polypropylene showed multiple melting peak from a seemingly single phase sample. The samples were considered to be solely monoclinic(α-crystals), therefore, the peaks were indicative of some crystallite differences, within the spherulite structure.

After number of experiments it was found that, a fast heating rate showed an abnormally high proportion of the lower melting phase as a result of poor heat transfer to the specimen. On the other hand at

low heating rate(2.5° and 5°K min^{-1}) showed different melting behaviour (transformation of β-type spherulites into the forms). It is believed slow heating would act similar to annealing of the specimen. Therefore, it was considered most likely that a heating rate of 10°K $min.^{-1}$ will show a true picture of the morphology. The DSC results relating to current work are presented in chapter 7.

3.11. Application of X-ray Diffraction Techniques to Study Crystalline Polymorphism in Extruded Polyolefin and Polyolefin Foam

3.11.1. Basic Concept of X-ray Diffraction

The X-ray diffraction can be used to determine detailed information on the state of order or disorder of a system. The diffraction of X-ray by gases or liquids give rise to diffuse haloes, whereas the diffraction of crystalline material gives sharp circles or spots (in the case of highly ordered crystalline structures). Also from the intensity and nature of the diffraction pattern, more detailed information can be deduced on the state of order of crystalline substances. In the case of semi-crystalline polymers, the information which can be collected from the X-ray analysis includes:

i) identification of material

ii) the relative orientation of the crystallites

iii) degree of crystallinity

When a crystalline material is exposed to a beam of X-rays, three dimensional arrays of atoms in the crystal scatters the radiation in a such a way that the scattered waves reinforce each other in specific directions. These directions, which are characteristic of the crystal orientation with respect to the beam and to the interatomic separation in the material, are governed by the Bragg's Law:

$$n\lambda = 2d_{hkl} \sin\theta \qquad 3.6$$

where;

- n is integer denoting the order of the diffraction
- λ is the wave length of the X-ray
- θ is the angle of incidence and reflexion
- d_{hkl} is the plane spacing designated by Miller indices

In this investigation extruded specimens were sectioned with a thickness of 500 μm along the flow direction and through its diameter. The sample was then mounted on the spinning stage (with skin side up) of a Philips PW 1050 diffractometer linked to a PW 1710 control terminal and software. The crystallographic analysis were made by scanning nickel filtered CuK_α radiation, collimated through a 0.2 mm slit, from 10 degrees in Bragg angle 2° up to 30° at a scan rate of 2° min^{-1}. The reflections from the spinning surface were collected

through a 1mm slit to the counter.

As it has been stated before, from the Bragg angles at which diffraction from a crystal occurs, it is possible to obtain information about the unit cell dimensions of a semi-crystalline polymer. For instance in this work the region between skin and foamed core showed a much higher degree of orientation crystallites. This also has been found to be consistent with work done on extrusion of blown film reported by Uejo (132).

Turner-Jones et al.(85,86) proposed an index based on the peak heights in the diffractogram to calculate β-phase concentrations. Recently Trotignon et al. (133) have used this method to study the α-phase orientation, β-phase distribution and crystallinity index C in injection moulded tensile test bars of isotactic polypropylene. The mathematical equations along with informations from X-ray diffraction based on peak heights can be used to determine the following indices:

i) α-phase orientation index A where

$$A = \frac{h\alpha_1}{h\alpha_1 + h\alpha_4} \qquad 3.7$$

it should be pointed out the value of A for any isotropic samples such as granules or powder is

equal to 0.57 (133).

ii) β-phase index B where,

$$B = \frac{h\beta}{h\alpha_1 + h\alpha_2 + h\alpha_3 + h\alpha_4} \qquad 3.8$$

iii) crystallinity index C where,

$$C = \frac{h\alpha_1 + h\alpha_2 + h\alpha_3 + h\alpha_4 + h\beta}{5ha} \qquad 3.9$$

where $h\alpha_1$, $h\alpha_2$, $h\alpha_3$, $h\alpha_4$, and $h\beta$ are the height of corresponding crystalline peaks, taken from the amorphous background, according to Turner-Jones (85, 86). ha is the maximum height of amorphous background. A typical X-ray diffraction of polypropylene is presented in Figure 3.4 (133).

Also it should be noted that C can not be directly related to crystalline fraction since this would require accurate separation of the background curve as has been reported by number of investigators (85,133), which requires corrections for incoherent radiation, thermal scattering, and polarisation.

In the case of high density polyethylene, the X-ray analysis was applied to analyse the relative degree of crystal orientation from skin to core layer by measuring their degree of intensity variations for both homo-polymer (solid) and foamed specimens. Also from the Bragg angle one can identify the plane spacing designated by Miller indices which can assist in

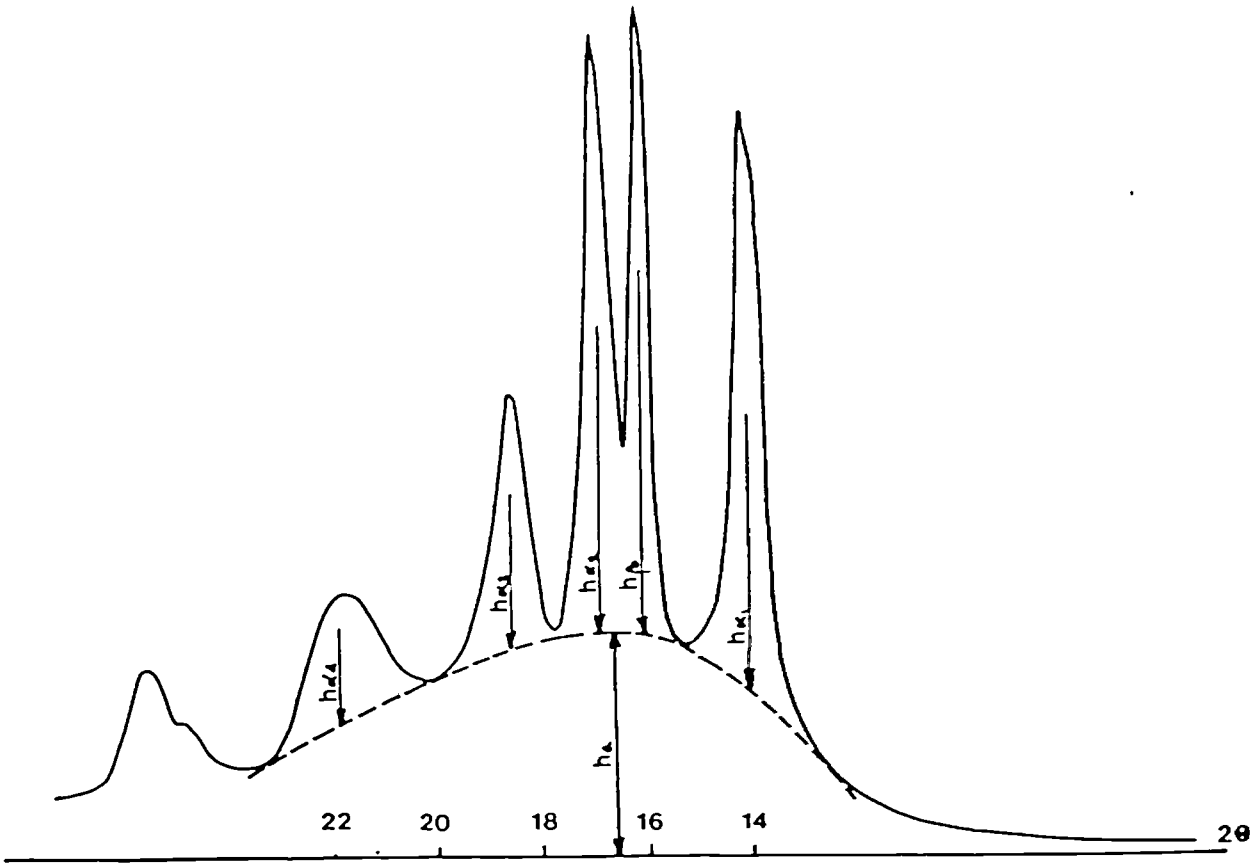

Figure 3.4. X-ray diffraction of polypropylene and a method of measurement of peak height (after 133).

identifying the form of crystalline structure. A typical X-ray diffraction analysis of semi-crystalline polyethylene is shown in Figure 3.5 (134).

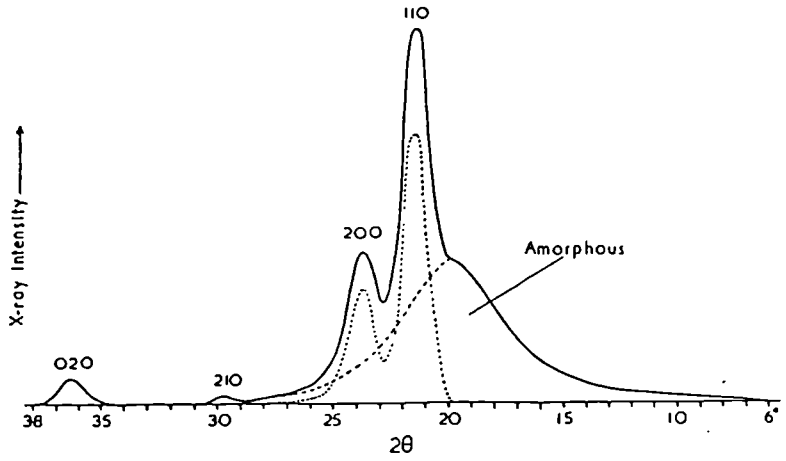

Figure 3.5. Intensity of X-ray diffraction in relation to angle of diffraction (after subtraction of background intensity). The curve is resolved graphically into a broad amorphous peak and sharp crystal peaks (after 134).

CHAPTER 4
REOLOGICAL PROPERTIES
OF
FOAMED AND UNFOAMED POLYOLEFIN

4. Rheological Properties of Foamed and Unfoamed Polyolefin

4.1. Introduction

A uniform dispersion of gas bubbles in a given amount of liquid in which the separation between bubbles is no more than the bubble diameter is termed a foam. Two extreme structural situations, depend on the gas to liquid volume ratio, are possible in a foam. The first type consists of spherical bubbles separated by rather thick liquid films. Such foams are term " wet " because of their low gas content. The second type contains mostly gas. Bubbles are polyhedral in shape separated from each other by very thin liquid films between the faces (Figure 4.1) these plane parallel films are called the lamella of the foam (135). Most common polymeric foams fall in the second category, and our study confined only to such systems.

Like most dispersed systems, foams are unstable in a thermodynamic sense. This is because the formation of gas bubbles results in a concomitant increase in surface energy, and the system tends to reduce the excess free energy by phase separation. Nevertheless, some foams can persist for a sufficiently long time to be put to useful purposes. Articles made of solid foams are examples of this. Here the liquid films undergo crosslinking reactions before the foam had

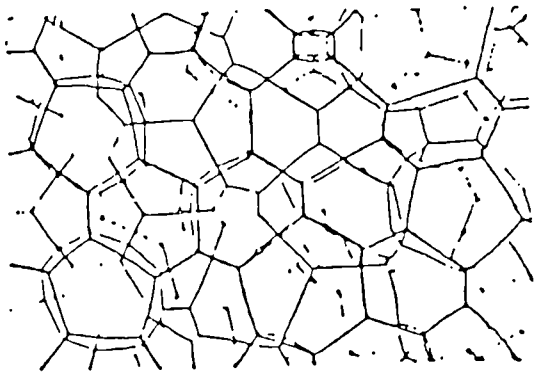

a

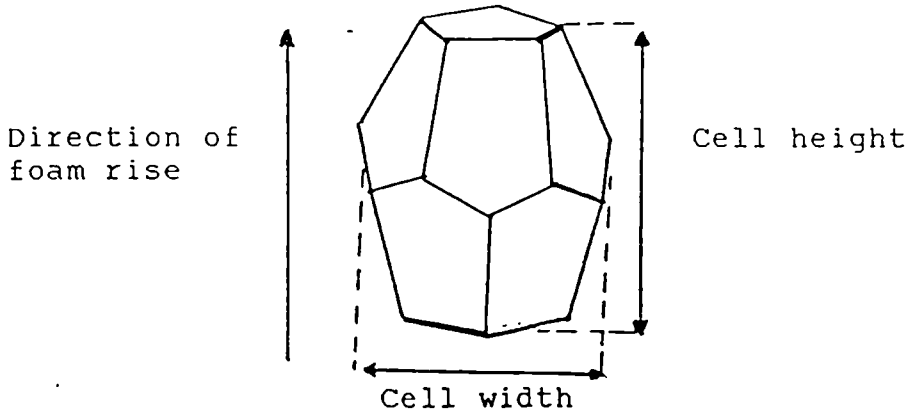

b

Figure 4.1. Schematic representation of a) real foam, b) a pentagonal dodecahedron cell (after 1).

time to collapse. Pure liquids do not foam. Generally, a surfactant, which can considerably lower the surface tension of the liquid to be foamed, has to be added in order to produce persistent ("metastable") foams. The formation of foam is followed by liquid drainage and cell collapse. Capillary pressure, present due to different radii of curvature at the gas-liquid interface because of polydispersity, and Van der waals attractive forces in the liquid films cause the lamella to become thinner with time. For the foam to be stable the liquid film must have some surface elasticity opposing this localised thinning. The most important source of this is the Gibbs Marangoni surface elastic effect (136). Here the change in liquid film area with drainage changes the equilibrium interfacial tension (Gibbs) as well as sets up a surface tension gradient (Marangoni), both of which provide a restoring force. In addition, surface viscosity and electric double layers resist drainage (137,138). A balance between all these forces determines the life time of a foam. Details of these, along with the kinetics of bubble collapse have been investigated by several researchers (139-141). This study, however, is restricted to the rheology of polyolefin foams only. Particular focus is given to the effect of gas concentration on the density and viscosity of foamed material during processing parameters.

4.2 Results and Discussion

4.2.1 The Effect of Molecular Weight and Molecular Distribution on Melt Viscosity of Polyolefin Homopolymers

Before attempting to present any of the rheological measurement of polyolefin foamed and homopolymer, it worth mentioning that the plunger type rheometer is not suitable for polymer-gas solution, since it cannot keep the gas generated from chemical blowing agent, dissolved into the polymer melt . Therefore the rheological properties presented in this chapter were carried out on the single screw extruder. To show the accuracy of rheological properties of polyolefin measured on a single screw extruder, rheological properties of polypropylene (GXM-43) at various melt temperatures were tested on both single screw extruder and Davenport rheometer.

Figures 4.2 and 4.3 exhibit relationship of true viscosity and true shear rate for polypropylene homopolymer (unfoamed) at different melt temperatures. it should be pointed out, by using two different dies, it has been possible to correct for the end effect, therefore, as has been stated by number of investigators (29-31) the shear rate and viscosity calculated by using Equation 2.16 and 2.17, are true shear rates and true viscosities. As it is noticed the

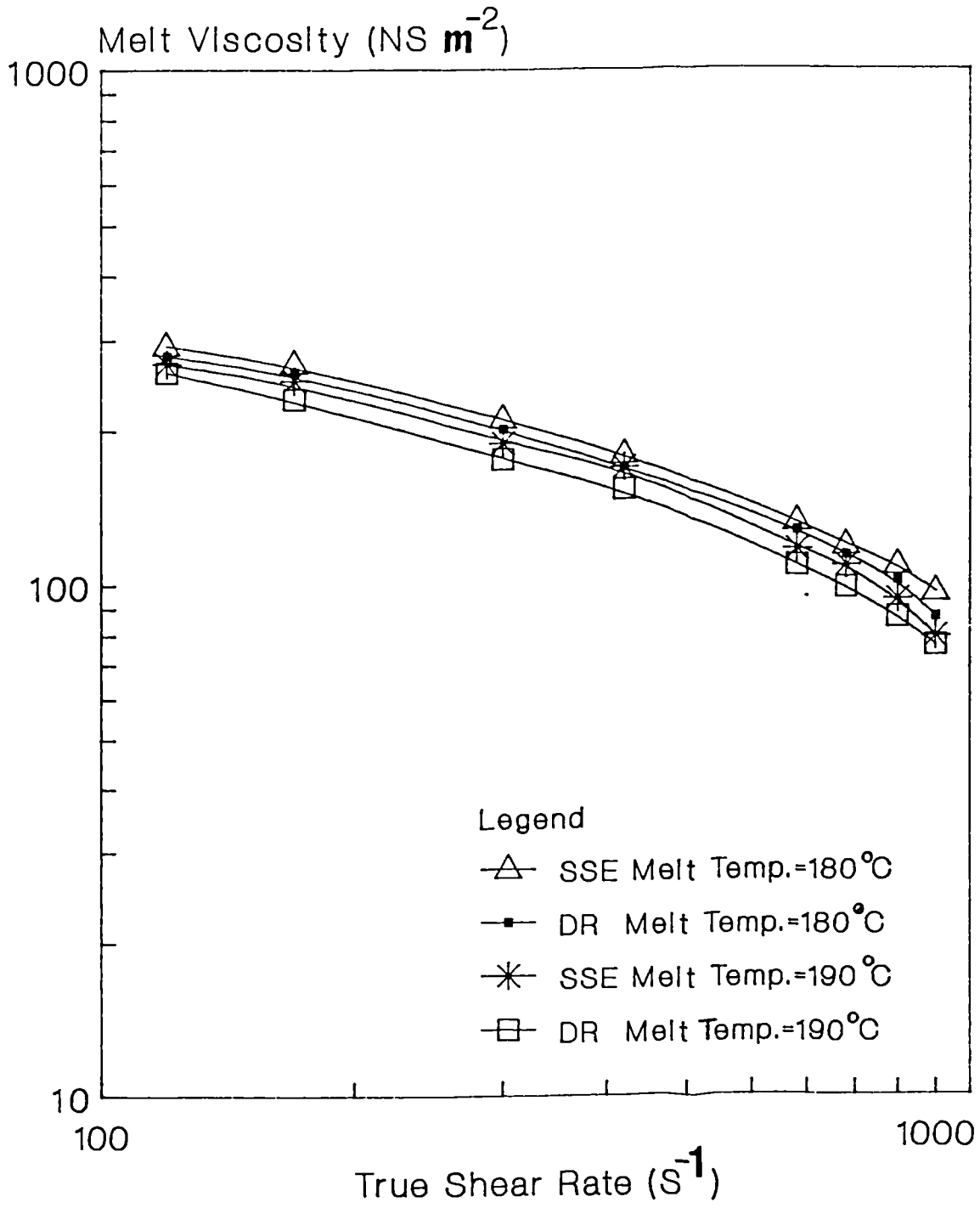

Figure 4.2. Relation of melt viscosity and true shear rate of PP (GXM-43) at various melt temperatures, measured on Single Screw Extruder (SSE) and Davenport Rheometer (DR).

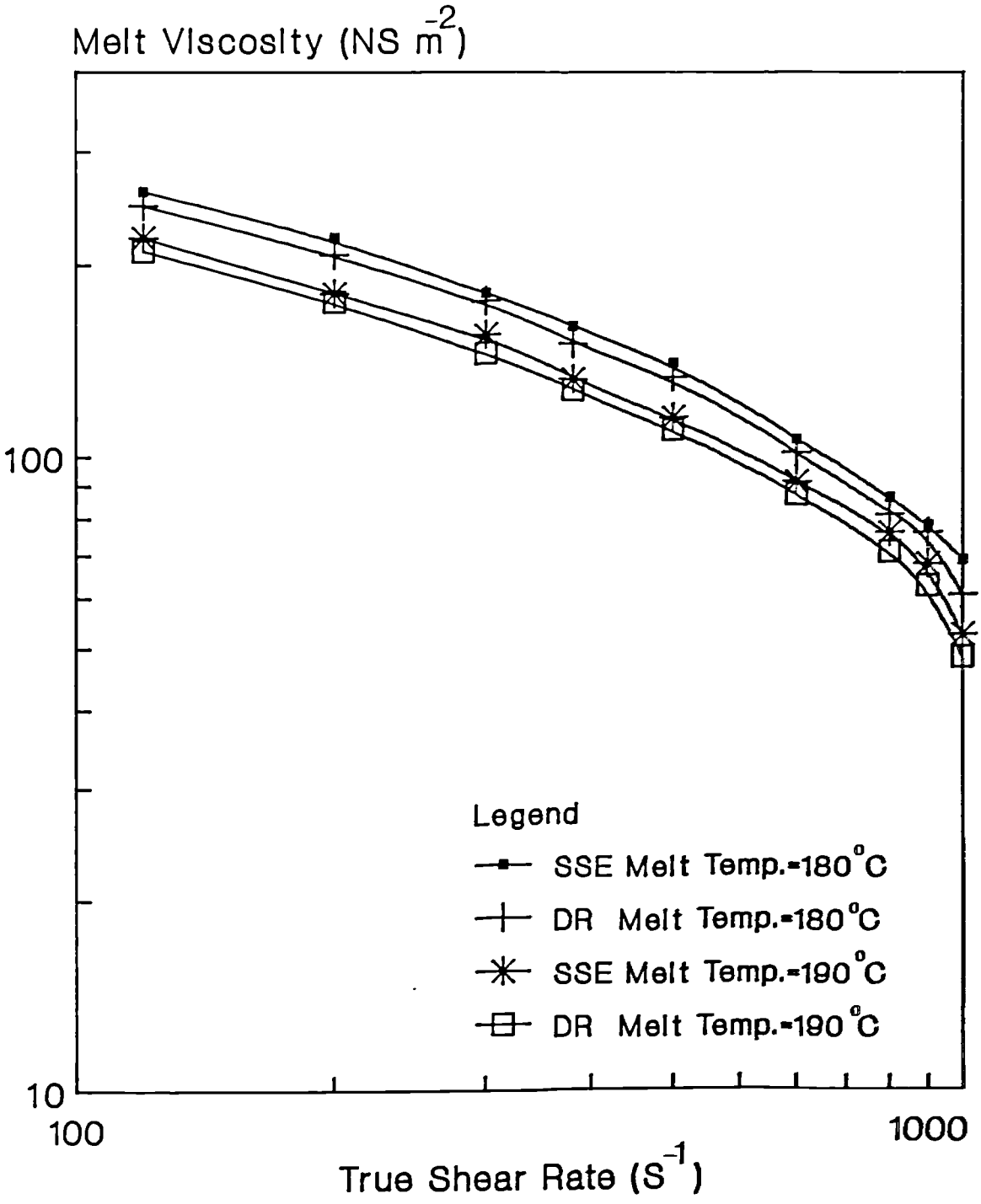

Figure 4.3. Relationship of melt viscosity and true shear rate of PP (GYM-45) measured at various melt temperatures measured on Single Screw Extruder (SSE) and Davenport Rheometer(DR).

results are in a good agreement and in most cases the difference is less than 5 percent.

Figures 4.4-4.7 show plots of shear stress shear rate relationships, for different grades of polyolefin in foamed and unfoamed stage. These materials follow a power law model of

$$\tau_w = K * t^n \qquad 4.1$$

where τ_w and t are wall shear stress and shear rate respectively. For the range of shear rates used, in which t is the true shear rate evaluated by use of the Rabinowitsch-equation. K is the material consistency, and n is the flow index. Table 4.1 presents the n values for these materials, indicating the relative degree of non-Newtonian flow behaviour. In the case of high density polyethylene the values of n decreases as the molecular distribution broadens. Similar results were reported by Guillet et al (142).

Figures 4.8-4.10 presents the relationship of true viscosity and true shear rate for high density polyethylene. The data presented here are shown up to the point of melt fracture. The effect of processing conditions on melt fracture will be consider later. Comparison of results presented in Table 4.1 and these figures suggest that the viscosity of the sample having a narrow molecular weight distribution is higher than that of samples with broad molecular weight distribution.

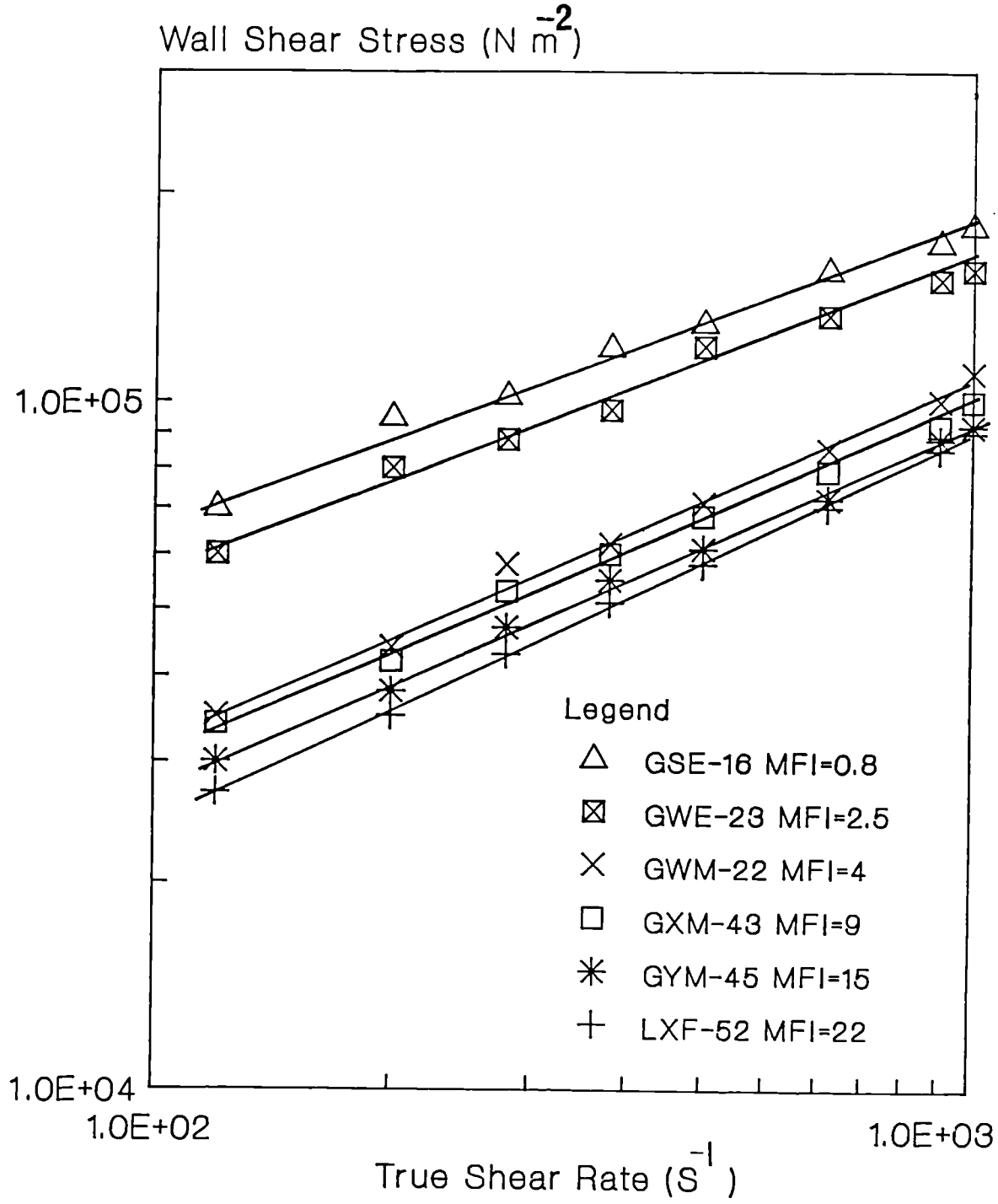

Figure 4.4. Relationship of wall shear stress and true shear rate for various grades of polypropylene. Melt temperature 180°C.

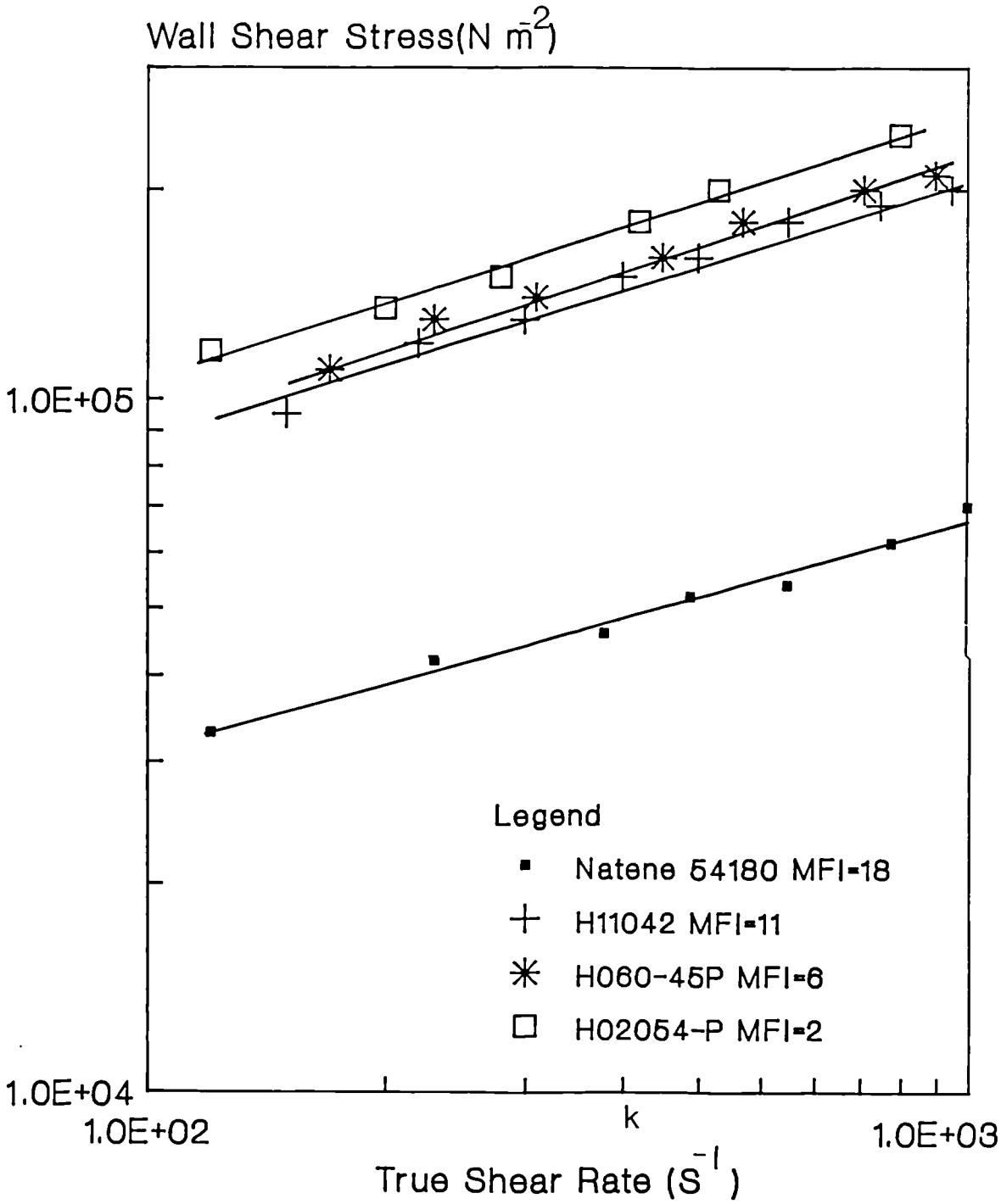

Figure 4.5. Relationship of wall shear stress and true shear rate for various grades of high density polyethylene. Melt temperature 245°C.

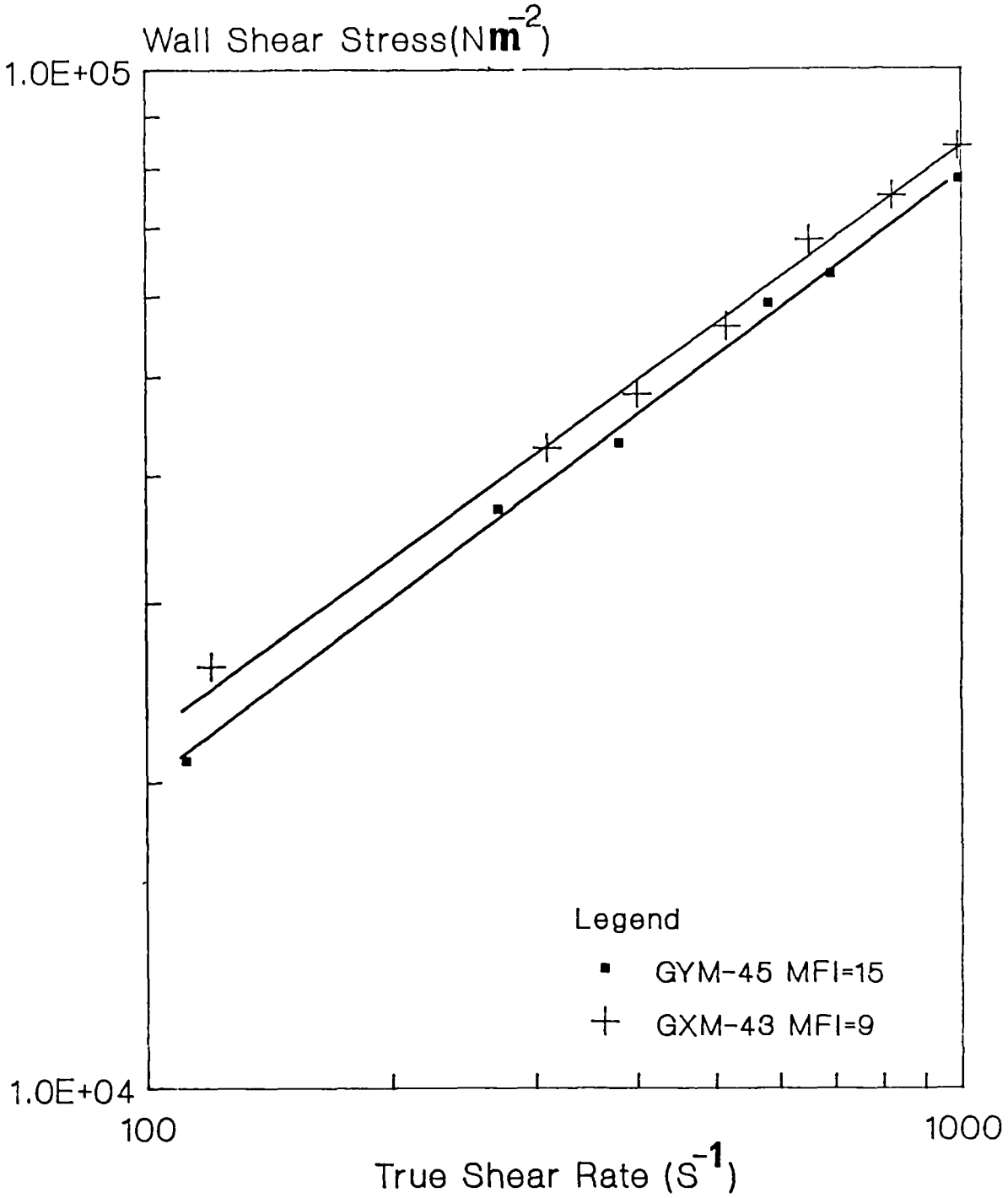

Figure 4.6. Relationship of wall shear stress and true shear rate for two grades of PP containing 5 wt.% chemical blowing agent (CBA). Melt temperature 180°C.

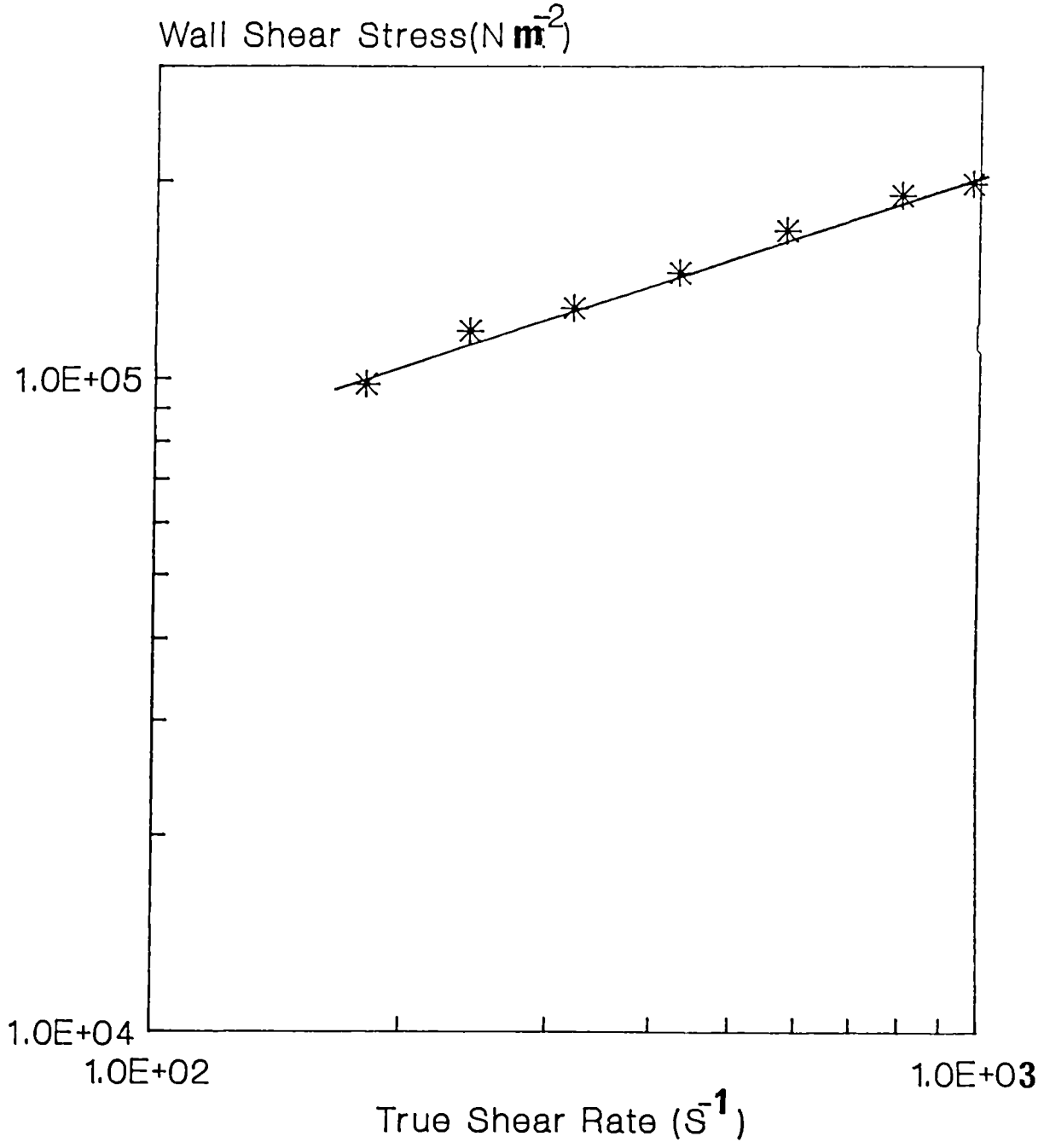

Figure 4.7. Relationship of wall shear stress and true shear rate of HDPE (H11042) containing 5 wt.% CBA. Melt temperature 245°C.

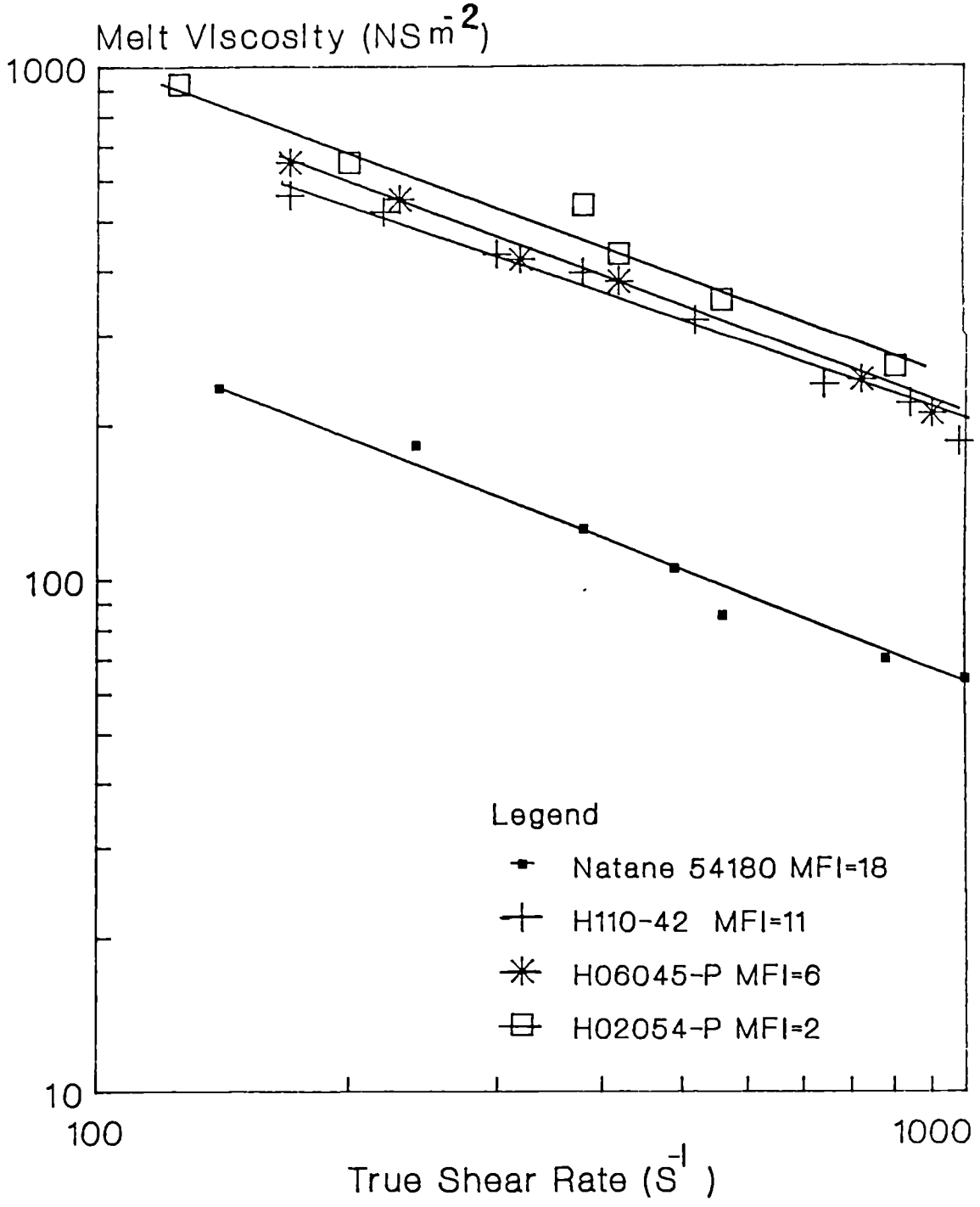

Figure 4.8. Relationship of melt viscosity and true shear rate for various grades of HDPE. Melt temperature 245°C.

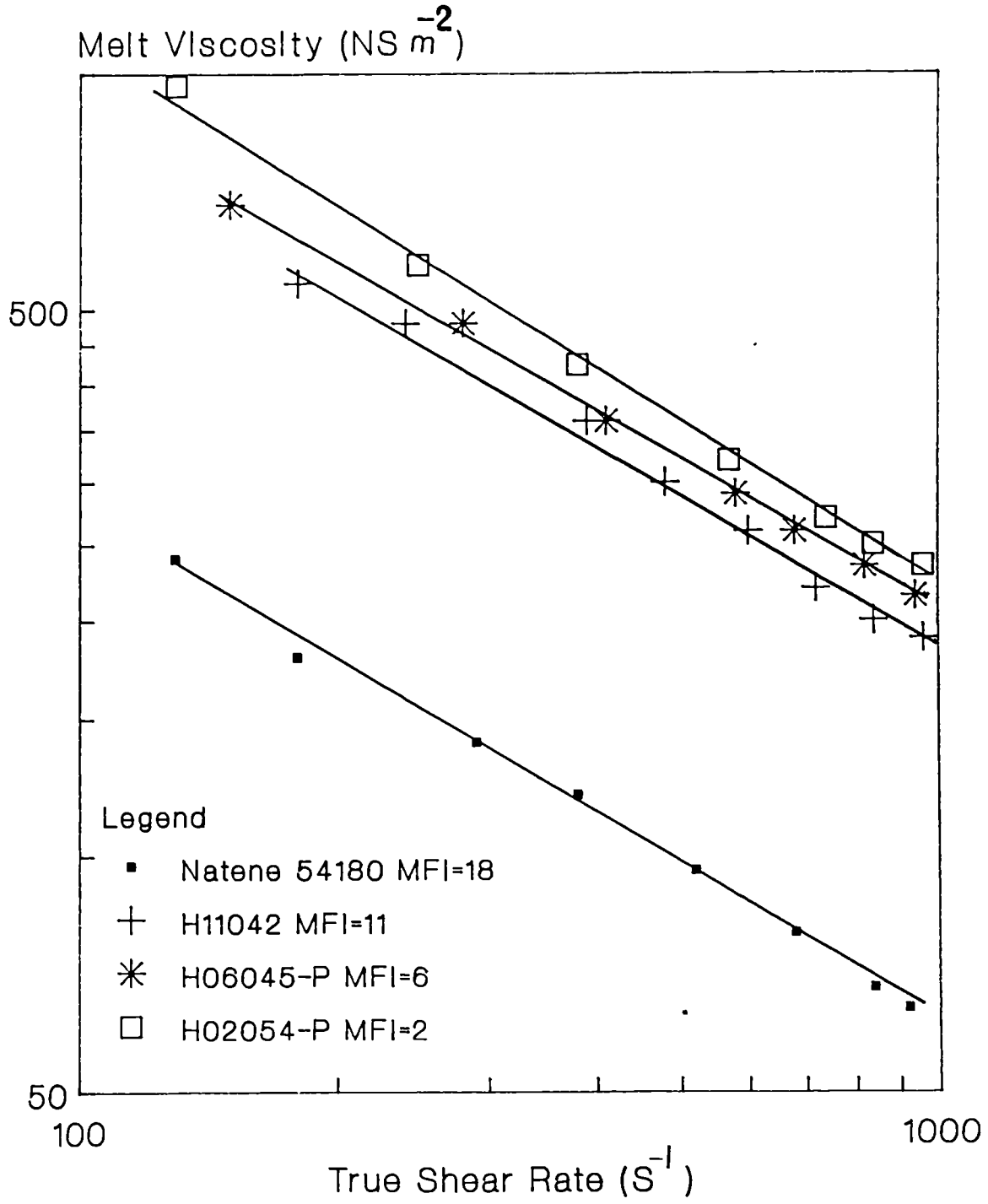

Figure 4.9. Relationship of melt viscosity and true shear rate for various grades of HDPE. Melt temperature 255°C.

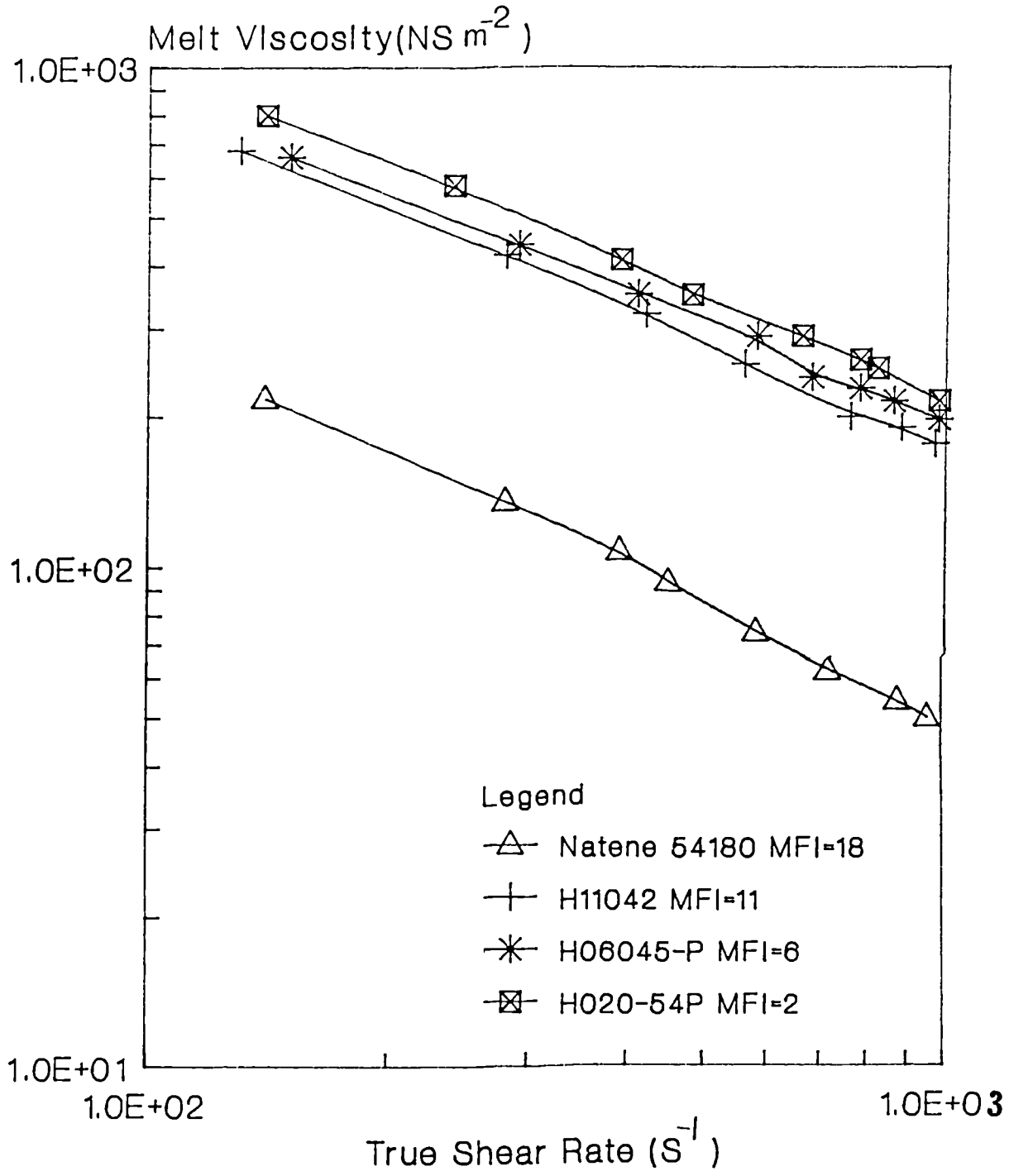

Figure 4.10. Relationship of melt viscosity and true shear rate for various grades of HDPE. Melt temperature 265°C.

this is attributed to the greater degree of chain entanglement and branching that occurs with a broad molecular weight distribution. The second interesting point which worth mentioning is, that the difference in melt viscosity of these samples at low shear rates is more pronounced than the difference at high shear rate. This is due to the fact that, the melt viscosity depends on the weight average molecular weight at low shear rate and on number average molecular weight at higher shear rate. Similar findings were reported by Ballman et al (143), where they study the melt viscosity of polydisperse polystyrene at different shear rates.

Table 4.1 presents the values of flow index n along with number average and weight average molecular weight and molecular weight distribution of polypropylene grades. It can be seen that the polydispersity is almost the same for all grades of polypropylene chosen for this study, but there is a large difference in their viscosity as it is presented in Figures 4.11-4.13. This can only be attributed to the difference in weight average molecular weight of these polymers. Cogswell (144) reported that a factor of two in molecular weight produces a tenfold change in viscosity, n at a given shear stress in the range of molecular weight, M, of interest for thermoplastics. He introduced following

Table 4.1a Molecular characteristics of polypropylene*

Polymer Grade	Weight Average Molecular Weight*10^{-5}	No. Average Molecular Weight*10^{-4}	Poly-dispersity	n Power Law Index	MFI g/10 min.
GSE-16	4.27	5.35	7.98	0.451	0.8
GWE-23	4.25	5.19	8.18	0.439	2
GWM-22	4.17	5.17	8.07	0.412	4
GXM-43	3.75	4.77	7.865	0.408	9
GYM-45	3.12	3.86	8.08	0.406	15
LXF-52	3.02	3.76	8.039	0.40	22

Table 4.1b Molecular characteristics of high density polyethylene**

Polymer grade	Wt.average molecular weight*10^{-5}	No.average molecular weight*10^{-4}	Polydis-persity	n power Law Index	MFI g/10 min.
HO20-54P	4.27	3.35	12.74	0.393	2
HO60-45p	3.00	2.12	14.19	0.385	6
H110-42	2.62	1.68	15.65	0.374	11
Natene 54180-AG	0.633	0.302	20.96	0.336	18

* All grades of PP were supplied by Imperial Chemical Industry (ICI) Co.

** All grades of HDPE were supplied by British Petroleum (BP) Co.

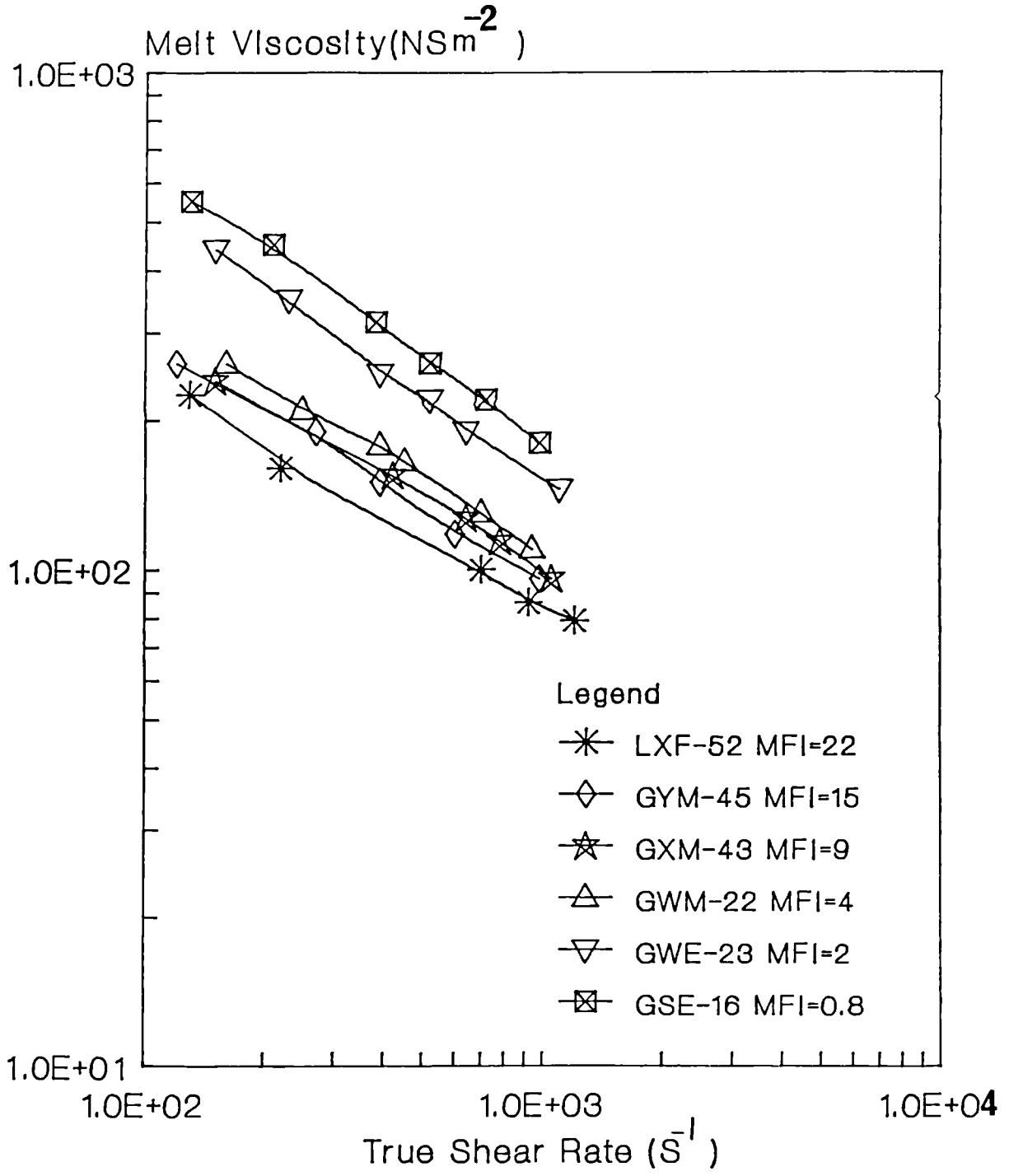

Figure 4.11. Relationship of melt viscosity and true shear rate for various grades of PP. Melt temperature 180°C.

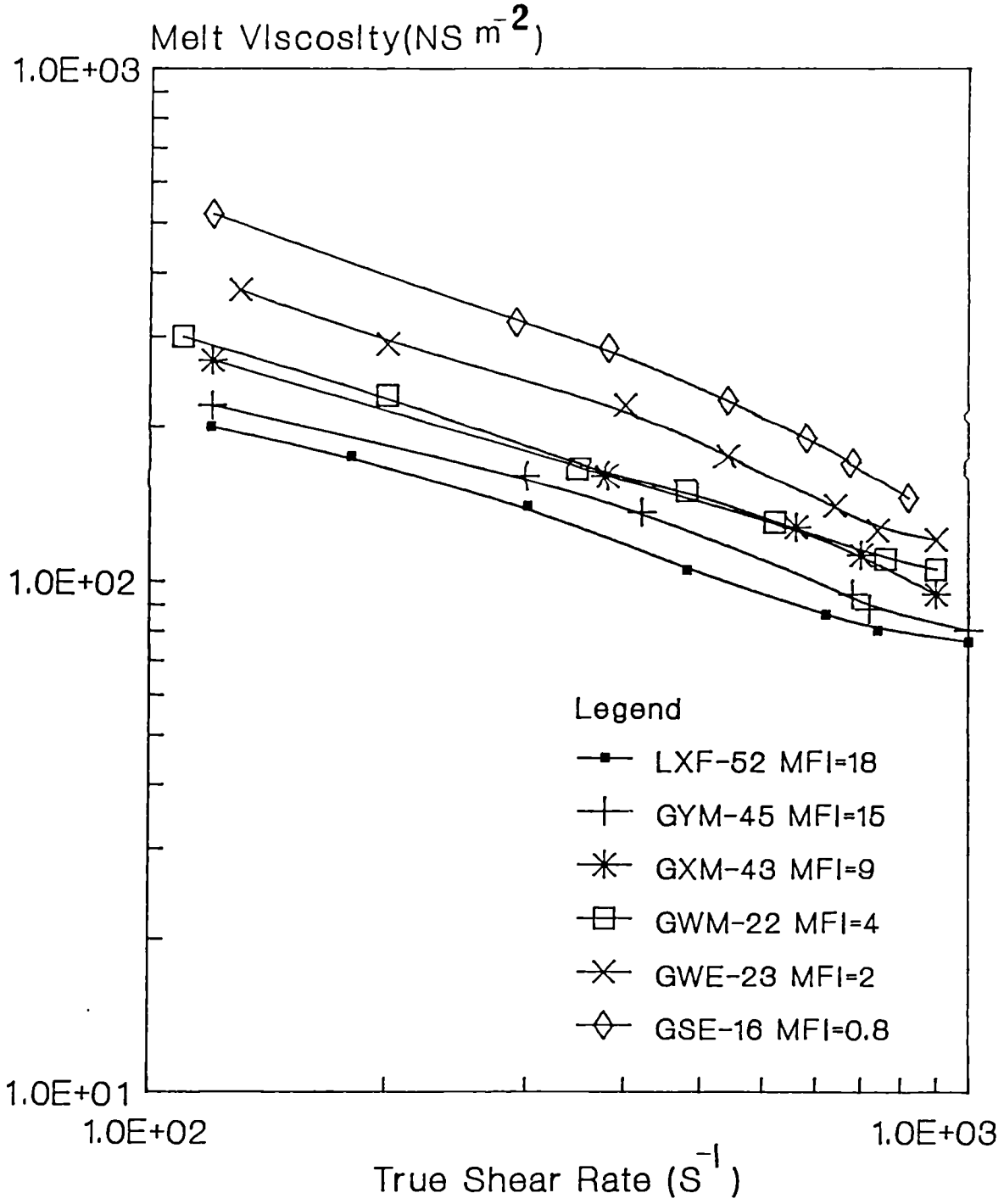

Figure 4.12. Relationship of melt viscosity and true shear rate for various grades of PP. Melt temperature 190°C.

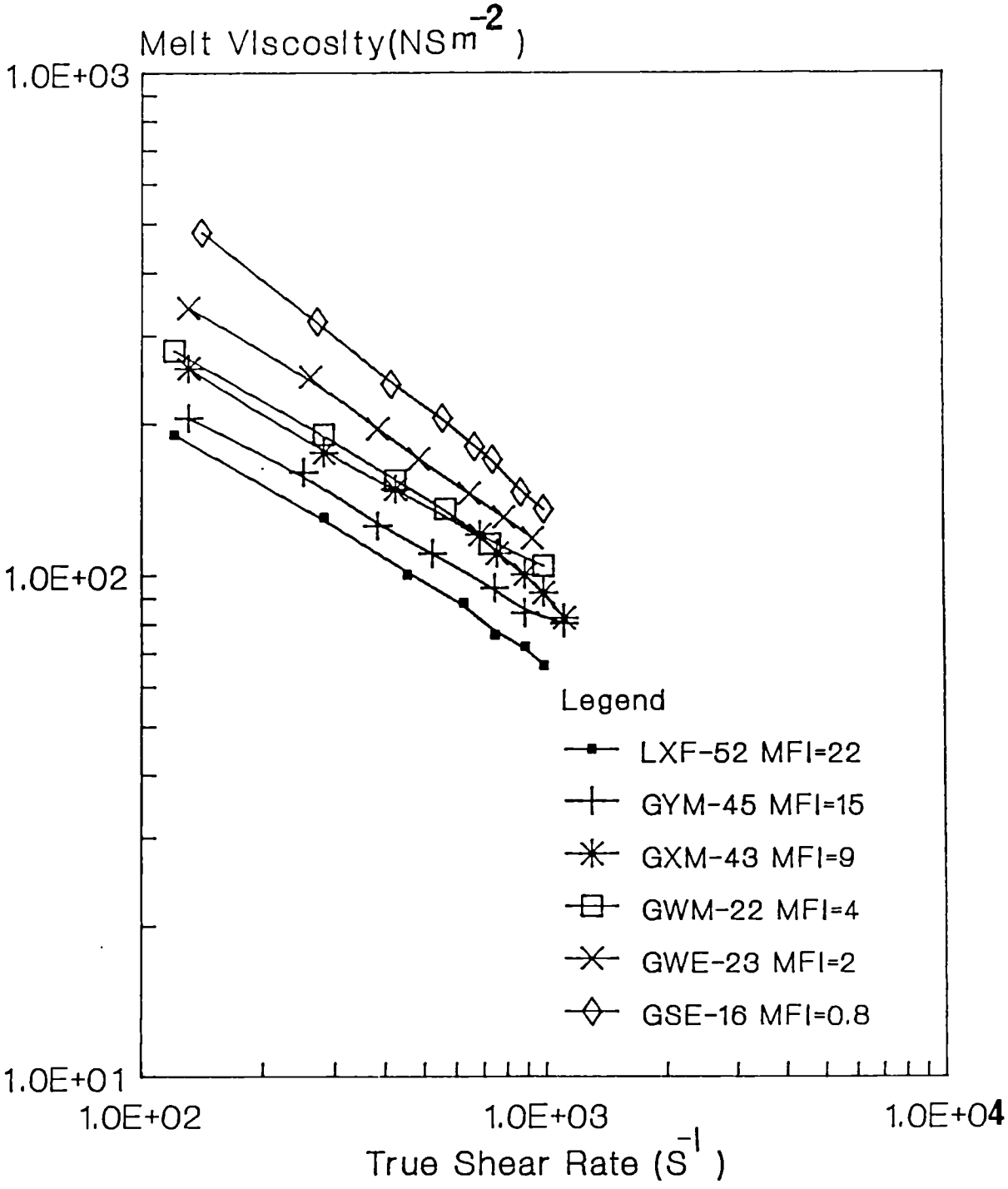

Figure 4.13. Relationship of melt viscosity and true shea rate for various grades of PP. Melt temperat 200°C.

relation between viscosity and molecular weight.

$$n = K * M^{3.5} \qquad 4.2$$

where K is the material consistency.

Figures 4.14-4.17 show the plot of wall shear stress of polyolefin against apparent shear rate, for a capillary L/D ratio of 1 and 20. It should be pointed out in order to show the effect of L/D, the data in these figures are uncorrected for the end effect. Below a critical shear stress shown by letter A in these figures, conventional viscoelastic flow was observed. Viscosity decreased with increasing shear rate, and a smooth extrudate was produced. However at and above the critical stress A, the emerging melt exhibited a surface roughness. The severity of surface roughness varied from one polymer to another and it depends on the molecular weight of the polymer. Tordella (145,146) suggest that the cause of the discontinuity is a fracture of the melt in die land due to possible slip-stick mechanism. Bartos (147) supports a slip-stick mechanism.

For all these materials the onset of melt fracture (indicated by arrow) is accompanied by a change in the slope of logarithmic flow curve or by a jump in the rate of output. Three interesting points can be deduced from these figures. Firstly at the same temperature, the melt fracture of the polymers with higher

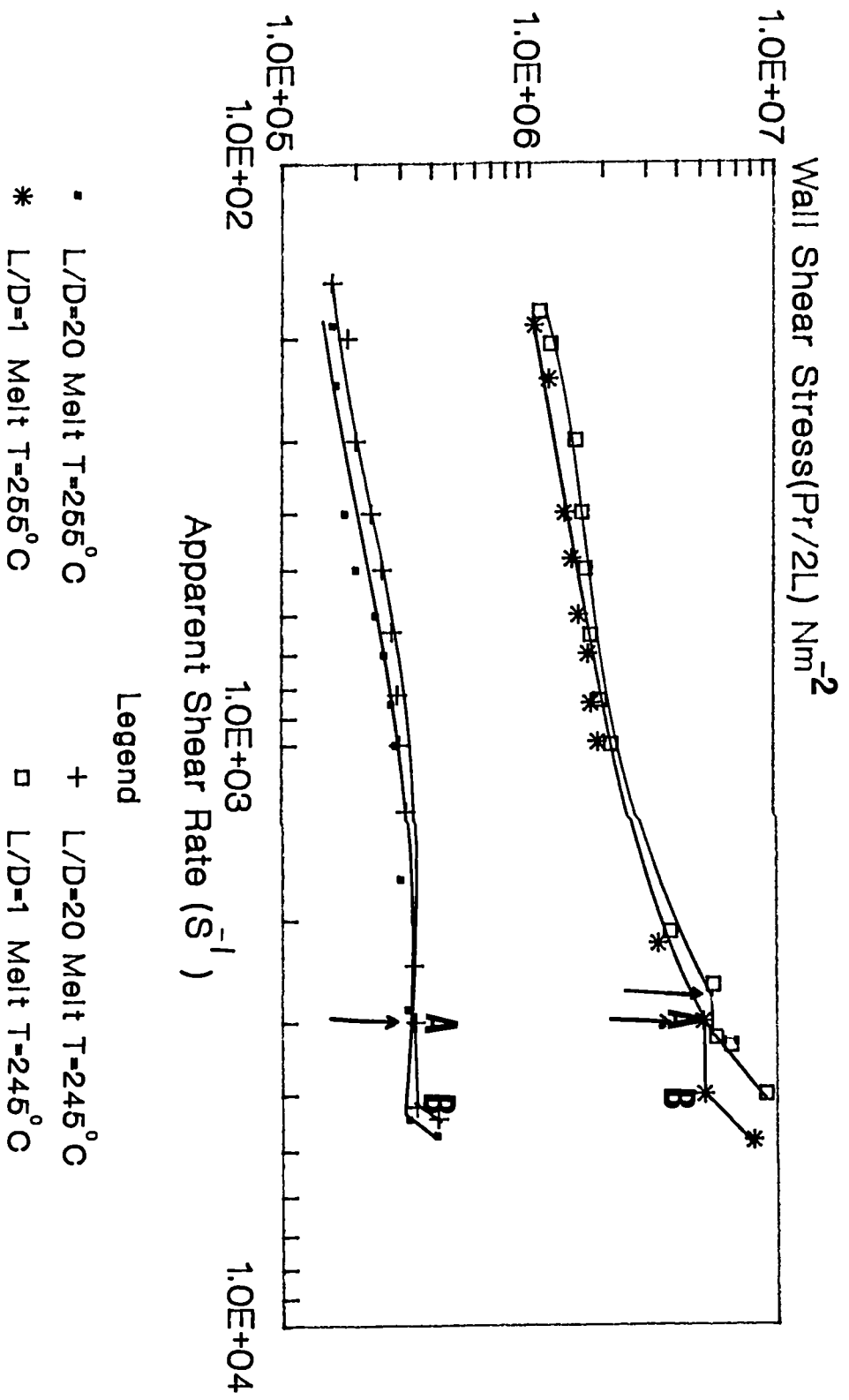

Figure 4.14. Schematic flow data for HDPE (H11042) at various melt temperatures and L/D ratios.

The arrow shows position of the melt fracture.

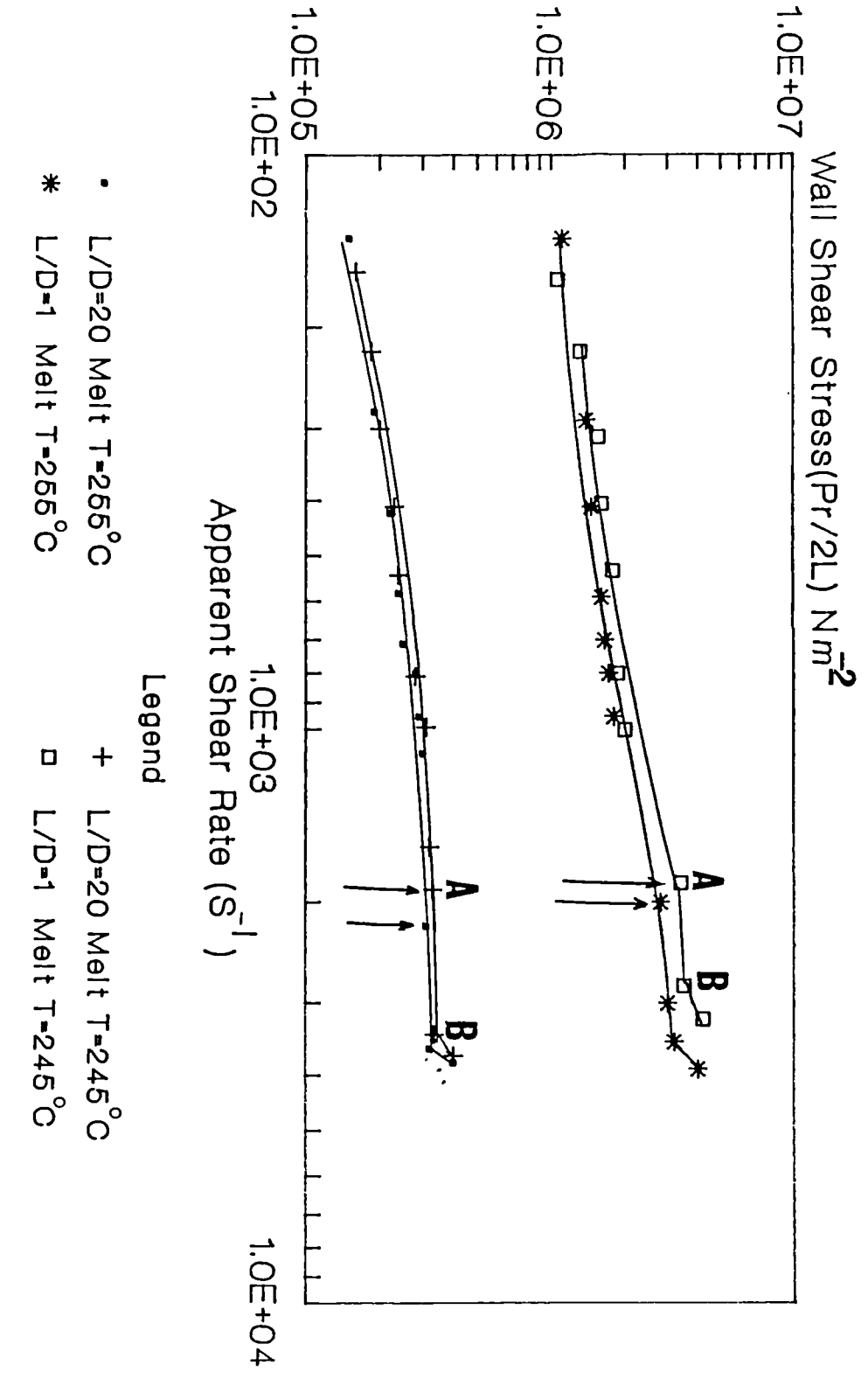

Figure 4.15. Schematic flow data for HDPE (H06045-P) at various melt temperatures and L/D ratios.

The arrow shows position of the melt fracture.

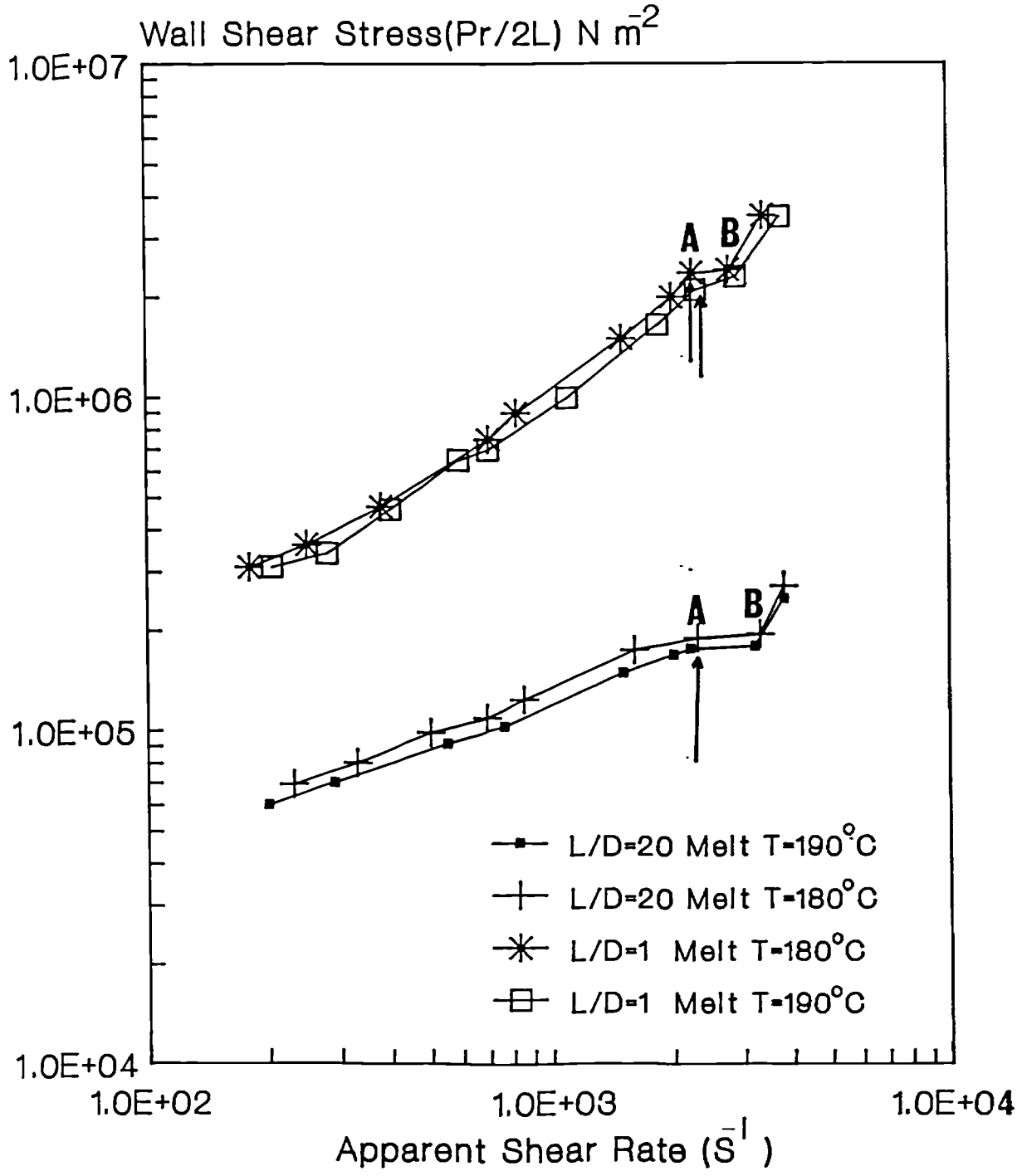

Figure 4.16. Schematic flow data for PP (GYM-45) at various melt temperatures and L/D ratios.

The arrow shows position of the melt fracture.

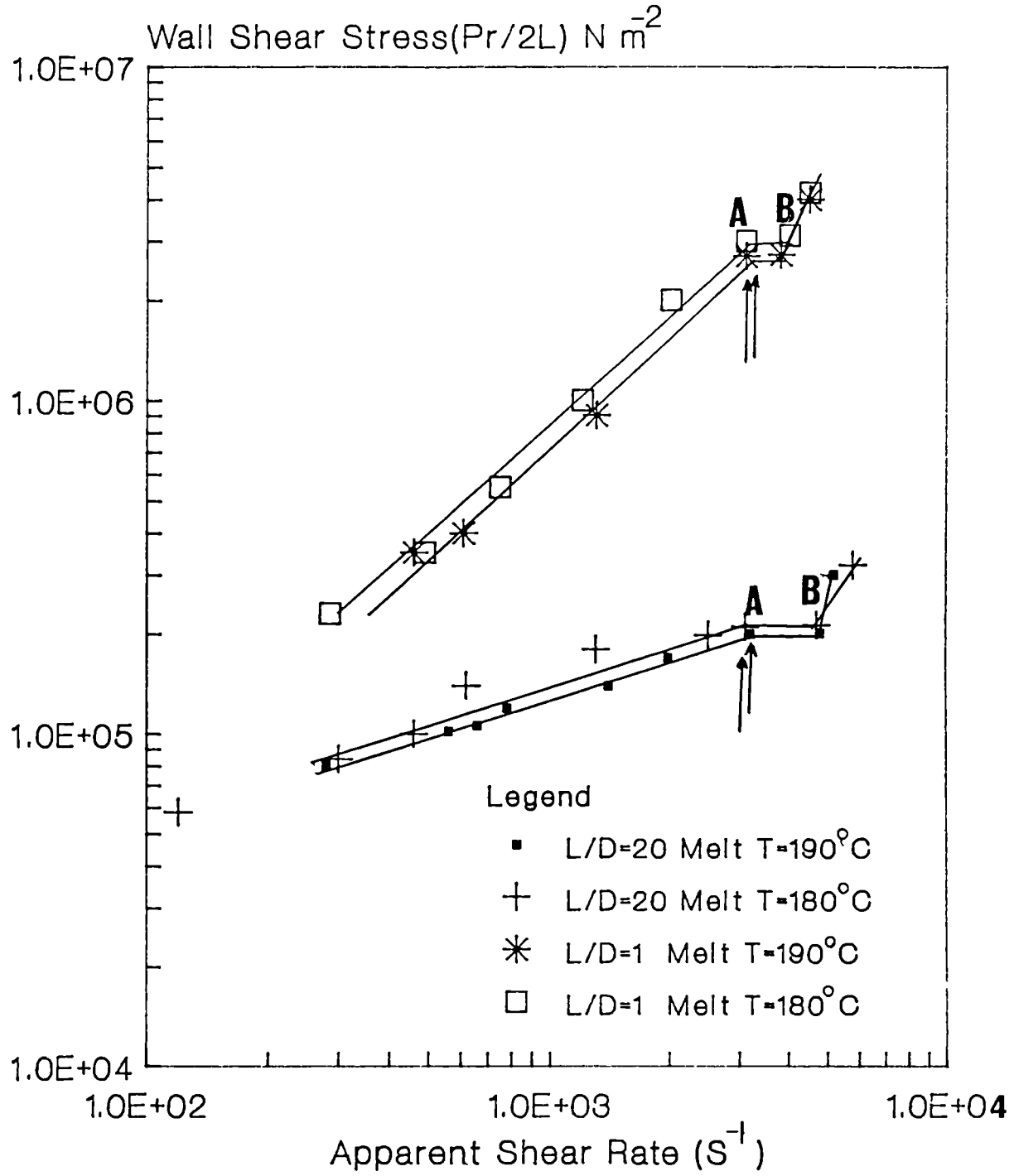

Figure 4.17. Schematic flow data for PP (GXM-43) at various melt temperatures and L/D ratios.

molecular weights occurs at lower shear rates. This phenomena is easily understood since longer chains are less flexible, therefore they are more susceptible to breakage than shorter chains. Den Otter (148,149) believes the discontinuity is a result of breakdown of the melt structure, this idea is also supported to some extent by Blyler et al. (150) and Pearson (151). In particular, the change in molecular weight dependence in the region of the discontinuity observed by Blyler et al.(150), seems to indicate a breakdown of the melt structure. Secondly it is evident that the capillary length has little or no influence at all on the position of occurrence of melt fracture. Thirdly the rate of increase in shear rate (almost at constant shear stress) tends to be more, for a higher L/D ratio, as denoted by letters of AB on the figures. An explanation for this type of behaviour could due to slippage at the capillary walls as proposed by Westover (152). Similar results are reported by Den Otter (35) and Tordella (146) where they have stated that the capillary length has no influence on the position of occurrence of the deformation due to melt fracture, but the L/D ratio of capillary has a pronounce effect on the melt fracture.

4.2.2 Effect of Temperature on Melt Viscosity of Polyolefin Homopolymers

Figures 4.8-4.13 exhibit plots of melt viscosity

against shear rate for high density polyethylene and polypropylene, at different melt temperatures. These figures demonstrate that the viscosity of these polymers are strongly influenced by melt temperature. This phenomenon is due to the fact that the free volume between the molecular chains increases with increasing the melt temperature, which as a consequence the molecules can rotate freely. At this juncture the Doolittle's equation can be introduced, which relates the melt viscosity to free volume. This equation is based on experimental data for monomeric liquids and gives (18).

$$n = a \, Exp \, (b * V/ Vf) \qquad 4.3$$

where a and b are constant and V and Vf are the total macroscopic volume and free volume respectively.

The flow behaviour of polyolefin homopolymers at diffe-different melt temperatures using different die lengths, can be studied from Figures 4.14-4.17. For the same reasons mentioned before the apparent shear rate and shear stress are reported here. The interesting points which worth mentioning are, as the melt temperature is increased the melt distortion due to melt fracture has reduced, and melt fracture occurs at higher shear rate. These figures also show that the die length has no influence on the position of occurrence of melt fracture and project the significance of knowledge of rheological properties for choosing the optimum conditions

for processing of polyolefin polymers.

4.2.3 Effect of Gas Blowing Agent on Rheological Properties of Polyolefin

4.2.3.1 Effect of Pressure and Temperature on Density of Molten Polymer Containing Gas

Melt pressure is one of the most important processing variables influencing the characteristics of polymers during foam extrusion. Several authors have shown, that gas bubbles, in form of microvoids are formed in the die, due to the pressure drop in this region, which tend to grow as they approach the die exit (22-25, 51-53). Studies of foam extrusion by Han et al shows, under low pressure (in die) considerable growth of gas bubbles have occur resulting in poor extrudate surface quality (22,25).

Tables 4.2-4.9 show the variation of density with pressure and apparent shear rate. At low shear rates (low throughput and pressure) the residence time is longer, therefore the microvoids have better chance to grow inside the die. This phenomena has resulted in lowering the density and apparently lowering the viscosity of molten polymer inside the die. Also the result presented in Tables 4.2-4.9 show the reduction of density of molten polymer in the die, is greater as the concentration of blowing agent is increased. This suggests, that with increase of blowing agent there

Table 4.2 Variation of density with shear rate for high density polyethylene(H11-042) containing 5 wt. % hydrocel CF-20 blowing gent at melt temperature 255°C. Die dimension L/D=1, D=2mm.

Shear rate (S^{-1})	Pressure M Pa	Melt density Kg m^{-3}
261	7.24	729
321	7.58	738
481	9.24	741
517	9.41	742
563	9.99	746

Table 4.3 Variation of density with shear rate for high density polyethylene (H11-042) containing 10 wt. % (hydrocerol CF-20) blowing agent at melt temperature of 255°C. Die dimension L/D=1, D=1mm.

Shear rate (S^{-1}	Pressure M Pa	Melt density Kg m^{-3}
235	6.83	725
343	7.45	735
474	9.00	739
529	9.31	741
620	9.65	752

Table 4.4 Variation of density with shear rate for high density polyethylene (H11-042) containing 5 wt.% blowing agent (hydrocerol CF-20). Die dimension (L/D=1 , D=2mm), melting temperature 265°C.

Shear rate (S^{-1})	Pressure MPa	Melt density Kg m^{-3}
250	6.860	721
340	7.033	726
424	8.515	736
520	9.239	739
600	9.515	743

Table 4.5 Variation of density with shear rate for high density polyethylene (H11-042) containing 5 Wt.% hydrocerol CF-20 blowing agent. Die dimension (L/D=1 , D=2mm), melt temperature 275°C.

Shear rate (S^{-1})	Pressure MPa	Melt density Kg m^{-3}
225	6.239	716
331	6.584	719
485	8.205	733
580	8.894	735
622	9.032	737

Table 4.6 Variation of density with shear rate for polypropylene (GXM-43) containing 5 wt. % blowing agent (hydrocerol CF-20) at melt temperature of 190°C. Die dimension, L/D=1 , D=2mm.

Shear rate (S^{-1})	Pressure KPa	Density Kg m^{-3}
220	344.7	259
378	551.6	313
635	965.3	342
847	1068.7	351
1153	1654.7	428
1278	1861.6	472

Table 4.7 Variation of density with shear rate for polypropylene (GXM-43) containing 10 wt. % blowing agent(Hydrocerol CF-20) at melt temperature of 190°C. Die Dimension, L/D=1 , D=2mm.

Shear rate (S^{-1})	Pressure KPa	Density Kg m^{-3}
120	206.8	173
343	275.8	182
563	413.7	194
644	551.6	207
732	620.5	226
1196	1447.9	390
1228	1551.3	404

Table 4.8 Variation of density with shear rate for polypropylene (GXM-43) containing 5 wt.% hydrocerol CF-20 blowing agent at melt temperature of 180°C. Die dimension, (L/D=1 , D=2mm).

Shear rate (S^{-1})	Pressure MPa	Density Kg m^{-3}
173	0.414	265
204	0.483	292
350	0.586	317
404	0.689	328
595	1.034	358
895	1.448	398

Table 4.9 Variation of density with shear rate for polypropylene (GXM-43) containing 5 wt.% hydrocerol CF-20 blowing agent at melt temperature of 200 °C. Die dimension, (L/D=1 , D=2mm).

Shear rate (S^{-1})	Pressure MPa	Density Kg m^{3}
200	0.207	179
350	0.517	302
510	0.931	339
718	1.172	341
900	1.517	391

will be more sites available for nucleation bubbles. These results are similar to the findings of Han et al. (25), where he has stated, as the molten polymer reaches the die exit and the pressure is reduced, the gas which present in excess of the solubility limit, comes off from the homogeneous melt, forming microbubbles. Hence, these microbubbles will grow as the pressure is reduced further, as more gas diffuses into them.

Another criterion which is important in processing of polymer foam is the melt temperature. Tables 4.2-4.9 show the effect of temperature on the density of polymer containing gas at various shear rate. As was mentioned before an increase in melt temperature will result in an increase in free volume, thereby, the material will flow easier and the melt pressure will decrease. This will cause phase separation and formation of gas bubbles inside the die.

4.2.3.2 The Effect of Blowing Agent on Melt Viscosity of Polyolefin Resins

Figures 4.18-4.21 exhibit plots of relationship of melt viscosity and true shear rate for various grades of polyolefin resins containing five and ten weight percent Hydrocerol CF-20 blowing agent. These data are compared with viscosity of their un-foamed state, at various temperatures. The viscosity of these grades of

polymers presented in these figures are shown up to the point of melt fracture. The effect of blowing agent on the position of melt fracture will be discussed later in this section.

As it is noticed from Figures 4.18-4.21, that the viscosity of foamed polymer has reduced with addition of blowing agent, this can be interpreted as the result of solubility (or plasticizing) the polyethylene or polypropylene molecules under the imposed extrusion conditions. This interpretation of course, assumes that the blowing agent is dissolved and distributed uniformly in the molten polymer. The extent to which a blowing agent reduces the viscosity of a molten polymer depends upon the processing conditions, which in turn determines the solubility. For instance with addition of 5 weight percent hydrocerol blowing agent at melt temperature of 180°C and shear rate of 130 S^{-1} the reduction of viscosity of polypropylene (GXM-43) foam as compare with its homopolymer is as much as 38%, but at shear rate of 1100 S^{-1}this difference is as little as 16%. One should notice that the apparent reduction in viscosity decreases with increasing shear rate and it reaches a point where this difference will stay constant. This critical point varies with temperature and gas volume fraction. Therefore, one might conclude that at high shear rates (high pressure)

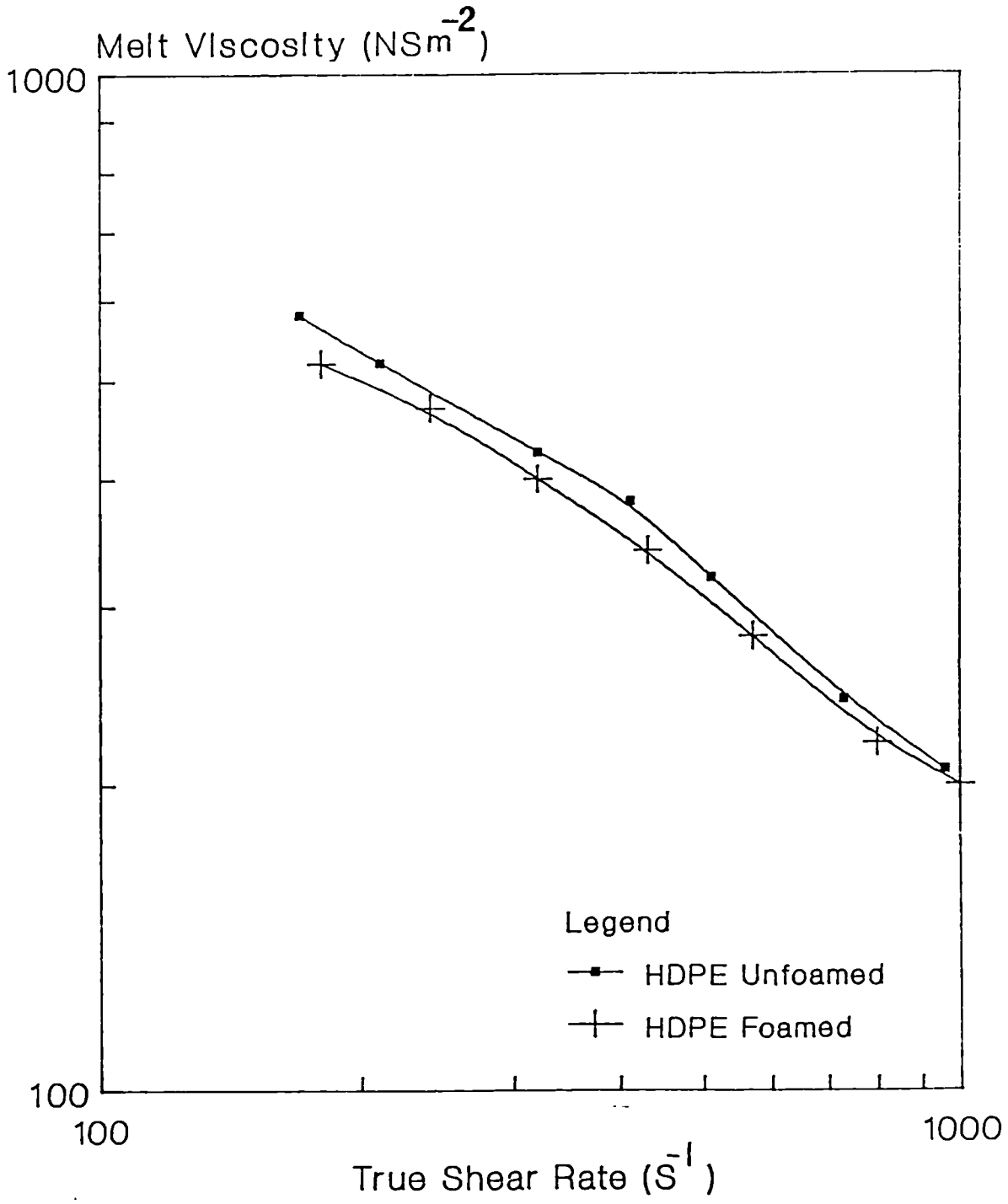

Figure 4.18. Relationship of melt viscosity and true shear rate of HDPE (H11042) in foamed (5 wt.% CBA) and unfoamed states. Melt temperature 245°C.

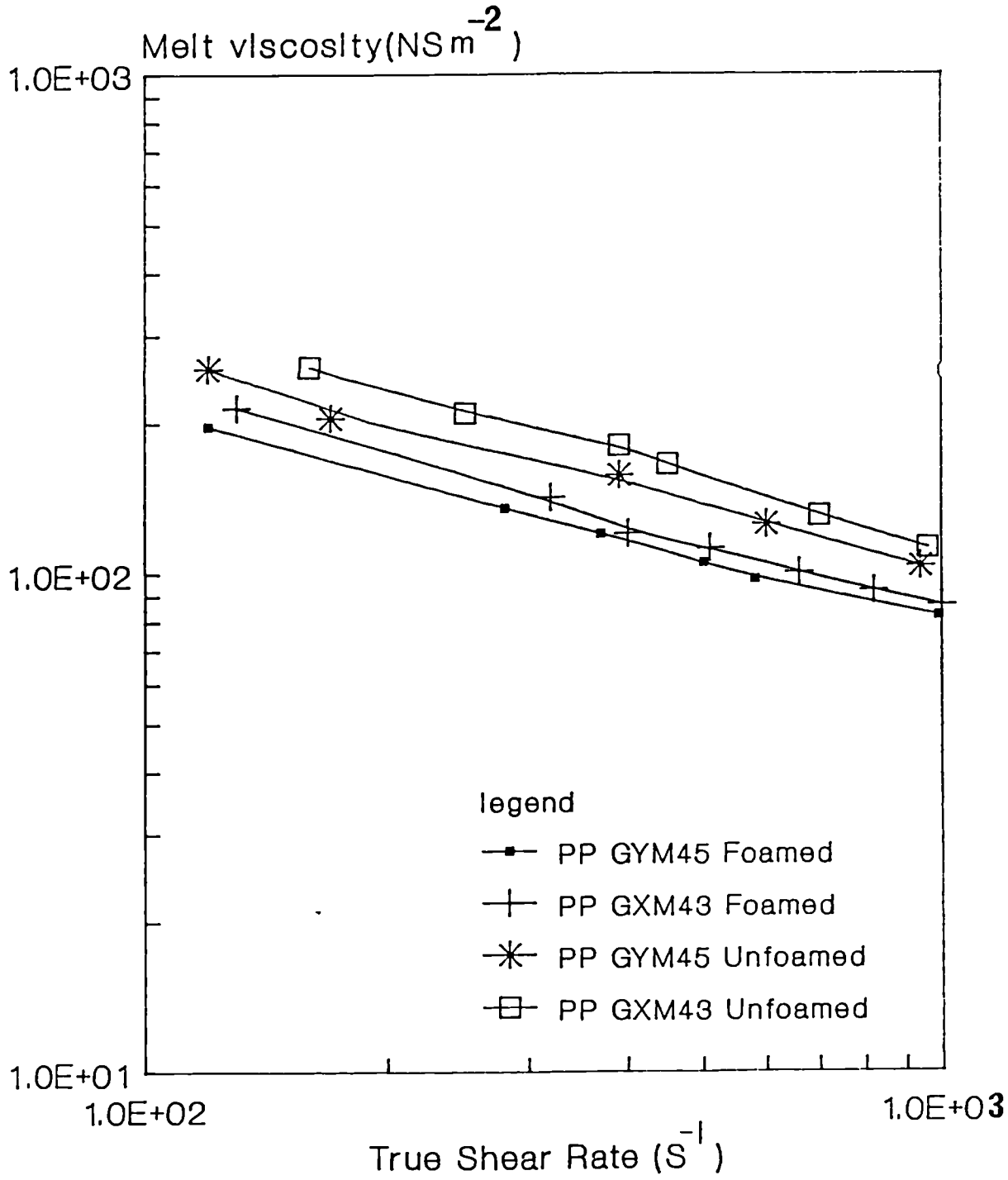

Figure 4.19. Relationship of melt viscosity and true shear rate of various grades of PP in foamed (containing 5 wt.% CBA) and unfoamed states. Melt temperature 180°C.

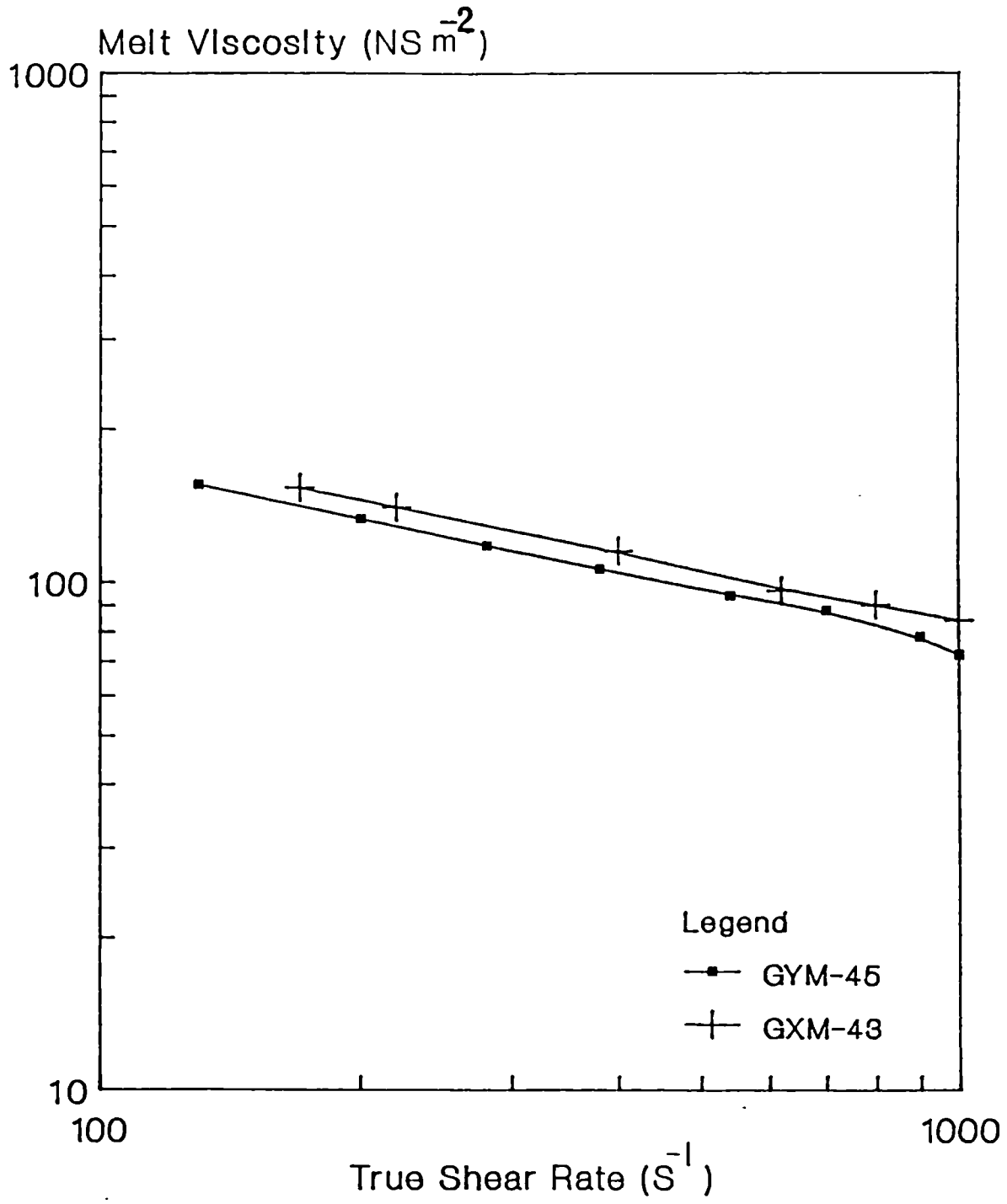

Figure 4.20. Relationship of melt viscosity and true shear rate of various grades of PP containing 5 wt.% CBA. Melt temperature 190°C.

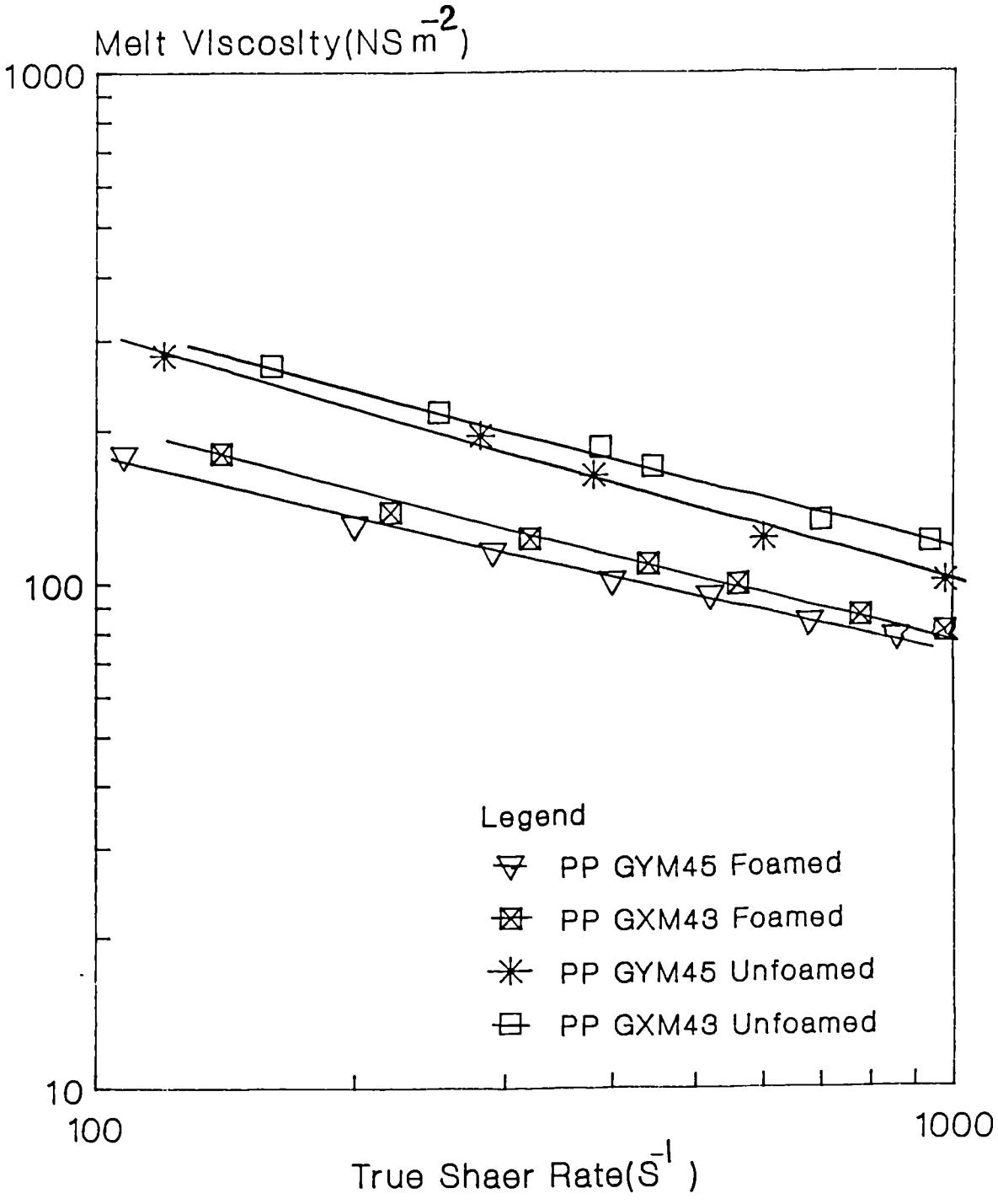

Figure 4.21. Relationship of melt viscosity and true shear rate of various grades of PP in foamed (containing 10 wt.% CBA) and unfoamed states. Melt temperature 180°C.

the gas bubbles are suppressed and dissolved in molten polymer and form a single phase system, whereas, at low shear rate the gas generated from blowing agent tends to form a separate phase and form microvoids in the die. Throne (28) has studied the effect of gas blowing agent concentration on injection moulding of thermo-plastics foam. He has shown with increasing the pressure on the melt in accumulator region, the solubility of gas in the melt has increased, hence, the reduction in melt viscosity decreased. Nikolaeva et al.(153) have also shown, with increasing the extrusion pressure on processing of low density polyethylene, the reduction in melt viscosity has also decreased. At the same time they have shown with increasing the blowing agent concentration the melt viscosity of low density polyethylene has decreased.

The influence of the blowing agent concentration on melt viscosity may be explained from the standpoint of the theory of free volume as is shown below.

For the purpose of comparing the viscosity of homopolymer with polymer containing gas, the Doolittle's equation can be employed which shows the viscosity of polymer melt ( ) as

$$= B * \mathrm{Exp} (B^{*} * V^{*} / Vf) \qquad 4.4$$

where V^{*} is the occupied volume, Vf is free volume and B^{*} and B are constants. A similar equation may be written

for the viscosity of polymer containing gas (n'), so that

$$n'/n = \mathrm{Exp}\left((B^* * V^* / VF) - (B^* * V^* / Vf')\right) \quad 4.5$$

in Equation 4.5 it is assumed that the occupied volume V^*, and constant B and B^* are not significantly altered by the addition of gas to the polymer.

The free volume of polymer-gas solution can be given from additivity law for free volume as,

$$Vf = \frac{(Xp\ Vp\ Mp + Xg\ Vg\ Mg)}{(Xp\ Mg + Xg\ Mg)} \quad 4.6$$

where X and M are volume fraction and molecular weight respectively. Here p and g denote for the polymer and gas respectively. Assuming the gas obeys Boyle's and Charles' law, Vg may be calculated at temperature and pressure of the experiment. Therefore one clearly sees that, the viscosity of polymer-gas system is function of operating conditions such as pressure and temperature and also the gas volume fraction.

The viscosity reduction factor (VRF) was used by Han et al (25) to find the effect of gas volume fraction on viscosity polymer melt.

$$VRF = \frac{\text{viscosity of molten polymer and blowing agent}}{\text{viscosity of molten homopolymer}}$$

Using the above formula, VRF has been calculated at various shear rates, for various combination of polyolefin grades and blowing agent concentrations.

Tables 4.10-4.12 show summary of these results. The following conclusions can be drawn from these Tables. Firstly at a given blowing agent concentration, the value of VRF at low processing pressures, depends on shear rate and at high pressure (approximately greater than 5.5 MPa) is independent of shear rate. Secondly the value of VRF decreases with increasing gas volume fraction. In addition the values of VRF are smaller for polypropylene than high density polyethylene. This is probably due to the fact that the melt viscosity and processing pressure of high density polyethylene is far greater than polypropylene resins, and also it is likely that, the gas (e.g. CO_2), is more soluble in high density polyethylene than it is in polypropylene.

4.2.3.3. The Effect of Temperature and L/D Ratio on Apparent Viscosity of Polyolefin-Gas Solutions

As long as the blowing agent remains dissolved in a molten polymer over the range of temperature studied, an increase in temperature will lower the melt viscosity of the polymer-gas solution, as may be seen in Figures 4.18-4.21. Even though the solubility of blowing agent increases (a lower amount of gas will be available to form microbubbles) with increasing melt temperature, it turns out for the situation under consideration the extent of pressure decrease due to increase of temperature is far greater than the extent of pressure expected from the increase in flow rate.

Table 4.10 Viscosity reduction factor (VRF) for polypropylene (GXM-43) foam at various melt temperatures and chemical blowing (CBA) concentrations.

Melt temperature 180°C Shear rate (S^{-1})	VRF CBA Concentration	
	5%	10%
130	0.62	0.59
320	0.68	0.63
400	0.70	0.65
510	0.75	0.66
680	0.76	0.67
1100	0.84	0.72
Melt temperature 190°C Shear rate (S^{-1})		
170	0.57	0.54
220	0.59	0.57
400	0.62	0.61
620	0.65	0.62
800	0.78	0.74
1000	0.81	0.78

Table 4.11 Viscosity reduction factor (VRF) for polypropylene (GYM-45) foam at various melt temperatures and chemical blowing agent (CBA) concentrations.

Melt temperature 180°C	VRF	
	CBA concentration	
Shear rate (S^{-1})	5%	10%
120	0.66	0.62
280	0.68	0.64
370	0.71	0.66
500	0.74	0.69
580	0.75	0.69
980	0.82	0.73
Melt temperature 190°C		
Shear rate (S^{-1})		
130	0.68	0.53
200	0.70	0.58
290	0.73	0.645
380	0.77	0.71
540	0.79	0.72
700	0.81	0.74
900	0.84	0.765
1050	0.84	0.77

Table 4.12 Viscosity reduction factor for high density polyethylene (H110-42) foam at various chemical blowing blowing agent concentrations.

Melt temperature 245°C	VRF	
	CBA concentration	
Shear rate (S^{-1})	5%	10%
180	0.867	0.845
240	0.941	0.912
320	0.932	0.922
430	0.953	0.938
580	0.952	0.945
800	0.953	0.947
1000	0.963	0.948

Therefore, the gas bubbles will grow as the melt reaches the die exit. This phenomenon as mentioned before will result in lowering the melt viscosity. It should be added that the solubility of gas in polymer melt depends upon molecular structure of both polymer and gas. As stated by Throne (28), with increasing melt temperature, the solubility could increase for one polymer and decrease for another, and depends on molecular structure of polymer and gas.

The effect of gas blowing agent on position of occurrence of melt fracture at various L/D ratios can be studied from Figures 4.22-4.23. It is apparent that the gas blowing agent has similar effect on the viscosity and melt fracture of polyolefin foam, as melt temperature. Another point which can be deduced from these figures is that, the position of occurrence of melt fracture for high density polyethylene foam is similar to its unfoamed state, whereas, the melt fracture of polypropylene has occurred at higher shear rate as compare to its unfoamed state (compare Figures 4.14 with 4.22 and 4.17 with 4.23). This could be due to the higher melt pressure involved in processing of high density polyethylene. The high pressure in the die will suppress the formation of gas bubbles, therefore the solution will behave as single phase system.

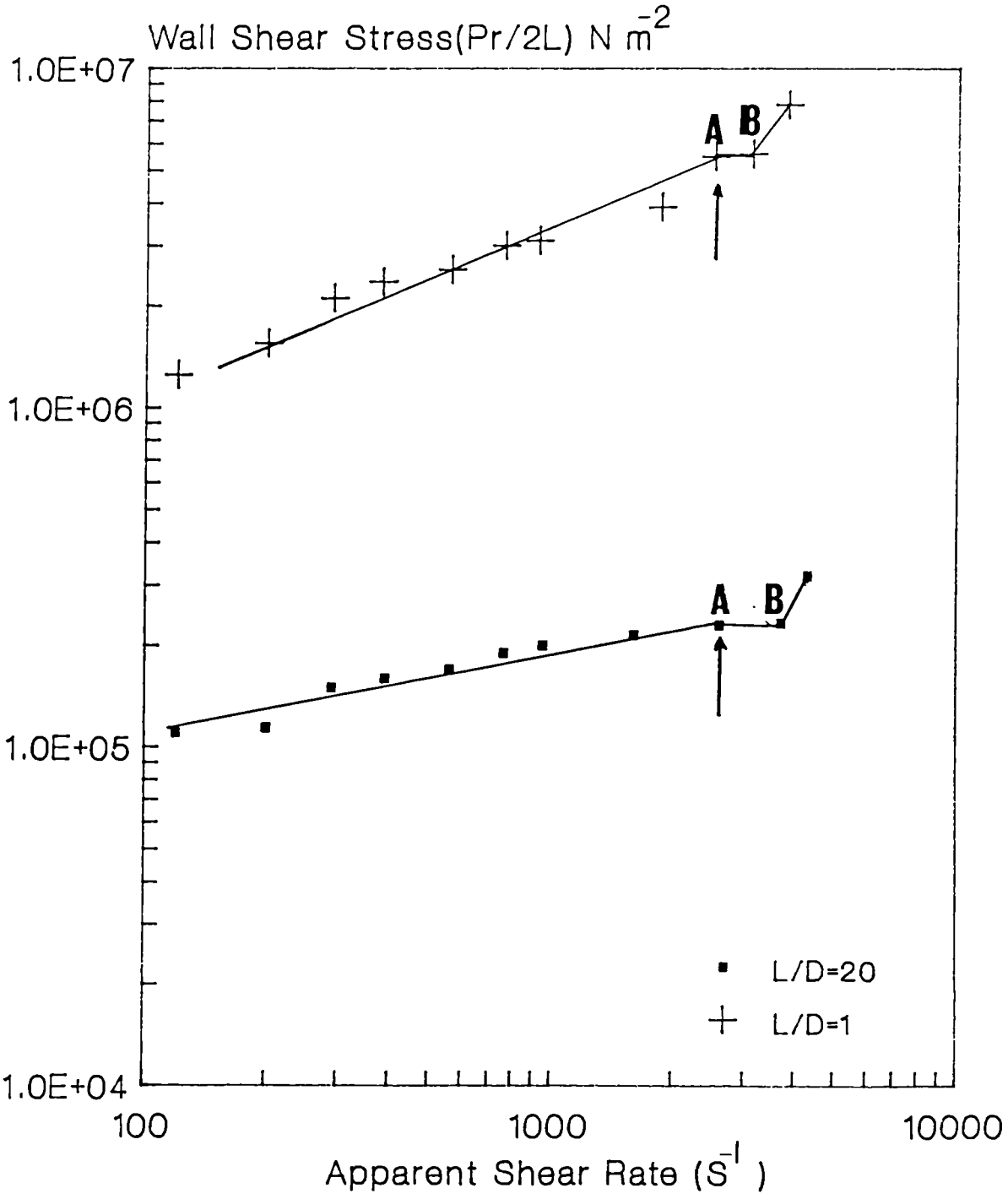

Figure 4.22. Schematic flow data of HDPE (H11042) containing 5 wt.% CBA.

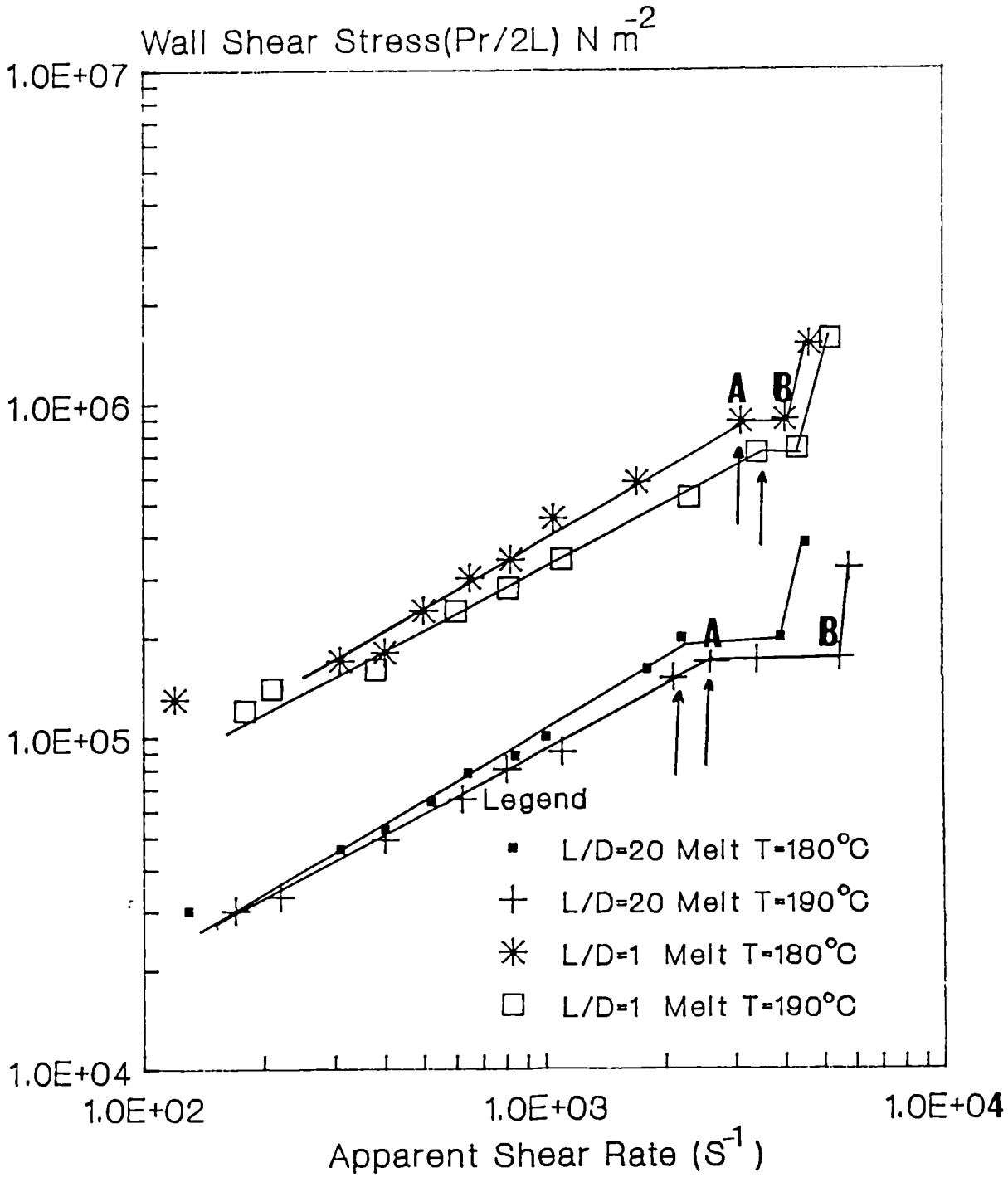

Figure 4.23. Schematic flow data of PP (GXM-43) containing 5 wt.% CBA at various melt temperatures and L/D ratios.

CHAPTER 5
PRELIMINARY INVESTIGATION
OF
EXTRUDED POLYOLEFIN FOAM

5. Preliminary Investigation of Extruded Polyolefin Foam

5.1. Introduction

In order to optimise the reduction of density as well as achieving high open cell fraction during production of polyolefin foam, a thorough understanding of effect of processing conditions on the foam quality is required. For this purpose it is intended to study the influence of the following prameters on the density (in molten and solidify stage) and rheological characteristics of polyolefin foam.

i) Die characteristics, such as die entry angle and land length.

ii) Processing conditions, such as melt pressure and temperature and cooling regime.

iii) Polymer type (effect of molecular weight, [molecular weight distribution] hence, melt viscosity

and,

iv) Concentration of chemical blowing agent.

Also it will be shown how one can optimise the uniformity of the cross section and stabilisation of cell walls, through refinement of the die geometry and control of the crystallisation temperature and melt strength of the material.

Figure 5.1 gives an over view of the experimental steps which will be followed in this chapter.

5.2. Some Aspects of Die Design

The function of extrusion die is to direct the molten polymer delivered by the screw into a required cross section. The die is, therefore, a channel whose profile changes from that of the extruder bore to an orifice which produces the required form. In order to predict the behaviour of the melt in a such a channel, one should characterise the viscosity of the material over the shear rate and temperature under study, in order to be able to correlate this viscosity with the flow of the melt under pressure through the different sections which define the channel. The design and construction of dies is complicated and, is based mainly on experience. It is more difficult to design dies for foaming process in general than it is for compact unfoamed material, since apart from cross sectional area, flow rate, flow resistance and viscoelastic swelling, one must take into account the expansion of the extruded strand, as well as minimisation of premature foaming inside the die.

The factors which influence extrudate characteristics

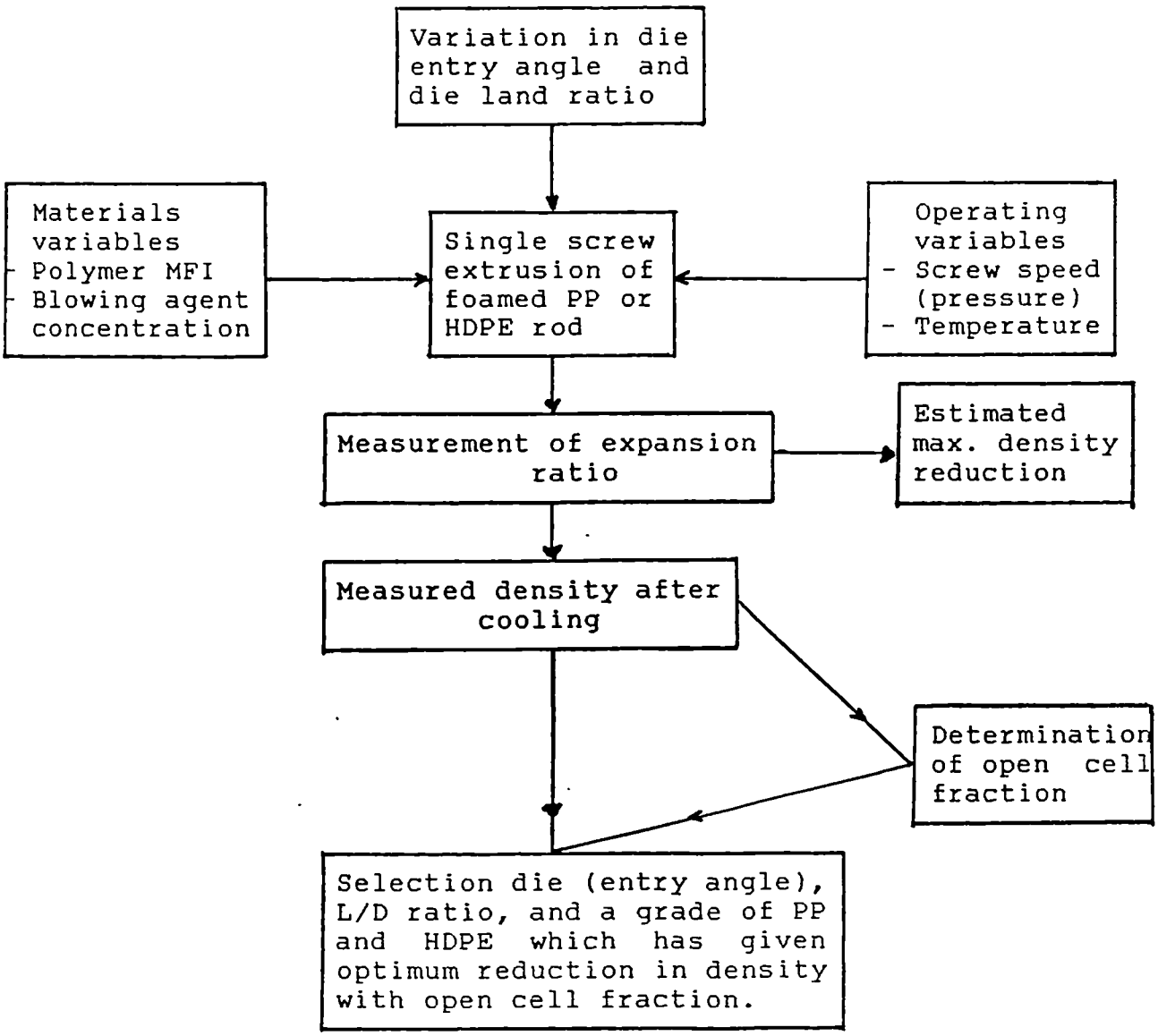

Figure 5.1. a) Summary of first stage of the programme.

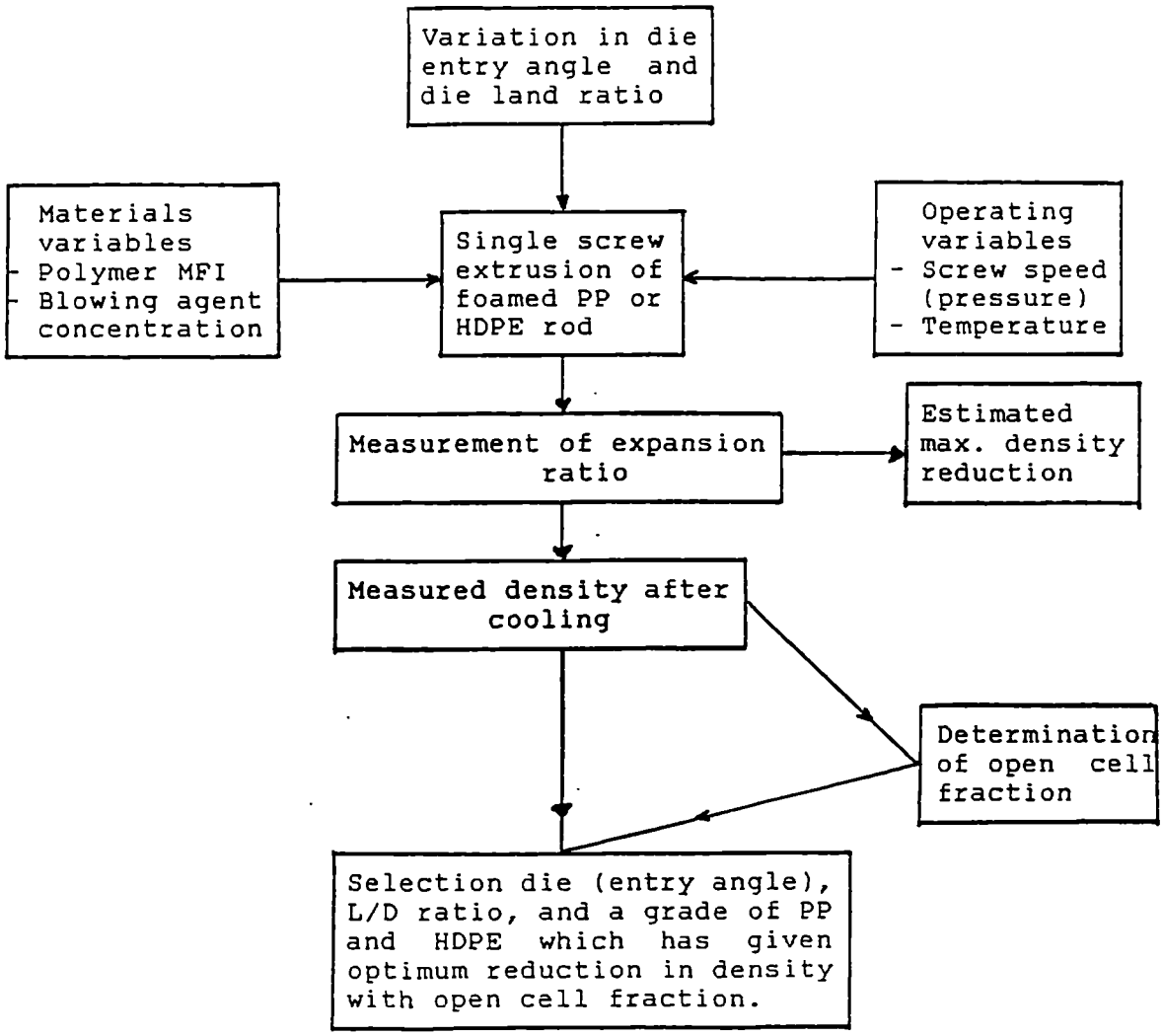

Figure 5.1. a) Summary of first stage of the programme.

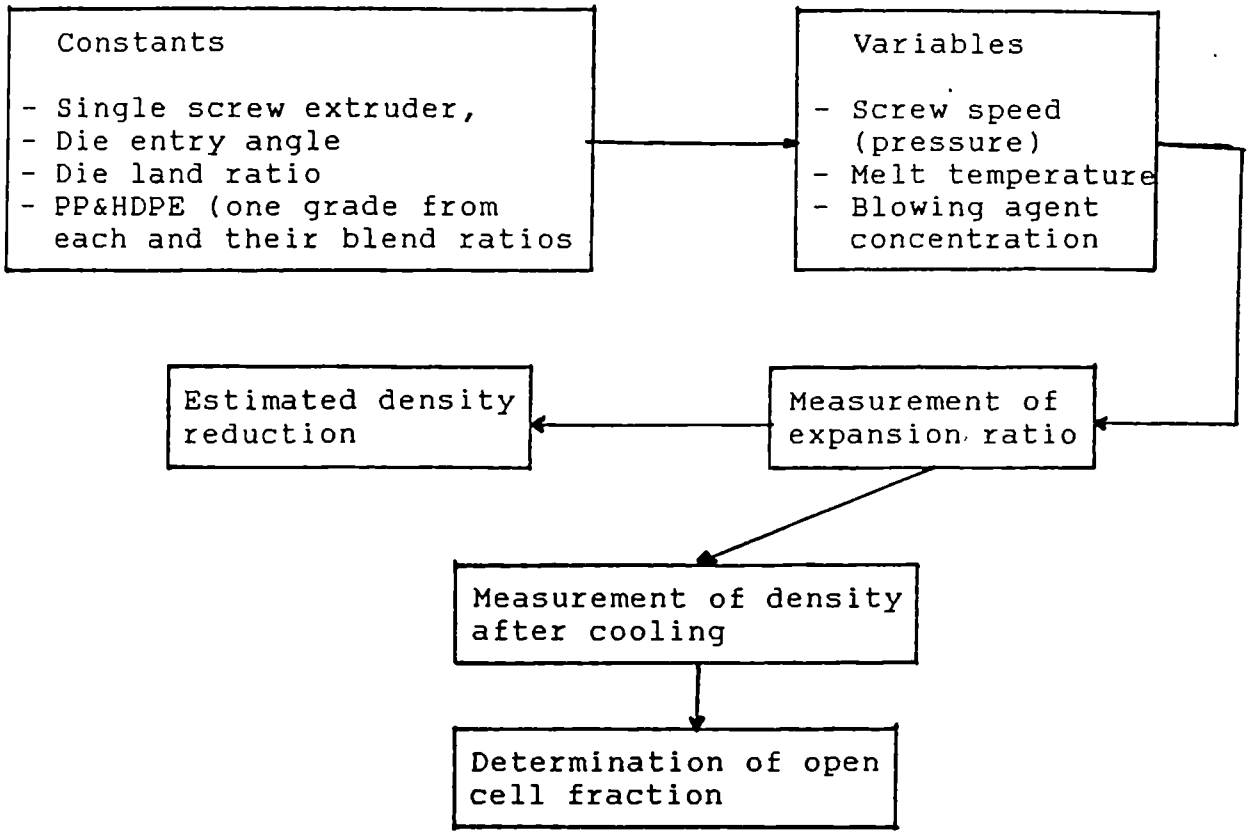

Figure 5.1. b) Summary of second stage of experimental programme.

after the strand has left the die, are the rate of drawdown, elastic effects and expansion behaviour.

In extrusion dies the zones of influence are the feed zone, the inlet zone (performing zone) and the die land (in the die orifice). The schematic representation of these areas are shown in Figure 5.2.

The feed zone is the transition from the circular or in the case of twin screws octagonal cross section at the extruder exit where it meets the die inlet zone. The melt stream coming from the screw is moved to the die inlet with increasing speed. Since the cross sectional differences between the die inlet and die exit are great, the channel should be tapered to avoid any stagnation. In the inlet or pre-forming zone the melt stream must be controlled so that its speed in the various cross sectional zone flow channel is as uniform as possible.

In converging flow, such as occurs in tapered entry of a die, an extensional flow superposed on a shearing flow (see Figure 5.3). The ratio of the magnitudes of the two types of flow varies with the angle of convergence of the taper, the elongational flow component increasing with increase in angle of the die (154). The total pressure drop changes with

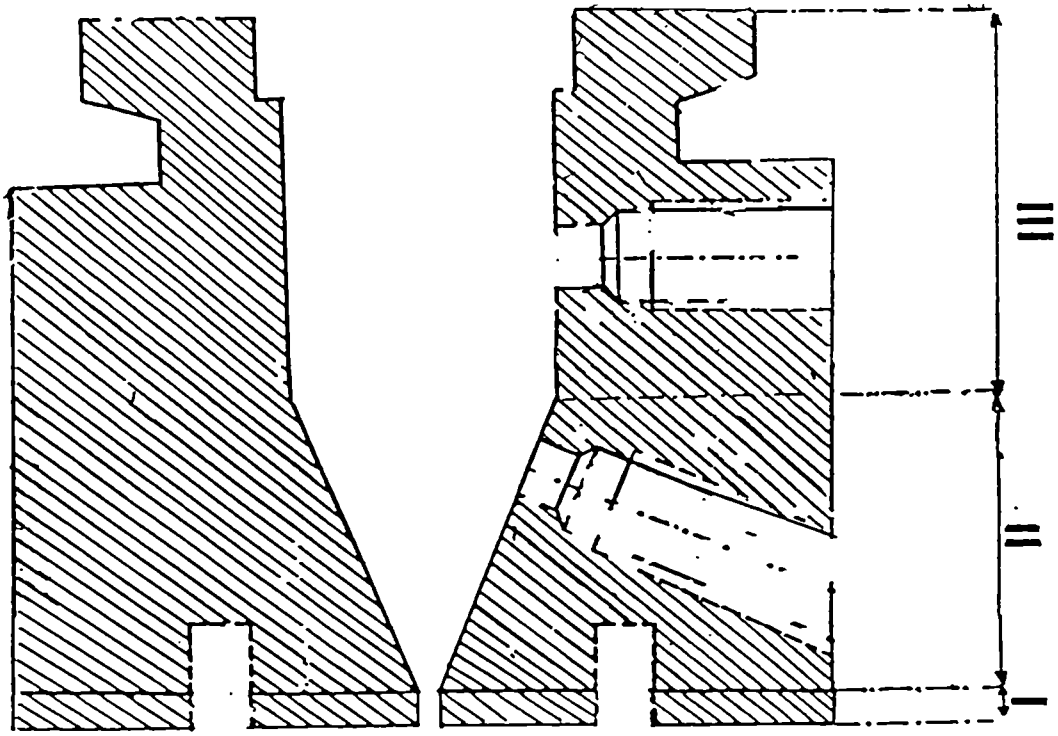

Figure 5.2. Schematic representation of an extrusion die, I=die land, II=inlet zone, and III=feed zone.

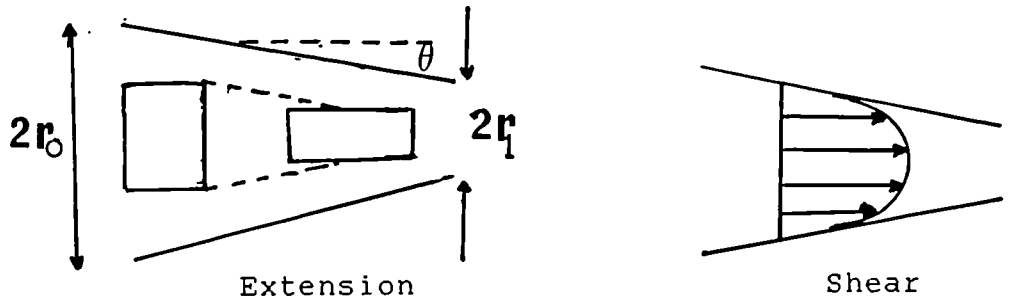

Figure 5.3. Extensional flow and shearing flow in a tapered die entry (after 153).

convergence angle so as to give a minimum value as the angle is increased.

In designing the optimum die a balance must struck between too much and two little streamlining. If the die has inadequate streamlining, the stretching rate may exceed that which the melt can accommodate without rupture, the streamline pattern will break down and extrudate becomes distorted. At the other extreme, if convergence angle is too narrow, the die becomes restricted so that the pressure drop unacceptably would be high, as it is shown in the proceeding sections.

For the purpose of investigating the effects of die geometry (die entry angle and land ratio) on processing conditions as well as foam quality (mainly density and open cell fraction), of polyolefin, several dies with different entry angle have been designed. The schematic representation of these dies are shown in Figure 5.4.

5.3 Method of Stabilisation of Cross Sectional Area of the Foam Extrudate

Polyolefins (in particular high density polyethylene and polypropylene) have a moderately sharp melting point,

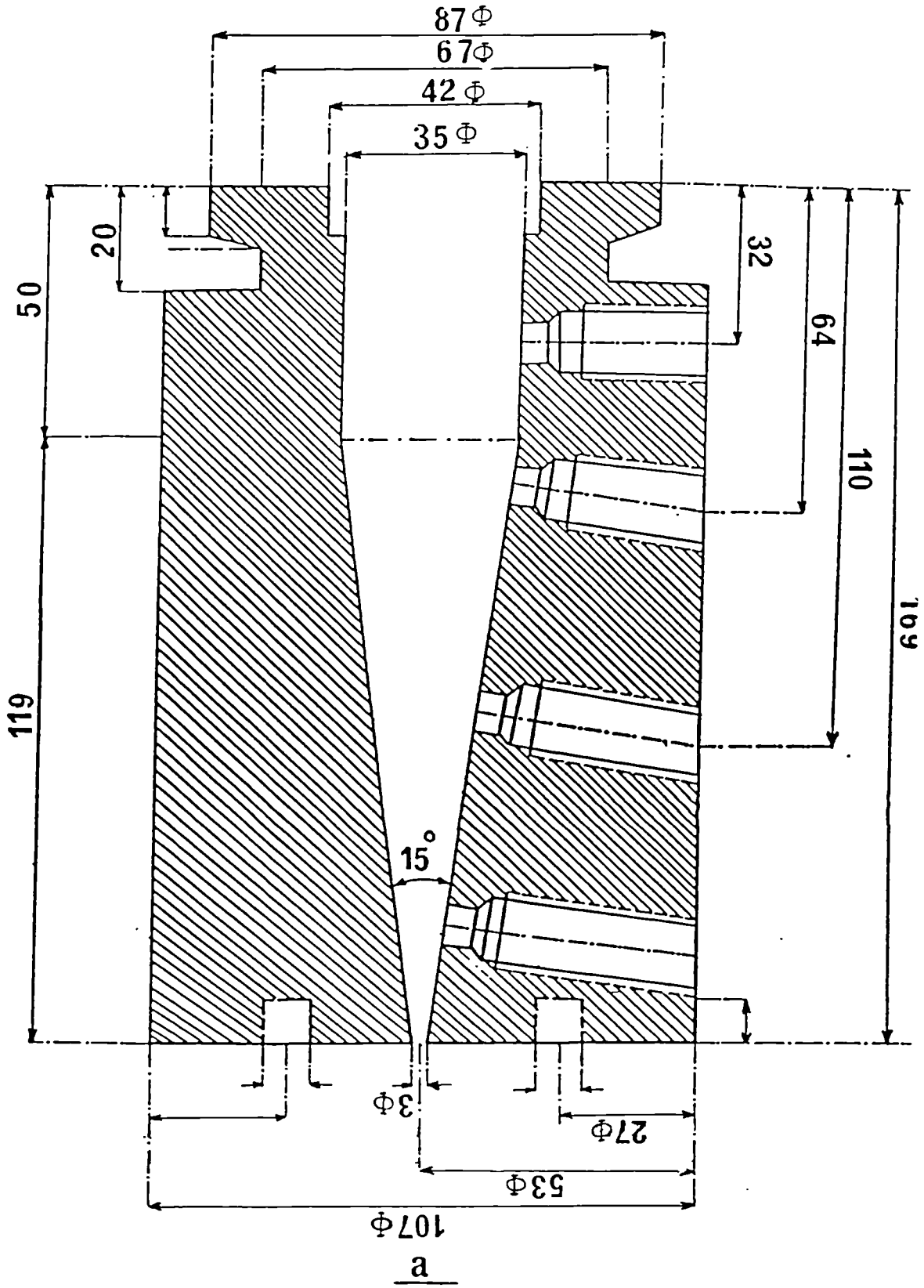

Figure 5.4. Schematic representation of dies used in this project. Die entry angle; a) 15°, b) 30°, c) 45° and d) 60°. All dimensions are in mm.

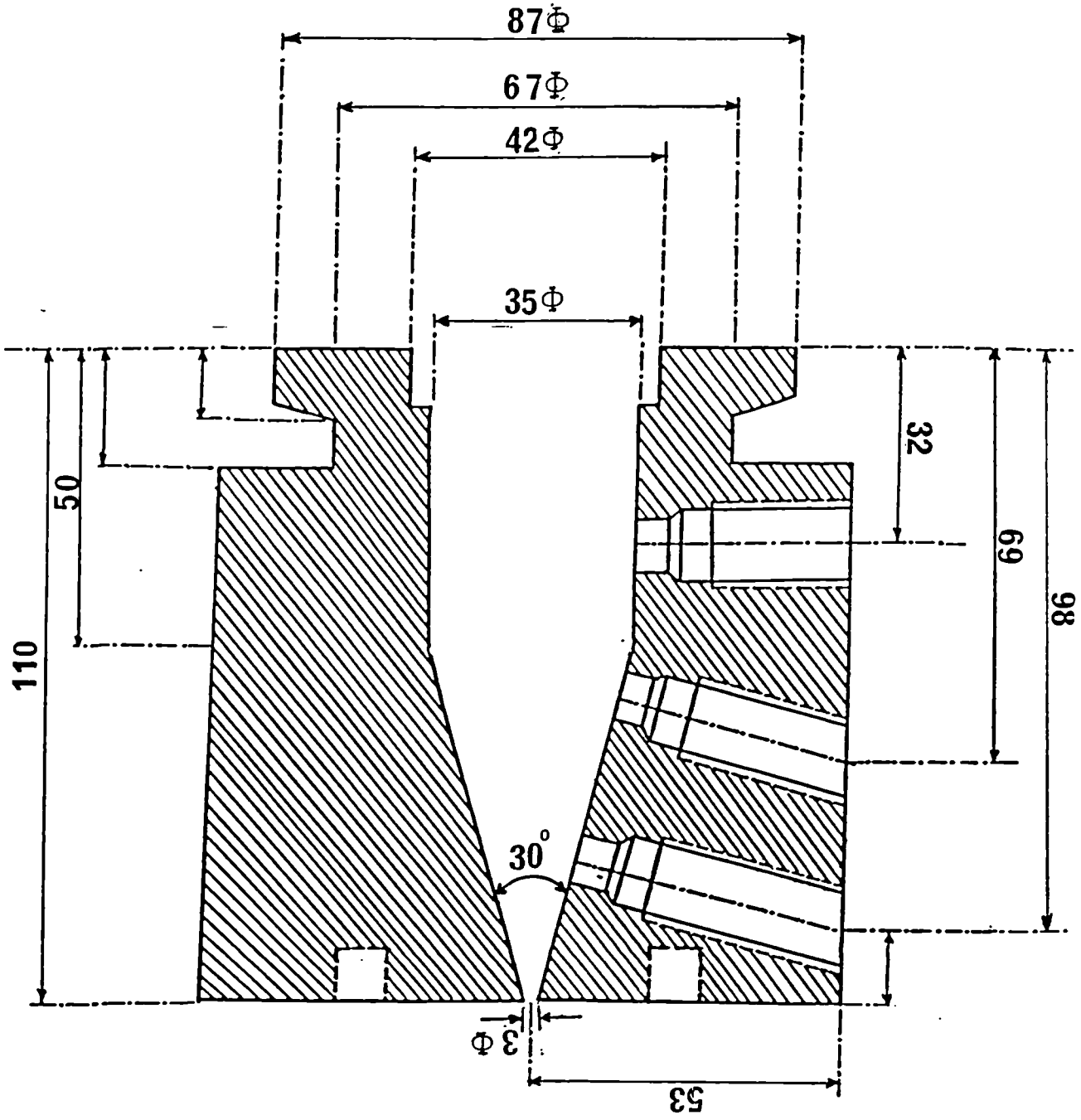

b

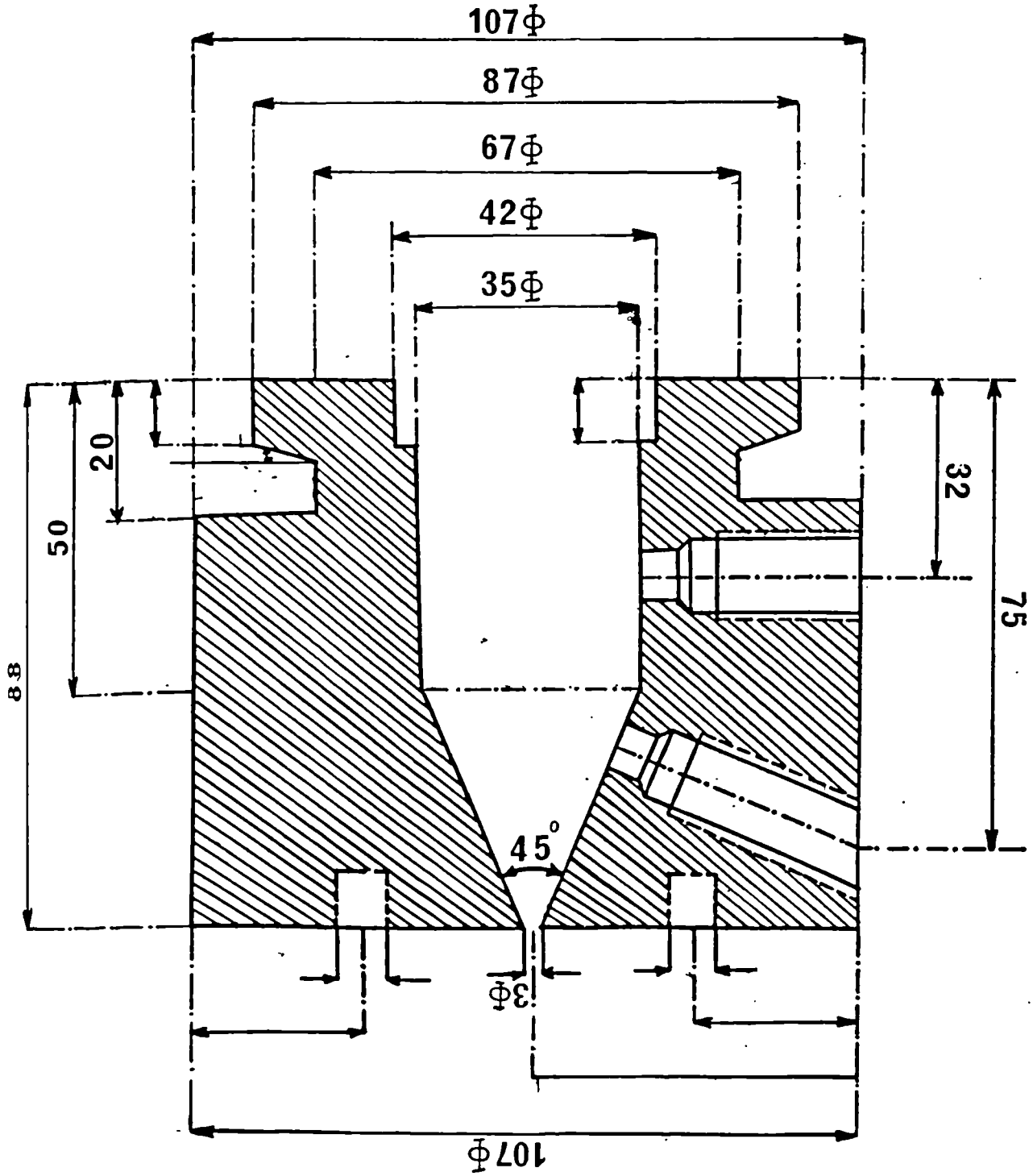

C

d

hence, their melt viscosity decreases rapidly over a narrow range of temperature above the melting point as it was shown in the previous chapter. This phenomenon makes it difficult to produce a low density foam with chemical blowing agents or even any physical blowing agent for that matter. The reason is that the foam collapses before it can be stabilised. For several years this problem has been approached by cross-linking the resin (in the case of polyethylene), chemically or by high energy radiation with X-ray, before it is foamed. This method has its limitation, especially if the foamed extrudate material is going to be used for an application which will come in contact with human body.

In an attempt to overcome the stabilisation problem encanntesed with polyolefin foams a calibration sleeve (the diameter of the tube should be large enough not to prevent the expansion of extrudated foam) was connected to the end of the die land adapter and the temperature of this tube regulated to control viscosity of the resin. In this way it was possible to support the foam extrudate emerging from the die and then to drop its temperature prior to entering the cooling tank. Also it should be added, it was found by trial and error, that a distance of 4-6 cm should be maintained between the end of this tube and the cooling tank so that a further drop in the temperature of extrudate

partially solidifies the melt to some extent, prior entering the sizing unit in the cooling tank .

In addition to this procedure it was necessary to pass the foaming extrudate through a calibration sleeve. The sizing sleeve should be long enough to provide sufficient time for cooling of the extrudate, whilst the external geometry was controlled. Combination of these two modifications helped to achieve more uniformity in cross section of extrudated foam material, and preventing premature collapse of foam.

5.4. Results and Discussion

5.4.1. Effects of Die Design Variables on Foam Extrusion Characteristics of Polypropylene

The extrusion characteristics of foamable polypropylene have been investigated by varying the die entry angle (15°, 30°, 45°, and 60°) and die land (capillary length to diameter, L/D ratio). Over the range of dies used through this investigation, it was found that, both the die entry angle as well as the L/D ratio play a significant role in influencing the foam extrusion characteristics of polypropylene.

Tables 5.1-5.4 display the effect of die entry angle on the axial pressure generated inside the die at various screw speeds, using a single screw extruder.

Table 5.1. Axial pressure profile of polypropylene (GXM-43) foam prepared at various screw speeds. Die entry angle 15°, melt temperature 195°C. L/D=0, blowing agent concentration (BAC) = 4 wt.%.

Screw Speed (rpm)	Apparent Shear Rate(S^{-1})	Axial Pressure* (MPa) P1	P2	P3	P4
10	934	1.172	0.905	0.689	0.620
20	1495	1.654	1.31	0.827	0.620
30	1979	1.93	1.69	1.103	0.896
40	2366	2.344	2.068	1.516	1.172
50 !	3389	2.62	2.275	1.691	1.310
60	4113	3.102	2.275	1.999	1.585
80	5025	3.447	3.172	2.137	1.654

Table 5.2. Axial pressure profile of polypropylene(GXM-43) foam prepared at various screw speeds. Die entry angle 30°, melt temperature 195°C. L/D=0, BAC= 4 wt.%.

Screw Speed (rpm)	Apparent Shear Rate(S^{-1})	Axial Pressure** (MPa) P1	P2	P3
10	981	1.241	0.965	0.896
20	1551	1.654	1.379	1.034
30	2037	1.999	1.858	1.517
40 !	2322	2.48	2.272	1.827
50	3425	2.584	2.346	1.930
60	4180	3.206	2.805	2.413

* and ** The axial distance from the die entrance are given in Figures 5.4.a and 5.4.b respectively.

! Melt disturbance began to appear.

Table 5.3. Axial pressure profile of polypropylene(GXM-43) foam prepared at various screw speeds. Die entry angle 45°. Melt temperature195°C.

Screw Speed (rpm)	Apparent Shear Rate(S^{-1})	Axial Pressure* (MPa) P1	P2
10	1035	1.275	1.034
20	1626	1.723	1.310
30	2008	1.965	1.827
40 !	2344	2.550	2.275
50	3482	2.69	2.413
60	4081	3.10	2.827
80	5077	3.654	3.412

Table 5.4. Axial pressure profile of polypropylene(GXM-43) foam prepared at various screw speeds. Die entry angle 60°. Melt temperature 195°C.

Screw Speed (rpm)	Apparent Shear Rate(S^{-1})	Axial Pressure** (MPa) P
10	1111	1.310
20	1635	1.723
30	1994	1.931
40 !	2361	2.517
50	3502	2.757
60	4109	3.137
80	5121	3.723

*and**, The axial distance from the die entrance are given in Figures 5.4.c and 5.4.d respectively.

! The melt disturbance began to appear.

The specification of the single screw extruder is given in the section 3.4.1. As it is noticed, as the entry angle gets shallower (the length of the die increases) greater pressure drop occurs inside the die. As it has been described previously this phenomenon could result in a poor cell stability and, therefore, will result in a product with higher density. On the other hand a die with steep angle (such 60°) is much shorter in the length than the one with smaller entry angle. Therefore, at high shear rate the streamline pattern will break down at lower shear stress and the extrudate becomes distorted. The foregoing results show that, the die with entry angle of 45° was identified as being most suitable for this process. Another important point which should be added is at apparent shear rate higher than 1500 S^{-1}, the behaviour of the pressure drop along the axial distance of the die approaches to a linear relationship as it observed in Figure 5.5. This change in behaviour of pressure drop (dp/dz) with apparent shear rate is most likely due to the greater solubility of the gas in the molten polymer with increasing melt pressure.

Figure 5.6 shows the effect of L/D ratio on the expansion ratio of the extrudate(df/dp), where df and dp are maximum diameter of foamed and unfoamed extrudate prior to cooling. Note that, the expansion ratio decreases

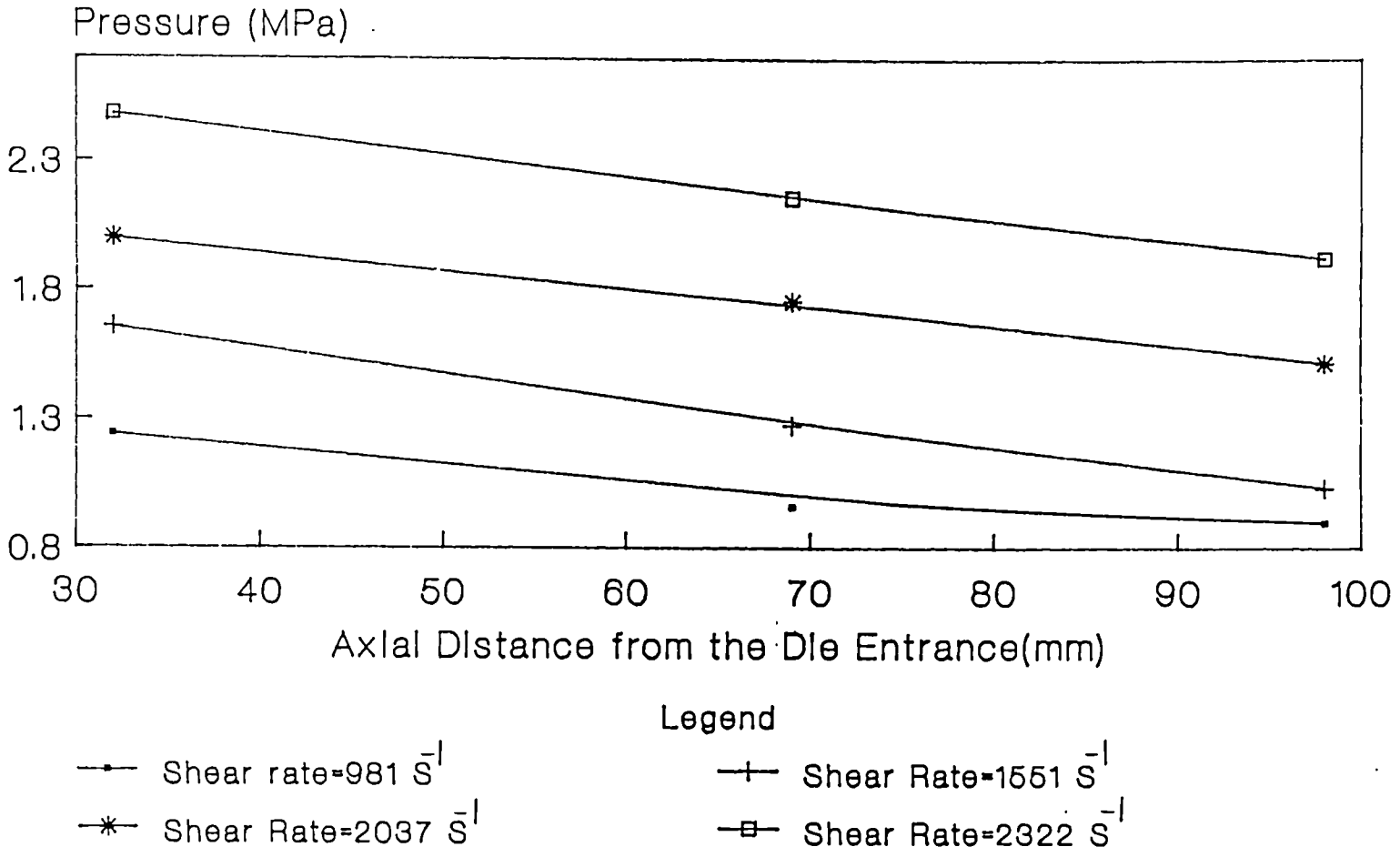

Figure 5.5 Axial Pressure profile of PP (GXM-43) containing 4 wt.% CBA in the die. Die entry angle=30°, L/D=0, Melt Temperature=195°.

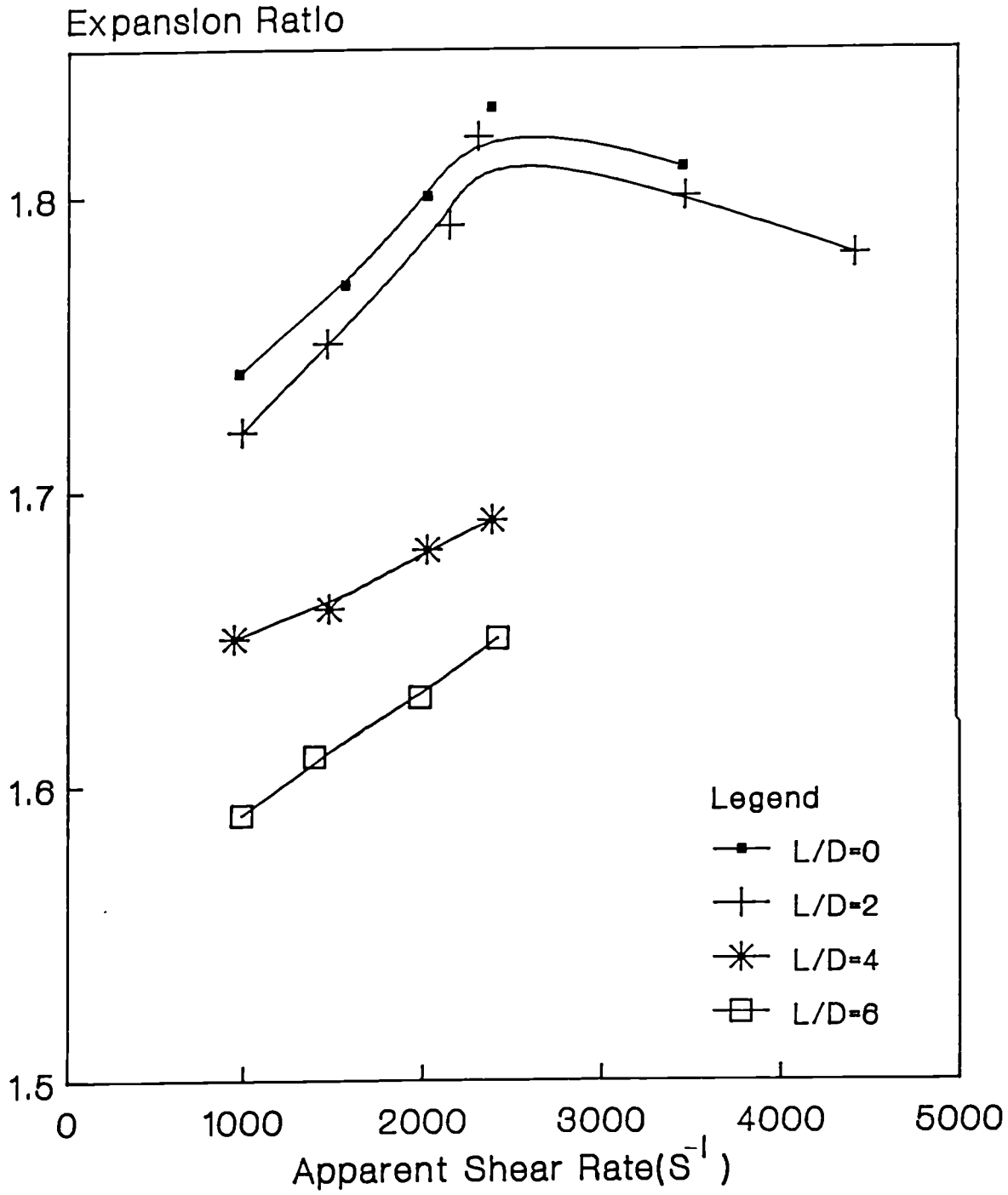

Figure 5.6. Relationship of expansion ratio and apparent shear rate of PP (GXM-43) foam. Die entry angle=45°, melt temperature=195°C.

with increasing L/D ratio. Also make a note that, except for L/D ratios of zero (i.e. a conical die) and 2 the expansion ratio shows little dependence on apparent shear rate.

The effect of L/D ratio on the solid state density appears to be rather complex as indicated in Figure 5.7. It was stated previously that, as the die length increases, the chance of premature foaming will be enhanced. Therefore, with increasing the die land ratio, the chance of premature foaming toward the end of the die land would be greater, hence, the cell walls will collapse prior to solidification. Effect of L/D ratio on open cell fraction is also shown in Figure 5.8. Note that the open cell fraction goes through a minimum at L/D ratio of 2 and then it increases for L/D ratio of 4 and 6, in spite of the fact that the die pressure increases with L/D ratio. This is attributable to the fact that although there is less chance of premature foaming occurring in the die section for the dies of having L/D ratio of 4 and 6, but still as is stated above, it is likely that premature foaming could be taking place in the capillary section of the die adapter (die land) as the mixture of molten polymer containing gas approaches the die exit.

From the results of the foregoing figures a compromise

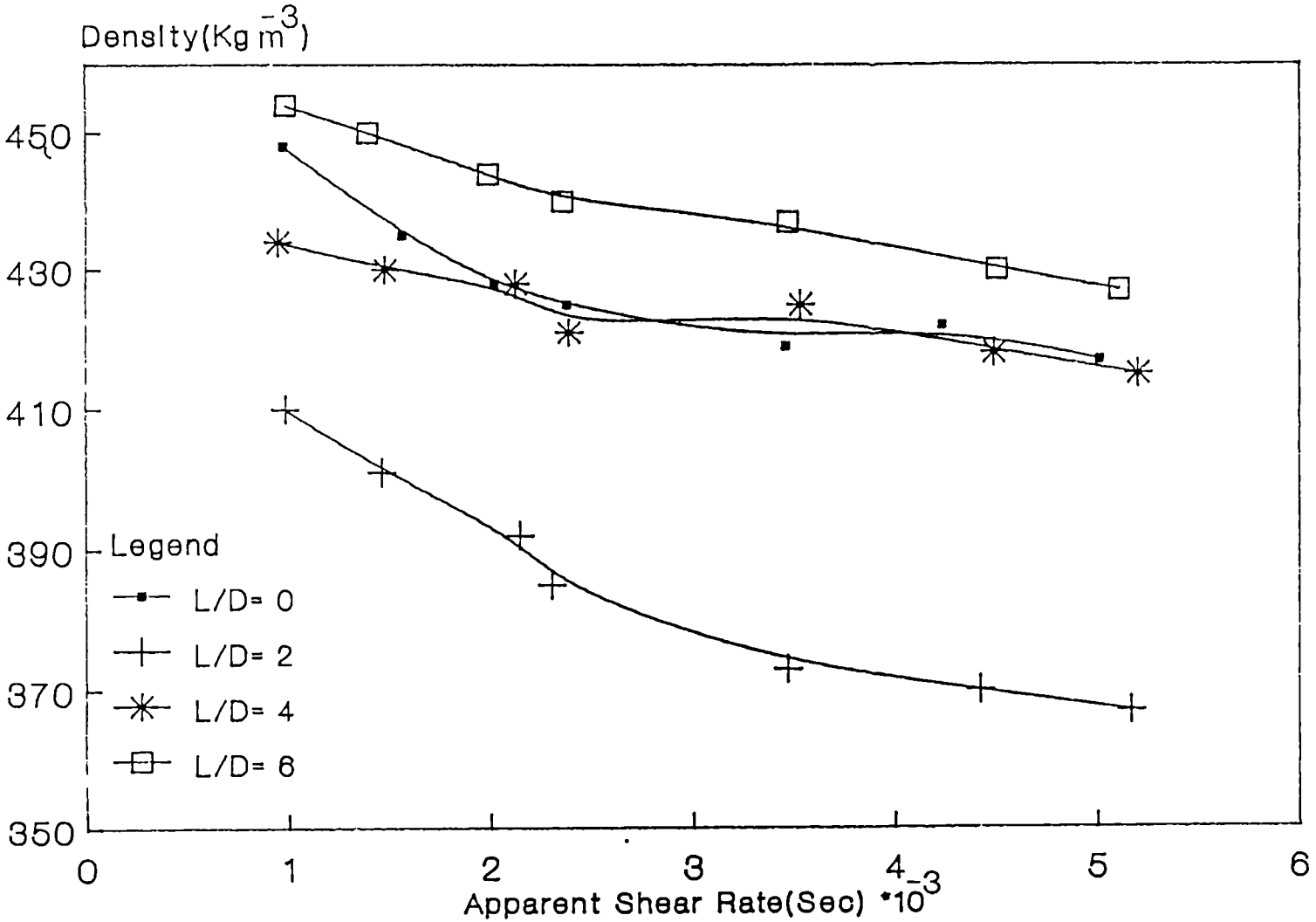

Figure 5.7. Relationship of density and apparent shear rate for PP foam at various L/D ratios. Melt Temperature 195°C.

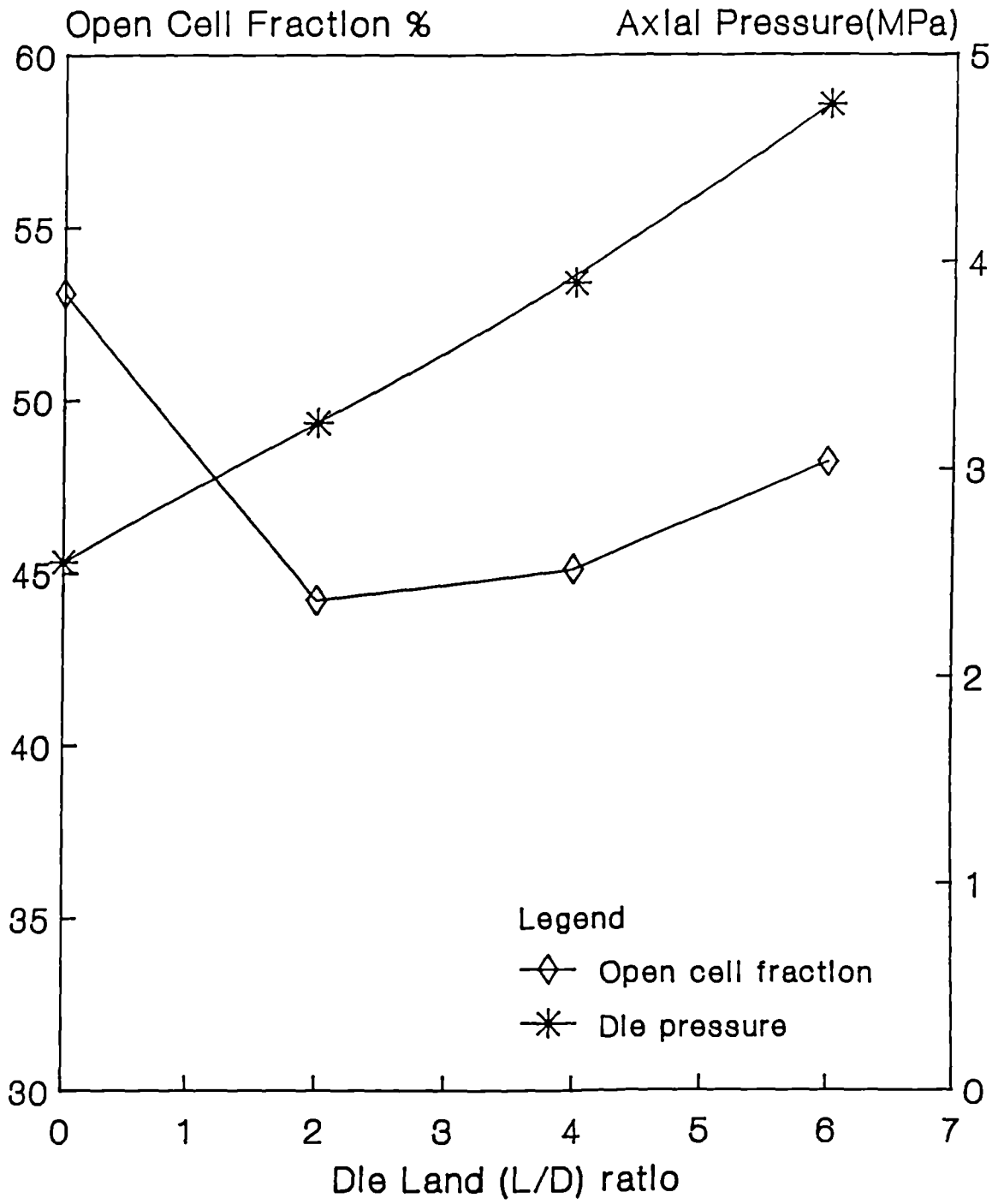

Figure 5.8. Schematic representation of open cell fraction and die pressure versus L/D ratio, for PP foam. Melt temperature 195°C.

can be made between open cell fraction and solid state density. Such results are presented in Figure 5.9, where, the optimum die land for this process to achieve lowest density is found to be around 2. Therefore, for the further studies in this section, die with entry angle of 45° and L/D ratio of 2 have been used.

5.4.2. Effect of Melt Temperature on the Foam Extrusion Characteristics of Polypropylene

The expansion ratios (df/dp) for different melt temperatures and at various apparent shear rates are shown in Table 5.5. These results show that the expansion ratio goes through a maximum and then decreases with further increase of melt temperature. This phenomenon is attributed to the lowering of melt viscosity with increasing the melt temperature, resulting in less restriction of bubble growth, but, further reduction of melt viscosity (with further increase of melt temperature) will result in the drainage of the cell walls and eventually to collapse of the bubbles prior to solidification. This type of behaviour was more pronounced when higher concentration of blowing agent was used, as it will be discussed later in this chapter. One would also expect that a higher shear rate would have the same effect on the expansion ratio as increasing melt

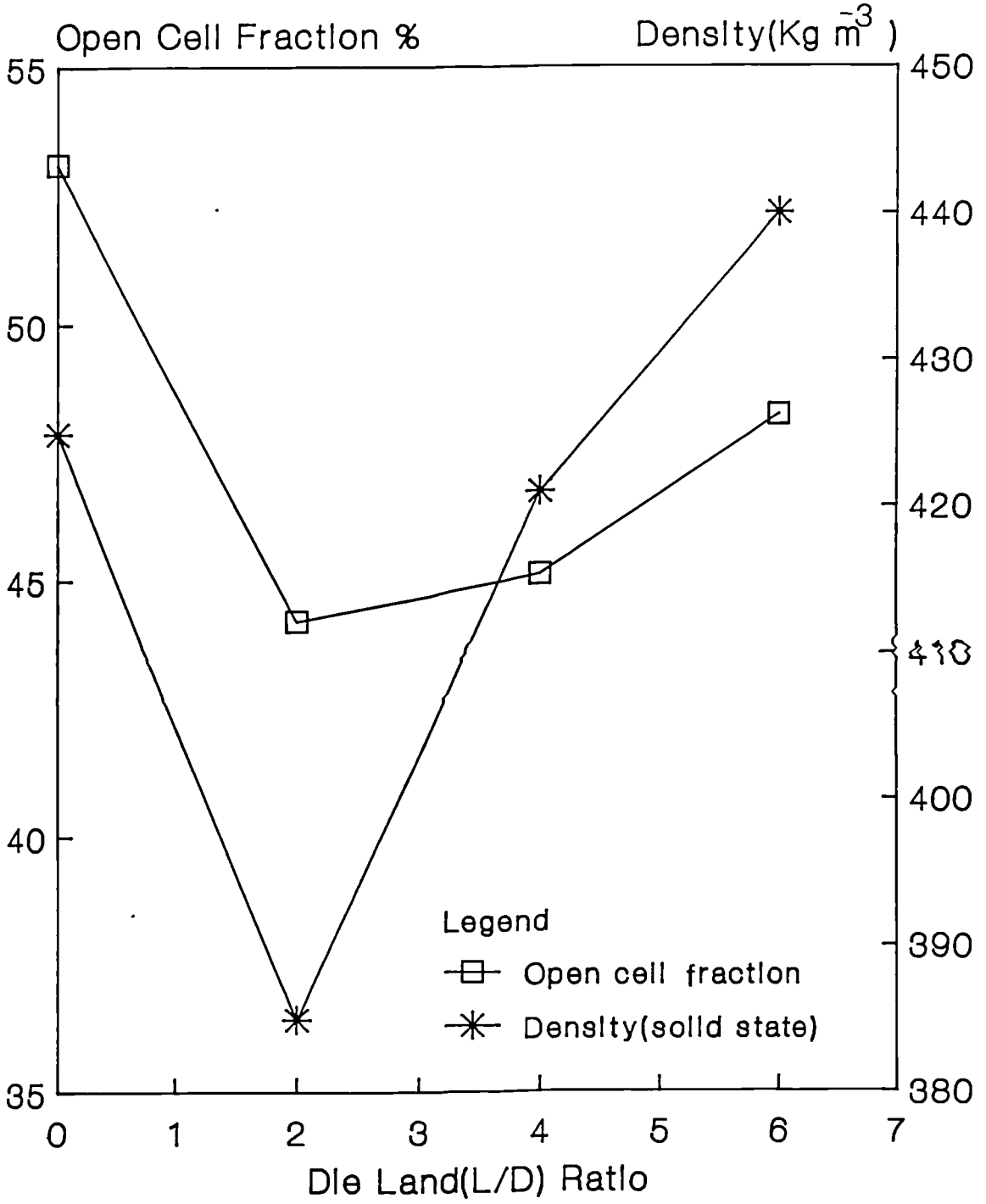

Figure 5.9. Schematic representation of open cell fraction and density (solid state) vs. L/D ratio for PP foam. Melt temperature 195°C.

Table 5.5. Relation between shear rate and expansion ratio for polypropylene(GXM-43) foam.
Die entry angle 45°, BAC = 4 wt.%.

Melt Temperature=175°C

Apparent Shear Rate(S^{-1})	Expansion Ratio
975	1.70
1386	1.75
2178	1.77
2345	1.83
3477	1.85
4089	Unstable melt
5155	Unstable melt

Melt Temperature=185°C

Apparent Shear Rate(S^{-1})	Expansion Ratio
950	1.72
1343	1.75
2109	1.83
2388	1.89
3424	1.89
4300	Unstable melt
4991	Unstable melt

Table 5.5. continues

Melt Temperature=195°C

Apparent Shear Rate(S^{-1})	Expansion Ratio
988	1.72
1465	1.75
2145	1.79
2305	1.82
3469	1.80
4421	1.79
5168	1.79

Melt Temperature =205°C

Apparent Shear Rate(S^{-1})	Expansion Ratio
963	1.65
1285	1.67
2236	1.70
2418	1.71
3469	1.70
4358	1.70
5138	1.69

temperature, but it is noticed the effect of shear rate is less pronounced than raising of melt temperature. The reason behind this behaviour is due to higher pressure involved with higher shear rates which prevent premature foaming of the material inside the die.

Figure 5.10 shows the relation of density of the foamed material, in both the melt and solid states at different temperatures. The density of foamed material in the melt condition was calculated according to the procedure described in section 3.5.2. Due to the same reasons previously described, the density of foamed polymer in the solid as well as in the melt state, is dictated by the melt temperature as it can be seen from Figure 5.10.

Also it should be pointed out that the density of extrudated foam in the solid state is up to 43% greater than its density in melt stage. This value is far greater than what it actually was expected, mainly due to collapse of the cell walls. It is believed that this draw back can be rectified by optimisation of the melt strength (melt viscosity) of the material, which will be discussed later in Section 5.4.10.

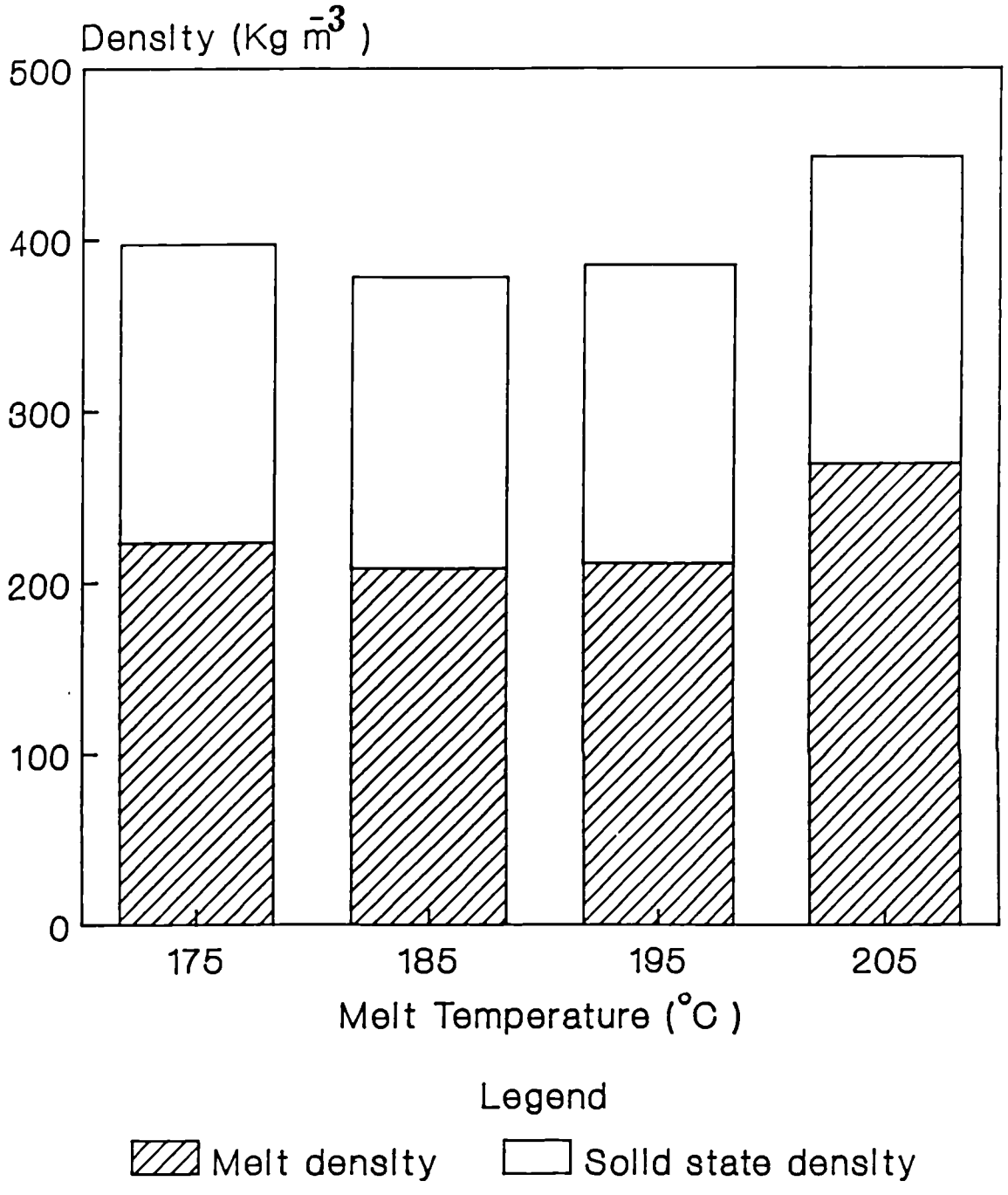

Figure 5.10. Relationship of density and melt temperature of PP (GXM-43) containing 4 wt.% CBA. L/D=2.

5.4.3. Effects of Melt Flow Index (MFI) on the Foam Extrusion Characteristics of Polypropylene

Several grades of polypropylene with different molecular weights have been chosen for this study. The general data on these grades are given in Section 3.2.

Figure 5.11 displays the relation of foam density in melt and solid state for different grades of polypropylene at various melt temperatures. In general the maximum reduction in density (in solid state) occurs at melt temperature between 185°C and 195°C depending on the grade of polymer used. The main reason behind this phenomenon (beside the melt viscosity previously described), is that the maximum amount of gas available (in the die region) from the chemical blowing agent is when the processing temperature of the polymer melt is around 185°C. It should be pointed out that, the chemical blowing agent is more efficient when, it decomposes in the last stage of the barrel of extruder or in the die region, where the escape of gas to the hopper is minimum, and also when its decomposition temperature " Td " is close to melting point of polymer material. Therefore, one can clearly see that the maximum reduction in density should occur at melt temperature of 185° C, which indeed is the case. Another point which can deduced from these figures is that, the

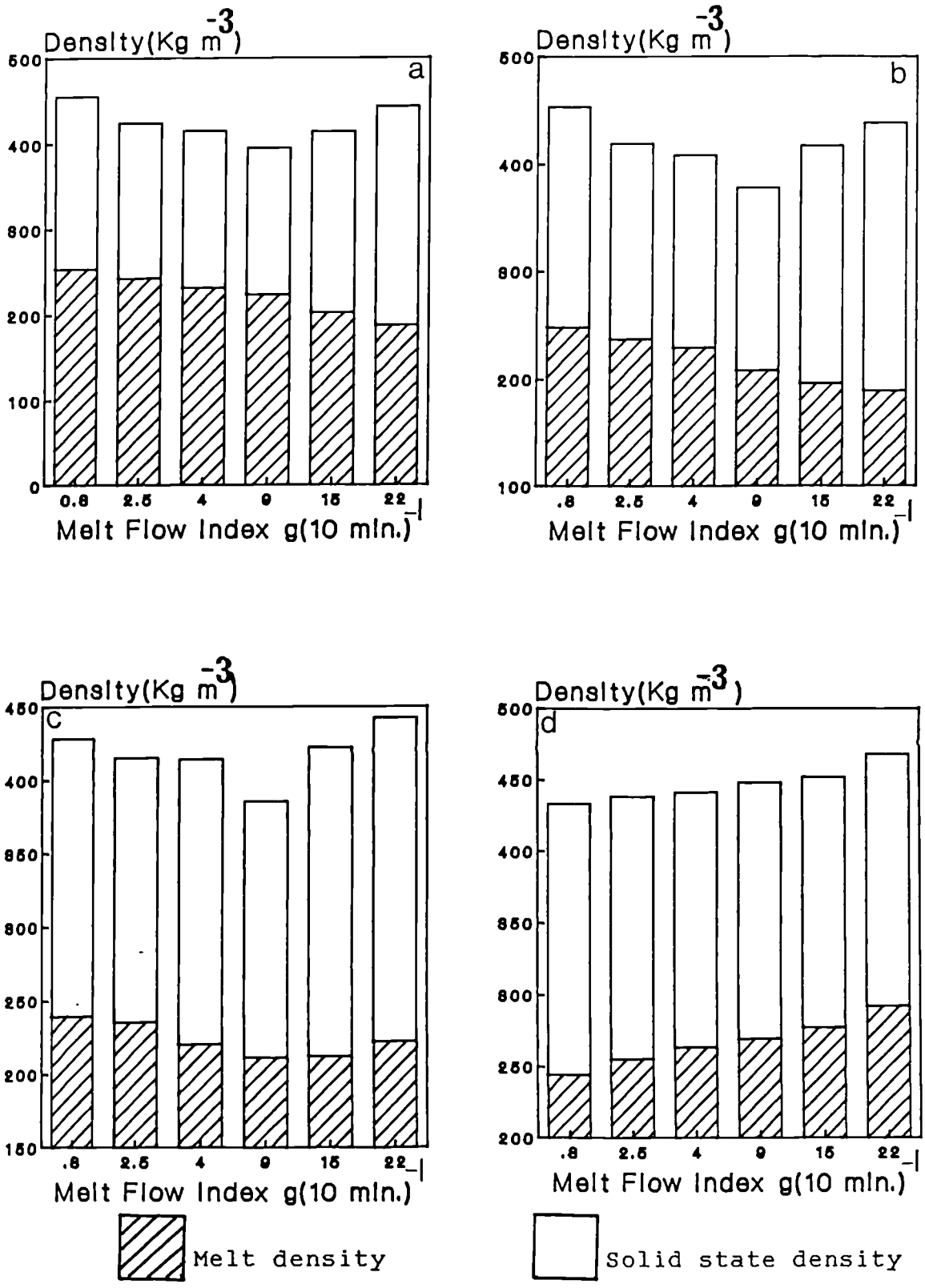

Figure 5.11. Relationship of MFI and density of PP containing 4 wt.% CBA at various melt temperatures; a)175°C b)185°C c)195°C and d)205°C.

density of the polymer foam (in the molten state) decreases with increase of MFI of the virgin resin (except for the melt temperature of 205°C where, a continuous increase in density was observed with increase of MFI of the material). This can be attributed to the fact that the resistance to expansion would decrease with increase of MFI (decrease of melt viscosity) of the polymer material, it reaches a point where, further reduction in melt viscosity will enhance the cell collapse as soon as the material emerges from the die exit. Therefore, one will expect density of the foam specimens increase beyond this point (critical viscosity).

The density of the material in the solid state goes through a minimum and then increases with a further increase the MFI of the feed stock (except for melt temperature of 205° C). As it has been explained before, this behaviour is due to lowering of melt viscosity and enhancing the movement and growth of the bubbles within the melt, but beyond a critical viscosity the melt strength of the polymer will be too low which can not withstand the external pressures (such as residual stresses and surface energy upon solidification). As with melt temperature of 205°C, one should bear in mind that, not only the melt viscosity of the material has been dropped (due to high

melt temperature) but also in order to increase the temperature of the polymer melt, it was necessary to increase the temperature of the barrel of extruder, which, this phenomenon has resulted in activation of the chemical blowing agent in the early stages of the extruder, and enhancing the premature foaming of the polymer melt.

The relation of open cell fraction of various grades of polypropylene foam and melt temperature are exhibited in Figure 5.12. As it was expected the resin with high melt flow index showed higher open cell fraction at lower temperature, whereas at high temperature (205° C and 215° C) higher open cell fraction was noticed with high viscous material (low MFI resin). As it has been mentioned before, in order the cell walls withstand the force exerted on them by the gas pressure as well as the surface forces upon solidification, the matrix should posses enough melt strength to balance out these foreign forces. Therefore, there is a critical viscosity below which the cell collapse are more readily and beyond that the melt resistance would be so high which will suppress the cell growth and due to thermo-dynamic principle the cells will tend to join one another. The foregoing results show that the resin with melt flow index of 9 g $(10\ min)^{-1}$ has shown highest open cell fraction with higher density

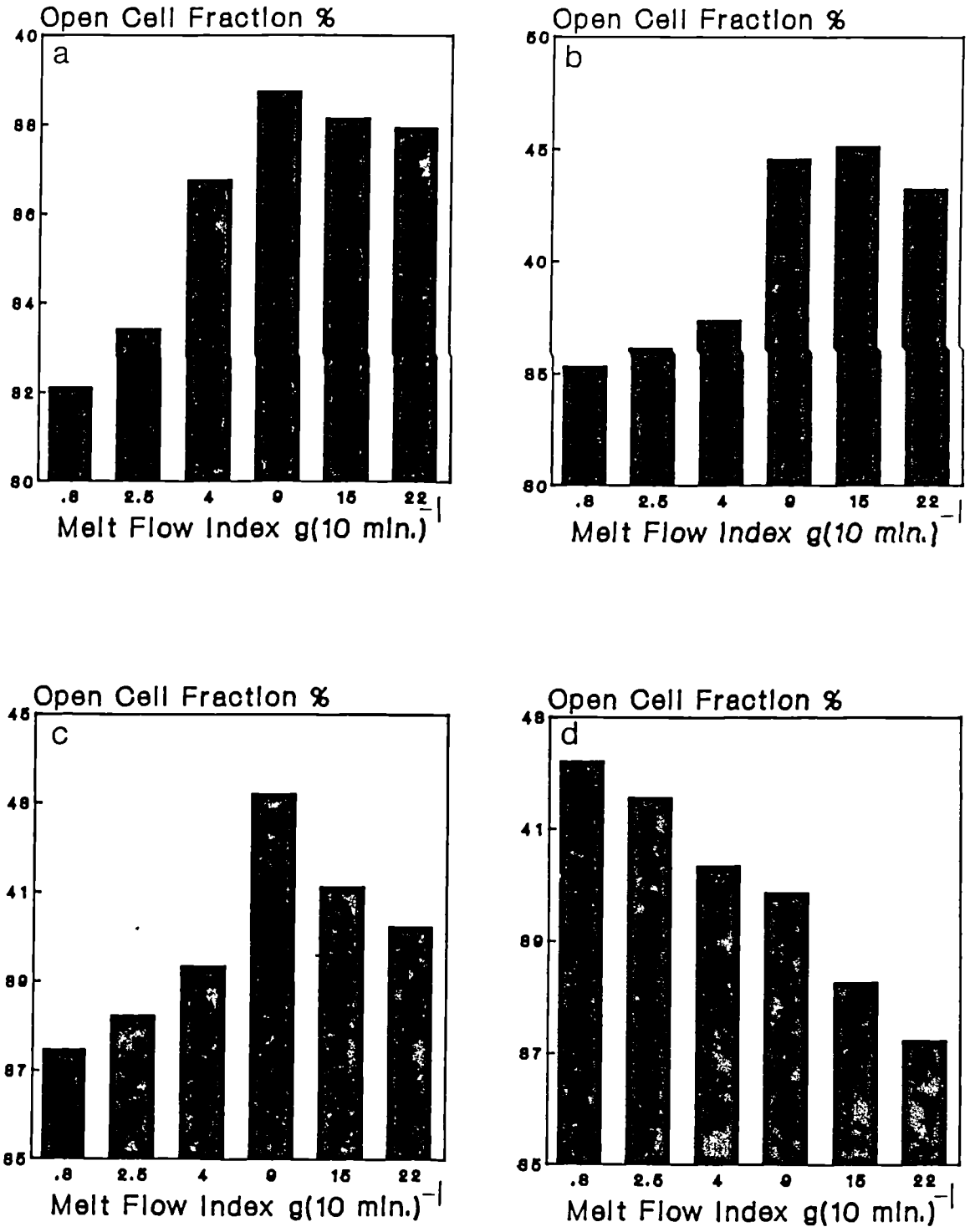

Figure 5.12. Relationship of MFI and open cell fraction of PP containing 4 wt.% CBA at various melt temperatures; a)175^{o}C, b)185^{o}C, c)195^{o}C, d)205^{o}C, e)215^{o}C.

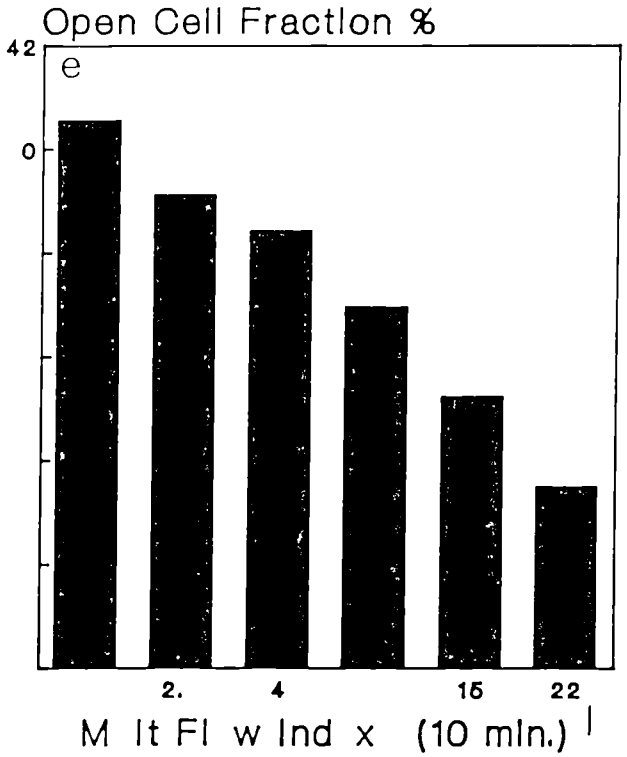
Open Cell Fraction %
42
e
0
2.
4
15
22
M It Fl w Ind x (10 mln.)

reduction as compare to the other grades of polypropylene used, but should be emphasised that the density and open cell fraction still are far from optimum condition.

5.4.4. Effects of Chemical Blowing Agent Concentration on the Foam Extrusion Characteristics of Polypropylene

Figure 5.13 shows the relationship between expansion ratio and weight percent blowing agent concentration in polypropylene extruded at various apparent shear rates. It is seen that, as the blowing agent concentration increases the expansion ratio also increases passing through a maximum. This trend is most probably due to super-saturation of the molten polymer with the excess amount of gas generated by the blowing agent. This phenomenon not only reduces the melt viscosity of the polymer, but also generates excess microbubbles in the melt, which upon entering the die, they will start to grow (due to pressure drop). These bubbles collapse as they emerge from the die exit and as it has been noticed during extrusion, the gas escapes through the skin of the extrudate.

Figure 5.14 displays the influence of chemical blowing agent concentration on density (in the solid and melt state), for various melt temperatures. It

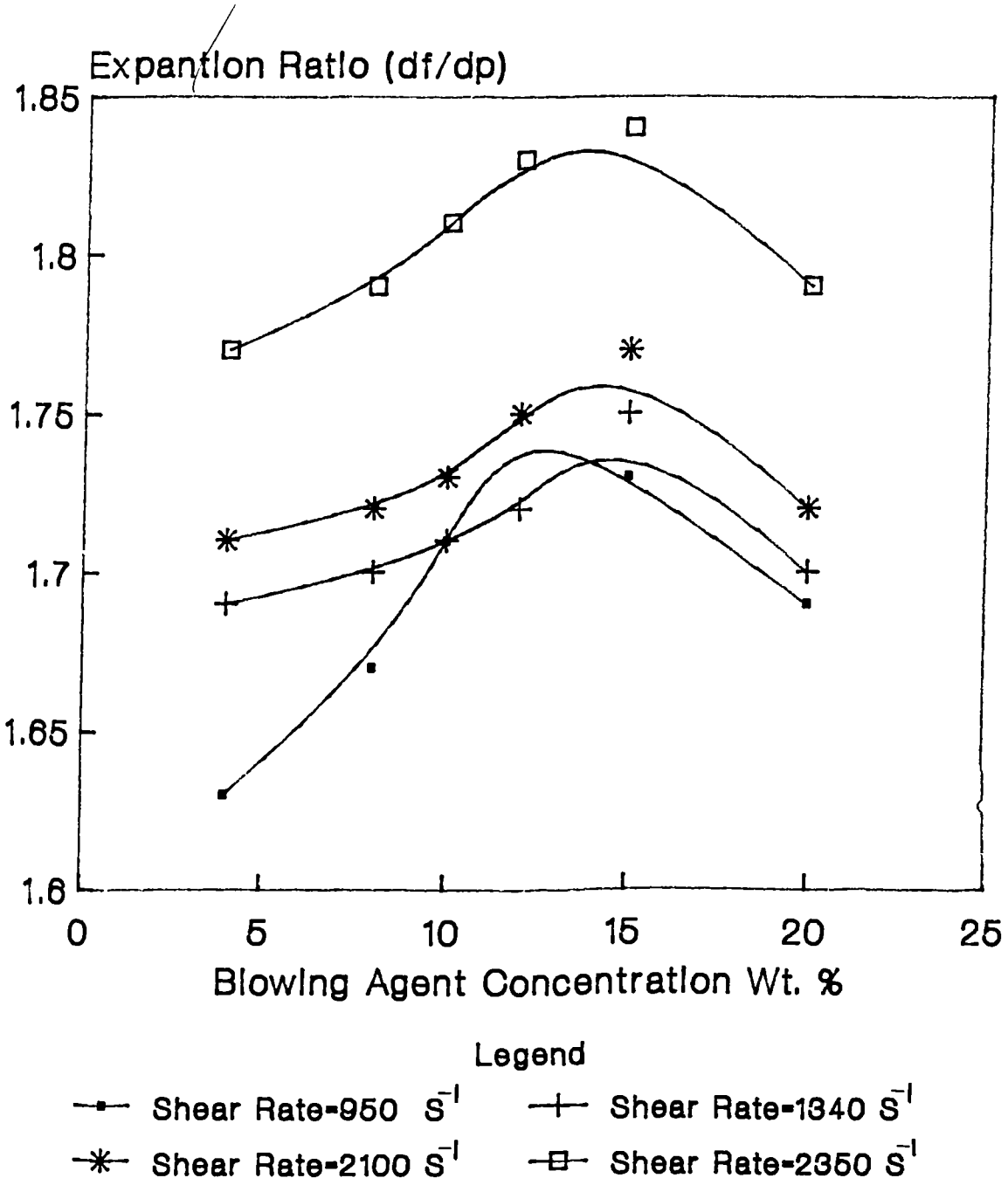

Figure 5.13. Relationship of expansion ratio and CBA concentration at various apparent shear rates for PP (GXM-43). Melt temperature 185°C.

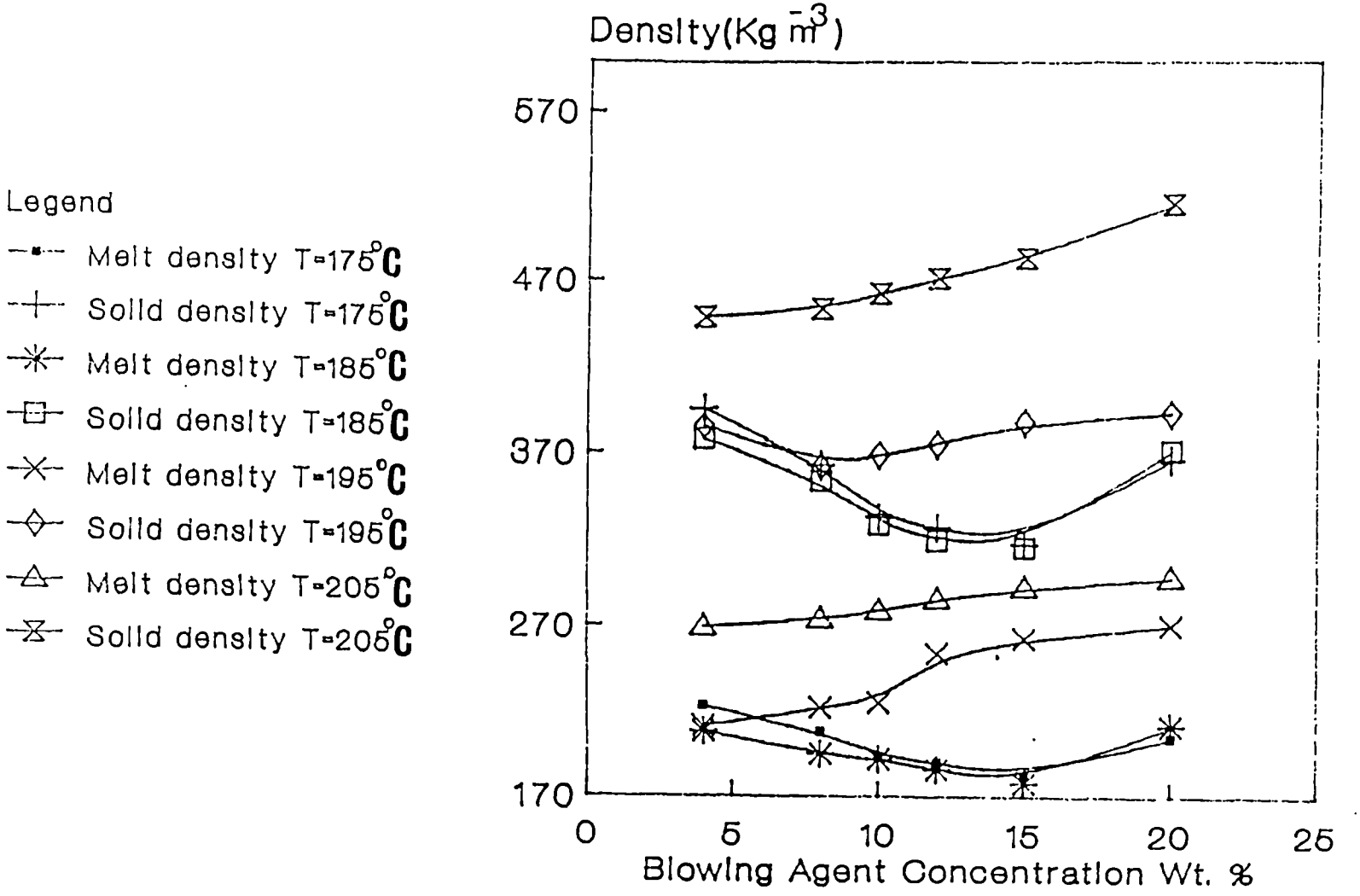

Figure 5.14. Relationship of PP (GXM-43) foam density and CBA concentration at various melt temperatures.

can be seen that at low melt temperature (175°C and 185°C), both the density in melt and solid state decreases with increasing blowing agent concentration, and it goes through a minimum at a blowing agent concentration of 15 wt%. But at temperatures higher than 185°C the density both in the melt and solid states, increases with increasing the blowing agent concentration. This is attributed to, not only the reduction in melt viscosity as the temperature is raised, but also to the lower efficiency of the chemical blowing agent (it was explained in previous section, at temperatures higher than 185°C, due to early activation of blowing agent in the barrel of extruder, less gas will be available in the die region, hence, the efficiency of chemical blowing agent is expected to drop, and also premature foaming would occur in the barrel). It should be pointed out on the average there is a 43% difference between the density in the melt and solid state, which still shows there is considerable cell collapse upon cooling.

5.4.5. Effects of Die Design Variables on the Foam Extrusion Characteristics of High Density Polyethylene

The foaming characteristics of high density polyethylene were investigated, using the same dies, which were designed for processing of polypropylene foam.

Tables 5.6-5.9 displays the effects of die entry angle on the axial pressure at various apparent shear rates, using a single screw extruder. As was expected, as the entry angle increases the pressure drop through the die decreases. It should be added that due to high entanglement and chain branching the melt viscosity of the high density polyethylene is far greater than polypropylene. Also due to the same reason, melt flow irregularities (i.e. melt fracture) noticed in the extrusion process, occurs at lower shear rate for polyethylene foam than for polypropylene foam. Also it should be mentioned that the melt disturbance with high density polyethylene foam is effected by the choice of die entry angle, melt temperature and blowing agent concentration, as can be seen from the results presented in Tables 5.6-5.9. These findings are in good agreement with the results obtained in the previous chapter. It should be pointed out that the relation of pressure drop within the die at different axial positions, for high density polyethylene(foamed and unfoamed) follows a fairly linear relationship as it is seen in Figures 5.15 and 5.16 respectively. It is interesting to compare the foregoing results with those of polypropylene foam presented in the Figure 5.5. One can clearly see that even at low shear rate the high density polyethylene shows a more linear pressure drop through the die as compare to polypro-

Table 5.6. Axial pressure profile of high density polyethylene(H11042) foam prepared at various screw speeds. L/D=0, Die entry angle 15°. Melt temperature 245°C. BAC=8 wt.%.

Screw Speed (rpm)	Shear Rate (S^{-1})	Axial Pressure* (MPa) P1	P2	P3	P4
10	910	7.584	6.894	6.550	6.205
20	1425	8.274	7.997	7.584	6.963
25 !	1789	8.618	8.204	7.756	7.239
30	2078	8.963	8.480	8.067	7.584
40	2411	9.307	8.874	8.342	8.135
50	3496	9.791	9.239	8.618	8.412

Table 5.7. Axial pressure profile of high density polyethylene(H11042) foam prepared at various screw speeds. L/D=0, die entry angle 30°, melt temperature 245°C.

Screw Speed (rpm)	Apparent Shear Rate (s^{-1})	Axial Pressure** (MPa) P1	P2	P3
10	955	7.722	7.039	6.756
20	1435	8.273	7.928	7.653
25 !	1798	8.687	8.173	7.791
30	2133	9.101	8.549	7.997
40	2496	9.514	8.963	8.549
50	3562	9.997	9.445	8.897

* and ** The axial distance from the die entrance are given in Figures 5.4.a and 5.4.b respectively.

! Melt disturbance began to appear.

Table 5.8. Axial pressure profile of high density polyethylene(H11042) foam prepared at various screw speeds. Die entry angle 45°, L/D=0, melt temperature 245°C, BAC=8 wt.%.

Screw Speed (rpm)	Apparent Shear Rate (S^{-1})	Axial Pressure* (MPa) P1	P2
10	962	7.722	7.308
20 !	1427	8.204	7.929
25	1812	8.756	8.342
30	2154	9.170	8.584
40	2514	9.584	9.032
50	3603	10.066	9.480

Table 5.9. Axial pressure profile of high density polyethylene(H11042) foam prepared at various screw speeds. Die entry angle 60°, L/D=0, melt temperature 245°C, BAC = 8 wt.%.

Screw Speed (rpm)	Apparent Shear Rate (S-1)	Axial Pressure** (MPa) P
10	1002	7.791
20 !	1442	8.274
25	1818	8.756
30	2183	9.238
40	2669	9.722
50	3657	10.135

* and ** The axial distance from the entrance are given in Figures 5.4.c and 5.4.d respectively.

! Melt disturbance began to appear.

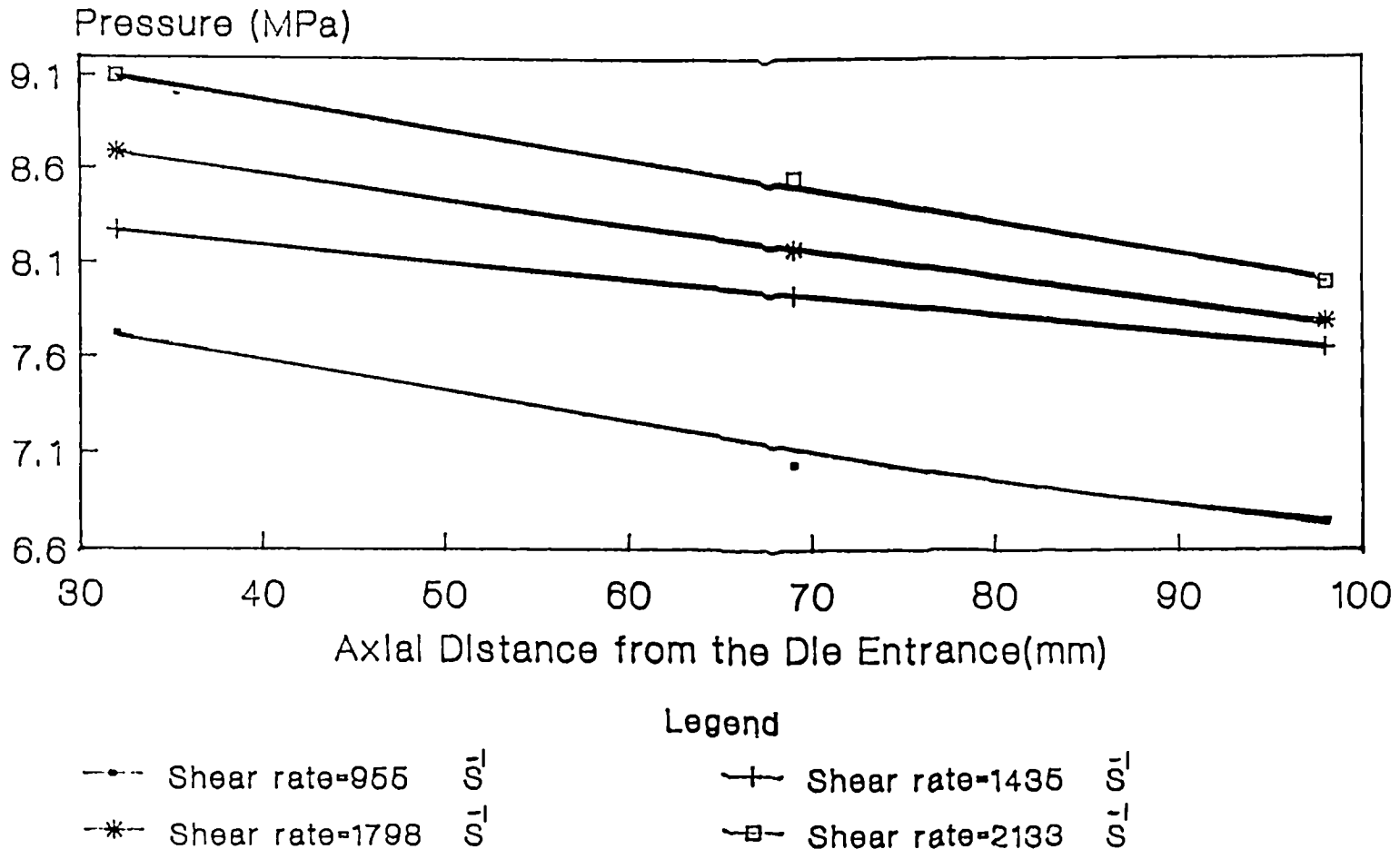

Figure 5.15. Pressure profile of HDPE (H11042) foam inside the die. Die entry angle=30°, L/D=0, CBA concentration=8 wt.%, melt temperature 245°C.

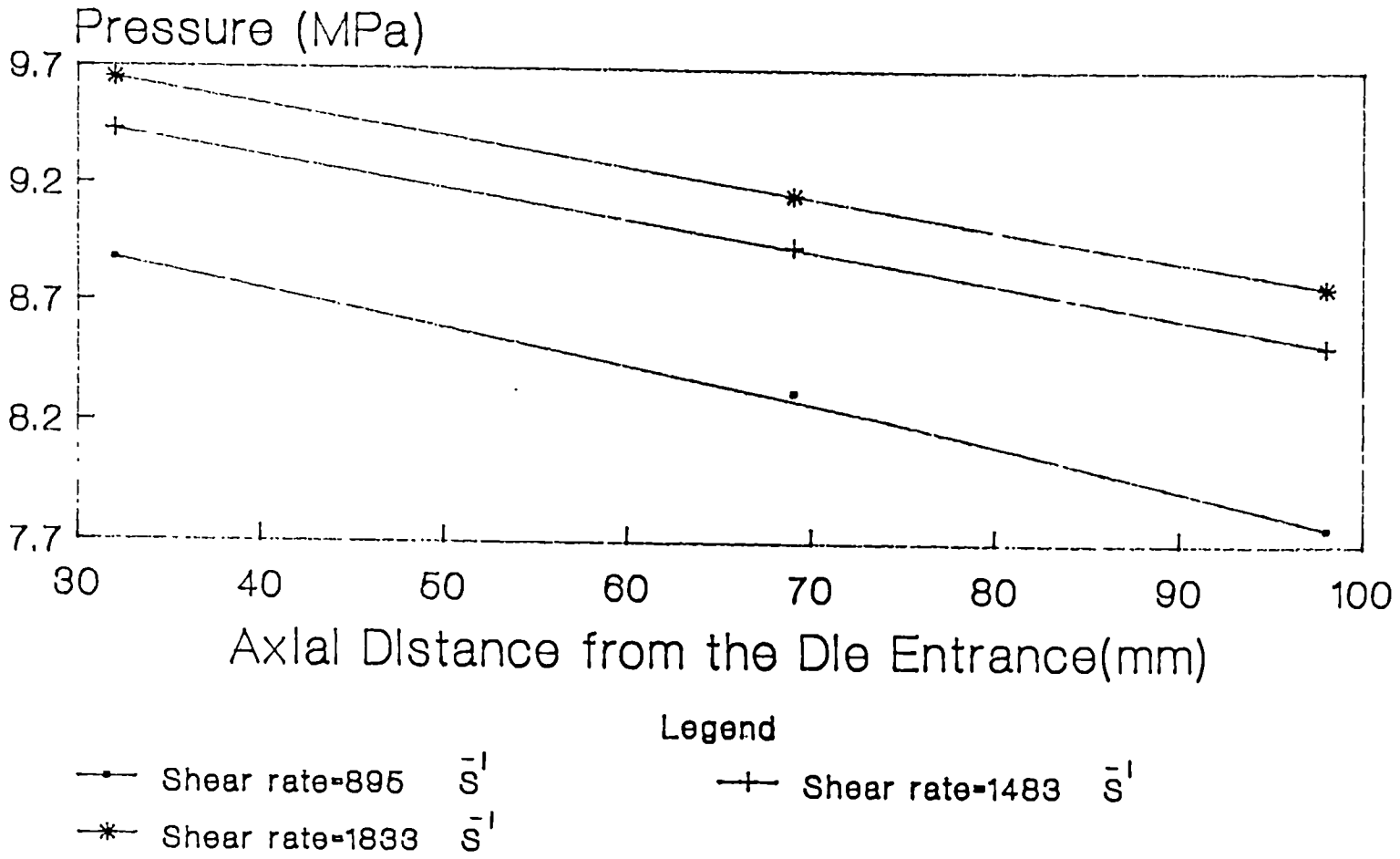

Figure 5.16. Pressure profile of HDPE (H11042) inside the die. Die entry angle 30°, L/D=0, melt temperature 245°C.

pylene foam. This suggest that, due to high pressure involved in processing of high density polyethylene foam, less premature foaming has taken place in the die than with processing of polypropylene foam.

The effect of L/D ratio on the expansion ratios of high density polyethylene at various shear rates has been investigated and these results are presented in Table 5.10. It is noteworthy that the expansion ratio decreases with increasing L/D ratio. This phenomenon is attributed to the longer relaxation time provided for molecular chains through a die with a high L/D ratio, which consequently, reduces the swelling ratio of the melt.

The effects of L/D ratio on the foam density (in the solid state) and open cell fraction of high density polyethylene foam are shown in Figures 5.17-5.18, respectively. Due to the same reasons mentioned above, the solid state density increases with increasing L/D ratio, whereas, the open cell fraction was slightly increased with higher L/D ratio.

From these results the die with entry angle of 30° and L/D ratio of zero is seen to give greater reduction in density and achievement of higher open cell porosity in high density polyethylene foam extrudate. Therefore, for the further studies in this section,

Table 5.10. Relation between expansion ratios of high density polyethylene foam prepared at various screw speeds. Die entry angle 30°, melt temperature 245°C, BAC = 8 wt.%.

L/D=0

Screw Speed (rpm)	Shear Rate (S^{-1})	Expansion Ratio (df/dp)
10	955	1.51
20	1435	1.54
25	1798	1.55
30	2133	1.57
40	2496	1.62
50	3562	Unstable melt

L/D=2

Screw Speed (rpm)	Shear Rate (S^{-1})	Expansion Ratio (df/dp)
10	928	1.46
20	1469	1.49
25	1833	1.50
30	2188	1.53
40	2525	1.56
50	3632	Unstable melt

Table 5.10. Cont.,

L/D=4

Screw Speed (rpm)	Shear Rate (S^{-1})	Expansion Ratio (df/dp)
10	978	1.43
20	1455	1.45
25	1769	1.48
30	2141	1.52
40	2532	Unstable melt
50	3589	Unstable melt

L/D= 6

Screw Speed (rpm)	Shear Rate (S^{-1})	Expansion Ratio (df/dp)
10	948	1.40
20	1473	1.43
25	1845	1.44
30	2176	1.46
40	2554	Unstable melt
50	3596	Unstable melt

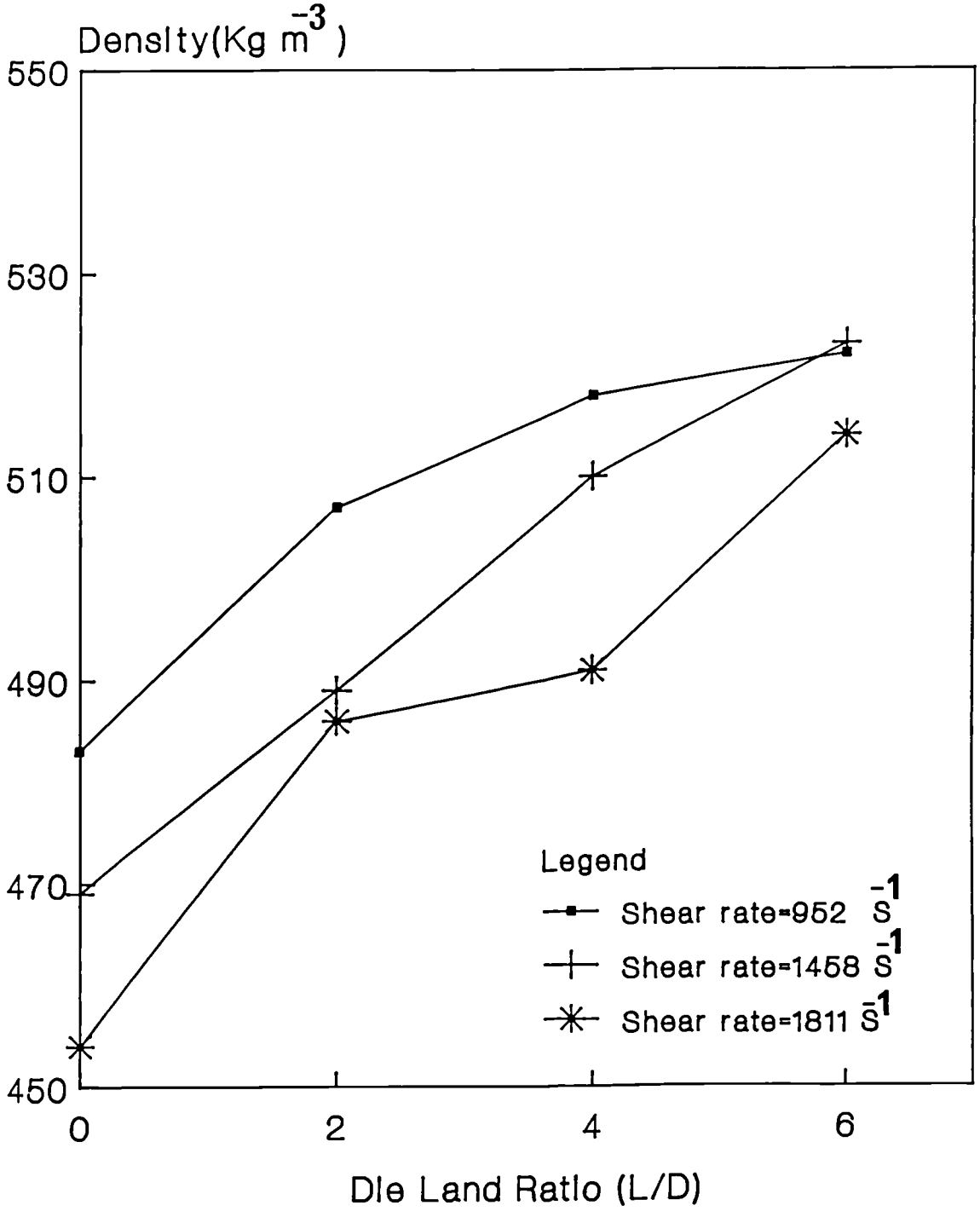

Figure 5.17. Relationship of density (solid state) and L/D ratio for HDPE (H11042) containing 8 wt.% CBA at various apparent shear rates.

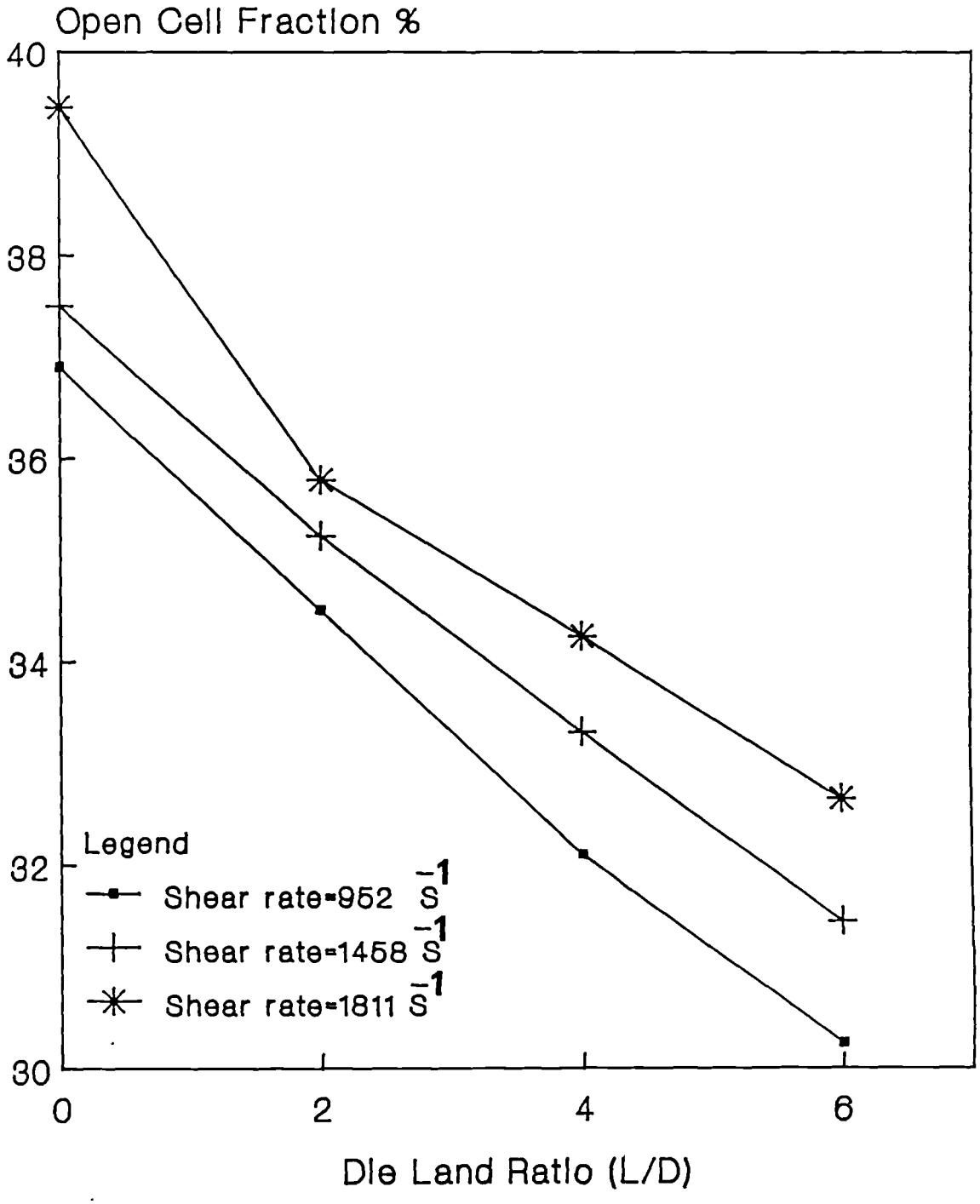

Figure 5.18. Relationship of open cell fraction and L/D ratio for HDPE (H11042) containing 8 wt.% CBA, at various apparent shear rates.

the die with an entry angle of 30° and L/D ratio of zero has been used.

5.4.6. Effects of Melt Temperature on the Foam Extrusion Characteristics of High Density Polyethylene

Figure 5.19 demonstrate the effect of melt temperature on the expansion ratio of high density polyethylene prepared at various apparent shear rates. It should be pointed out that, the apparent shear rates specified in Figure 5.19 and Figure 5.20 are the average values (since a small variation in screw speed could lead to different output, therefore, it was difficult if not impossible to set the extruder at the same screw speed for the 4 different L/D ratios). The actual values of the shear rates could be $\pm 30\ S^{-1}$. Figure 5.19 shows that the expansion ratio increases with the melt temperature and then around melt temperature of 255-265°C (depending on the shear rate) it goes through a maximum, and then decreases with further increase of melt temperature. Also it should be pointed out, for each shear rate, the temperature of the die and the screw in the last zone were altered, in order to keep the melt temperature at a fairly constant value (± 4°C). It should be added that, the results were reproducible, and standard deviation was found to lie between 0.014-0.018. From the results

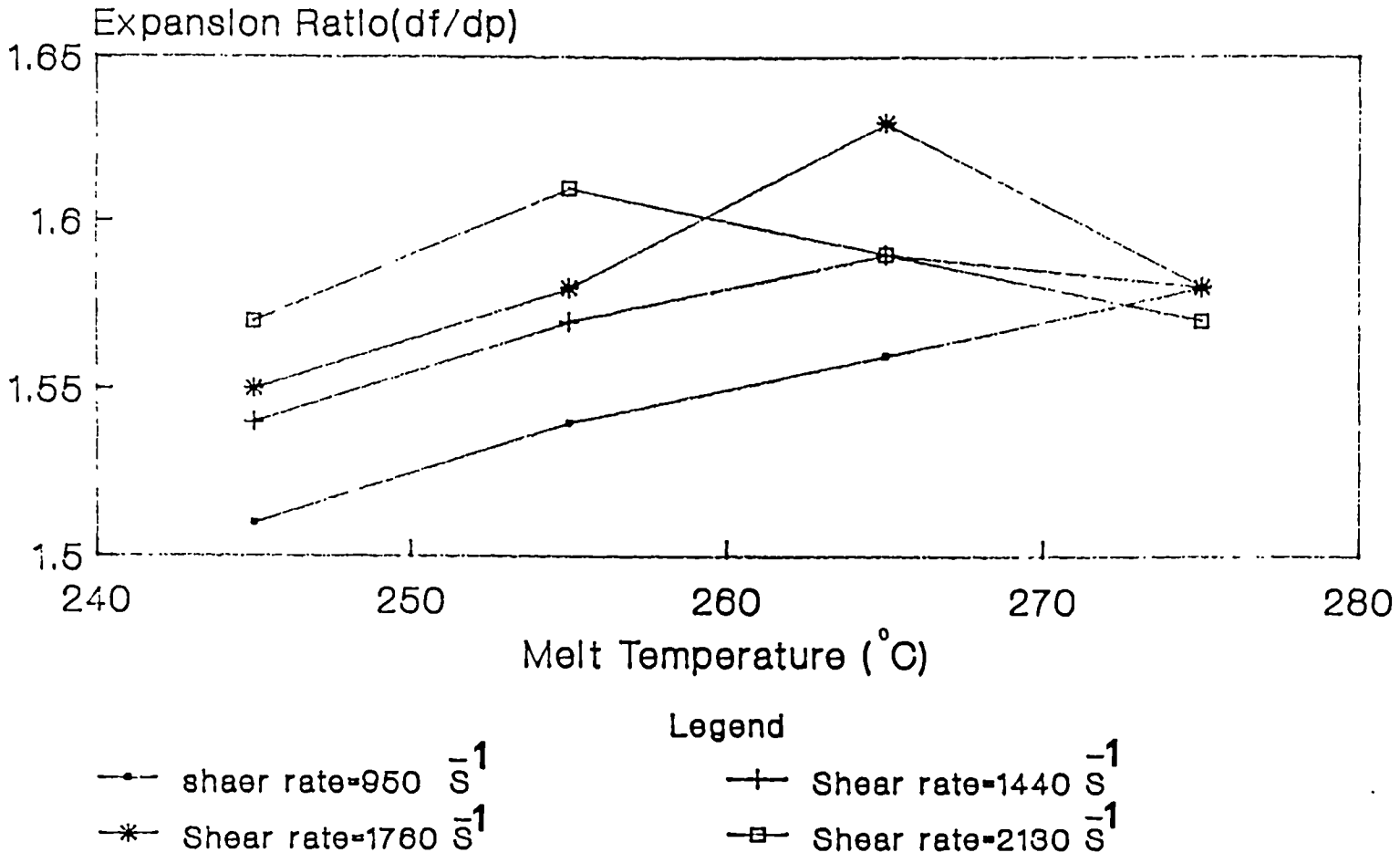

Figure 5.19. Relationship of expansion ratio and melt temperature for HDPE containing 8 wt.% CBA.

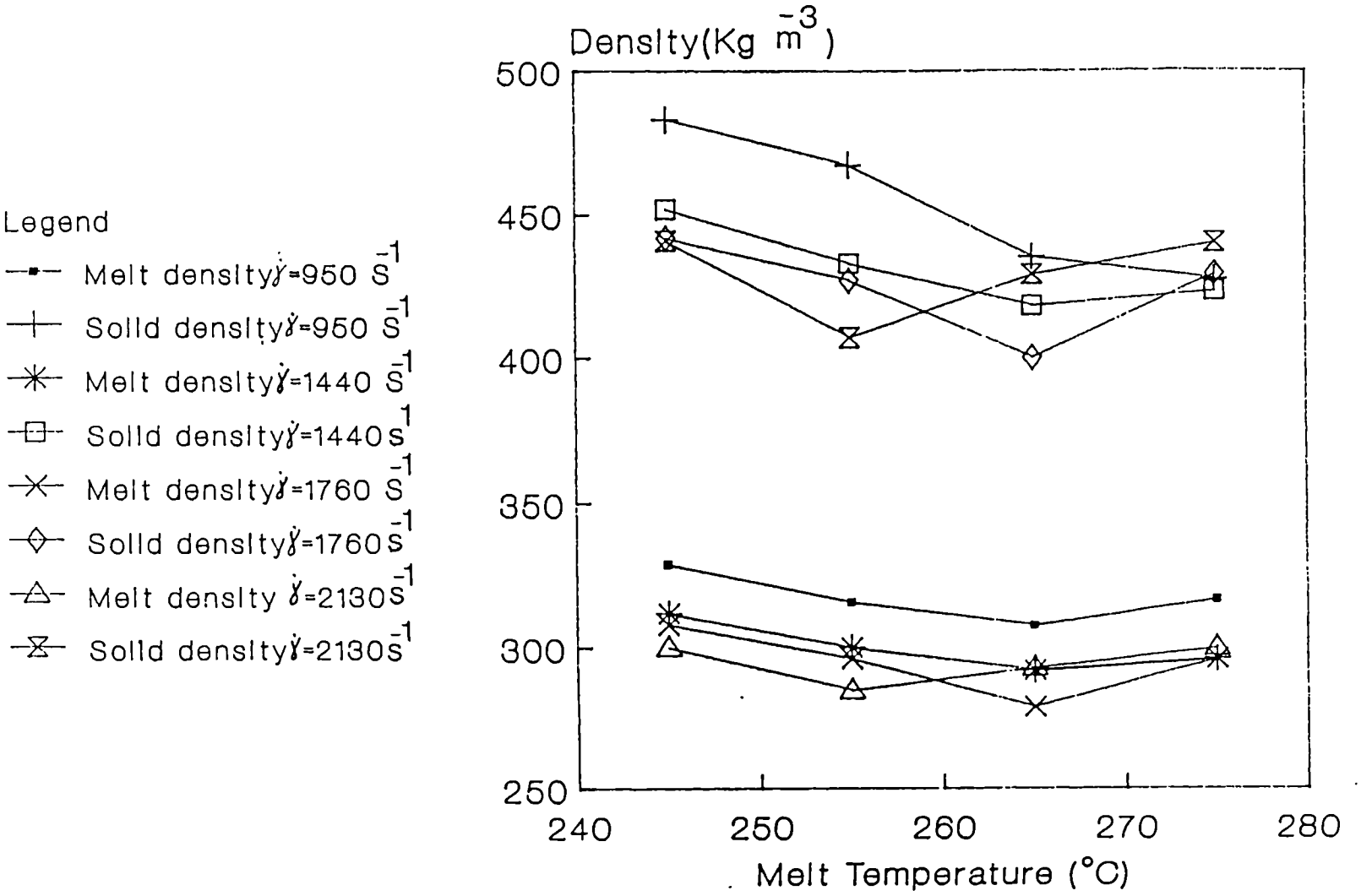

Figure 5.20. Relationship of density of HDPE foam with melt temperature at various apparent shear rates.

described above one can clearly see how the processing conditions (mainly the melt temperature and pressure) are influencing the expansion ratio of the foamed polymer. Also it is interesting to compare the above mentioned results with those for polypropylene foam, presented in Table 5.6. Clearly one can see, the expansion ratio of polypropylene foam is far greater than those of high density polyethylene which shows the dependency of foam characteristics on the melt strength (hence, melt viscosity) and molecular structure of polymeric material.

The density of extrudated foam in the melt and solid states have been measured and their findings are presented in Figure 5.20. It is illustrated that the relation of the density with respect to melt temperature is similar to those of expansion ratio which had been described previously. Also it should be mentioned that, the density of the foamed material in the solid state is around 31% greater than its density in the melt stage. Therefore, this shows, the extent of cell collapse in the high density polyethylene is less than that observed for polypropylene foam.

5.4.7. Effects of MFI on the Foam Extrusion Characteristics of High Density Polyethylene

Several grades of high density polyethylene with

different melt flow indices were extruded on a single screw extruder and the effects of melt viscosity on the density and open cell fraction of the foamed material was recorded.

Figure 5.21 displays the change in foam density, in the melt and solid states, for different grades of high density polyethylene, at various shear rates. In general it is seen that the density (in the solid state) of foamed polymer decreases with increasing MFI and it reaches to a minimum level at MFI=11 g $(10min.)^{-1}$, and increases again for the grade which has MFI=18 g $(10min.)^{-1}$. On the other other hand the density in melt stage continuously drop with increase of MFI of the virgin resin. The comparison of the density of these grades of high density polyethylene in the melt and solid conditions suggests that, the optimum density reduction would be achieved when the melt viscosity is optimised and its value lies between the melt viscosity of the resins with MFI indices of 11 and 18 g$(10\ min)^{-1}$. Also it should be added that with increasing temperature, the density (in solid state) decreased (except for the grade of Natene 54180 MFI of 18 g$(10\ min.)^{-1}$ and reaches to a minimum value at melt temperature 265° C, beyond which the density increases with further increase of the temperature (see Figure 5.21). It should be pointed out, due to the high temperature require for processing of high density

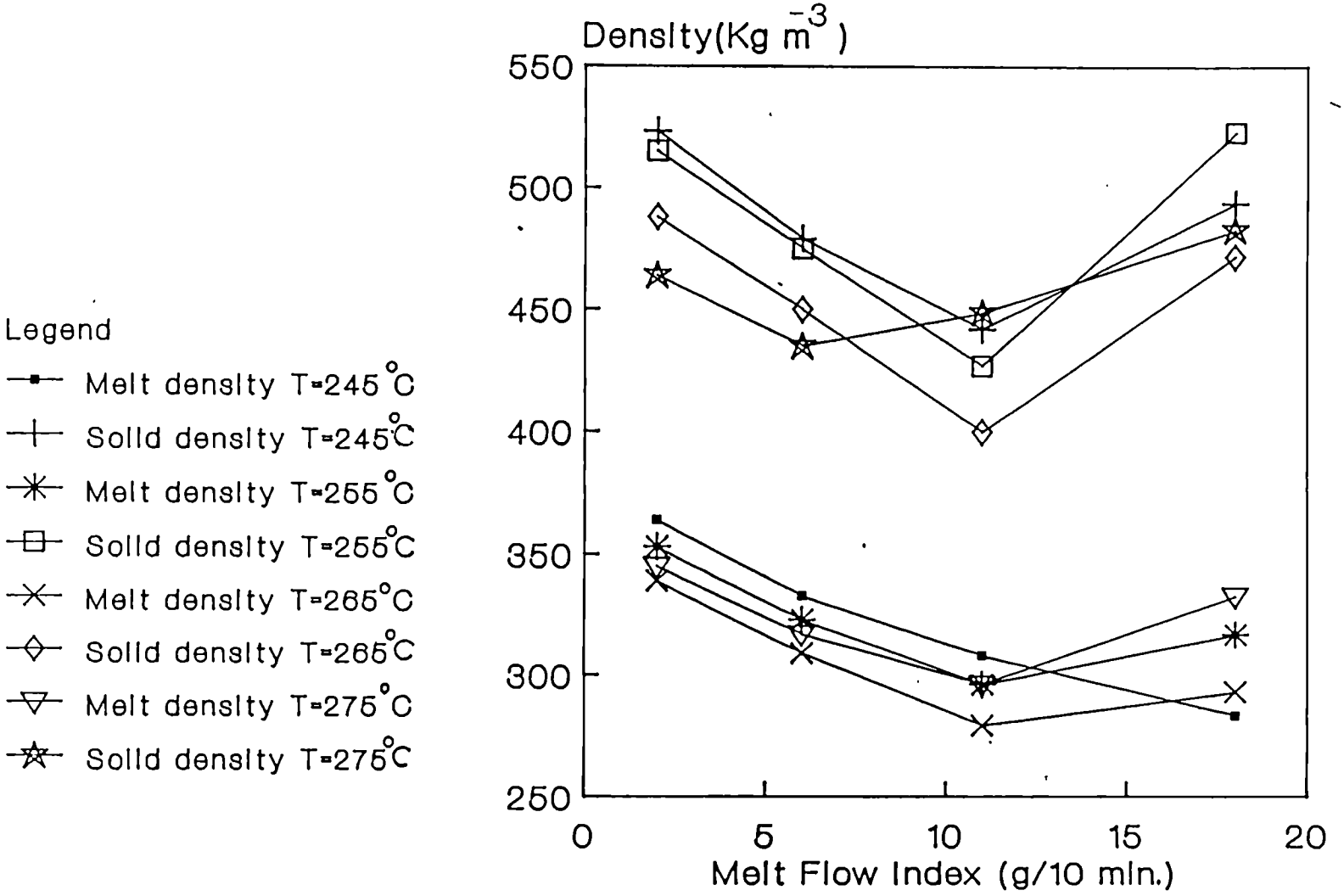

Figure 5.21. Relationship of MFI and density of HDPE containing 8 wt.% CBA.

polyethylene, the efficiency of the blowing agent would be much lower than when the same blowing agent is used with polypropylene. Therefore, the density of foamed specimens in both melt and solid conditions are far greater than those observed for polypropylene foam.

The open cell fraction for all these grades of high density polyethylene was investigated and their findings are presented in Figure 5.22. As it can be seen the open cell fraction of all grades of high density polyethylene foam (at various processing temperature), increases with increasing MFI of the virgin resin and goes through a maximum at MFI of 11 g(10min)$^{-1}$, except for the resin with MFI of 18 g(10 min)$^{-1}$ (Natene 54180) at melt processing temperature of 245°C. This phenomenon is due to drop in melt viscosity of the polymer with increasing the melt temperature, which promote the growth of the bubbles within the melt. It should be added further increase in melt temperature will result a drop in the melt strength of the material and promote the cell drainage, hence, the cells will collapse more readily.

5.4.8. Effects of Chemical Blowing Agent Concentration on the Foam Extrusion Characteristics of High Density Polyethylene

The grade of polymer which showed optimum density

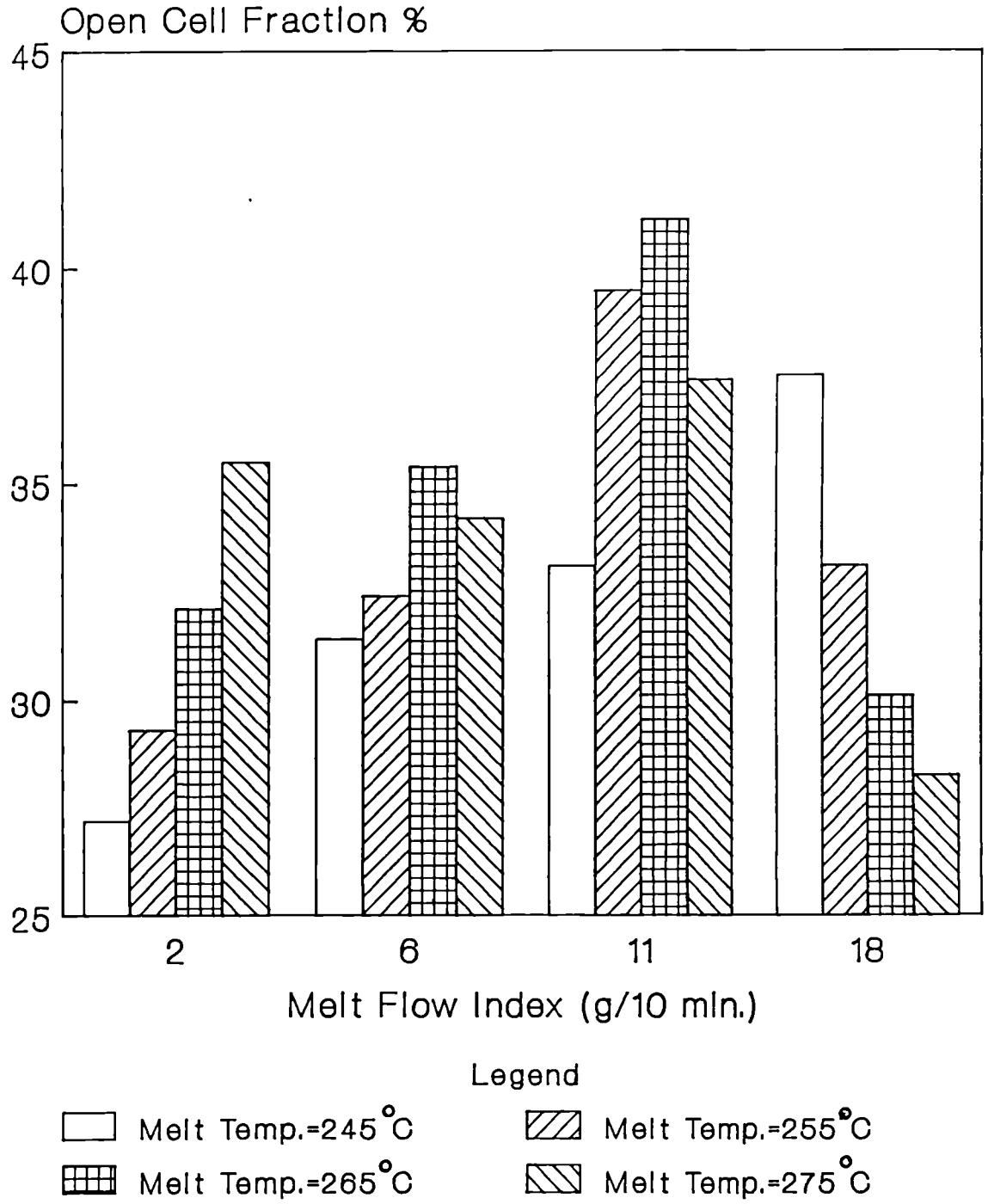

Figure 5.22. Relationship of open cell fraction and MFI of HDPE containing 8 wt.% CBA. Die entry angle 30°.

reduction (Rigidex H11042 MFI=11 g (10 min.)$^{-1}$ was chosen for further evaluation and its expansion ratio was determined with different blowing agent concentrations and at various shear rates. The findings of these results are presented in Figure 5.23. It is clearly seen that as a consequence of over foaming of the melt, at high blowing agent concentrations, the expansion ratio of high density polyethylene foam has been dropped. This is due to premature foaming together with a drop in melt viscosity of the polymeric material, which leads to collapse of the cell walls as soon as the melt emerge from the die exit.

The measurement of density (in the solid state) passes through a maximum at blowing agent concentration of 15 wt.% and decreases with further increase of blowing agent, on the other hand open cell fraction exhibit similar trend as those of expansion ratio, as concentration of blowing agent is changed (Figures 5.24 and 5.25 respectively. It seen that the drop in melt viscosity of the foamed polymer, as well as super saturation of the melt (at high blowing agent concentration) have resulted in premature foaming and collapse of the cell walls prior to solidification.

It has been shown that the foam characteristics are strongly affected by die design (entry angle and die land length), melt pressure, melt temperature, MFI of

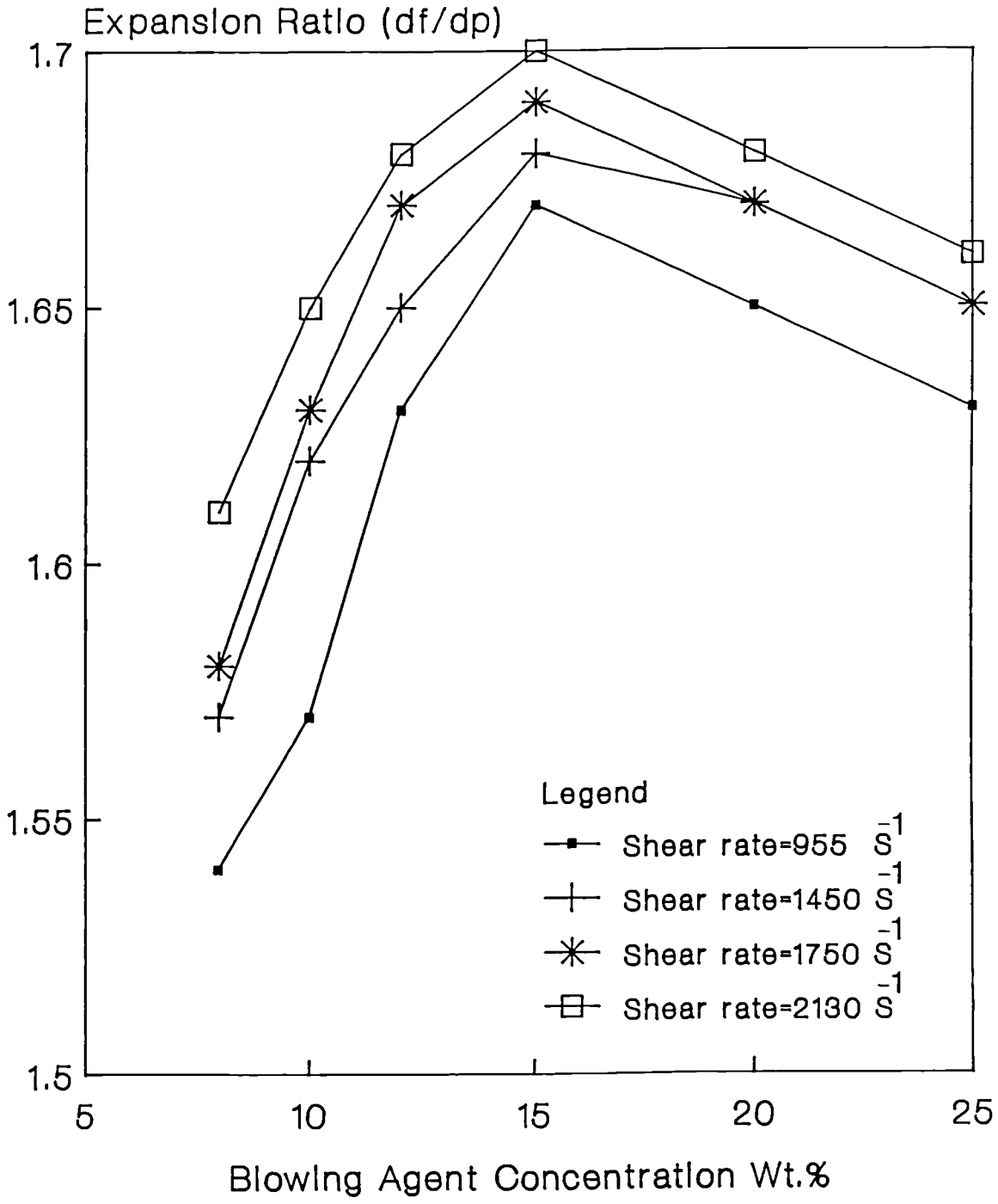

Figure 5.23. Relationship of expansion ratio and CBA concentration for HDPE foam. Melt temperature 255°C.

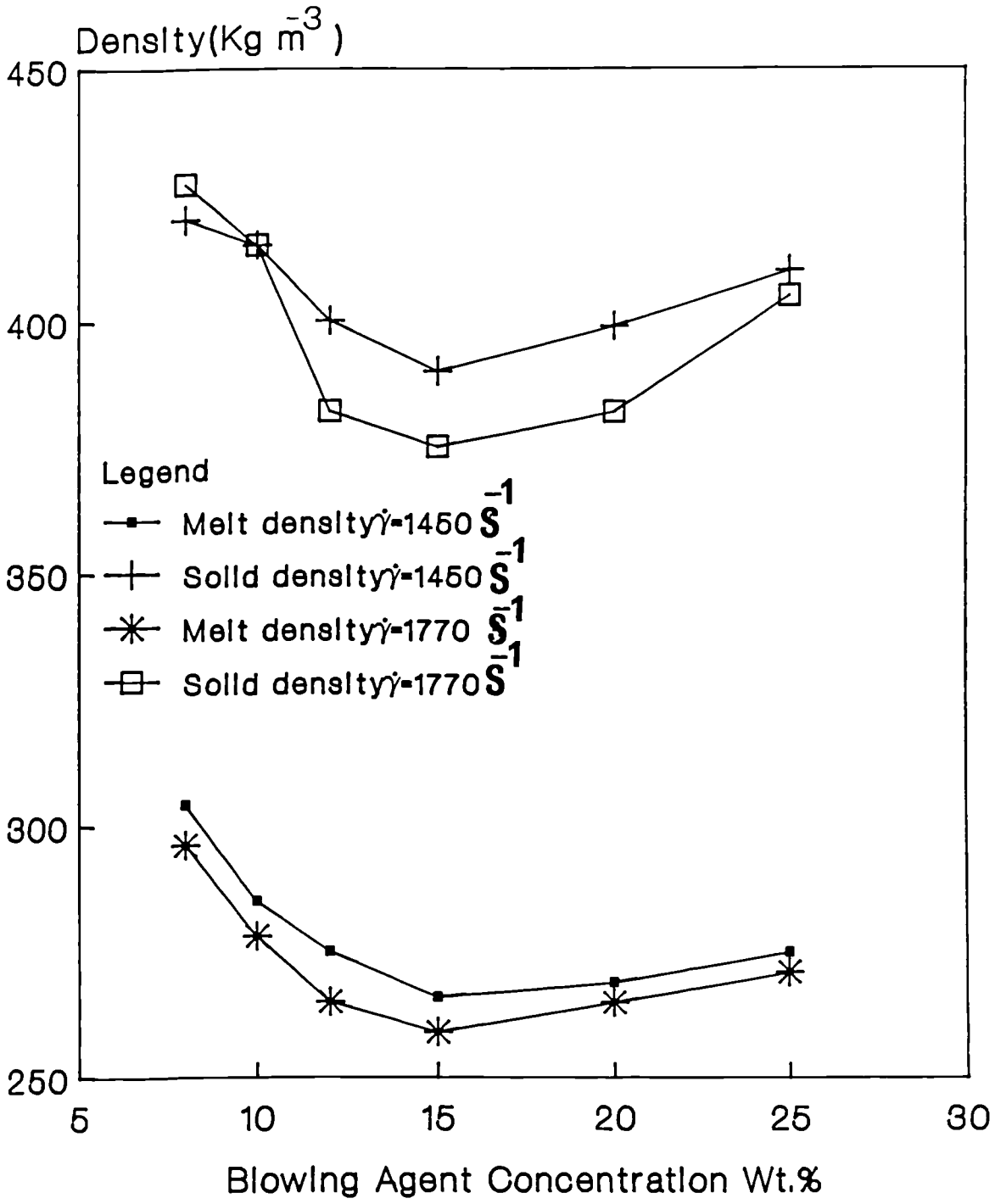

Figure 5.24. Relationship of CBA concentration and density of HDPE foam at various apparent shear rates. Melt temperature 255°C.

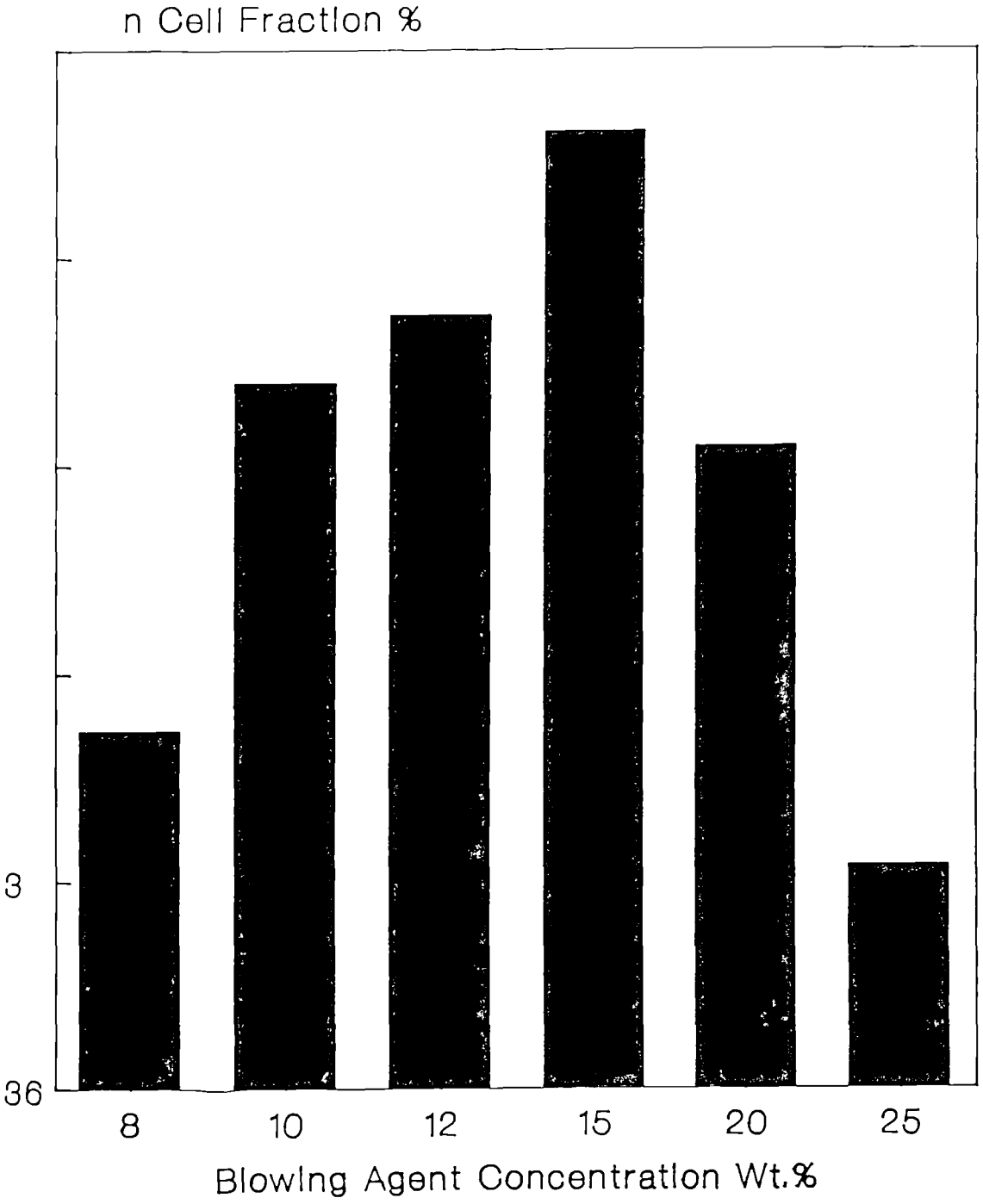

Figure 5.25. Relationship of CBA concentration and open cell fraction of HDPE foam. Apparent shear rate 1770 S^{-1}.

material, and gas blowing agent concentration. In all cases it was concluded in order to prevent premature foaming, the pressure should be maintained on the melt in the die region. This can be achieved by processing the material with a die angle of 45° with Polypropylene, or 30° in the case of high density polyethylene. Also it was shown for achievement of low density and high open cell fraction L/D ratios of zero and two are most suitable in high density polyethylene and polypropylene foam respectively.

Melt flow index also strongly affected the maximum reduction in density and open cell fraction in extruded foam. From the six different grades of polypropylene and four grades of high density polyethylene used, the grades with melt flow index of 9 and 11 $g(10min.)^{-1}$, were found to give optimum reduction in density and high fraction of open cell porosity. But still the density of these extrudated foam in solid state is far greater than their density in the melt condition. As was discussed earlier, this is mainly due to collapse of cell walls which is the consequence of low melt strength of the material, allowing premature foaming inside the die. It is consider that the melt strength of the material could be enhanced by physical blending of polypropylene and high density polyethylene. To this end, the PP(GXM-43

MFI=9 g(10 min)$^{-1}$ and HDPE (H11042 MFI=11 g(10 min)$^{-1}$, were blended and extruded through a die entry angle of 45° and with L/D ratio of 2 at various melt temperatures, pressures and blowing agent concentration. The findings of this investigation are presented in the following section.

5.4.9. Effects of Melt Temperature on Extrusion Characteristics of Binary Blends of PP/HDPE Foam

The two grades of polypropylene (GXM-43) and high density polyethylene (H11042) were physically melt blended in a co-rotating screw extruder. The extrudate was granulated, and then tumbled mixed with chemical blowing agent. The effects of processing conditions on density and open cell content were determined on foam prepared using a single screw extruder. The specification of the extruder is given in Table 3.3. The findings of this investigation are listed below.

Figures 5.26 and 5.27 display the effects of melt temperature and apparent shear rate on the expansion ratio, for various blends of polypropylene and high density polyethylene. As it is noticed, the expansion ratio increases with increasing the concentration of polypropylene in the blend and then decreases when polypropylene concentration is at 100%. It should be

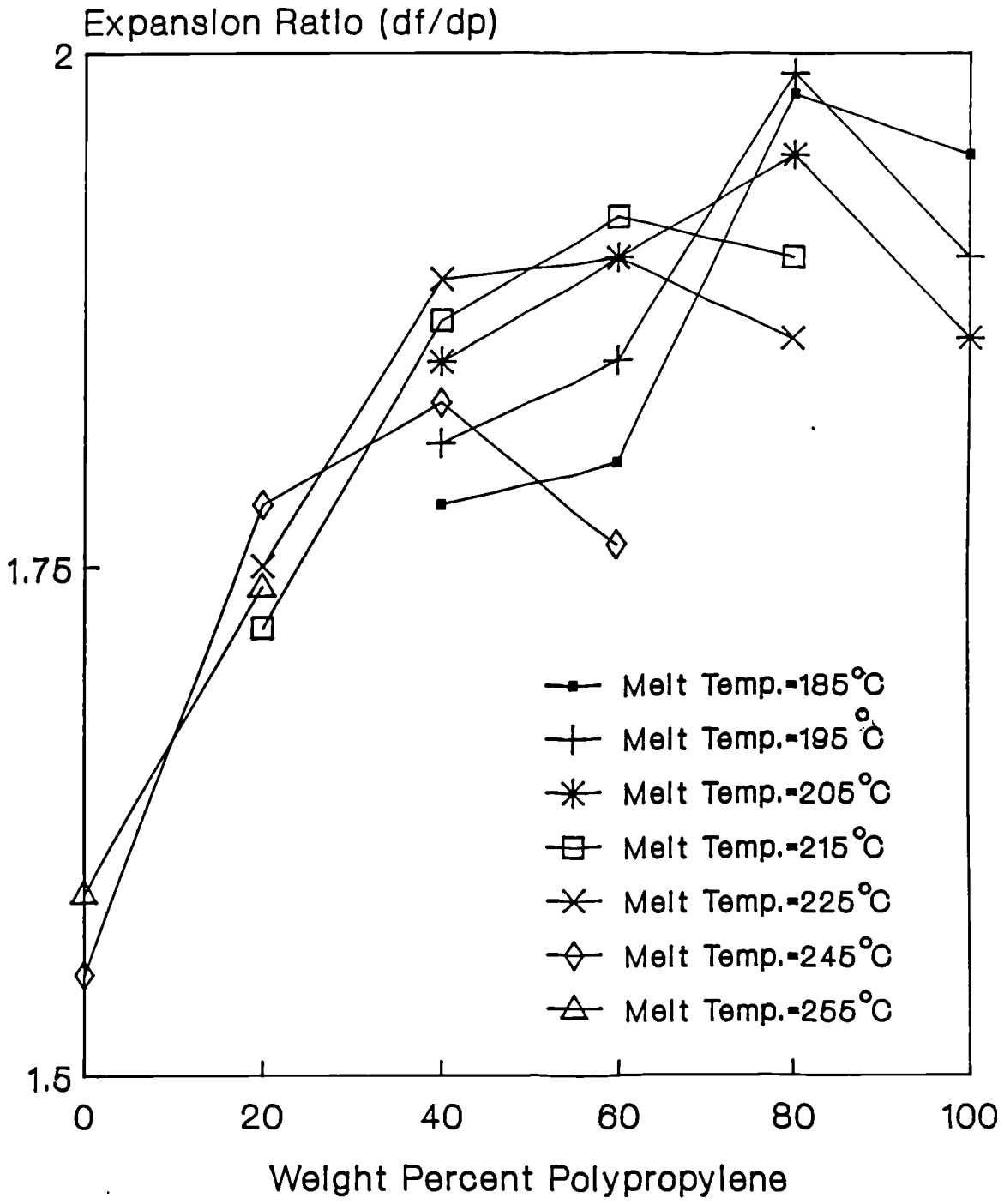

Figure 5.26. Relationship of expansion ratio with concentration of PP in binary blends of PP/HDPE foam. CBA concentration 8 wt.%, L/D=2, die entry angle 45°.

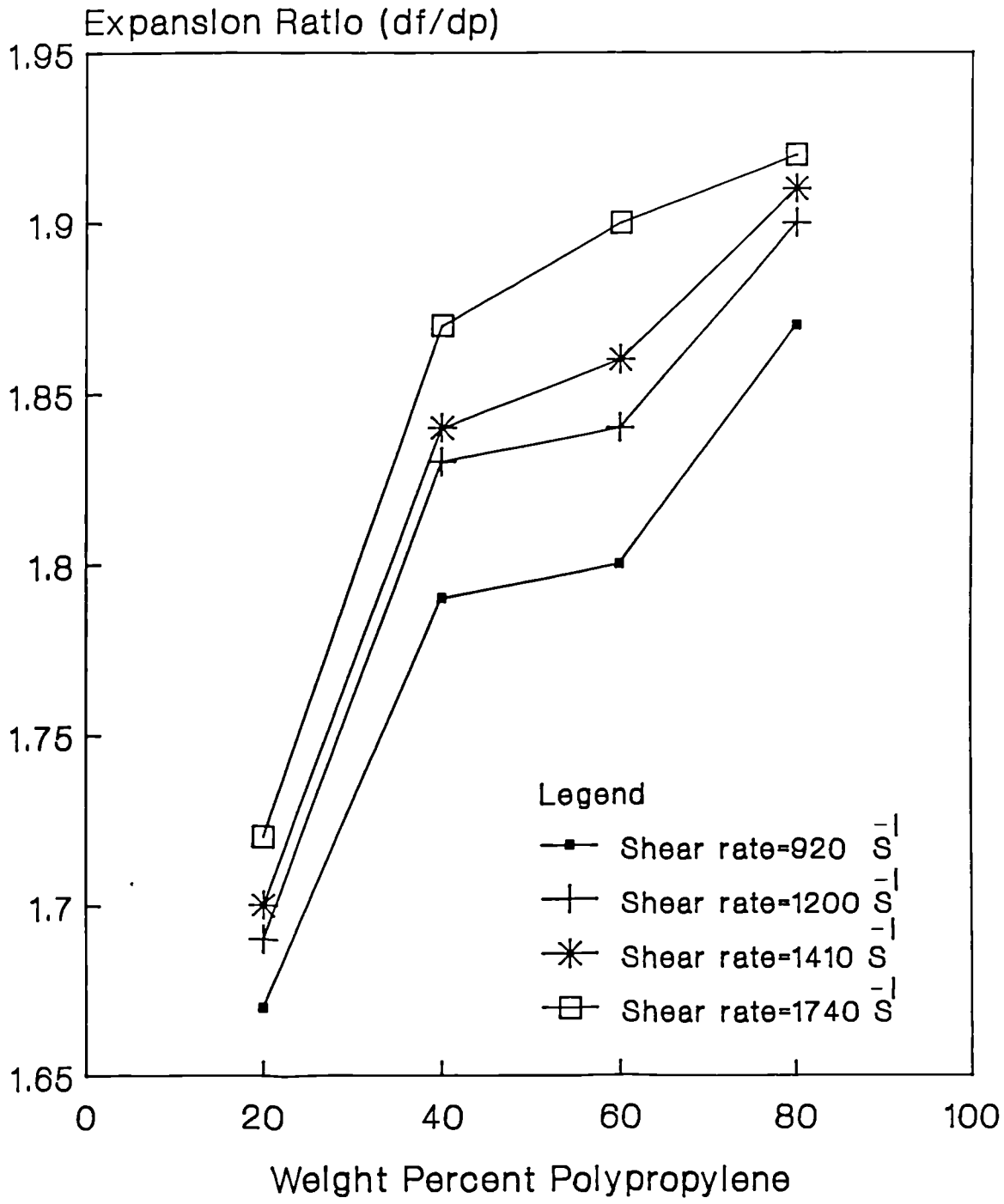

Figure 5.27. Relationship of expansion ratio and concentration of PP in binary blends of PP/HDPE foam. CBA concentration 8 wt.%, die entry angle 45°.

stated that the concentration at which the expansion ratio goes through a maximum depends on melt temperature.

The effect of melt temperature on the density of the foam, in both the melt and the solid states, has been recorded and their findings are presented in Figure 5.28. Several interesting points can be deduced from this figure. Firstly, it is evident that the density (in the melt and solid states) decreased with increasing polypropylene concentration in the blend and it goes through a minimum at the ratio of 80/20 PP/HDPE, and then increases with increasing high density polyethylene concentration. This effect is attributed to the fact that below a blend ratio of 80/20 PP/HDPE, the melt strength of the material is low, and upon cooling some of the cell walls collapse resulting in as much as of 43% difference between density in the melt and the solid states. However, above this blend ratio even though the difference in the density in molten and solid state is lower than 43% but due to a higher melt viscosity, the resistance to expansion is greater and therefore some of the cells are suppressed and were not allowed to fully develop. Secondly, at melt temperatures higher than 195°C, one can see that with increase of PP concentration, the reduction in density (in melt stage) is less as compare to melt

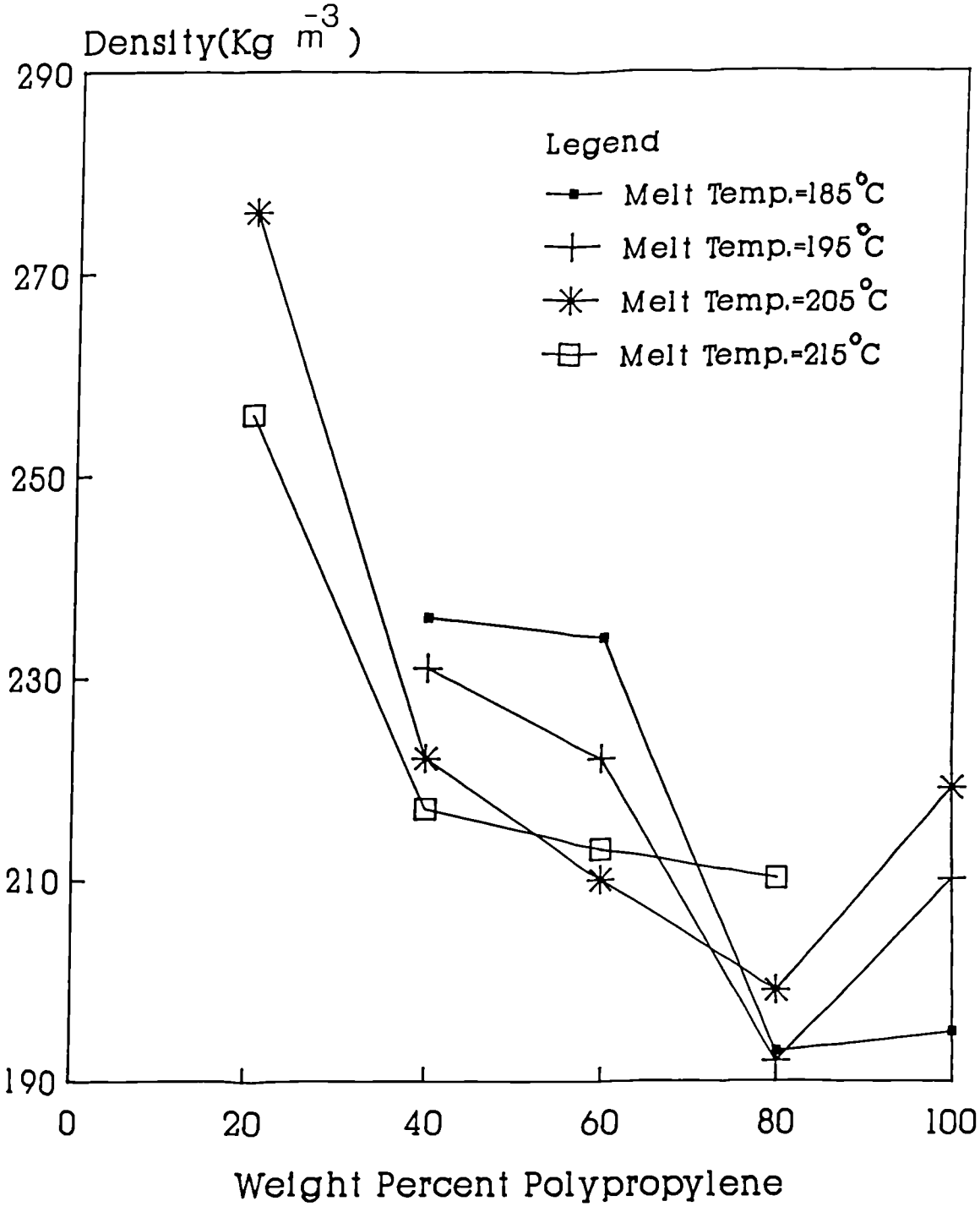

Figure 5.28.a Relationship of density (melt state) and PP concentration in binary blends of PP/HDPE foam.

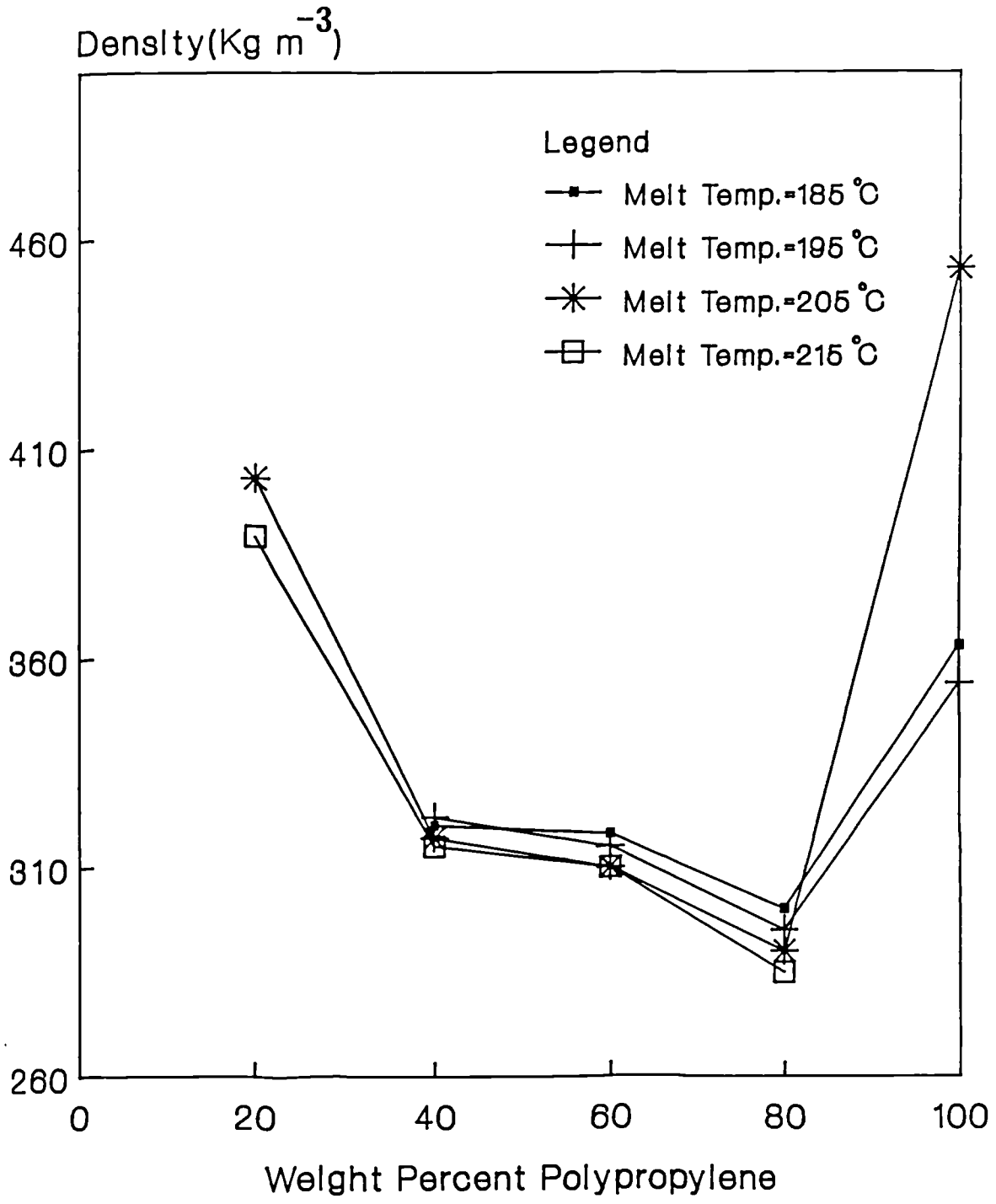

Figure 5.28.b. Relationship of density (solid state) and concentration of PP in binary blends of PP/HDPE foam.

temperatures of 185-195°C. This phenomenon is due to decrease in melt viscosity together with premature foaming of the melt in the die region, resulting in collapse of the bubbles as the melt emerges from the die exit.

Results for open cell fraction determined at ratios of PP/HDPE blend and at different melt temperatures are presented in Figure 5.29. Again as it is noticed the open cell fraction maximised at blend ratio of 80/20 and 40/60 PP/HDPE (depending on the melt temperature). This demonstrate that although the cell walls have ruptured, they still have enough strength to withstand the stresses exerted on them upon cooling.

5.4.10. Effects of Chemical Blowing Agent Concentration on Foaming Characteristics of Binary Blends of PP/HDPE

The variation of density in both molten and solid states and also open cell fraction of the extruded foam prepared using various blowing agent concentrations and polyolefin blend ratios have been studied and their results are displayed in Figures 5.30-5.31, respectively. As long as the blowing agent remains dissolved in a molten polymer over the range of temperatures studied, an increase in its concentration or an increase in melt temperature decreases the viscosity of the mixture,

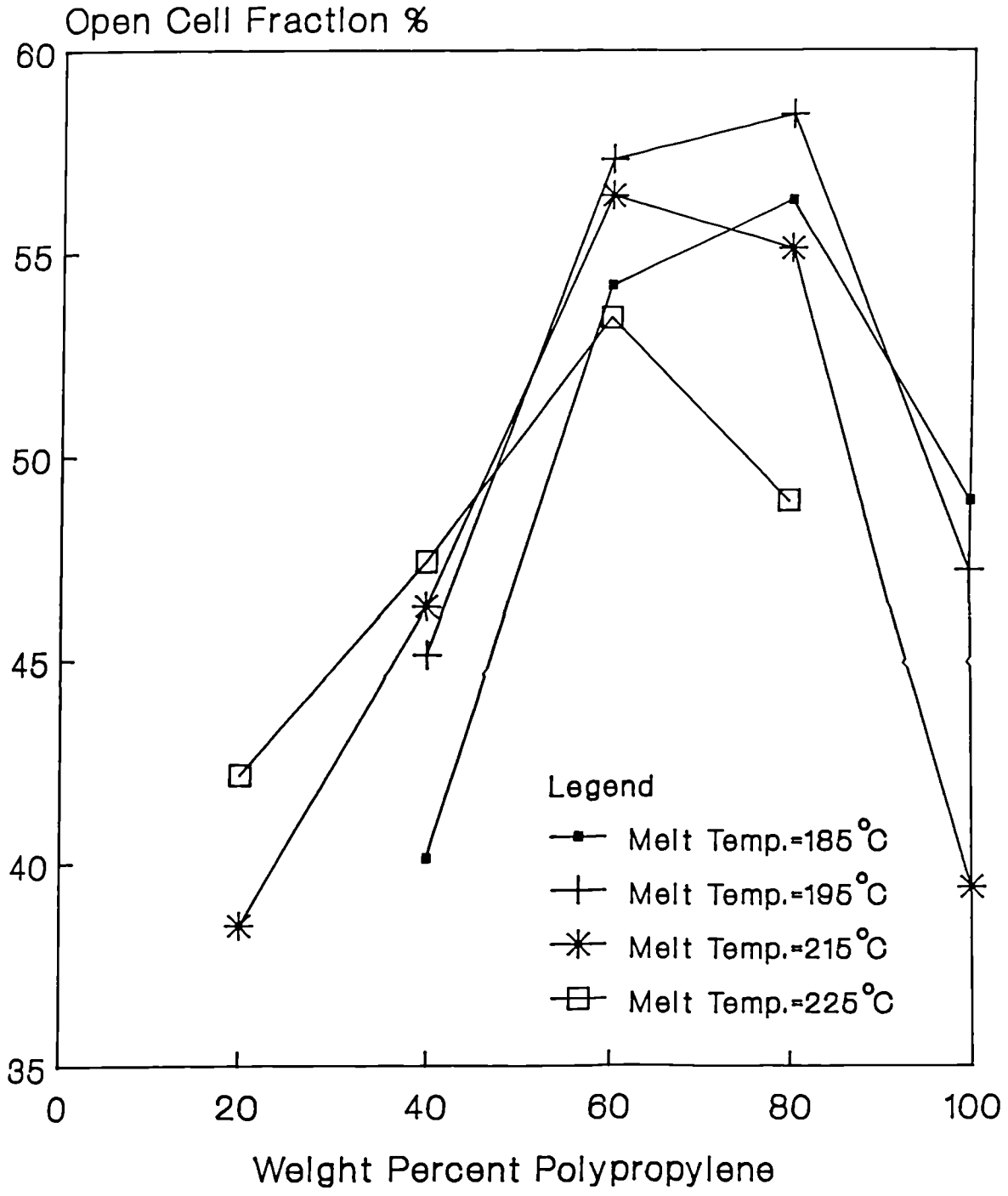

Figure 5.29. Relationship of open cell fraction and concentration of PP in binary blends of PP/HDPE foam. CBA concentration 8 wt.%.

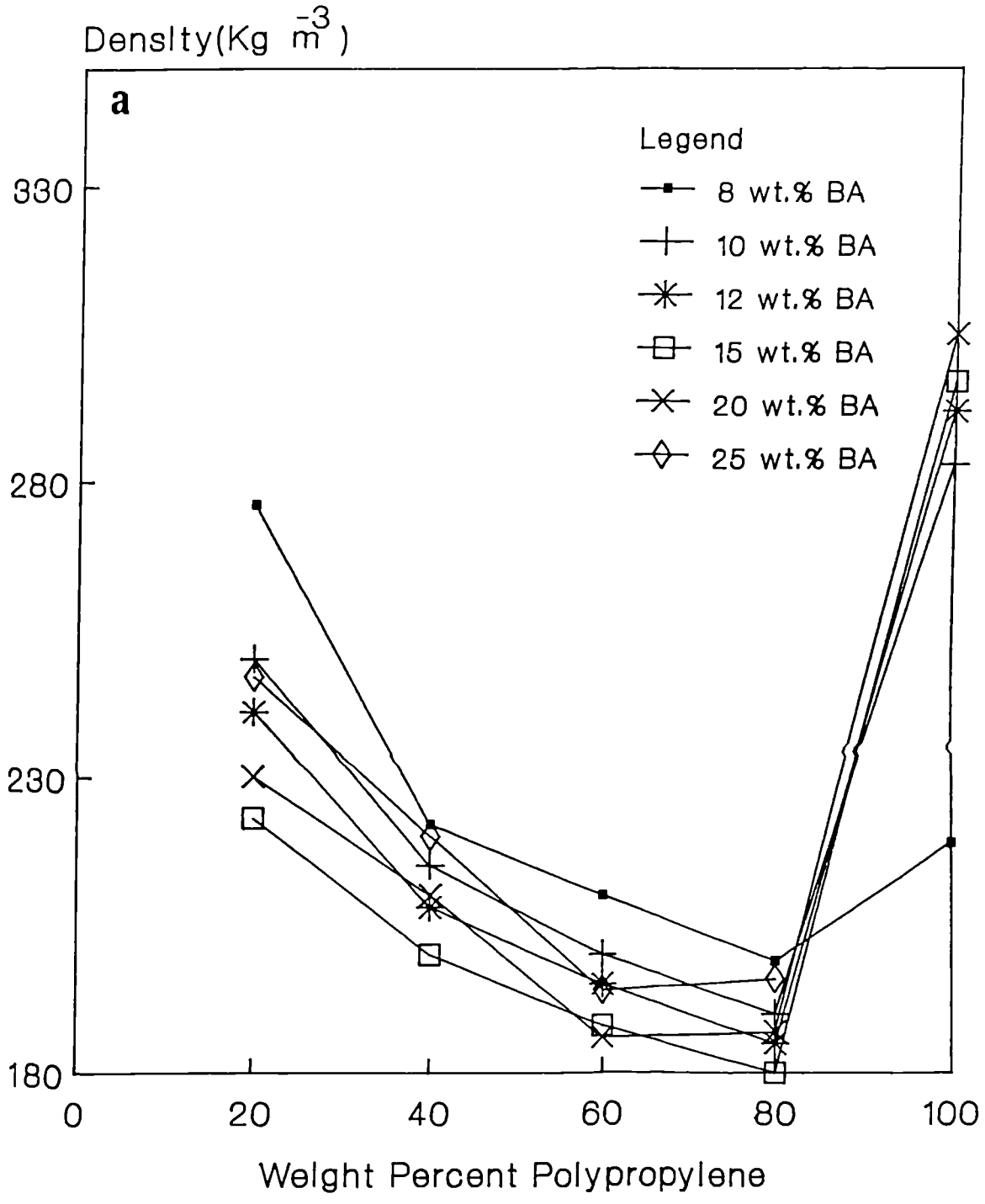

Figure 5.30. Relationship of density and CBA concentration in PP/HDPE foam. a) Melt density b)solid state density.

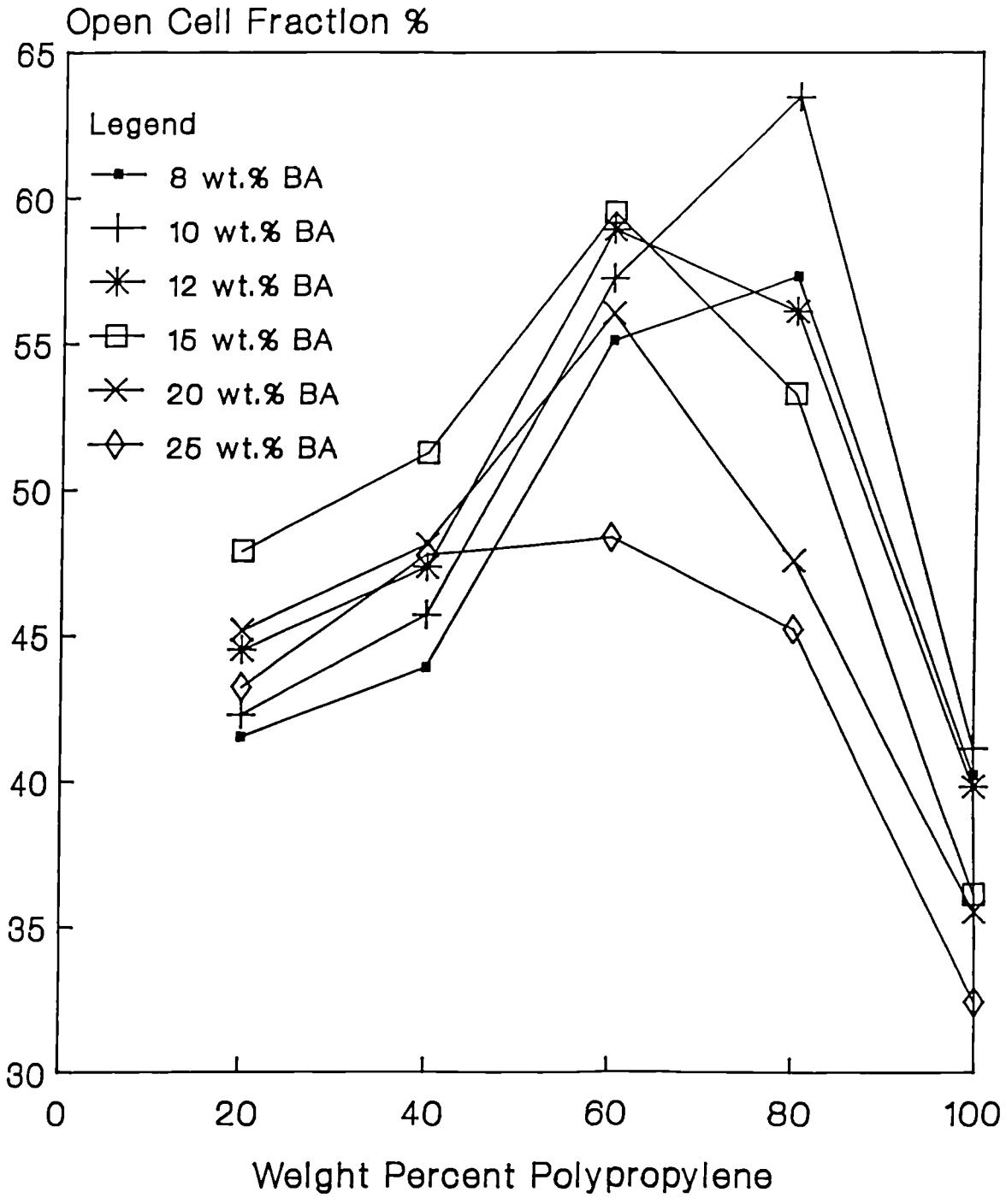

figure 5.31. Relationship of open cell fraction and CBA concentration in PP/HDPE foam.

hence, results in reduction of the density in the melt state as may be seen in Figures 5.30a. The influence of the blowing agent concentration on melt viscosity of the polymer may be explained from the standpoint of the theory of free volume for concentrated solution of polymers. The free volume increases with addition of gas into the polymer, hence the melt viscosity will decrease (20). However, if the blowing agent increases beyond the super saturation of the melt, the excess gas present in the melt tends to form a separate phase (i.e. forms gas bubbles) and lead to premature foaming and increase in density in both melt and solid states.

The results of open cell fraction at various blend ratios and blowing agent concentrations are presented in Figure 5.31. For the same reasons explained above open cell fraction goes through a maximum at blend ratio of 80/20 PP/HDPE.

The following points have been observed regarding the effects of die entry angle, die land ratio (L/D), melt viscosity, processing condition and blowing agent concentration on density (melt and solid state) and open cell fraction of polyolefin foam.

i) It was shown the density and open cell fraction of polypropylene foam is affected by

die design and die land ratio. Considerable pressure drop was recorded for dies with entry angle of 15° and 30°, whereas, die with entry angle of 60° showed considerable melt fracture at lower shear stress and shear rate as compare to die entry angle of 45°. Due to branching of high density polyethylene, hence, higher melt viscosity than polypropylene, the die with entry angle of 30° was more suitable for processing of this polymer.

ii) Over the range of L/D ratios studied, it was found that L/D ratio of 0 and 2 were more appropriate for achievement of low density and high open cell fraction in high density polyethylene and polypropylene foam respectively.

iii) Melt viscosity also strongly affected the maximum reduction in density and open cell fraction. Grades of polymer with high melt viscosity resisted the expansion, thereby, the bubble growth was suppressed, and due to thermodynamic principle the small cells will join the large ones. This phenomenon has resulted to a foam specimen with high density and low open cell fraction. On the other hand, resins with high MFI have lower melt strength, therefore, the cell walls could not withstand the stresses exerted on them upon solidification.

From six different grades of PP and four different grades of HDPE used for this study, the grades with MFI of 9 and 11 g(10 min)$^{-1}$ were found to give maximum reduction in density and a high fraction of open cell porosity, as compare to the other grades of these polymers.

iv) in order to optimise the viscosity of the polymer melt, PP (GXM-43 MFI = 9 g (10 min.)$^{-1}$) and HDPE (H11042 MFI = 11 g (10 min.)$^{-1}$), were physical blended in a co-rotating screw extruder. Results of this investigation showed the blend ratio of 80/20 PP/HDPE, was more suitable for achieving maximum reduction in density with high percentage of open cell porosity as compare to other blend ratios of these polymers.

CHAPTER 6
MACROMORPHOLOGY OF POLYOLEFIN FOAM

6. Macromorphology of Polyolefin Foam

6.1. Introduction

During the past few years, several theories (155,156) have been proposed which attempt to describe the mechanism by which cells are formed during the extrusion of resin/foaming agent mixtures. These theories all assume complete decomposition of foaming agent prior to extrusion resulting in the formation of small gas bubbles, well dispersed in the polymer melt. Final cell formation and its structure is then controlled by proper choice of processing conditions such as melt temperature and pressure (screw speed) and weight percent concentration of added blowing agent. In this chapter the attention will be focused on the effect of the above mentioned parameters on the number of cells, cell size, and cell size distribution.

The number of cell per cubic centimetre of foam has been found to be a very useful parameter for describing nucleation efficiency of the blowing agent used, and, also evaluation of overall foam quality (157). This parameter is a function of both the average cell size and the density of extruded foam. The number of cells per cubic centimetre can easily be calculated from the following relation (157);

$$Nc = [\ 1 - (Pf/Pr)\ ] \ / \ \{(3.14 * Dc^3\ )/6000\} \qquad 6.1a$$

or

$$Nc = 1910 * [(Pr - Pf) / (Dc^3 * Pr)] \qquad 6.1b$$

where

Nc is the number of cells per cubic centimetre

Pf is the density of foam in g cm^{-3}

Pr is the density of resin in g cm^{-3}

Dc is average cell diameter in mm

It should be pointed out that all cells were assumed to be spherical through the whole sample.

6.2. Results and Discussion

6.2.1 Cell Size Measurement of Polypropylene Foam

6.2.1.1. Effects of Melt Viscosity on the Cell Size and Cell Size Distribution of Polypropylene Foams

In order to investigate the effect of processing conditions on cell size and cell size distribution of polypropylene foamed rod, the samples were prepared in the form of disks. The cross section of the disks were coated with gold-palladium according to the procedure mentioned in section 3.9.3. The cross sections of these specimens were examined by SEM. The pictures produced from the cross section was used to count the chord size by the Image Analysis (model Optimax, System IV). The raw data measured by the central processing unit was processed by the computer and cell diameter was measured per unit volume using the Schwatz-Saltikov analysis.

The tabulated results are shown in Table 6.1, and a

Table 6.1. Cell size analysis of different grades of polypropylene foam containing 4 wt% chemical blowing agent (CBA).

Polymer Grade	MFI g/10 min	Mean Cell Diameter (mm)	Largest Cell Diameter (mm)	Standard Diviation	Area Fraction Occupied by the Cells %	No. of Cells per cm^3 $*10^{-5}$
GSE-16	0.8	0.184	0.330	0.08	29.4	1.283
GWM-23	2.5	0.2912	0.687	0.1325	33.59	0.4215
GWE-22	4	0.3060	0.650	0.154	34.37	0.3732
GXM-43	9	0.162	0.450	0.0815	58.187	2.828
GYM-45	15	0.3465	0.660	0.1369	38.88	0.2502
LXF-52	22	0.4513	0.75	0.1508	33.68	0.1085

graphical representation of cell size distributions exhibited in Figure 6.1. Furthermore, representative views showing cross section of corresponding samples are presented in Figure 6.2. Several interesting points can be drawn from these results:

i) Generally large bubbles were observed for grades of polymers either with very low MFI or with very high MFI. It is also noteworthy that for low MFI resins, the area fraction occupied by cells is smaller than with polymers with high MFI.

ii) The bubbles are not uniformly distributed through the cross section of the samples.

iii) The shapes of bubbles are not uniform through the cross section, changing from circular to elliptical form, from core to skin regions.

The first phenomenon could be due to the fact that with very low melt flow index polymers, the melt viscosity is very high which restricts the growth of the cells within the melt, thereby, due to thermodynamic principles the small cells will join the larger ones (as it was described in chapter 2, the gas pressure within the smaller cells is greater than the large cells, therefore, the small bubbles will diffuse into the large ones), and result in very non-uniform cell distribution within the sample. On the other hand, with high melt flow index polymer, the melt resistivity is so low the cell walls cannot withstand the pressure generated within them by the

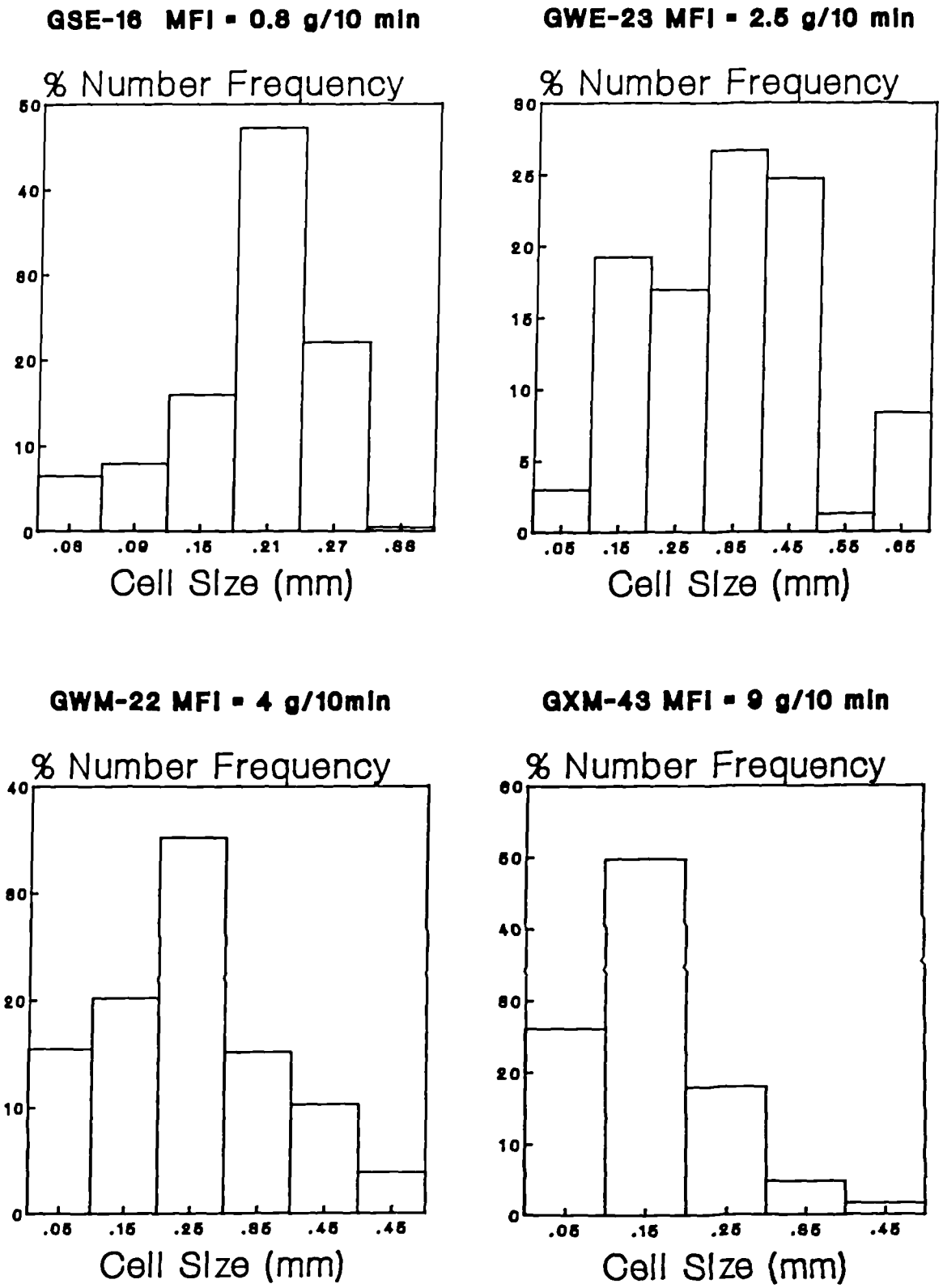

Figure 6.1. Cell size distribution of various grades of PP foam containing 4 wt% chemical blowing agent (CBA). Melt temperature 195°C.

GYM-45 MFI = 15 g/10min

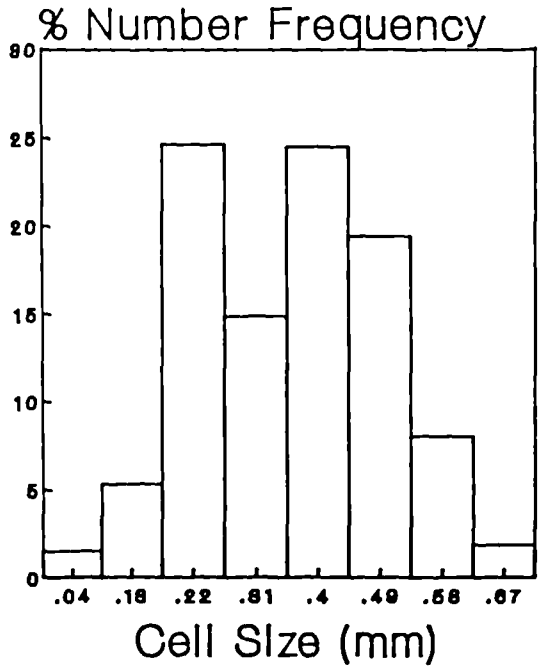

LXF-52 MFI = 22 g/10 min

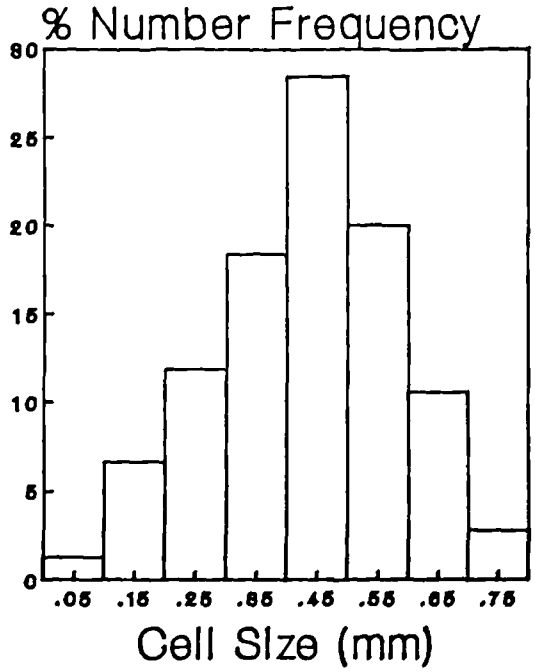

Figure 6.2. Cross sectional area of various grades of PP foam. Scale bar is equal to 1 mm unless otherwise is stated.

A) GSE-16 MFI = 0.8 g/10 min.
B) GWM-23 MFI = 2.5 g/10 min.
C) GWE-22 MFI = 4 g/10 min.
D) GXM-43 MFI = 9 g/10 min.
E) GYM-45 MFI = 15 g/10 min.
F) LXF-52 MFI = 22 g/10 min.
G) Higher magnification of E

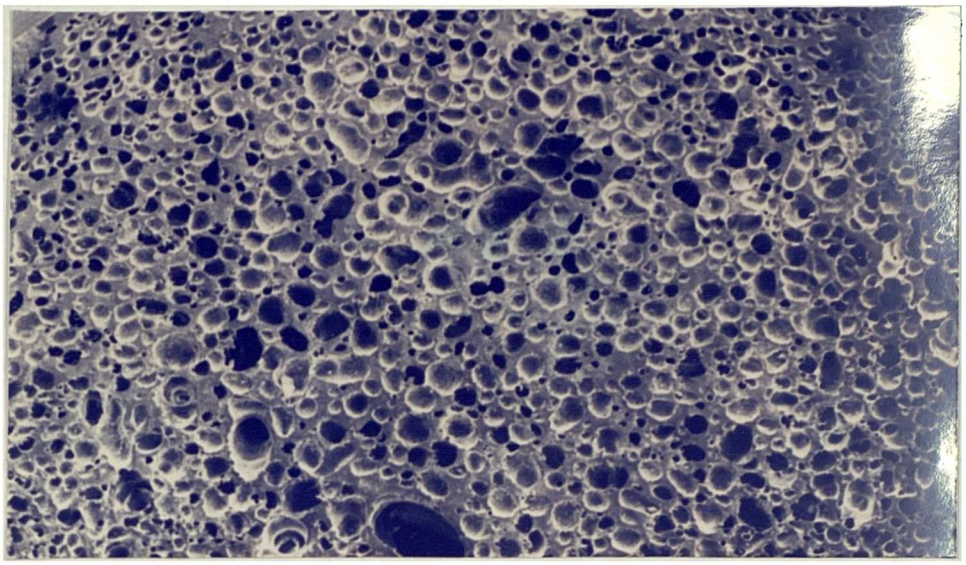

a

1mm

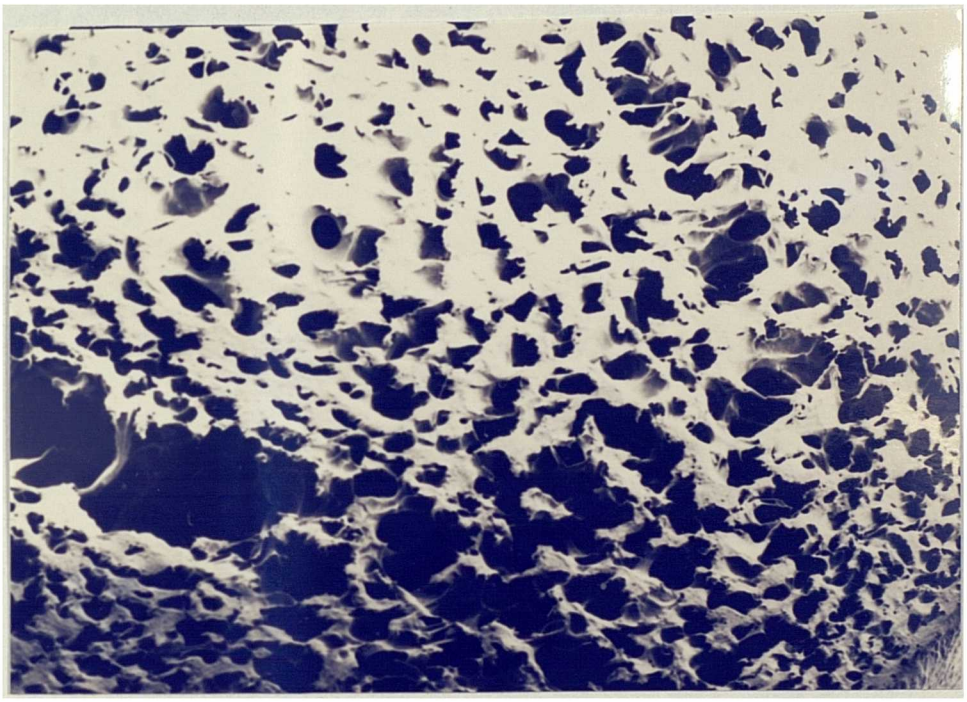

b

1mm

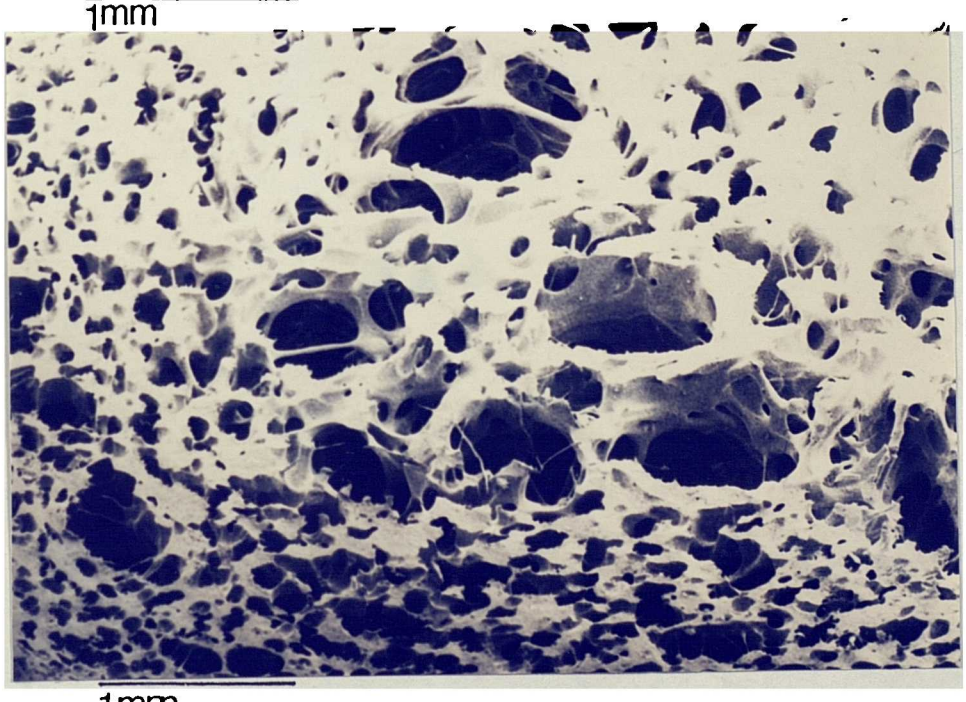

c

1mm

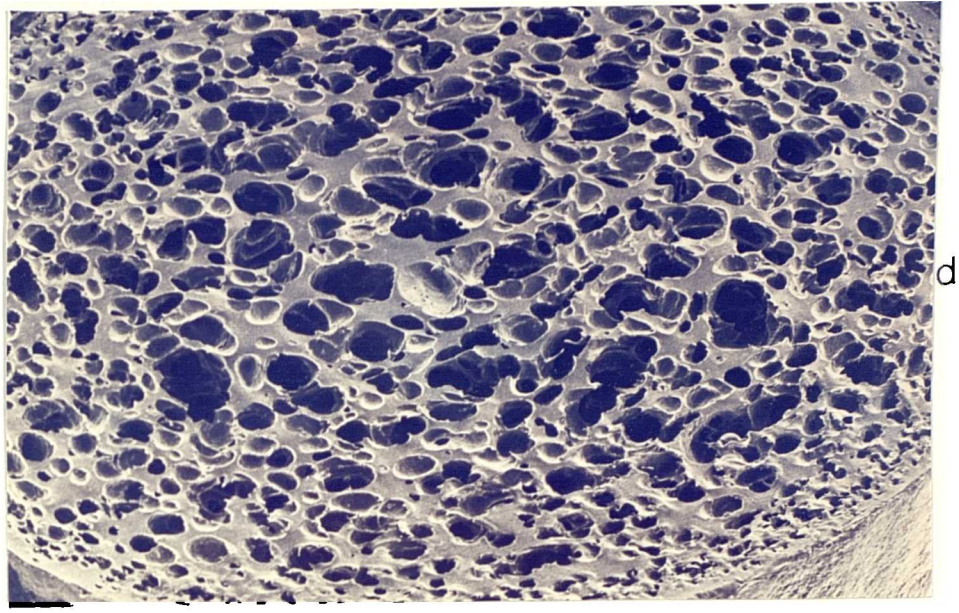

d

1mm

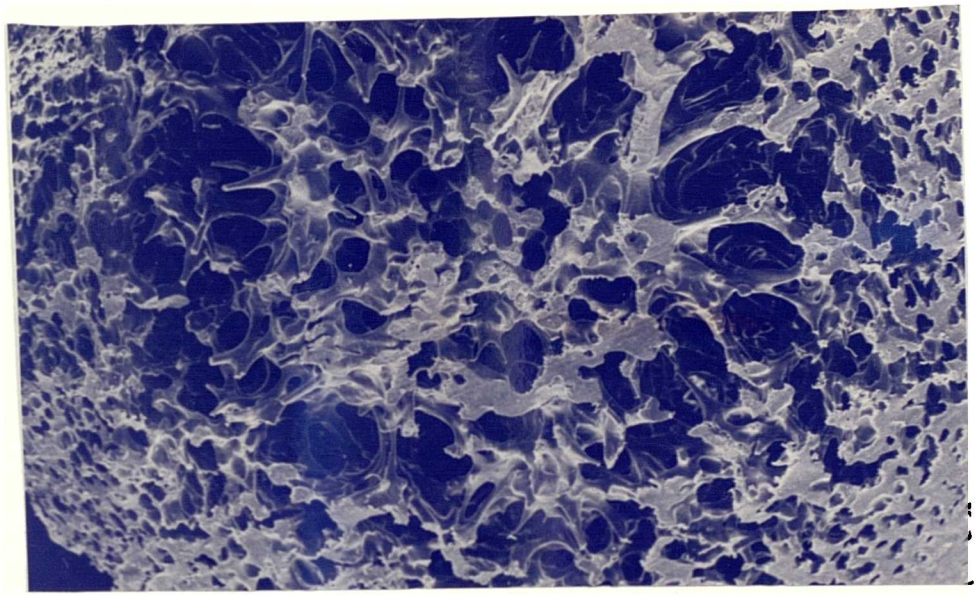

e

1mm

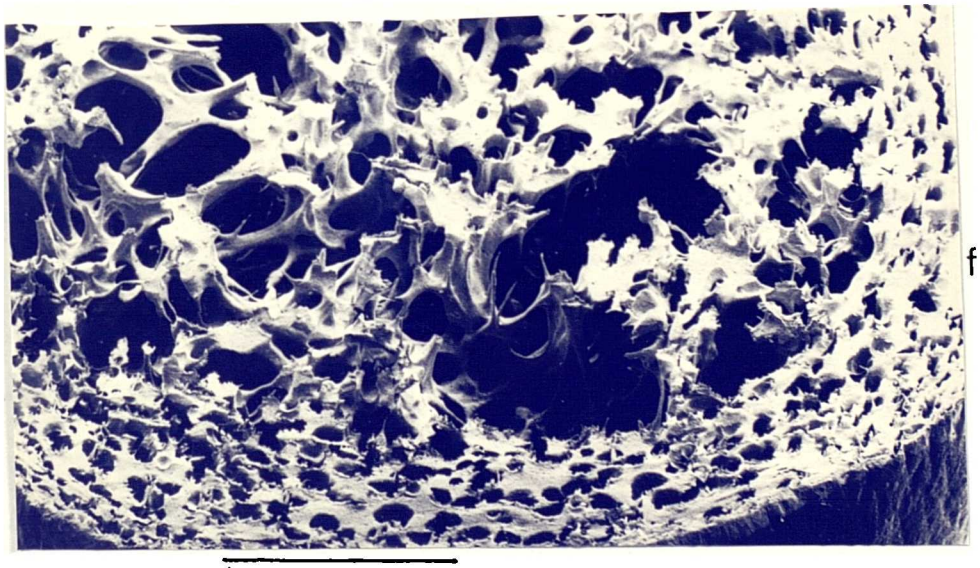

f

1mm

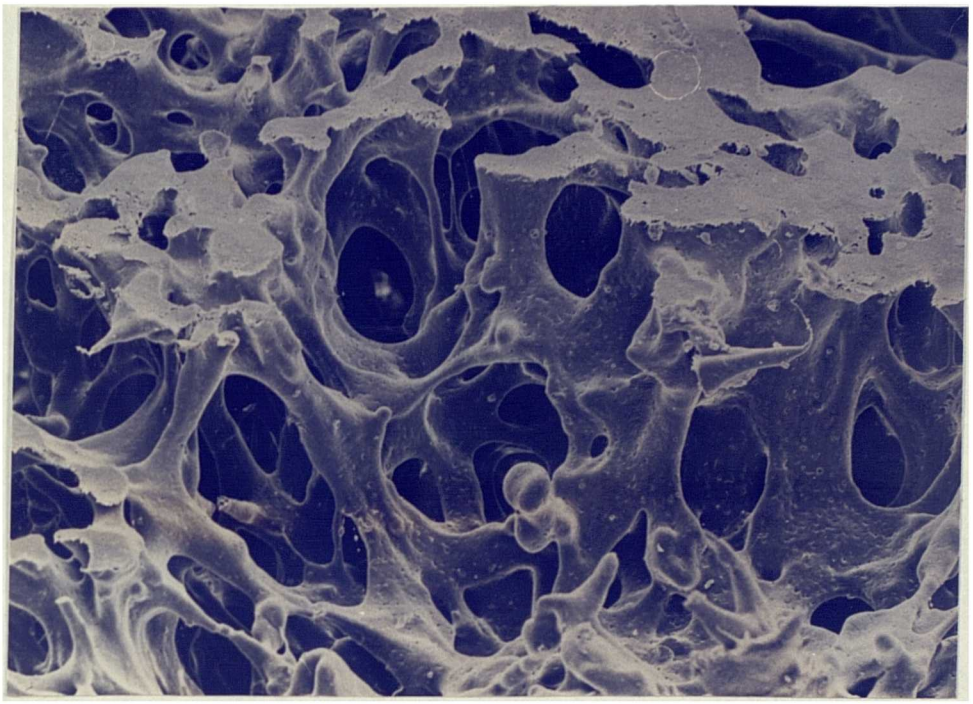

g

400 µm

chemical blowing agent. Therefore, the bubbles will collapse prior to cooling and this will results in formation of large holes in the specimens. For the second phenomenon two explanations can be given. Firstly, this can be caused by imperfect mixing of blowing agent and polymer, which is partly due to non-ideal mixing and also due to the fact that the polymer as well as blowing agent used in this study were in the form of granules hence, it reduces their contact areas which can significantly reduces the over all degree of mixing. Secondly, upon expansion of the polymer from the die exit the thermal conductivity of the extrudate will significantly decrease, therefore, this will create a greater differential cooling upon solidification, hence, the bubbles in the skin region will be suppressed where the cells away from the skin still have a chance to grow further. Bubble collapse is also evident in the core region, particularly with polymer of high MFI. This can be explained by differential cooling within the material, causing lower viscosity of melt in the core region than in the skin layer, thus, the cells in the core region will go through further expansion and eventually will result in rupture of the cell walls and collapse of the bubbles upon the solidification. The third phenomenon can be attributed to the shear flow differences in the cross section of the extrudate. Where the greater shear flow in the skin region will change the geometrical

shape of the cell from circular to elliptical. An expected shear rate profile across the extrudate is shown in Figure 6.3.

6.2.1.2. Effects of Processing Conditions on the Cell Size and Cell Size Distribution

Melt pressure in the die as well as melt temperature was altered and their effects were recorded (see ch. 5). The results of cell size measurement are shown in Tables 6.2 and 6.3. Their respective cell size distribution are presented in Figures 6.4 and 6.5 respectively.

Melt pressure has significantly affected the number of cells, cell structure and cell size through the cross section. The results of Table 6.2 and Figure 6.4 show that the uniformity of cell distribution along with area fraction occupied by the cells has increased with increasing melt pressure (increasing shear rate), resulting in a corresponding increase in the number of cells per cubic centimetre of foam (Nc). Han et al.(51, 158) achieved similar results with extrusion foaming of low density polyethylene and polystyrene using a physical blowing agent. Two proposals can be given to explain this type of behaviour. Firstly the solubility of gas will increase with increasing melt pressure, therefore, there will be less chance of premature foaming inside the die which can have an adverse

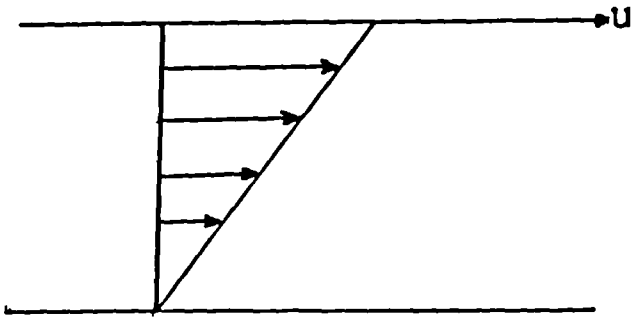

a

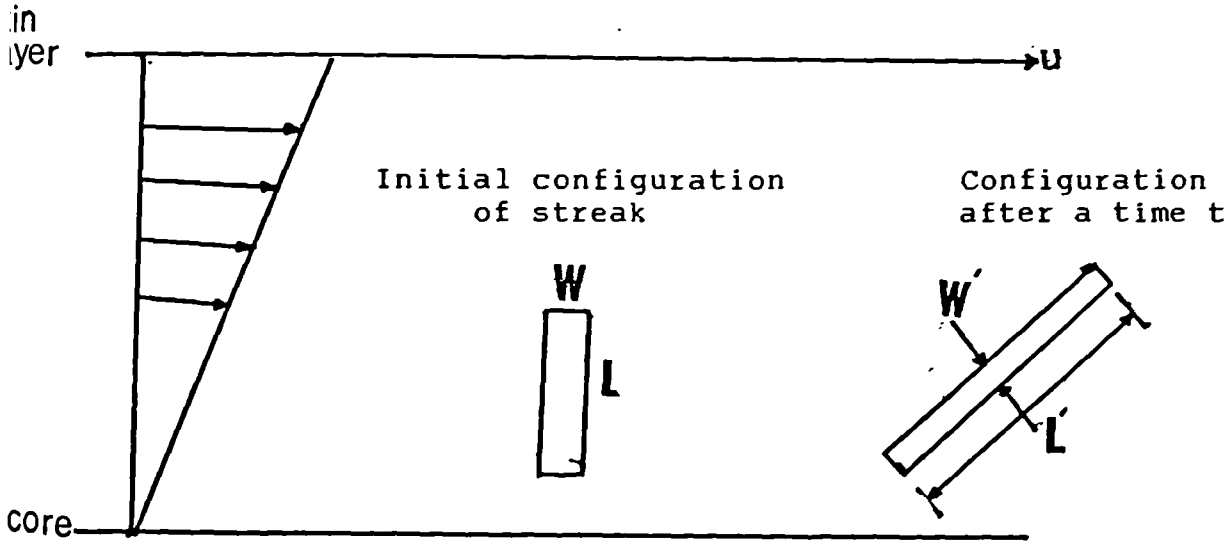

b

$$\dot{L}/L = [1 + (\dot{\gamma}t)^2]^{0.5}$$

L is initial length of streak
$\dot{L}$ is length of streak at time t
$\dot{\gamma}$ is shear rate

Figure 6.3. a) Velocity profile in extruder, b) Variation of shape of streak (bubble in this case) in simple shear flow (after 32).

Table 6.2. Cell size analysis of polypropylene (GXM-34) containing 4 wt% CBA at different apparent shear rates.

Shear Rate (S^{-1})	Mean Cell Diameter (mm)	Largest Cell Diameter (mm)	Standard Diviation	Area Fraction Occupied by the Cells %	No. of Cells per cm^3 $*10^{-5}$
950	0.224	0.331	0.148	41.25	0.944
1343	0.216	0.412	0.132	49.613	1.081
2109	0.612	0.450	0.0815	58.187	2.828
2388	0.151	0.489	0.0959	61.33	3.323
3424	0.253	0.439	0.111	51.11	0.672

Table 6.3. Cell size analysis of polypropylene (GXM-43) containing 4 wt% CBA at different melt temperatures.

Melt Temp. (C)	Mean Cell Diameter (mm)	Largest Cell Diameter (mm)	S.D.	Area Fraction Occupied by the Cells %	No. of Cells per cm^{-3} $*10^{-5}$
175	0.231	0.311	0.124	42.71	0.821
185	0.162	0.450	0.0815	58.187	2.828
195	0.165	0.393	0.0995	55.65	2.432
205	0.255	0.553	0.131	46.75	0.7616

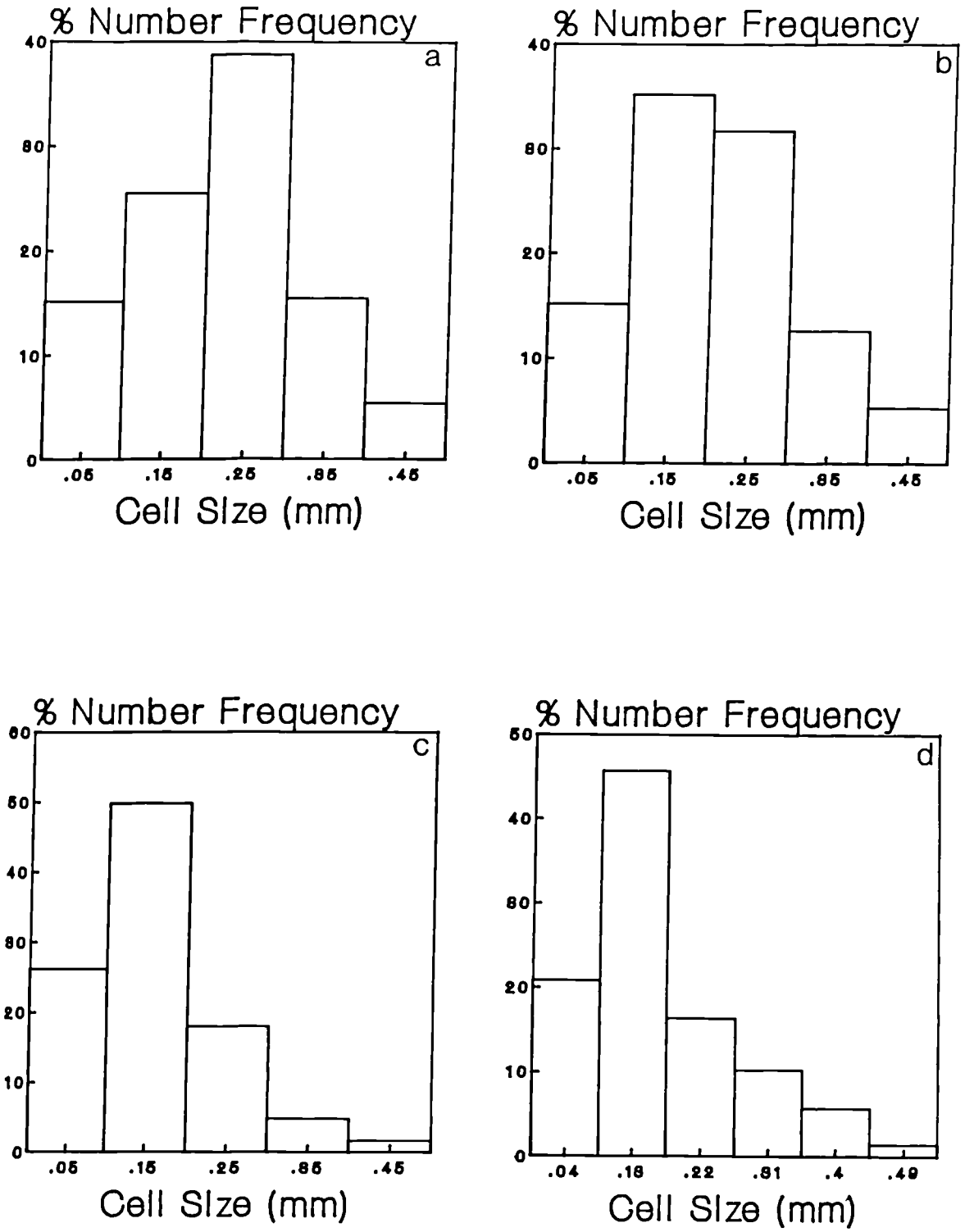

Figure 6.4. Cell size distribution of PP (GXM-43) containi 4 wt% CBA_1 at different apparent shear rates. a) 950 S^{-1} b) 1343 S^{-1}, c) 2109 S^{-1}, and d) 2388 S^{-1}, and e) 3424 S^{-1}.

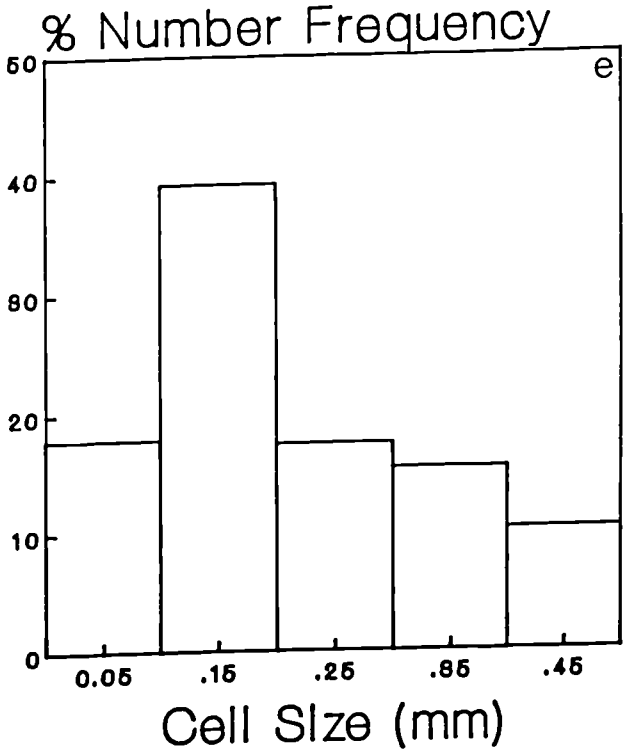
% Number Frequency
e
50
40
30
20
10
0
0.05
.15
.25
.35
.45
Cell Size (mm)

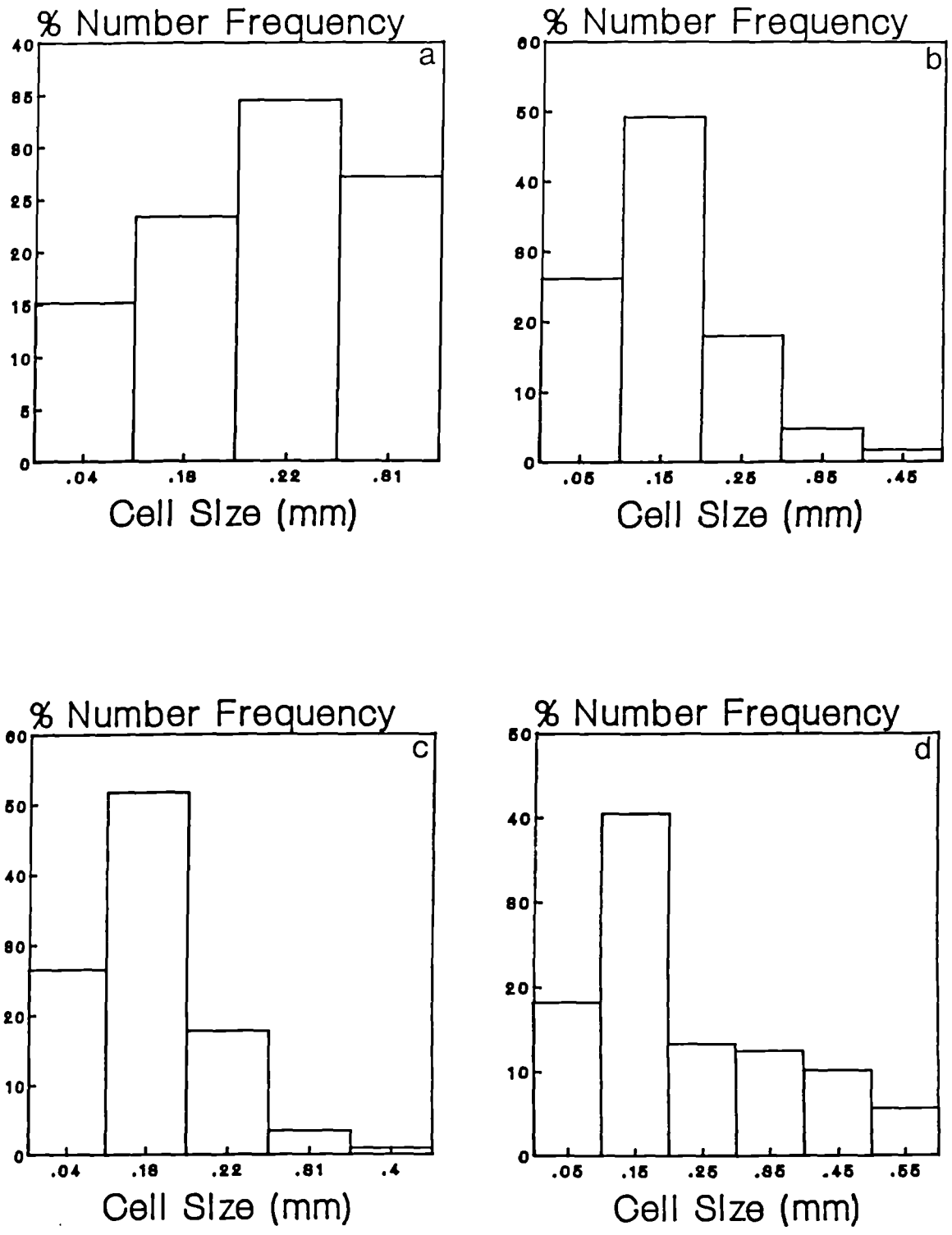

Figure 6.5. Cell size distribution of PP(GXM-43) foam at different melt temperatures.
a)175°C, b)185°C, c)195°C, and d)205°C.

effect on the foam density and foam quality. Secondly, the extrusion pressure can be at least qualitatively explained in terms of the swelling phenomenon exhibited by viscoelastic melts, such as polypropylene. Higher extrusion pressure produces an increase in the flow rate accompanied by a greater degree of swelling of the resin as it emerges from the die exit. This swelling phenomenon causes a differential cooling effect in the melt and thereby produces a greater temperature difference between the nucleating " hot spot " (mainly the blowing agent residual), and super-saturated gas/polymer solution. This situation could favour more efficient nucleation. In addition, the increased swelling assists in expansion of the foam, thereby, partially accounting for the lower densities observed at higher extrusion pressures.

As mentioned previously, the melt temperature has a pronounced effect on the foam quality as can be observed from Table 6.3 and also Figure 6.5. As it has been explained in chapter 4, the melt viscosity of poly-propylene decreases with increase of melt tempe-rature, thereby, due to drop in melt strength of the polymer the cell wall will collapse more readily prior to cooling. Therefore,one can notice for a self nucleating foamable mixture extruded near the decom-position temperature "Td" of the foaming agent, the

number of cells per cubic centimetre of foam was found to pass through a maximum with increasing melt temperature as is displayed in Table 6.3. This effect can be explained on the basis of the extent of foaming agent decomposition and the corresponding gas/nucleant ratio in the melt, as it leaves the extrusion die. At a low melt temperature (175°C), the percent decomposition is relatively low and therefore the gas/nucleant ratio is low. The result is fairly efficient nucleation, but leading to foamed specimens with high densities, as it was observed in the previous chapter. As the melt temperature is increased to and approaches the temperature giving maximum rate of blowing agent decomposition (185°C), the gas/nucleant ratio increases causing a decrease in the foam density, but at the same time cell size also decreases due to greater degree of supersaturation in the gas/polymer solution as it leaves the die exit. It has been suggested that such gas solutions are less stable and therefore cell nucleation is facilitated (157). Optimum foam quality is reached often when melt temperature is close to decomposition temperature "Td" of the blowing agent and also when the number of undecomposed nucleant particles is just adequate to provide efficient cell nucleation. Beyond this melting temperature (185°C), further increase serve only to premature decomposition of blowing agent in the early zones of extruder. This explains the decreasing trend in the number of cells.

6.2.1.3. Effects of Blowing Agent Concentration on Number of Cells, Cell Size and Cell Size Distribution of Polypropylene Foams

The experimental results indicated that cell structure is dependent on the concentration of foaming agent. For a foamable mixture, it was found that an increase in the concentration (up to 15 wt%) of blowing agent component produced a slight increase in the average cell size, whereas at concentration higher than 15 wt.%, the cell size abruptly increased with increasing blowing agent concentration as it is shown in Table 6.4. This behaviour is due to decrease of melt viscosity with increasing blowing agent concentration (as it was observed in chapter 4). The sudden drop in melt viscosity in the die region, will result in formation premature cell growth and rupture of the cell walls (due to drop in melt strength). This phenomenon will lead to joining of the bubbles and formation of a few large cell through the cross section of the extrudate. The over foaming of the polymer melt can be minimised, by optimisation of the melt strength of the polymer, either by selecting a grade of resin with lower MFI or lowering the melt temperature of extrudate. If the foaming agent concentration is too high in relation to the nucleant concentration, the pressure exerted on the melt by the expanding cells can only be relieved by gas diffusion toward and subsequently through the extrudate wall.

Table 6.4. Cell size analysis of polypropylene (GXM-43) foam at different CBA concentrations. Melt temp.=185°C.

Wt% CBA	Mean Cell Diameter (mm)	Largest Cell Diameter (mm)	S.D.	Area Fraction occupied by the Cells %	No. of Cells per cm^{-3} $*10^{-5}$
4	0.162	0.450	0.08152	58.187	2.828
8	0.161	0.321	0.088	63.161	2.795
10	0.519	0.373	0.0925	65.389	2.877
12	0.163	0.356	0.0836	64.89	2.646
15	0.254	0.542	0.132	57.25	0.6804
20	0.333	0.621	0.1396	47.25	0.294

Table 6.5. Cell size analysis of polypropylene (GXM-43) containing 4 wt% CBA and 1 wt% nucleating agent (talc).

Wt% CBA	Mean Cell Diameter (mm)	Largest Cell Diameter (mm)	S.D.	Area Fraction occupied by the Cells %	No. of Cell per cm^{-3} $*10^{-5}$
4	0.156	0.27	0.0915	60.25	3.019
8	0.147	0.291	0.108	68.35	3.71
10	0.139	0.307	0.111	68.25	5.11
12	0.150	0.319	0.107	67.11	3.365

For the purpose of studying the effect of increasing nucleating sites, 1 wt% nucleating agent such as talc was added to the composition, while holding the amount of blowing agent concentration at a constant level. The addition of nucleating agent resulted in the formation of a greater number of cells with smaller average diameter as it is noticed from comparison of Tables 6.4 and 6.5. This effect is simply due to a more complete fractionation of foaming gas between the number of nucleation sites.

6.2.2. Effects of Processing Conditions on Number of Cells, Cell Size and Cell Size Distribution of High Density Polyethylene Foams

High density polyethylene foam was prepared on a single screw extruder at different melt temperatures and pressures. The results of cell measurement and cell size distribution are given in Table 6.6 and Figure 6.6. The general view of cross sectional areas of corresponding specimens are presented in Figure 6.7. The effects of melt viscosity on the cell size and cell size distribution are similar to those of polypropylene foam, except that the uniformity in the cell size distribution is lower in the case of high density polyethylene foam. Also the open cell fraction content is much less in the case of high density polyethylene than polypropylene foam (see Figures

Table 6.6. Cell size analysis of various grades of high density polyethylene containing 8 wt% CBA.

Polymer grade	MFI g/10 min	Mean Cell Diameter (mm)	Largest cell Diameter (mm)	S.D.	Area Fraction Occupied by the Cells %	No. of Cells per $cm^3 * 10^{-5}$
H020-54P	2	0.201	0.35	0.089	21.49	1.083
H060-45P	6	0.347	0.75	0.154	28.31	0.2276
H11042	11	0.1828	0.35	0.0893	42.32	1.720
NATENE 54-180	18	0.3899	0.59	0.151	34.46	0.1635

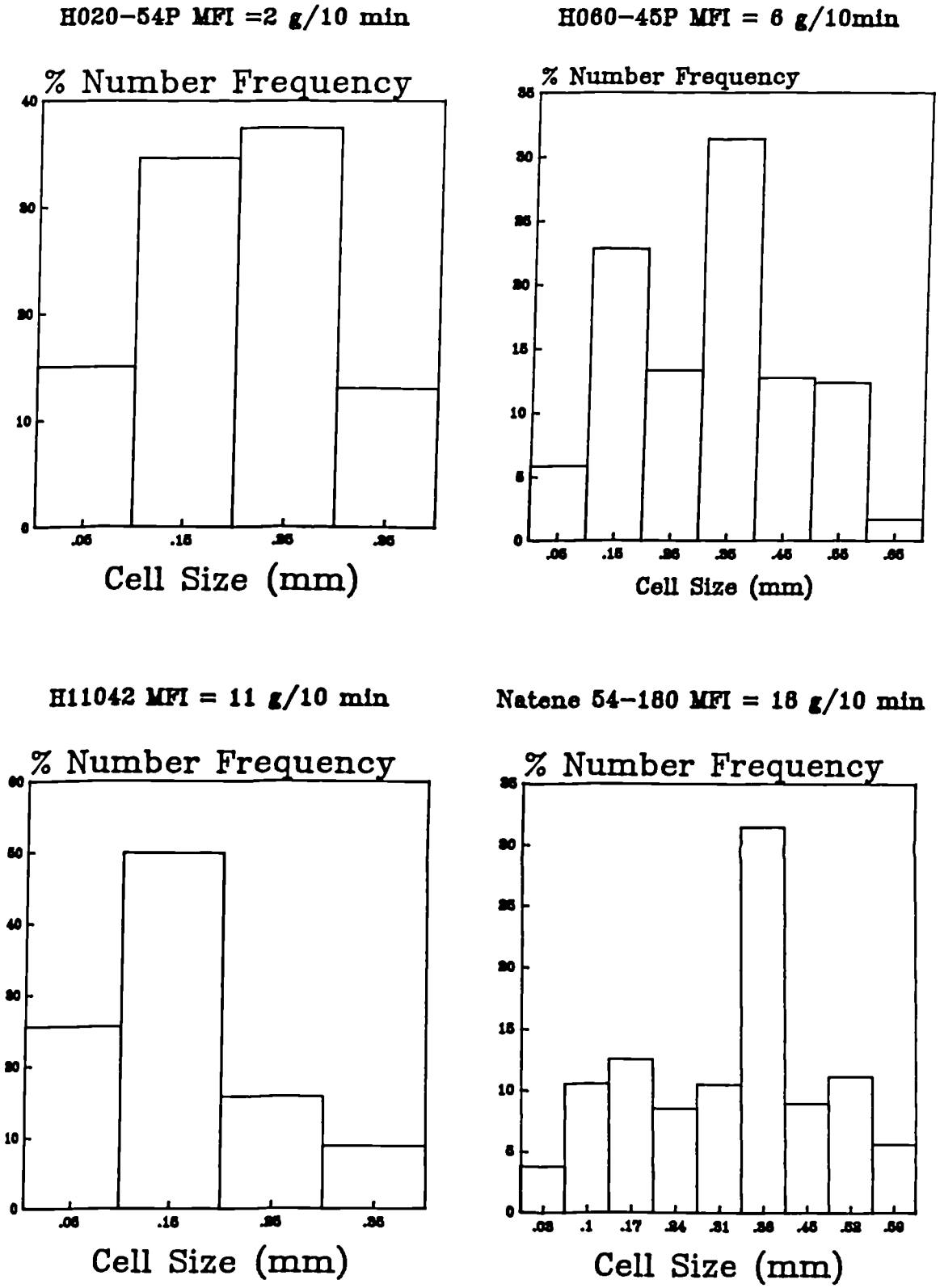

Figure 6.6. Cell size distribution of various grades of HDPE foam containing 8 wt% Chemical blowing agent.

Figure 6.7. Cross sectional area of various grades of HDPE foam containing 8 wt% chemical blowing agent. The scale bar is equal to 1 mm unless otherwise is stated.

a) H02054P MFI = 2 g/10 min.
b) H06045P MFI = 6 g/10 min.
c) H11042 MFI = 11 g/10 min.
d) NATENE 54-180 MFI = 18 g/10 min.
e) Higher magnification of c

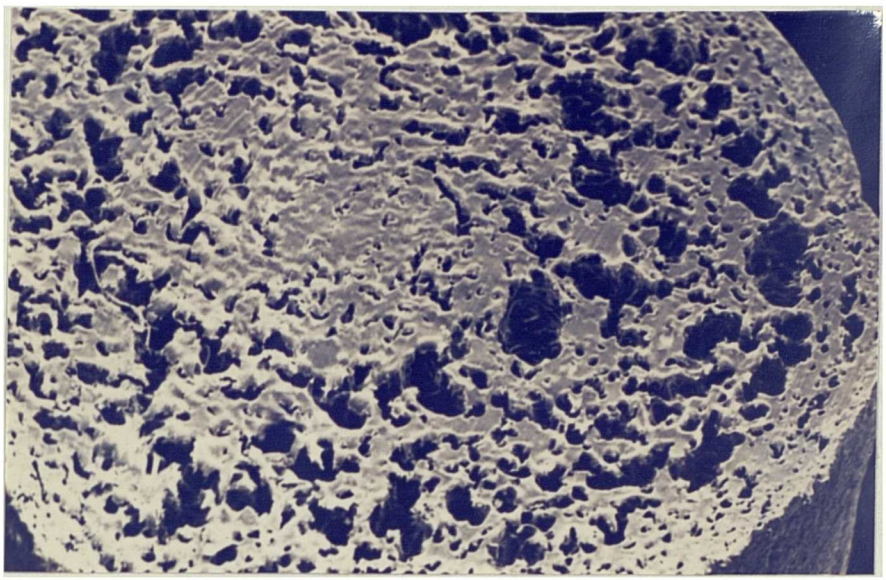

a

1mm

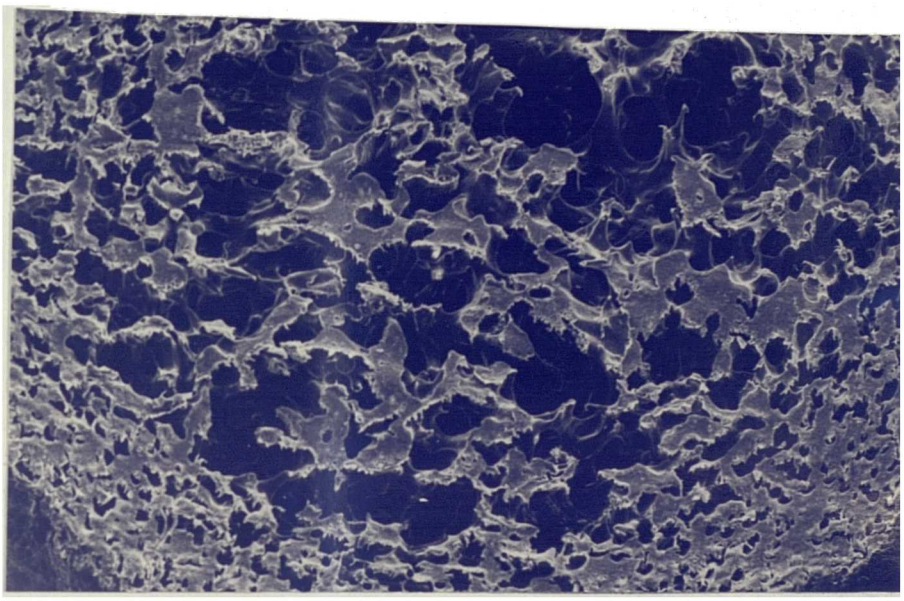

b

1mm

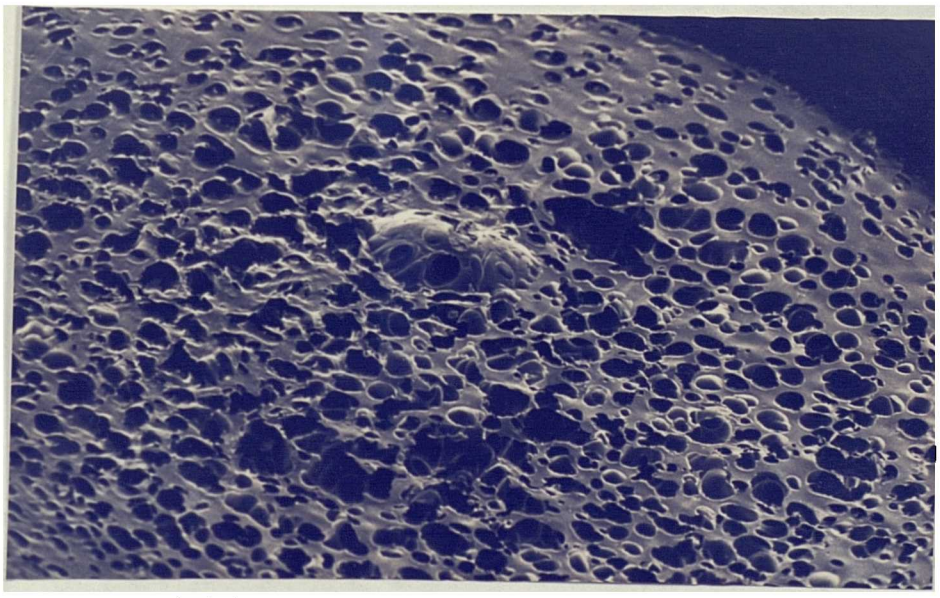

c

1mm

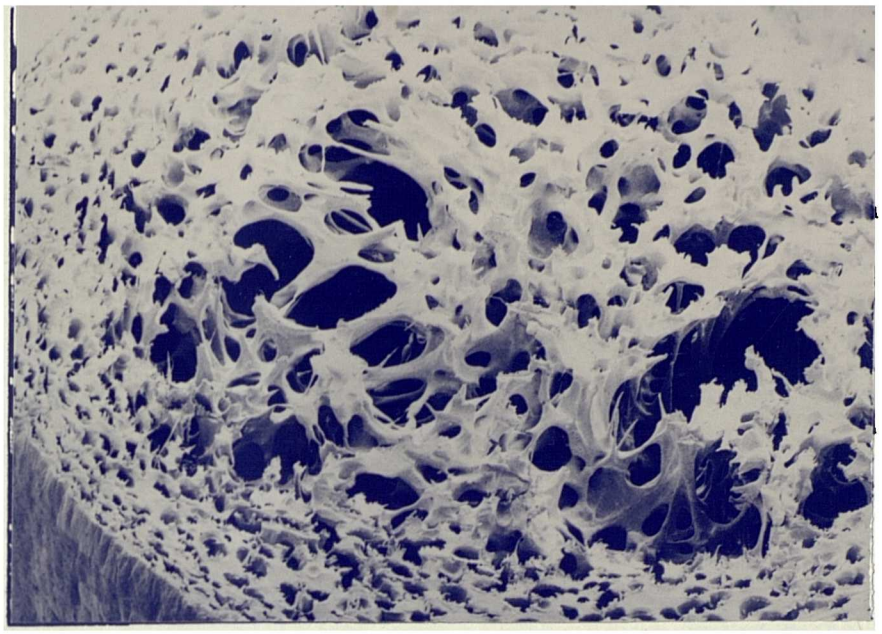

d

1mm

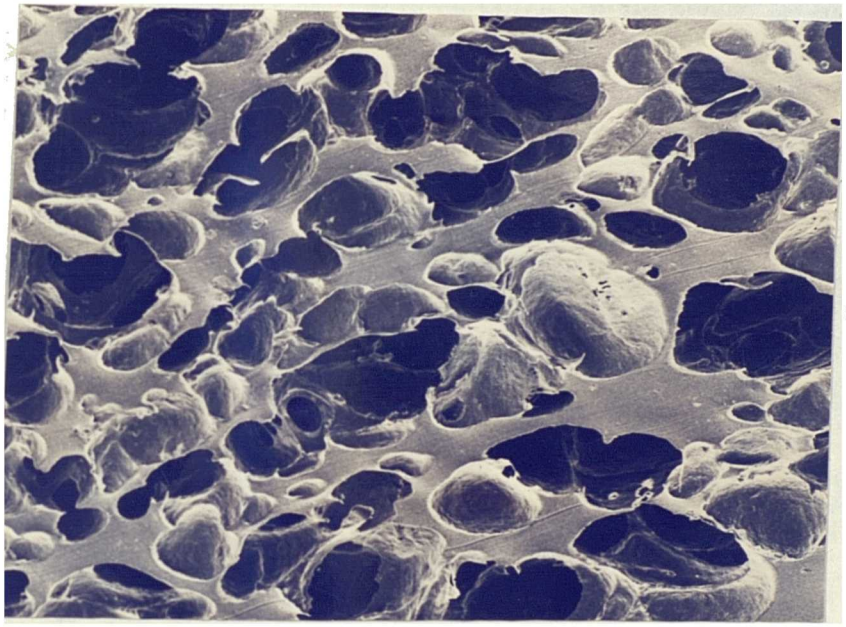

e

400μm

6.2.G and 6.7.E). This behaviour can be attributed to the different molecular branching of the macromolecules of high density polyethylene obtained during polymerisation. These macromolecules show a " tree type " branching which give rise to higher viscosity (159) and also more resistance to stretchability of the material during foaming action as compare to polypropylene. It is evident that increasing the branching, the viscosity of polymer melt increases (159), therefore, this might suggest the reason for higher melt viscosity as well as melt strength of the high density polyethylene as compared to polypropylene resin. The increase in viscosity will restrict the growth of the cells, therefore, as explained in the previous section due to thermodynamic principles the gas within the small cells will diffuse into the larger ones and a very non-uniform cell distribution will be formed prior to solidification (see Figure 6.6).

Also with the less viscous resins, it was observed that increasing the melt residence time (using lower screw speed, hence, lower die pressure), has resulted in more cell collapse and less uniformity in cell size throughout the cross section of the extrudate, (Table 6.7 and Figure 6.8). It appears reasonable to assume that with lower screw speed not only the pressure on the melt in the die region is lower, but also due to the fact that the material will remain for a longer

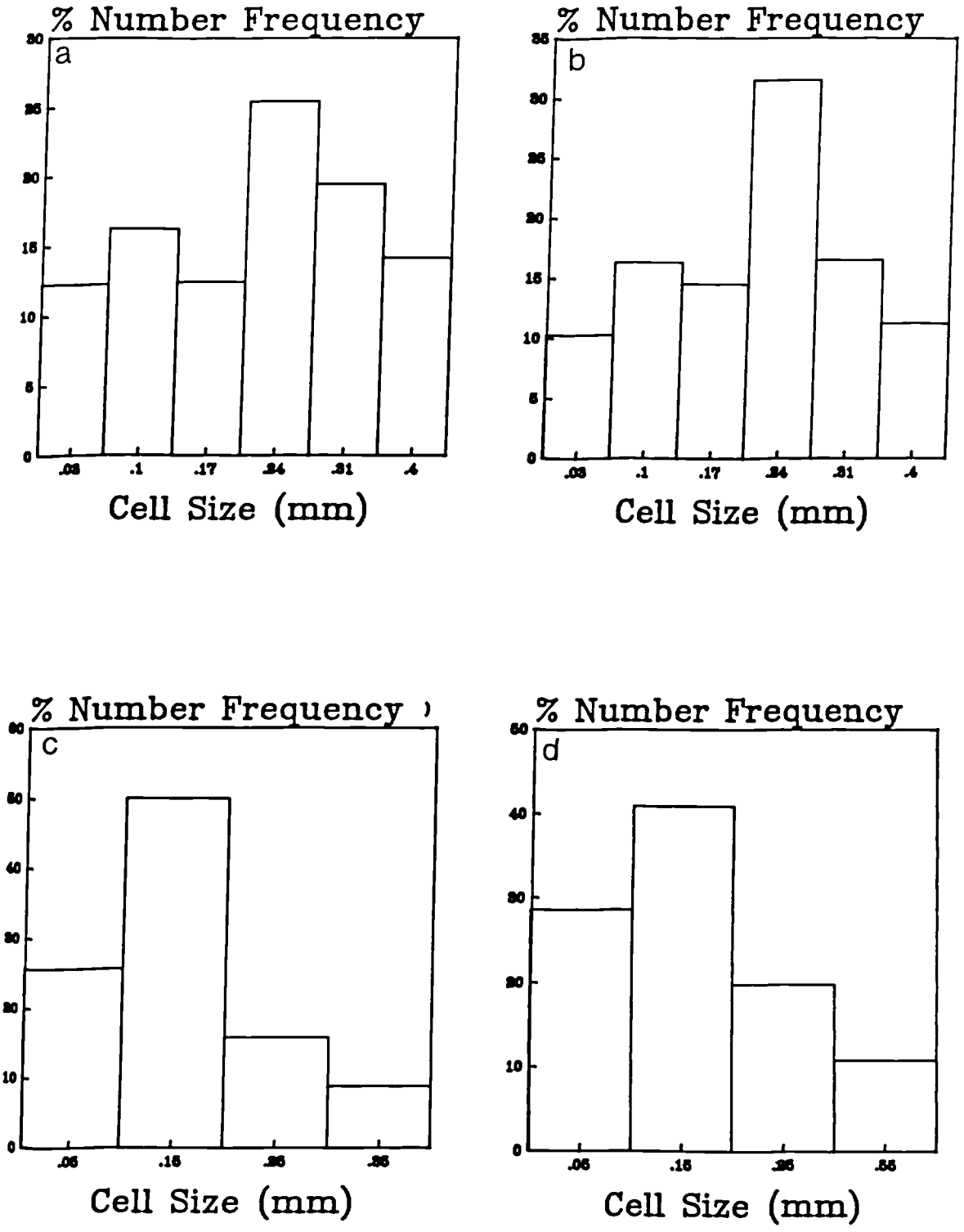

Figure 6.8. Cell size distribution of HDPE (H11042) foam containing 8 wt% CBA at various apparent shear rates. a) 950 S^{-1}, b) 1440 S^{-1}, c) 1760 S^{-1}, and d) 2130 S^{-1}.

Table 6.7. Cell Size analysis of high density polyethylene (H11042) containing 8 wt% CBA at different apparent shear rates.

Shear Rate (S^{-1})	Mean Cell Diameter (mm)	Largest Cell Diameter (mm)	S.D.	Area Fraction Occupied by the Cells %	No. of Cells per $cm^3 * 10^{-5}$
950	0.241	0.41	0.121	21.85	0.685
1440	0.219	0.408	0.110	32.48	0.945
1760	0.1828	0.35	0.0893	42.32	1.720
2130	0.167	0.37	0.098	45.65	2.3

Table 6.8. Cell size analysis of high density polyethylene (H11042) containing 8 wt% CBA at different melt temperatures.

Melt Temp. (C)	Mean Cell Diameter (mm)	Largest Cell Diameter (mm)	S.D.	Area Fraction Occupied by the Cells %	No. of Cells per $cm^3 * 10^{-5}$
245	0.228	0.357	0.0962	21.89	0.859
255	0.1828	0.35	0.0893	42.32	1.72
265	0.175	0.437	0.112	34.75	1.994
275	0.171	0.319	0.212	29.63	1.969

period of time in the barrel of extruder, the amount of gas escaping from the hopper would be greater. Therefore, premature foaming together with low gas/ nucleant ratios, are believed to be responsible for non-uniformity of cell structure, lower number of cells per unit volume and lower percentage of area fraction occupied by the cells, in specimens processed at low pressure (low screw speed, hence, low shear rate). The number of cells per unit volume slightly decreased with increasing the melt temperature. At the same time the area fraction occupied by the cells went through a minimum at a melt temperature of 255°C, as is evident from Table 6.8. As it has been mentioned earlier in this chapter, gas/nucleant ratio is one of the phenomena which affects the cell concentration per unit volume. Since high density polyethylene, is processed at a temperature much higher than " Td" of the blowing agent used, therefore, increasing the melt temperature tends to activate the blowing agent at an earlier stage in the barrel of extruder, resulting in greater gas leakage from the hopper during the processing (this was noticed visually).

The area fraction occupied by the cells reaches a minimum at melt temperature of 255°C. This is believed to be due to lowering of the melt viscosity, which will result in less restriction of movement of bubbles

within the melt, hence, less chance of bubbles joining one another and forming a large cell. This phenomenon will compensate for decrease of gas/nucleant ratio, which was explained to be a key factor in obtaining a low density foam with uniform cell size distribution. Further increase in melt temperature, will promote a reduction of melt viscosity together with a drop in gas/nucleant ratio, which will tend in lowering of number of cells per unit volume and a raise in density of foamed specimen as it was observed in the previous chapter.

6.2.3. Effects of Blowing Agent Concentration on the Number of Cells, Cell Size and Cell Size Distribution of High Density Polyethylene Foams

The results of the foregoing section suggest that the high density polyethylene with MFI of 11 g $(10\ min)^{-1}$ H11042, is most suitable for production of foam rod, as compared to the other three grades which studied. Further investigation has been undertaken to show the effect of chemical blowing agent concentration on the number of cell per unit volume, cell size, and cell size distribution of this grade of high density polyethylene. The outcome of these findings are listed in Table 6.9 and Figure 6.9.

It can be seen that as the blowing agent concentration increases, the uniformity of cell distribution, as well as number of cells per unit volume,

Table 6.9. Cell size analysis of high density polyethylene (H11042) foam at different CBA concentrations. Melt Temp.=255 C.

Wt% CBA	Mean Cell diameter (mm)	Largest Cell Diameter (mm)	S.D.	area Fraction Occupied by the cells %	No. of Cell per cm^3 $*10^{-5}$
8	0.1828	0.350	0.0893	42.32	1.72
10	0.173	0.373	0.0954	47.19	2.037
12	0.158	0.365	0.111	51.14	2.95
15	0.149	0.391	0.105	53.85	3.56
20	0.189	0.575	0.128	45.31	1.72
25	0.292	0.619	0.135	38.85	0.4235

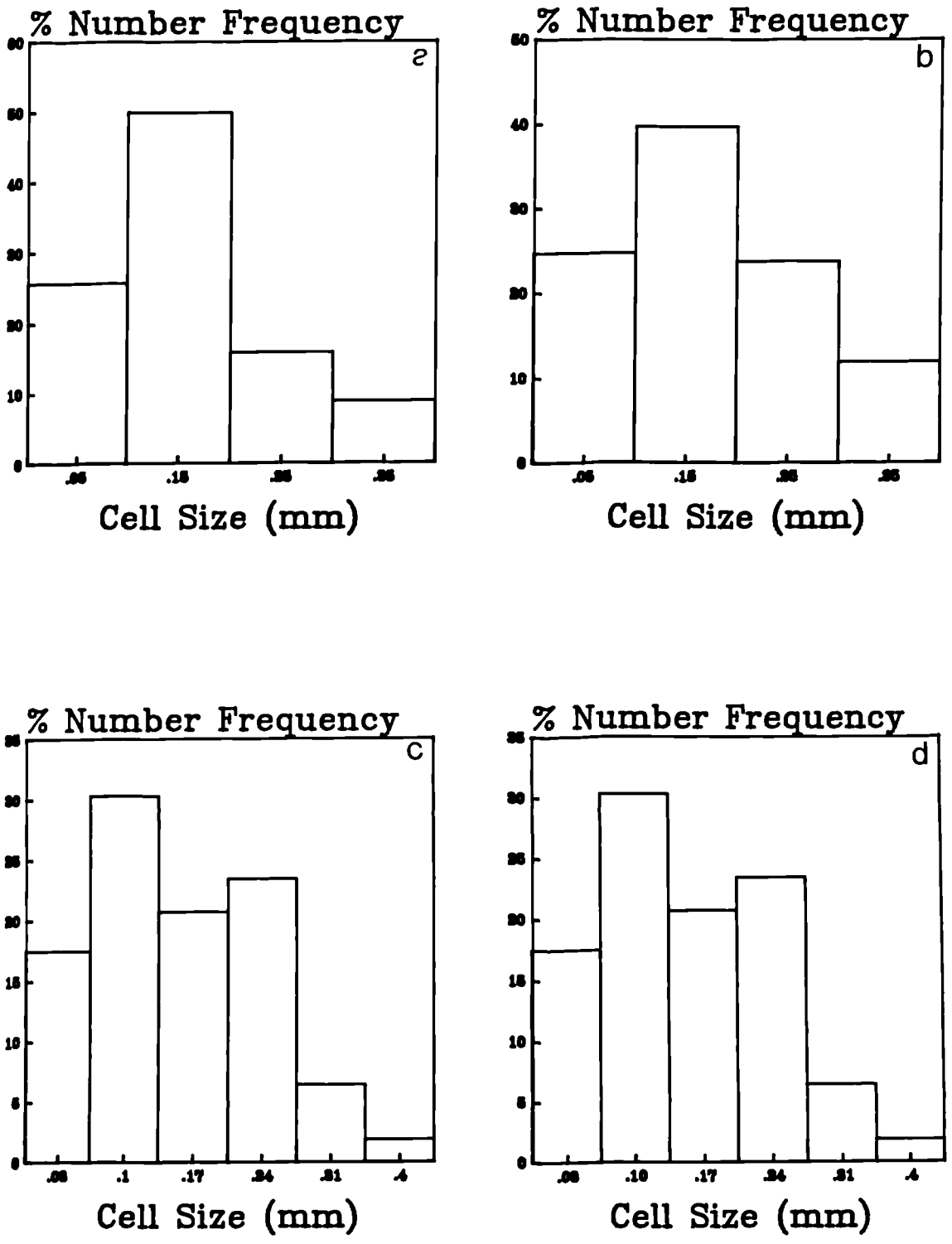

Figure 6.9. Cell size distribution of HDPE(H11042) foams at various CBA concentrations (wt.%).
a)8, b)10, c)12, d)15, e)20, and f)25.

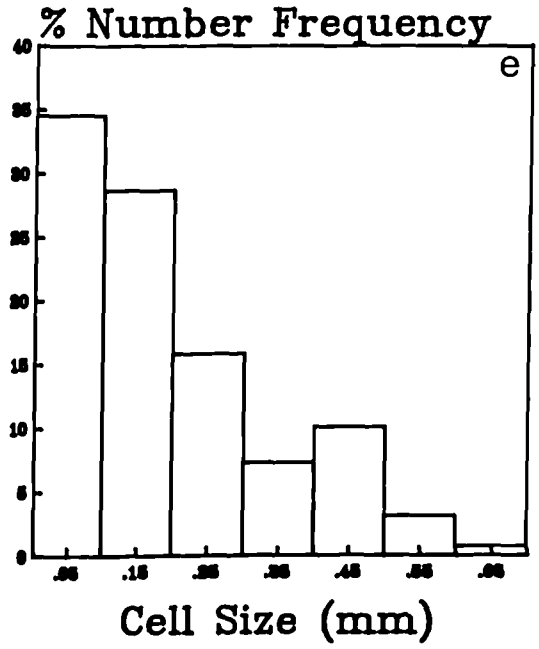
% Number Frequency
e
40
30
20
10
0
.05
.15
.25
.35
.45
.55
.65
Cell Size (mm)

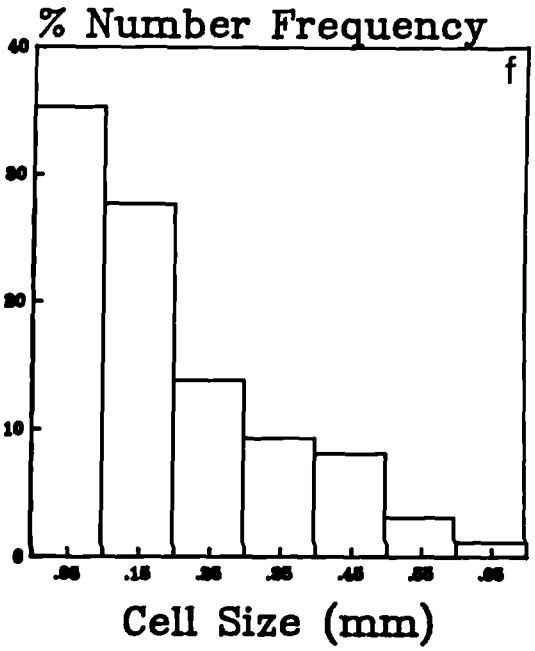
% Number Frequency
f
40
30
20
10
0
.05
.15
.25
.35
.45
.55
.65
Cell Size (mm)

increases through the cross section and it reaches a maximum at blowing agent concentration of 15 wt%. The reasons behind this phenomenon are clear, since increasing the blowing agent concentration tends not only to decrease the melt viscosity (which can help the movement of the cells), it also increases the gas/nucleant ratio. It should be pointed out that it reaches a point where the further increase in the gas concentration supersaturates the melt and the excess gas tends to rupture the cell walls and either form a blister on the extrudate skin or escape through surface of the extrudate melt. It should be emphasised that the concentration at which this maximum uniformity in cell distribution is achieved, also depends on processing conditions such as melt temperature and melt pressure, which were kept constant to isolate effects of the chemical blowing agent. It is interesting to point out that due to the preceding reasons, the area fraction occupied by the bubbles, as well as the number cells per unit volume, also go through a maximum with increasing blowing agent concentration. These results are in a good agreement with the analysis of the density of the foam specimens studied in the previous chapter.

6.2.4. Macromorphology Analysis of Blends of PP/HDPE Foams

6.2.4.1. Effects of Blend Ratio of PP/HDPE on the Number of Cells, Cell Size and Cell Size Distribution of PP/HDPE Foams

The results of the previous chapter and the foregoing sections show that the density, open cell fraction and uniformity of the extruded polyolefin foam, is strongly dependent on the melt viscosity and melt strength of the virgin resin. It has been shown that due to chain branching of high density polyethylene, the melt strength of this polymer is very high as compare to polypropylene homopolymer, hence, the expansion of the bubbles within the melt is restricted. This phenomenon has resulted in a foamed specimen with high density and non-uniform distribution of cells through its cross section. On the other hand the molecular structure of polypropylene comprises linear chains, which will lead to a lowering of melt viscosity see (chapter 4) and lower melt strength, compared to high density polyethylene. For this reason the cell walls readily collapsed upon cooling, which resulted in a foamed specimen with high density as well as low open cell fraction. Therefore, in order to achieve a foamed sample with uniform cellular structure along with low density, it was consider that the melt viscosity of the polymer required modification. For this reason, the grades of polypropylene (GXM-43) and high density polyethylene

(H11042), which resulted in more uniform cellular structure along with lower density and higher open cell fraction (as compared to the other grades of these polymers tested), were melt blended in varying ratios using a co-rotating twin-screw extruder.

Table 6.10 and Figure 6.10 present the cell size and cell size distributions of binary blends of PP/HDPE foam prepared at various blend ratios. The general view of cross sectional areas of corresponding specimens are displayed in Figure 6.11. From the results presented in the Table 6.10 and Figures 6.10 and 6.11 one can deduce the following points:

i) As the weight percent of polypropylene increased in the blend composition, the average cell size slightly decreased. At the same time uniformity of cell size distribution as well as area fraction occupied by the cells increased. This phenomenon is attributed to lower melt strength and lower melt resistivity which is associated with the polypropylene melt.

ii) Even though the average cell size has slightly decreased with increasing the polypropylene weight ratio, the change in number of cells per unit volume become more pronounced. The reason behind this behaviour is quite clear since, presence of polypropylene in the melt resulted in higher expandibility and at the same time presence of

Table 6.10. Cell size analysis of binary blends of PP/HDPE containing 8 wt% CBA.

Wt% of PP in the Blend	Mean Cell Diameter (mm)	Largest Cell Diameter (mm)	S.D.	Area Fraction Occupied by the cells %	No. of Cells per cm^3 $*10^{-5}$
0	0.1828	0.35	0.0893	42.32	1.72
20	0.175	0.373	0.117	47.51	2.03
40	0.168	0.385	0.095	57.14	2.658
60	0.159	0.345	0.101	64.35	3.13
80	0.153	0.407	0.0779	69.28	3.547
100	0.162	0.45	0.08152	58.187	2.828

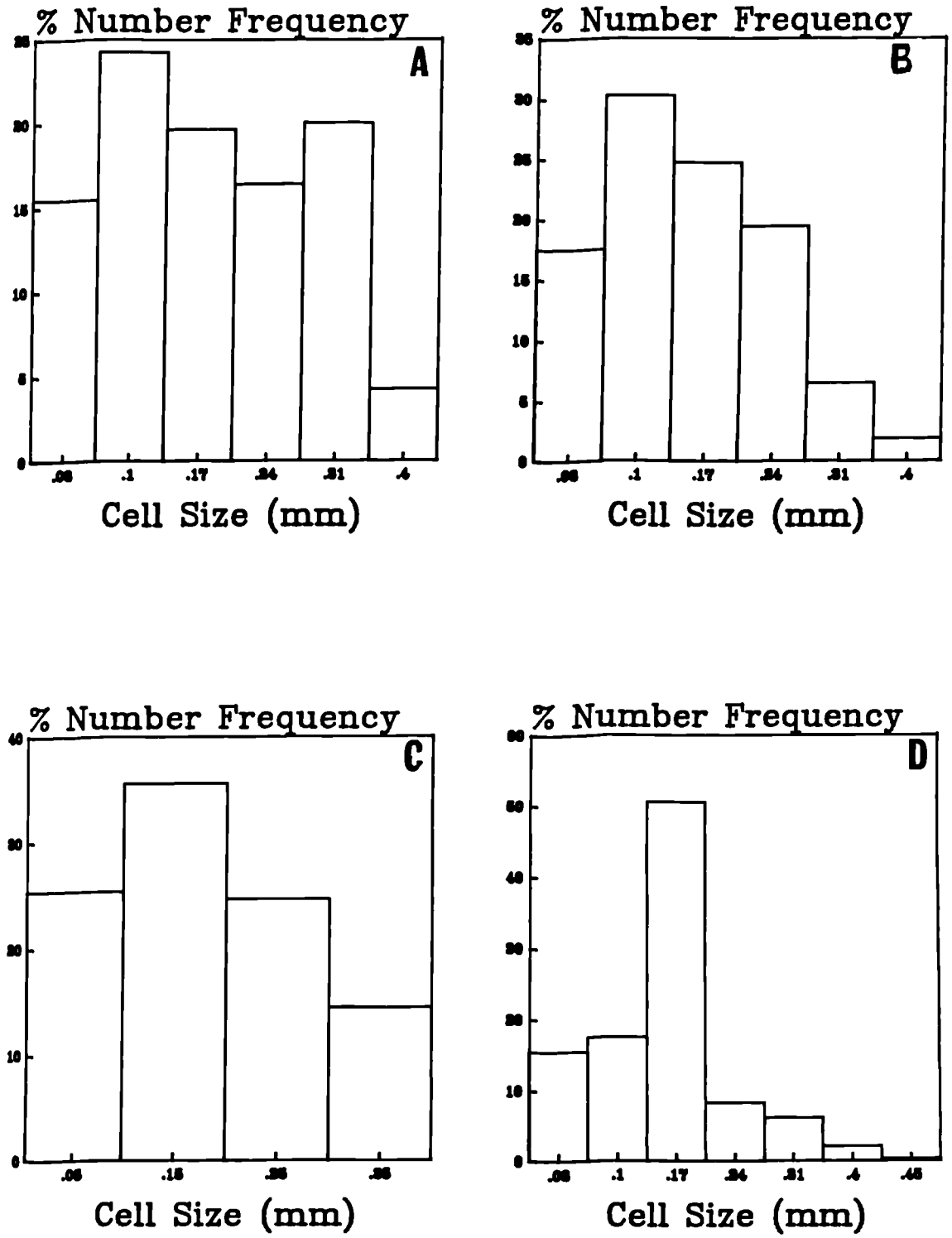

Figure 6.10. Cell size distribution of binary blends of PP/HDPE foams at various blend ratios.
A)20/80, B)40/60, C)60/40, and D)80/20.

Figure 6.11. Cross sectional area of binary blends of PP/HDPE foam, containing 8 wt% CBA.
a)20/80 PP/HDPE
b)40/60 PP/HDPE
c)60/40 PP/HDPE
d)80/20 PP/HDPE

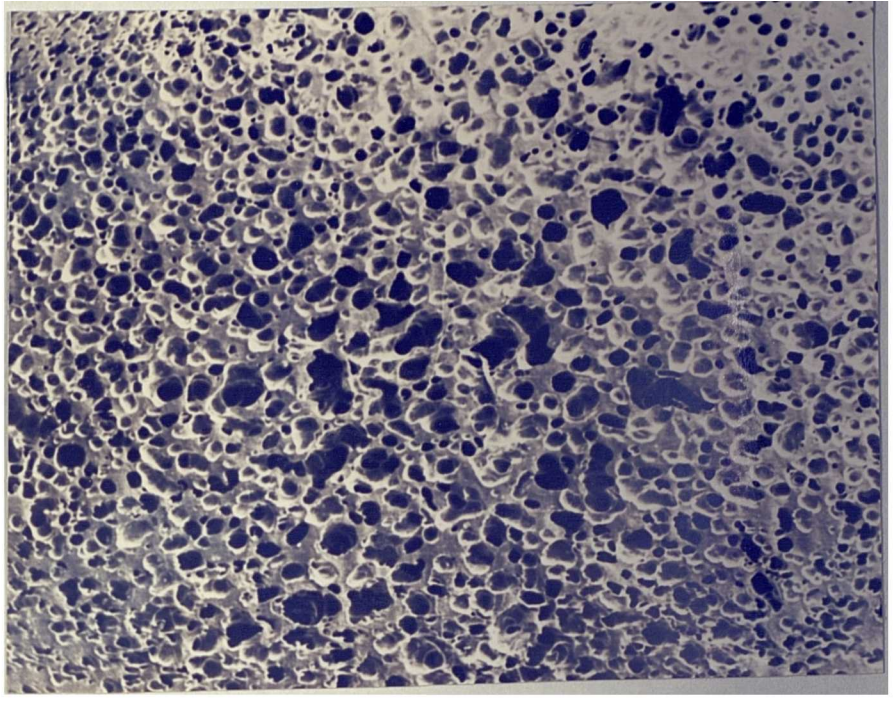

a

1mm

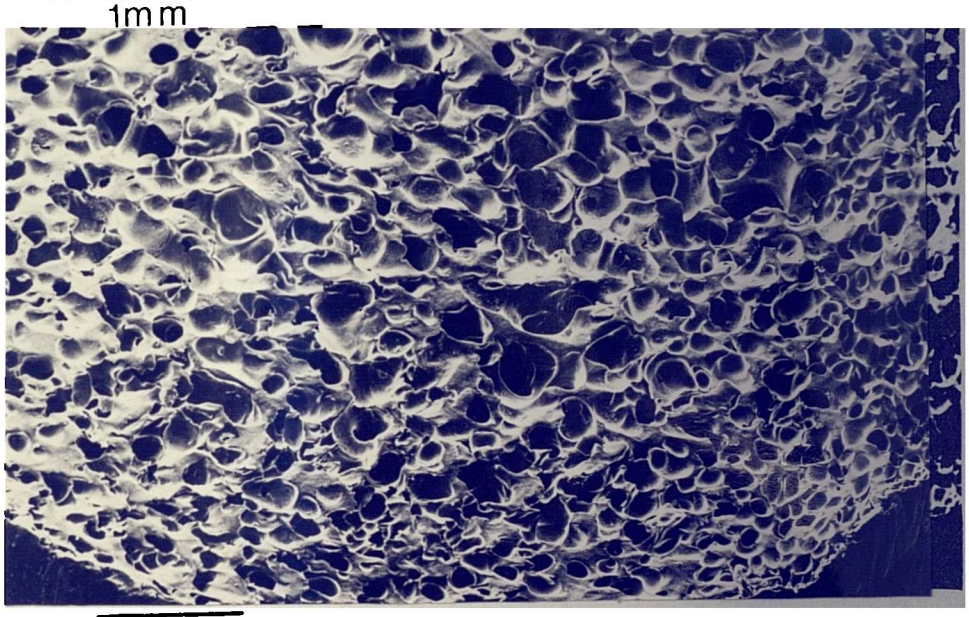

b

1mm

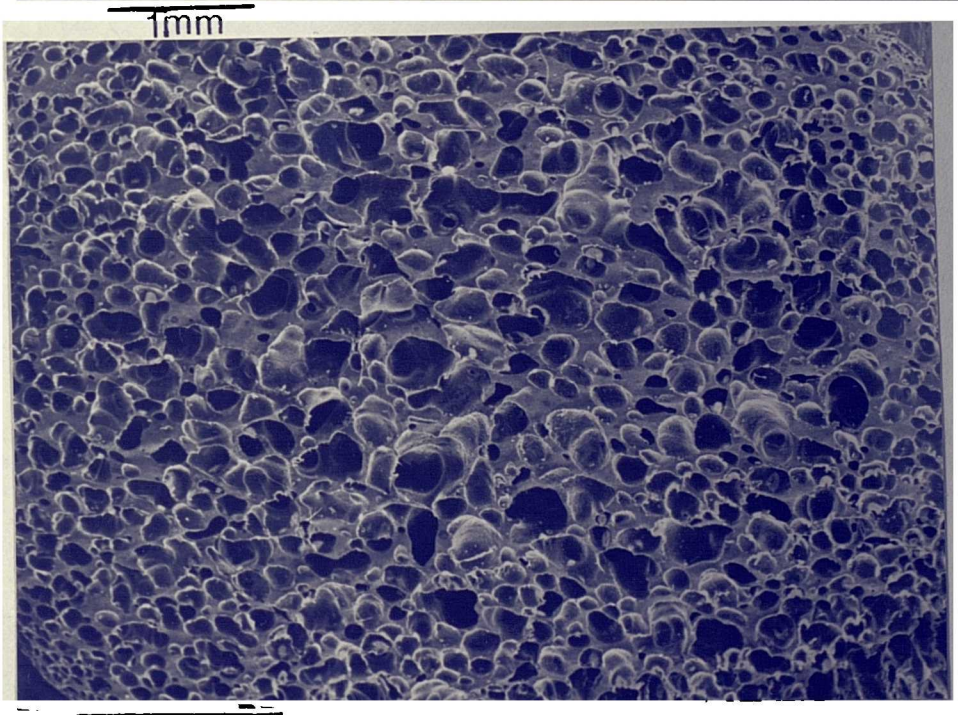

c

1mm

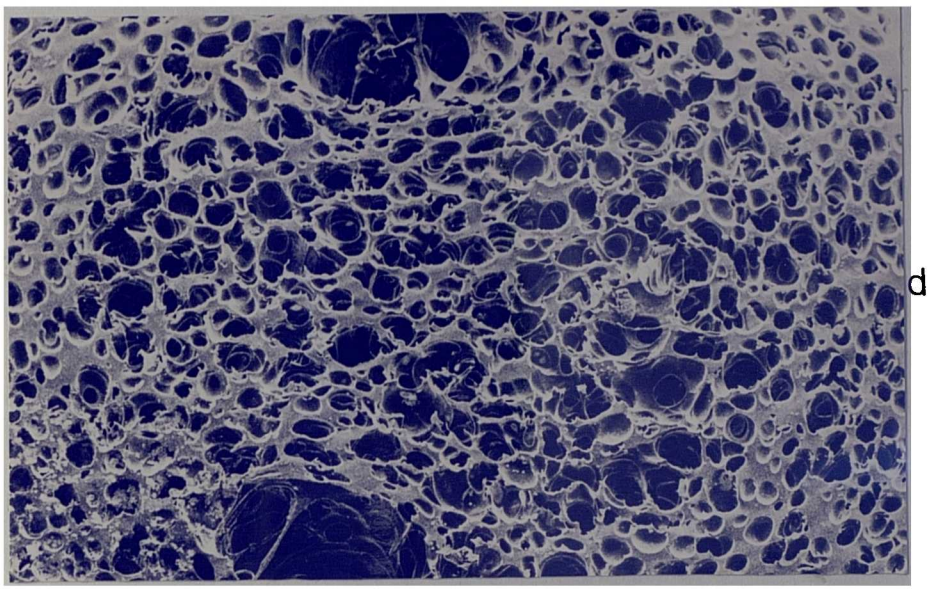

d

1mm

high density polyethylene increased the melt strength of the molten polymer and limited the prevention of cell collapse. Combination of these two phenomena has resulted in a larger area fraction occupied by cells as well as a foam specimen with lower density, as compare to their respective homopolymers (as it was observed in the earlier sections of this chapter).

6.2.4.2 Effects of Chemical Blowing Agent Concentration on Binary Blends of PP/HDPE Foams

Figure 6.12 exhibit the effect of chemical blowing agent concentration on the cell size distribution of binary blends of PP/HDPE foam. As it is noticed, at low concentrations of CBA, due to the low gas/nucleant ratio the cells formed are very small. The result is fairly efficient nucleation but as it was perceived in the previous chapter, the densities of foamed specimens are high. This situation is similar to extrusion at temperatures just below the " Td " of a self nucleating foaming agent. As the CBA concentration increased the gas/nucleant ratio increases causing a decrease in the foam density. Cells size also decreased due to a greater degree of supersaturation in the gas/polymer solution as it leaves the die. It has been postulated (157) that such solutions are less stable and therefore cell nucleation is facilitated. Optimum foam quality is reached at a critical blowing

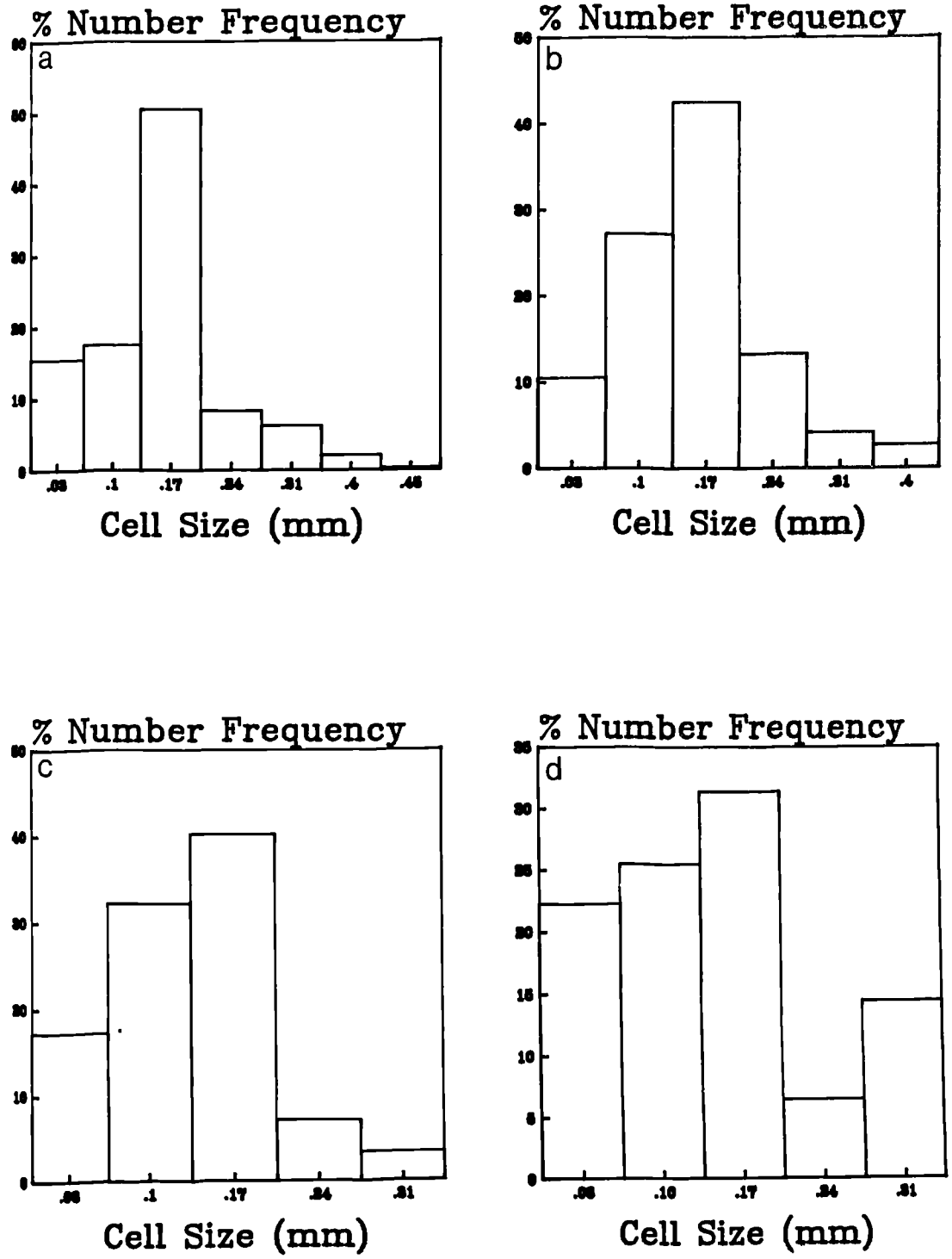

Figure 6.12. Cell size distribution of binary blend of PP/HDPE (80/20) foam at various CBA concentrations (wt.%). a)8, b)10, c)12, d)15, e)20.

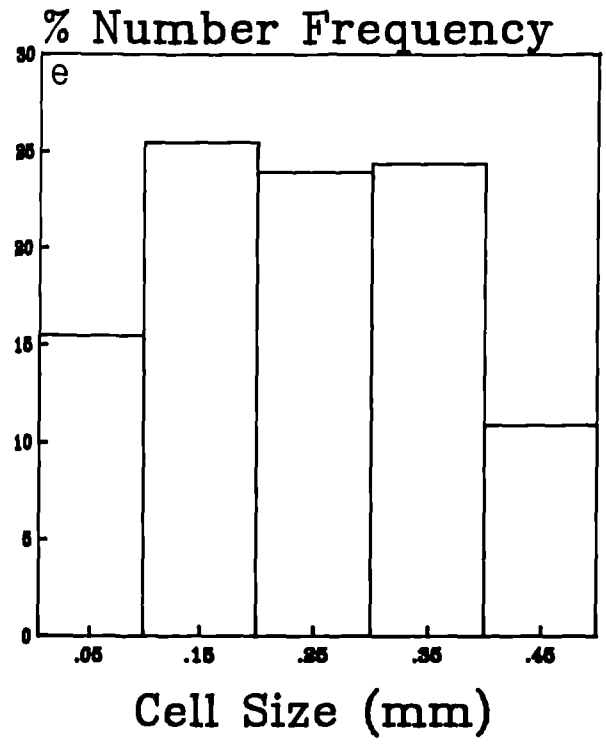
% Number Frequency
e
30
25
20
15
10
5
0
.05
.15
.25
.35
.45
Cell Size (mm)

agent concentration, when the number of nucleating sites (undecomposed BA or residual of CBA) are just adequate to provide efficient cell nucleation. Beyond this concentration, a further increase serves only to deplete the supply of nucleation sites by premature decomposition and a further drop in viscosity of the polymer melt. This explains the decreasing trend in the number of cells shown in Table 6.11. Ultimately as the gas/nucleant ratio becomes very large, the resulting lack of nucleation give rise to an over foamed product.

Table 6.11. Cell size analysis of binary blend of PP/HDPE (80/20) foam at various CBA concentrations.

Wt% CBA	Mean Cell Diameter (mm)	Largest Cell Diameter (mm)	S.D.	Area Fraction Occupied by the Cells %	No. of Cells per cm^3 $*10^{-5}$
8	0.153	0.407	0.0779	69.28	3.547
10	0.151	0.337	0.0811	71.28	3.721
12	0.147	0.295	0.0681	73.38	3.95
15	0.153	0.305	0.0836	72.65	3.547
20	0.211	0.419	0.124	62.46	1.33

CHAPTER 7
MICROSTRUCTURAL ANALYSIS OF EXTRUDED POYOLEFIN AND POLYOLEFIN FOAM

7. Microstructural Analysis of Extruded Polyolefin and Polyolefin Foams

7.1. Optical Characteristics of Extruded Polypropylene (Solid)

The microstructure at the surface of extruded polypropylene was analysed by polarised light microscopy. Thin films, 5-10 μm, were prepared by microtomy from the cross section of extruded samples. The specimens were examined on Richert Zetopan microscope and different regions which varied in width were identified across the section.

Figure 7.1 illustrate the typical banded morphologies through the cross section of polypropylene. As it is noticed the spherulitic structure has been poorly developed in the skin layer. This structure less band is probably due to rapid cooling, which do not allow sufficient molecular reorganisation for development of spherulitic morphology. Also the nucleation did not occur at the skin layer as was originally expected, but rather at varying distance into the bulk of the polymer (see Figure 7.1.a). Also it should be pointed out the bright spherulites appearing in the Figure 7.1 are due to presence of β-spherulites, therefore as one can notice these spherulites are only present in the vicinity of skin layer, and from almost 600 μm away from the skin layer up to core region the morphological structure were mostly found to be

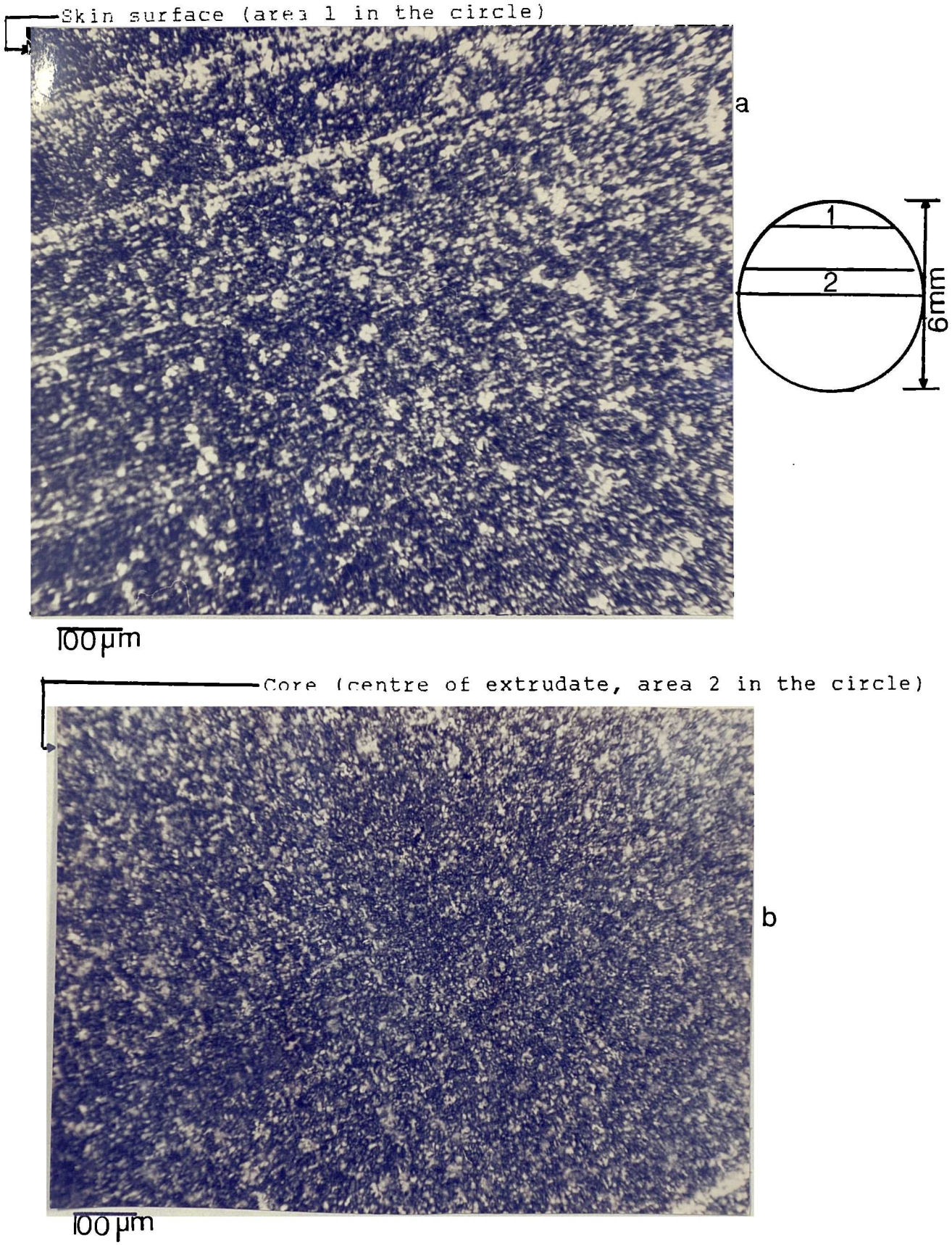

Fig. 7.1. a) Morphological analysis of skin layer of extruded polypropylene.
b) Morphological behaviour of core layer of extruded polypropylene.

monoclinic (α-phase structure) as it is evident from Figure 7.1.b. It is believed this behaviour is due to slower cooling of the foregoing region as compared to the skin layer.

The extent and width of structureless regions as well as the type of spherulites strongly depend on the processing condition such as take off speed as it is noticed from Figure 7.2. The foregoing material was processed at apparent shear rate of 1035 S^{-1} (the apparent shear rate is measured at the die exit), and take off speed of 0.06 m sec^{-1}. When the extrudate rod was processed at high screw speed, hence, high take off speed (.30 m sec^{-1}), the material beneath the skin layer (less than 1 mm away from the surface) still was in molten state and cooled at room temperature (faster cooling rate). This effect is similar to injection moulding of polypropylene at different mould temperatures studied by Kamal et al.(109).

7.2. Micromorphology of Extruded Polypropylene by Transmission Electron Microscopy (TEM)

The microstructural analysis of extruded rods of polypropylene was also characterised by TEM. The following studies were carried out on the skin and core layer of (approximately 3000 μm away from the surface of the rod) the extruded samples. A surface

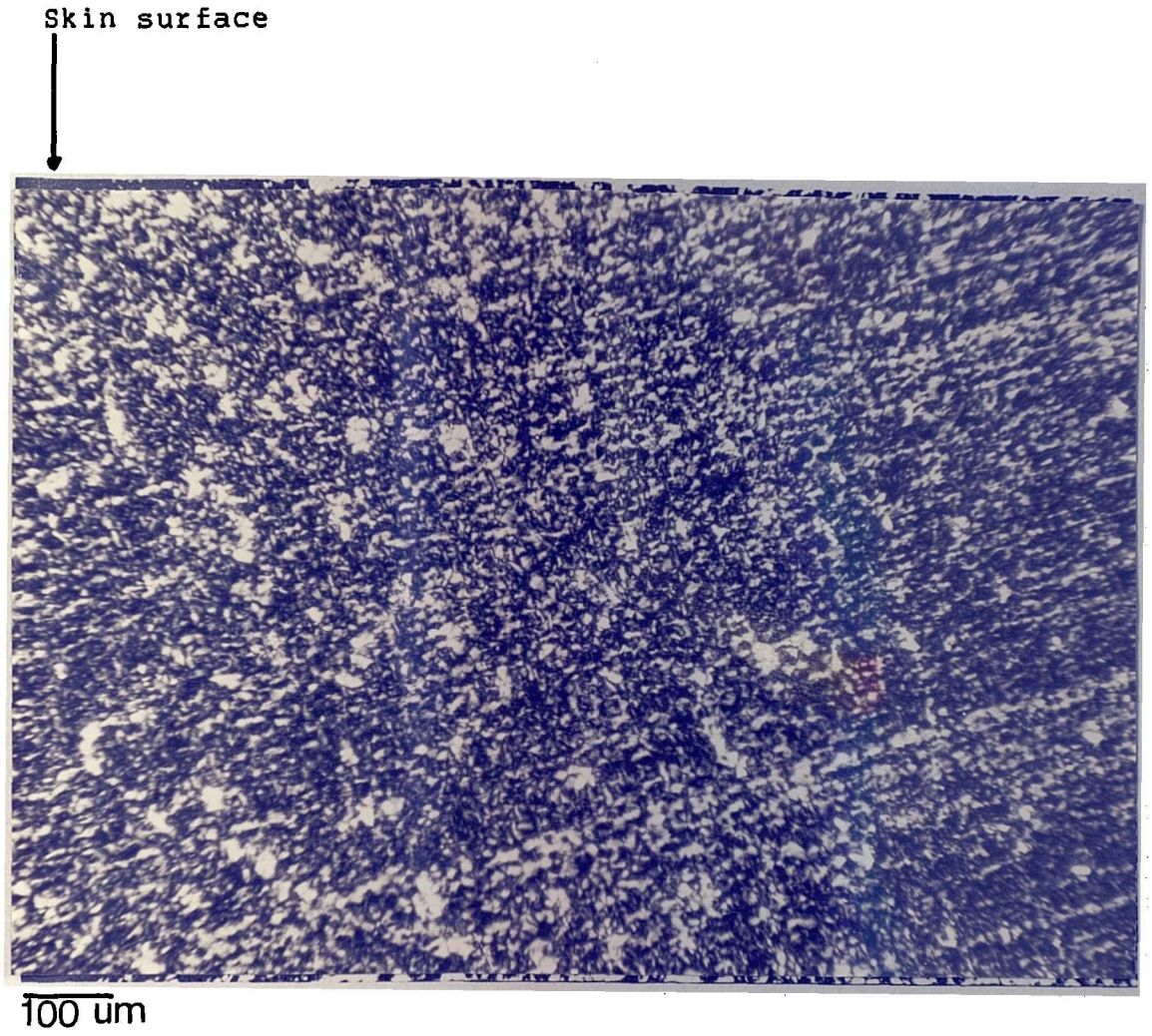

Fig.7.2. Morphological ana ys s of k n polypropylene processed a shea rate of 1035 S^{-1} (0rpm) and ake f speed of 0.06 m/sec

through the thickness parallel to the flow direction was exposed by microtomy and then it was carefully polished down to 1 μm finish (the microtomed surface was mounted in epoxy resin to prevent any distortion during polishing). Afterwards the surface was ultrasonically cleaned and then etching techniques described in section 3.9 were carried out for 20 hours at room temperature. The temperature and time of etching was determined by trial and error in order to achieve the best results. After the etching process the surface was cleaned ultrasonically according to the procedure of Norton (102), then the samples were vacuumed dried and two stage replication was applied. The surface of replica was analysed by TEM using a Philips EM301 microscope. Details of the findings are listed below.

Figure 7.3 shows the spherulitic structure of skin layer of extruded polypropylene. At high magnification, some of fine features of individual layers become more noticeable. As it was expected in the skin layer, mostly the lamellae have oriented in the flow direction as shown in Figure 7.4. This layer most likely consist of chain extended material, which is typical of oriented melt. It is also interesting to note that just below the skin layer, the spherulite has cracks running perpendicular to the flow direction (see Figure 7.3 and 7.4). The presence of

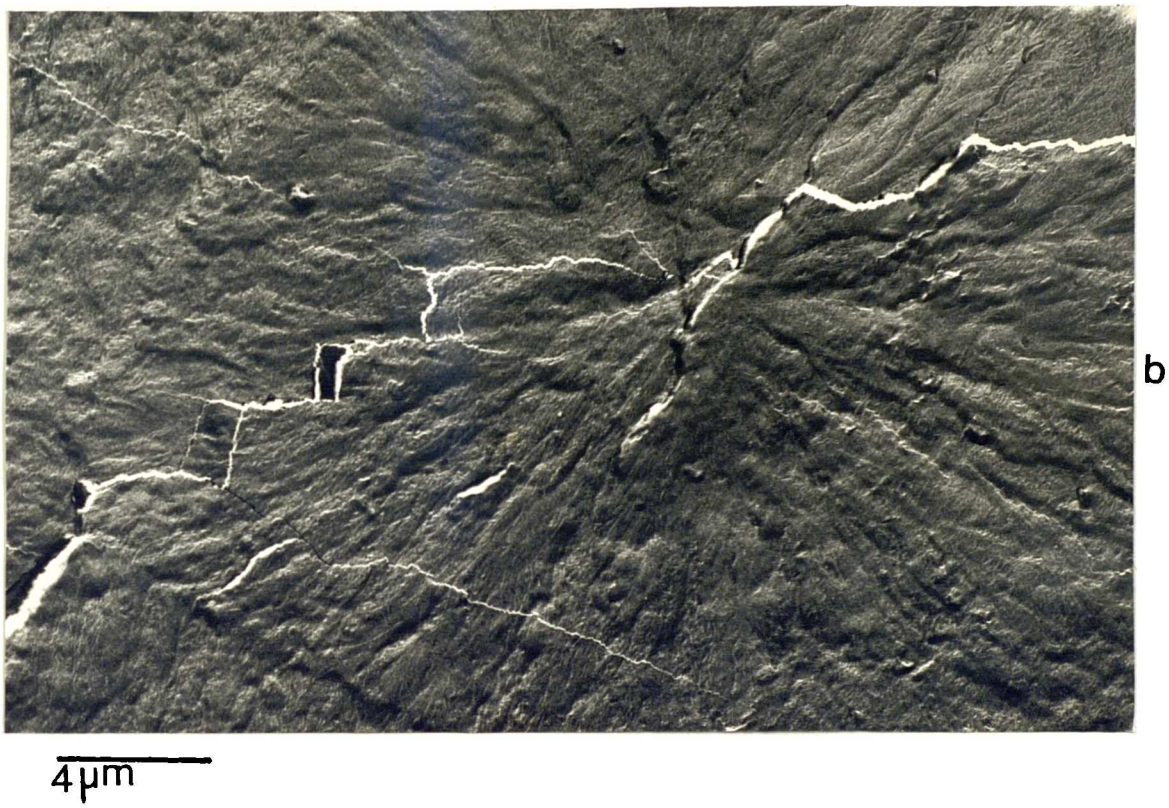

Fig. 7.3 a) Low magnification of α-phase spherulite in skin layer.
b) Removal of amorphous region in spherulite structure of polypropylene.

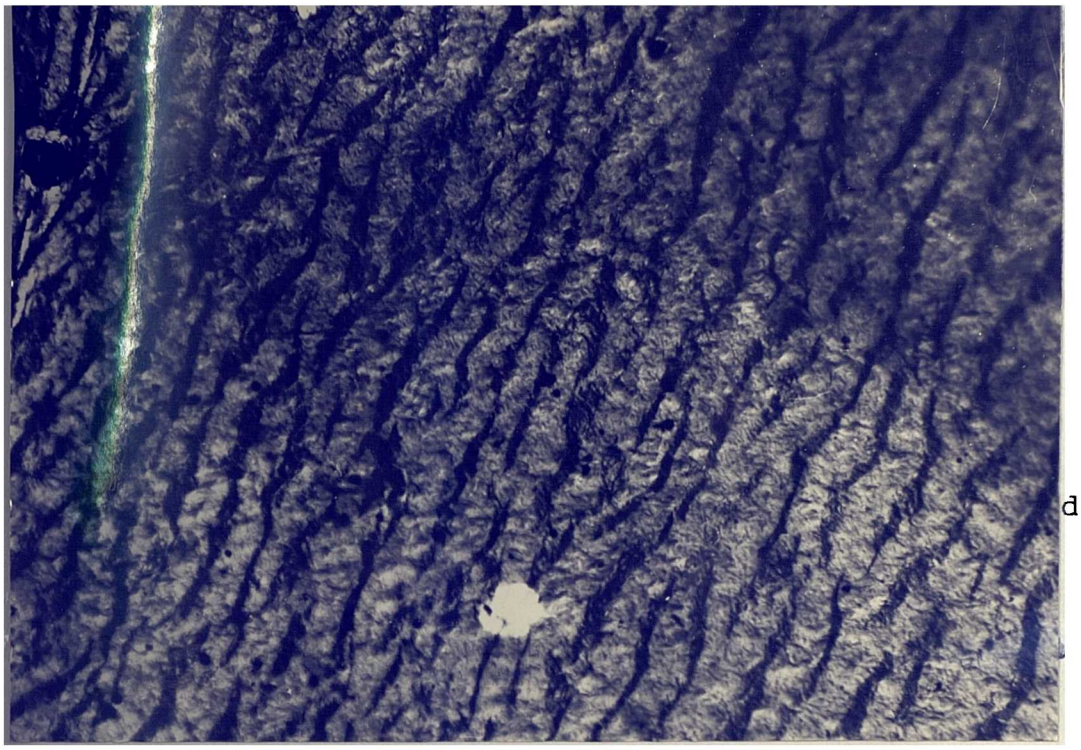

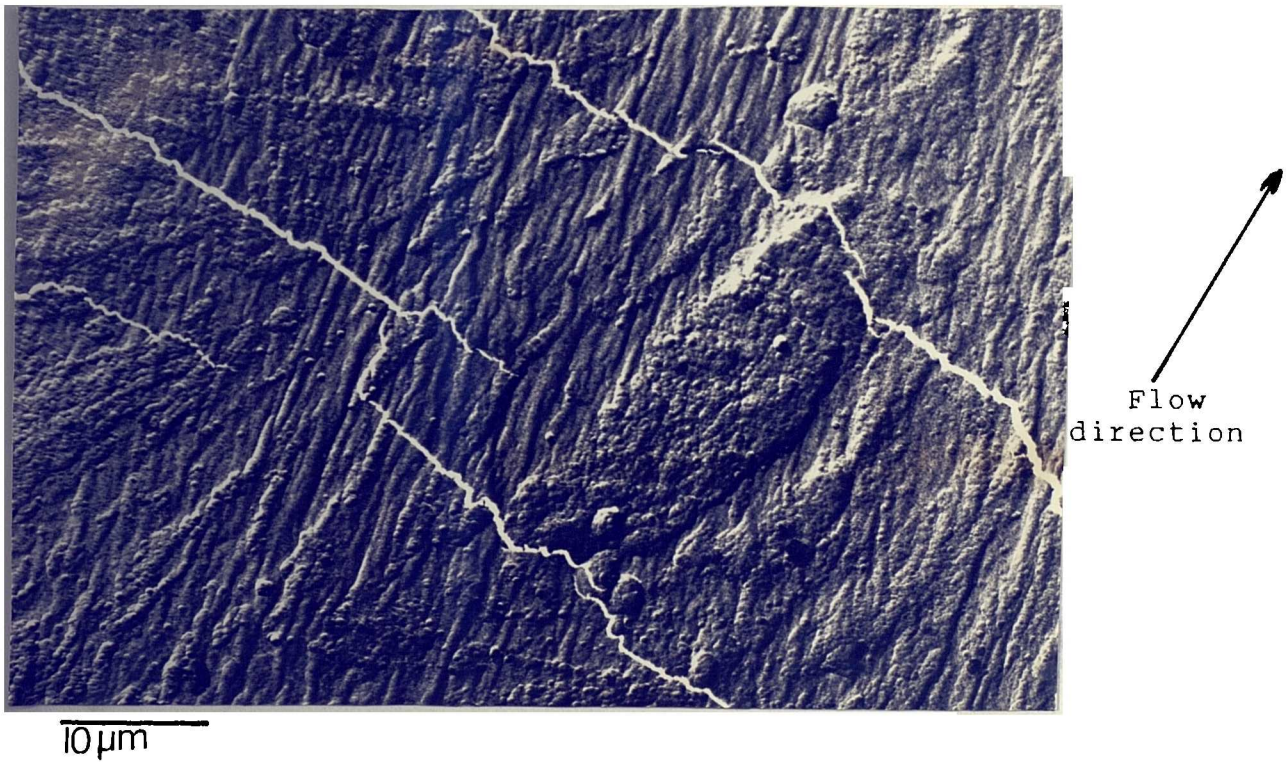

Fig. 7.4. Morphology in highly sheared area reavels typical row mucleation of lamellae laying perependicular to flow direction.

these cracks indicates that, amorphous material was present on the surface prior to etching. similar observation has been reported by Fitchmun and co-worker (160,161) using aqueous chromium trioxide and chromic-sulphuric acid etchants.

Microstructural analysis of the core of the extrudate rod revealed the unique feature of cross hatched type lamellae branching which occurs in all types of α-phase monoclinic polypropylene (98,102,162). Figure 7.5 display a low magnification appearance of these spherulites which occurs up to 40 μm in diameter towards the core of extrudate rod. This figure shows how the branching affects the lamellar morphology bestowing upon it what is essentially a bimodal orientation, where radial lath like lamellae nucleate tangential and cross-hatched overgrowths of lamellae are oriented nearly orthogonally. Cross-hatched morphology is also shown in Figure 7.6, where in this figure R represents the radial direction within the spherulite whilst T represents the branched, tangential direction of the cross-hatched overgrowth. The intercrossing and shorter lamellae T, were measured to be at angle of approximately 80°with respect to radial direction which is in good agreement with finding of Khoury (98). Norton (102) in an investigation on the morphological studies of isotactic polypropylene from melt, found that at a

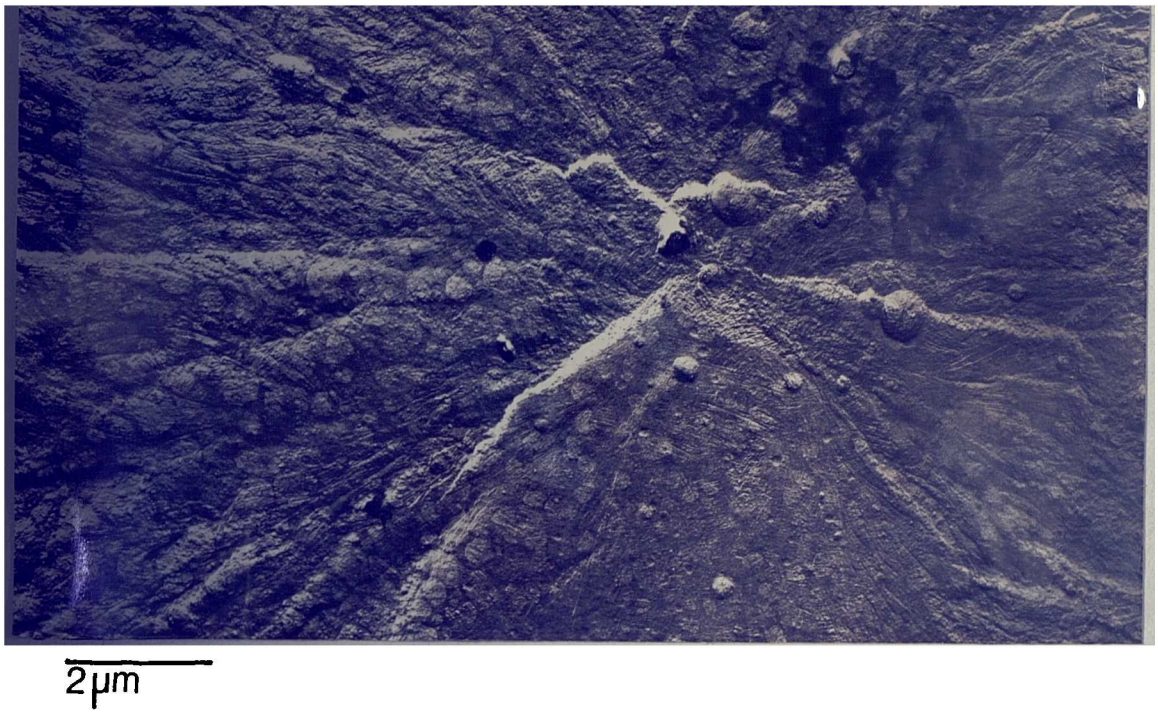

Fig. 7.5. Typical of cross-hatched morphology of α-phase spherulite.

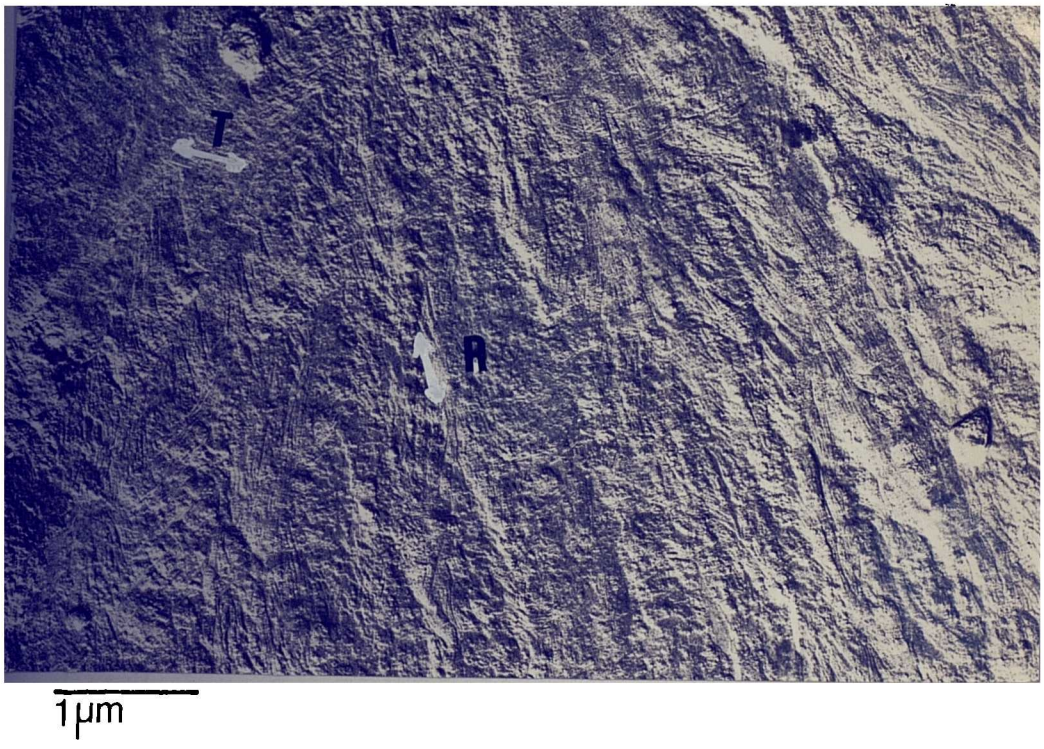

Fig. 7.6. Appearance of features of cross-hatched morphology R=radial; T=tangential direction.

crystallisation temperature of 148°C the difference in the respective thickness of the two components can be identified, the radial lamellae being slightly thicker ca. 50 nm for the radial component and ca. 40 nm for the tangential component.

The effect of this twinning provides the explanation for the change of birefringence of spherulites of monoclinic polypropylene as observed by many investigators (80,82,102). The net birefringence and its sign depends on the relative proportion of twinned and untwinned components. Lamellae with radial growth display negative birefringence (as with β-spherulites) whereas lamellae with tangential growth display positive birefringence (102). In type I α-phase spherulites the T and in type II β-phase spherulites the R lamellae should predominate in the cross-hatched (80).

7.3. Thermal Analysis of Extruded Polypropylene Homopolymer

Differential scanning calorimetry (DSC) was used to characterise the thermal behaviour of extruded samples of polypropylene along the flow direction. Layers of 500 μm were cut and then tested according to the procedure described in section 3.10. The technique itself was found to be available and convenient tool for comparative analysis of

microstructure of crystalline polymers such as polypropylene, whilst the results indicated many interesting thermal transitions.

Figure 7.7 exhibit the thermal analysis of extruded polypropylene carried out on the Perkin Elmer DSC II. As it is noticed the melting curves of skin layer display one major peak corresponding to an α-phase melting endotherm at 437°K and one minor peak on the shoulder of major peak at 422.1°K. The latter peak agrees with β-phase melting endotherm reported by Lovinger (101). It is interesting to show that when a sample from same layer was first heated to above the melting temperature of polypropylene and cooled at slow rate (5°K min^{-1}.) and then reheated, the first peak which appeared previously in Figure 7.7.a at 422.1°K was absent (see Figure 7.7.b) which proves the point that β-spherulites form due to fast cooling. Beyond this point only one endothermic peak was observed around 437°K.

From these results, it is concluded that with fast cooling a two phase system is observed in the crystal structure of extruded polypropylene and also due to alignment of the chains (1000-2000 μm from the surface), the degree of crystallinity is highest in this region as it is shown in Table 7.1. A summary of melting behaviour observed in skin and core layer is

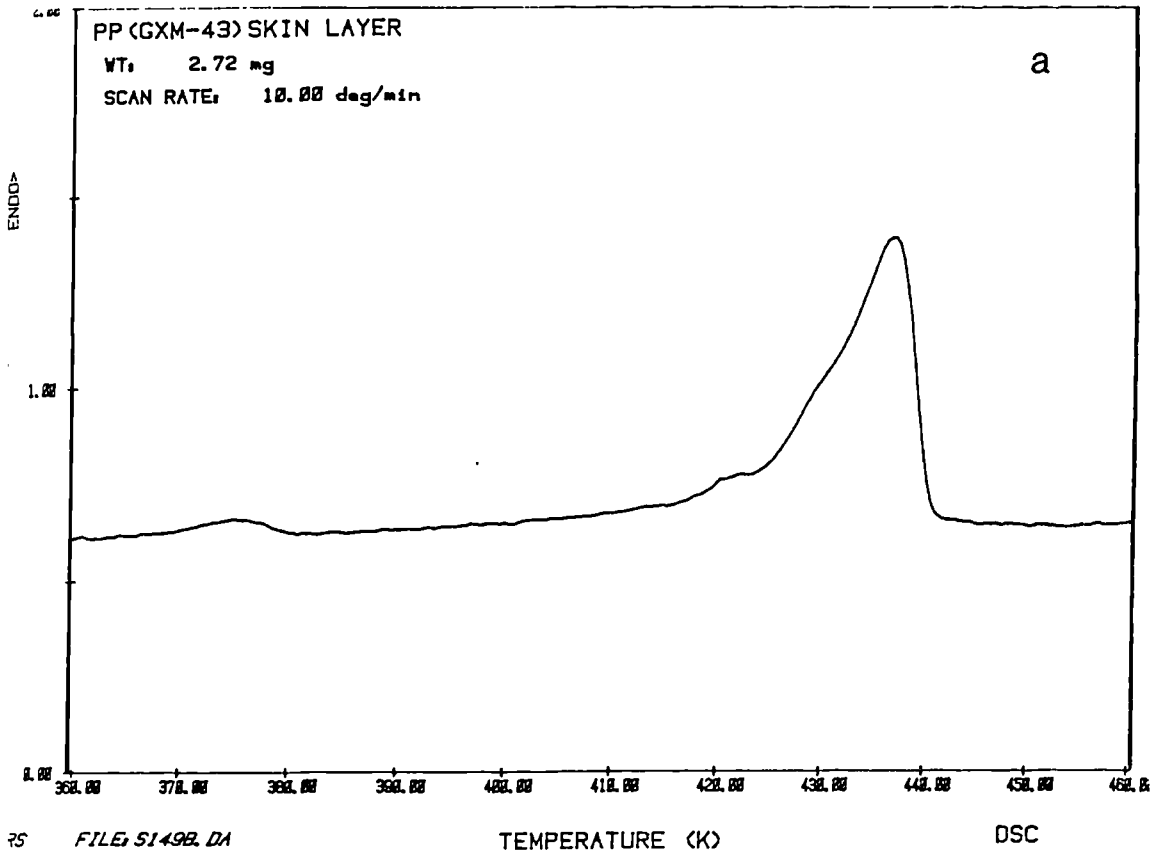

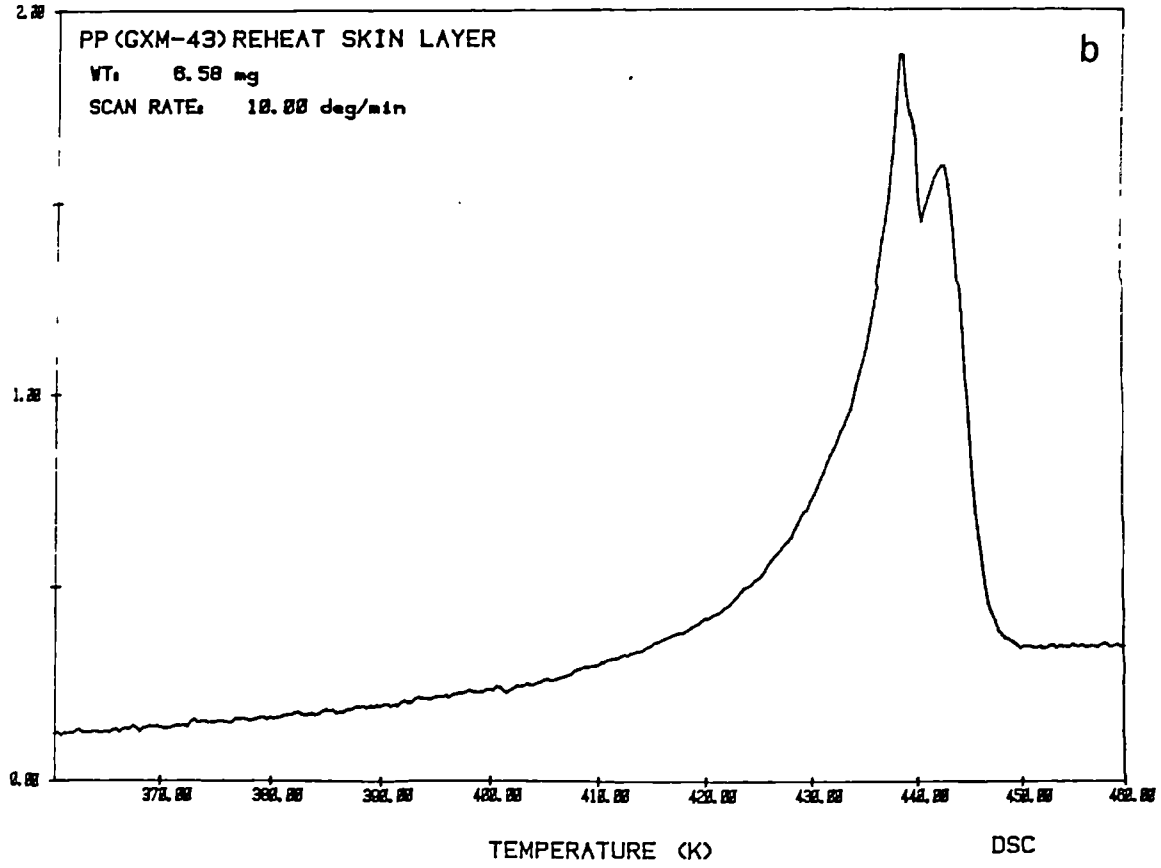

ig.7.7 a) melting behaviour of skin layer of extruded polypropylene.
b) melting behaviour of slowly cooled ($5\,^{\circ}K\ min.^{-1}$) sample of polypropylene.

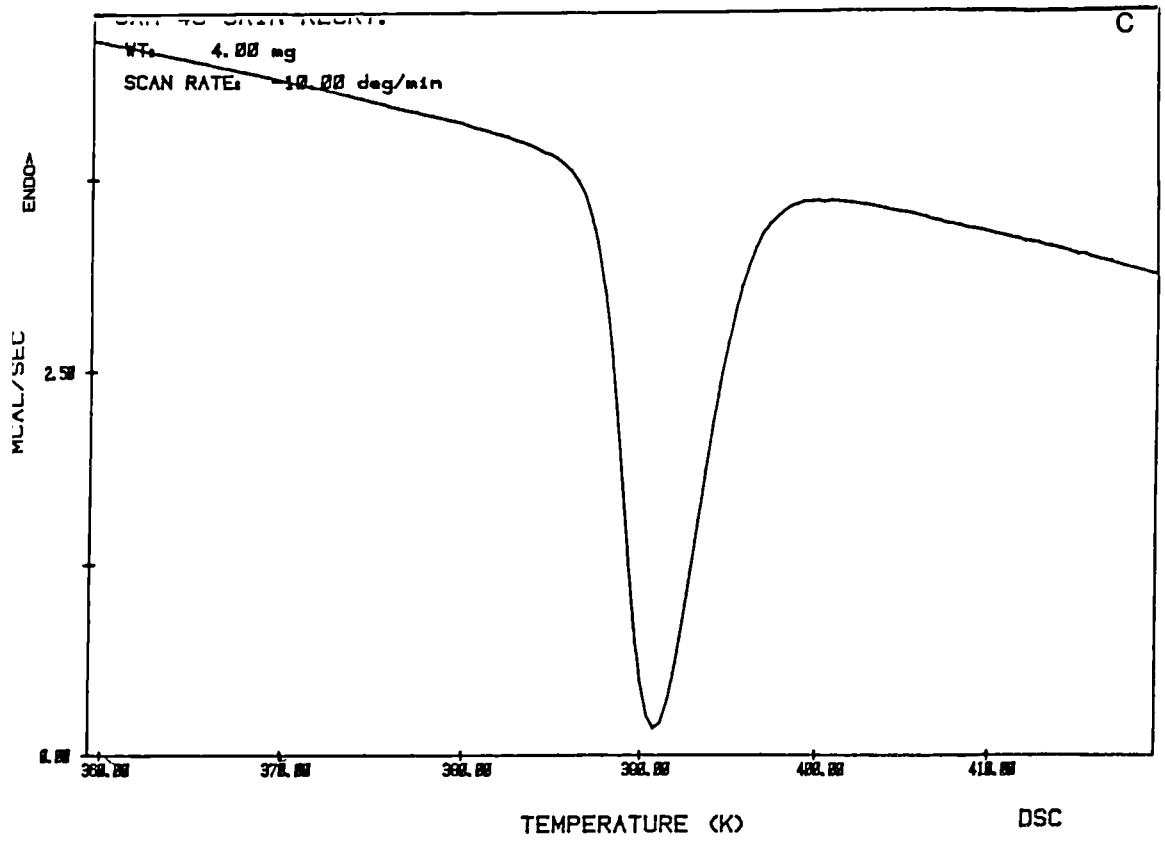

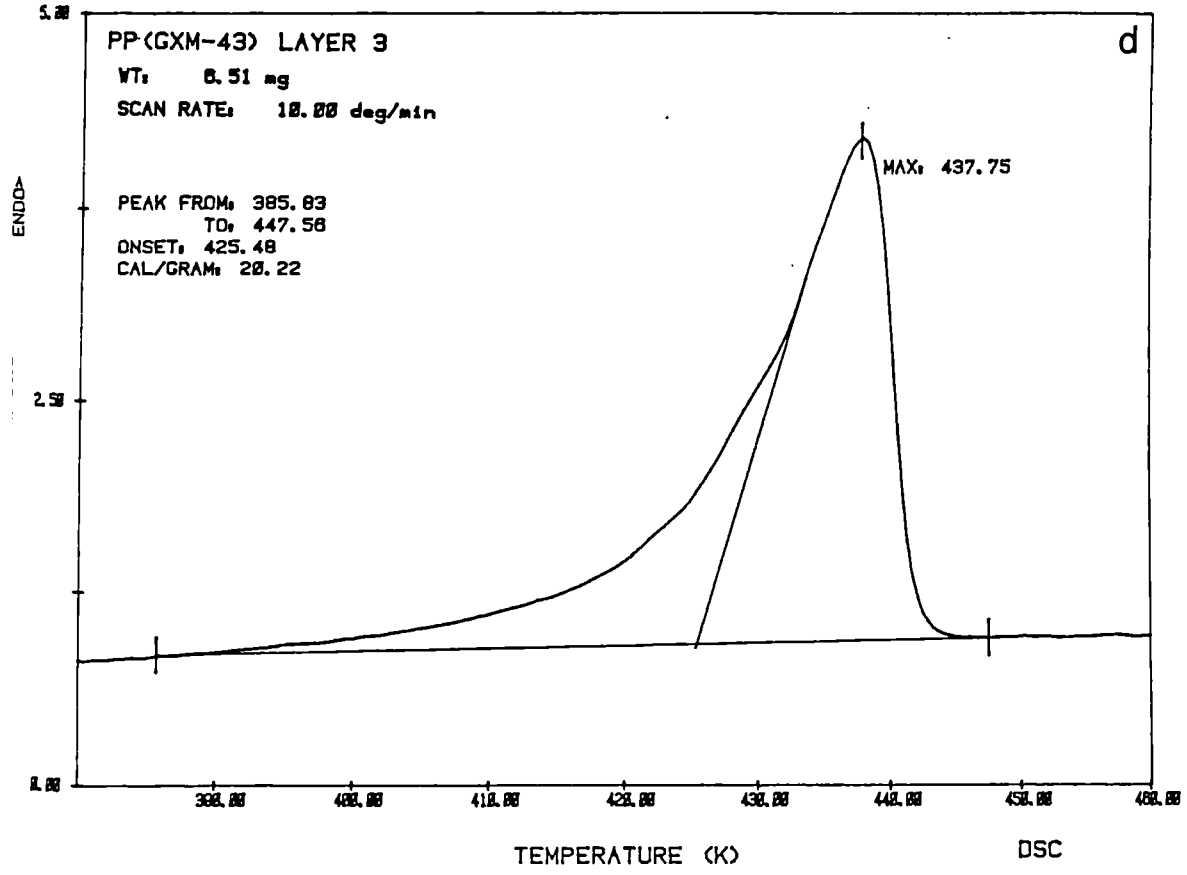

ig. 7.7 c) recrystalisation behaviour of polypropylene.
d) melting behaviour of polypropylene (1500 µm away from skin).

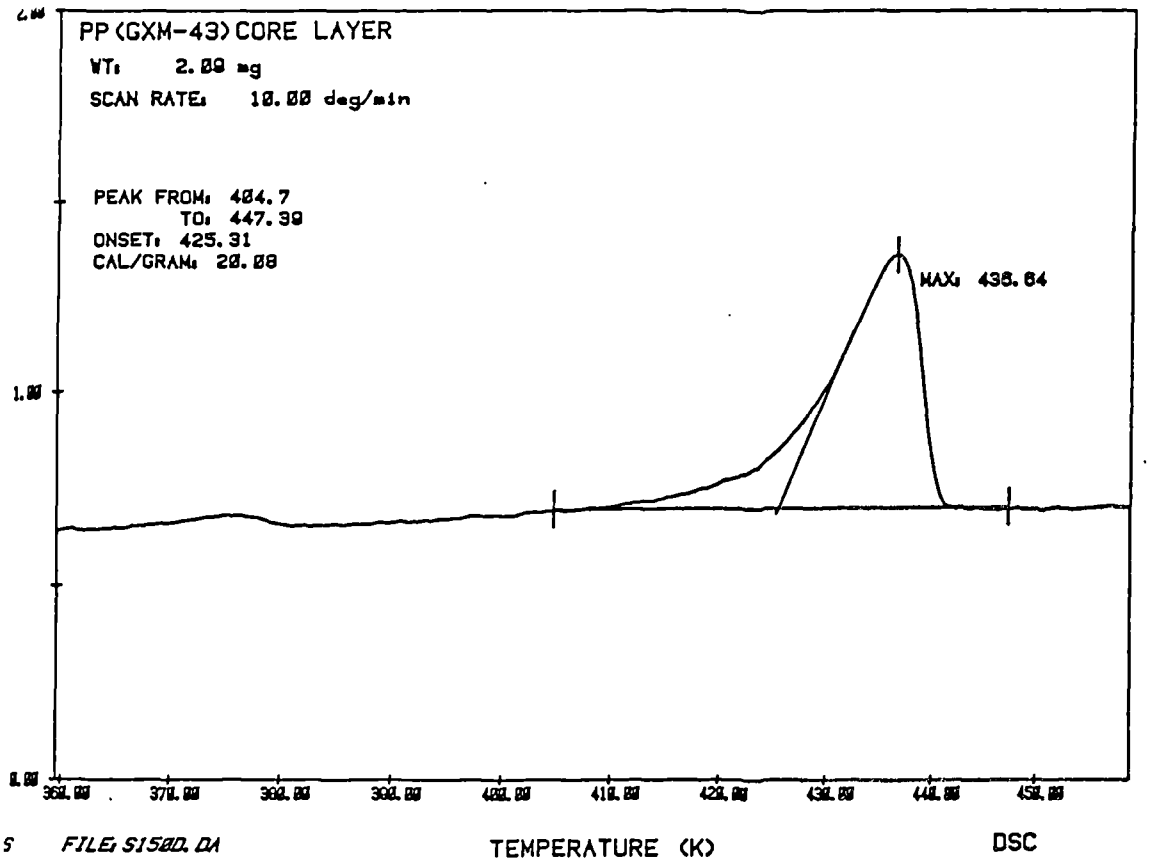

igure 7.7. e) melting behaviour of core layer extruded polypropylene.

Table 7.1 DSC analysis of extruded polypropylene. Screw speed 60 rpm, temperature of cooling media 60°C.

Thickness of layer from the surface (μm)	Melting peak temp.(°K) β	α	Degree of super-cooling (°K)	Degree of crystal.* %
10-500	422.1	436.83	46.28	34.14
500-1000	-	437.1	44.55	37.56
1020-1500	-	437.75	45.25	36.27
2000-2500	-	437.52	46.15	35.88
2500-3000	-	436.64	45.38	33.03

* Heat of fusion for 100% crystaline polypropylene was taken as 247 J g^{-1} (163).

presented in Table 7.1.

Degree of crystallinity and crystalline structure of extruded polypropylene were not altered by varying the processing conditions such as melt temperature and pressure, whereas cooling rate (temperature of cooling media) has effected the degree of crystallisation through the thickness of the sample as it is evident from Tables 7.2 and 7.3, respectively.

7.4. Scanning Electron Microscopy (SEM) Studies on Extruded Polypropylene

From a practical standpoint the adaptation of the permanganic etching technique for use with the more easily used SEM should provide a tool for the rapid identification of bulk morphologies at the spherulitic level. Although the resolution is decreased, and the possible effects of beam damage may be present, an advantage of such method lies in the ease and consistency of sample preparation. This stems from the obviated need for replication.

The low magnification available using SEM proved to be adequate in assessing the crystalline morphology of extruded polypropylene. The following figures typify the results.

Table 7.2 DSC analysis of extruded Polypropylene. Screw speed 10 rpm, temperature of cooling media 60°C.

Thickness of layer from the surface (μm)	Melting peak temp.(°K) β	Melting peak temp.(°K) α	Degree of super-cooling (°K)	Degree of cryst.* %
10-500	-	437.25	43.55	36.22
500-1000	-	437.9	42.85	35.05
1020-1500	-	438.1	44.83	34.91
1500-2000	-	436.25	42.57	35.54
2000-2500	-	436.43	42.78	34.26

* The heat of fusion for 100% crystalline polypropylene was taken as 247 J g^{-1} (163).

Table 7.3 DSC analysis of extruded polypropylene. Screw speed 60 rpm, temperature of cooling media 80°C.

Thickness of layer from the surface (μm)	Melting peak temp. β	Melting peak temp. α	degree of cryst.* %
0-500	-	438.1	38.37
500-1000	-	437.45	39.73
1020-1500	-	437.7	35.68
2000-2500	-	436.9	35.2
2500-3000	-	436.25	33.83

* The heat of fusion for 100% crystalline polypropylene was taken as 247 J g^{-1} (163).

An overall examination of Figure 7.8, which is a SEM micrograph of an etched cross section cut perpendicular to the extrusion direction, reveals a texture remarkably similar to that seen in polarised light microscopy (see Figure 7.1). Figure 7.8 is interpreted as showing crystalline material forming poorly defined spherulites beginning near skin layer and ending in a well developed spherulite core. It is noticed that the structureless layer is about 40 μm thick. In the second layer the spherulites are prematurely developed. This layer is about 200 μm thick. The third layer which is about 2000 μm away from the skin layer is consist of only α-spherulites (see Figure 7.8.b and 7.8.c). The core layer is basically consists of monoclinic (α-phase) spherulites. It is interesting to compare the above findings with the results of microstructural analysis of injection moulded of isotactic polypropylene witness by Fitchmun et al.(160), where he has noticed that the size of the crystalline structures at boundaries (transition between skin and core layer) are abruptly changed and the spherulite close to the skin layer appear to have developed in row as opposed to randomness of spherulites found above this layer. This sort of pattern was not observed in this study, mainly due to high shearing of molecular chains and also different cooling process associated in the injection moulding process.

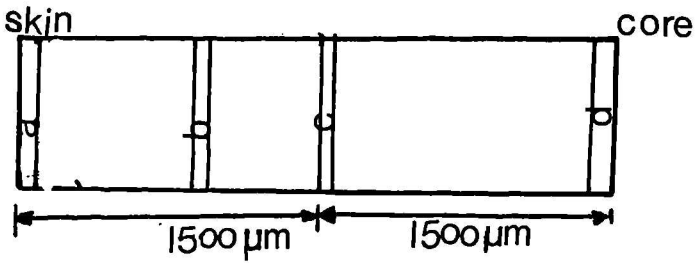

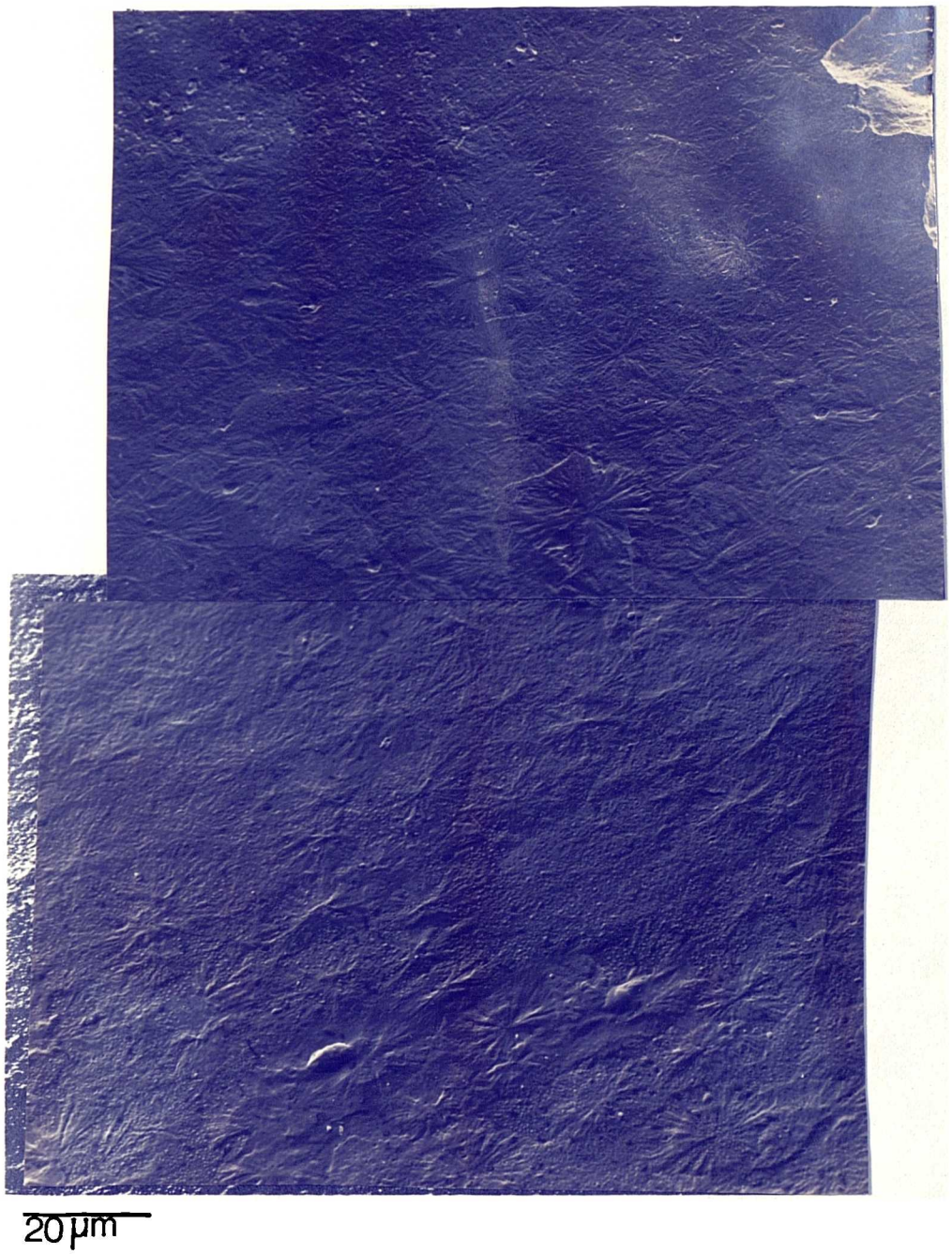

Fig. 7.8 a) Skin layer analysis of extruded polypropylene. Position of areas covered in Figures 7.8 a-d are shown in above diagram.

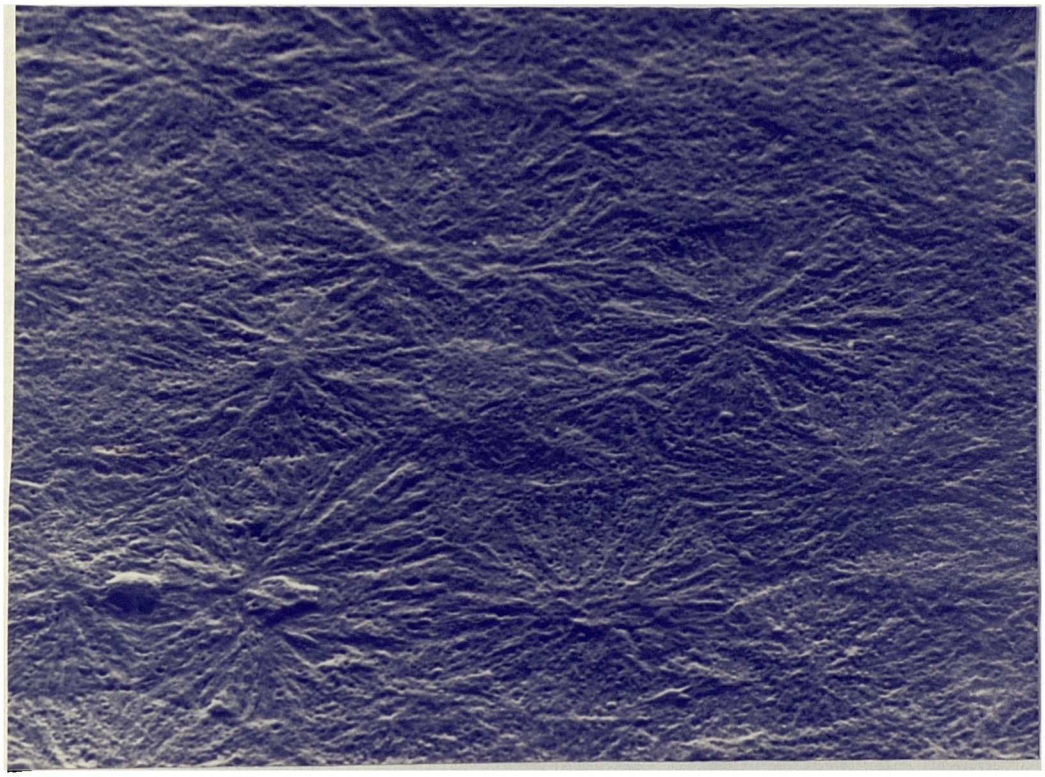

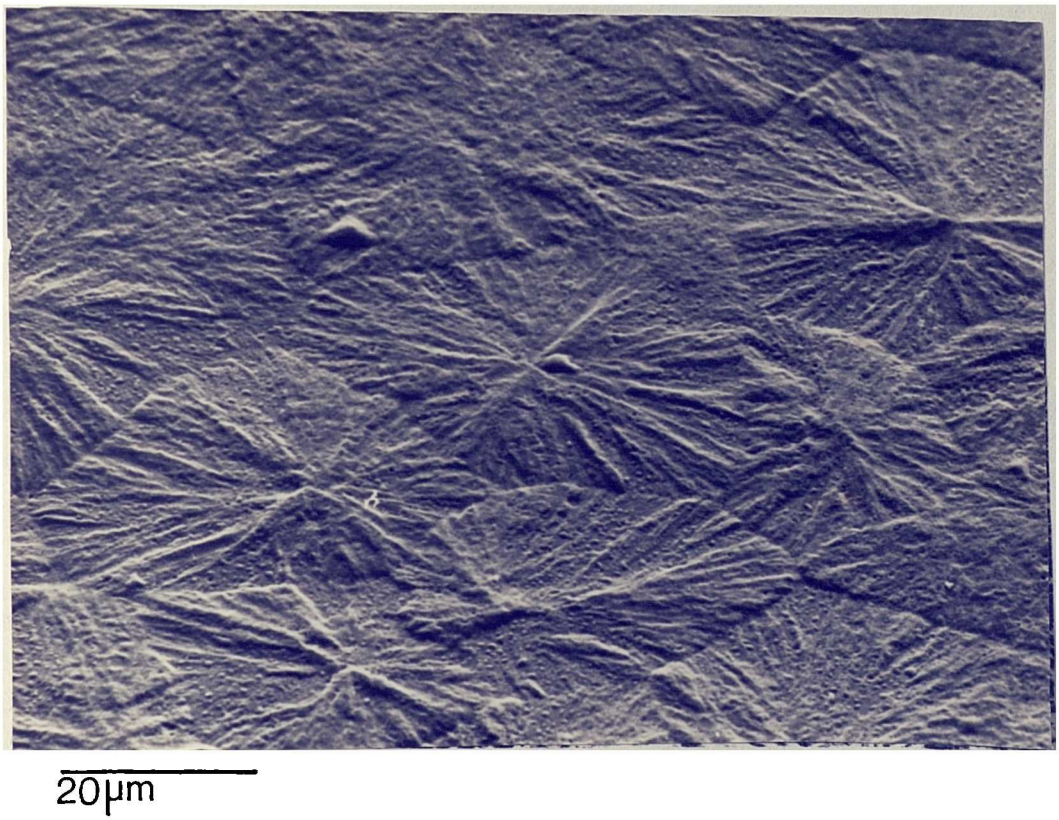

Fig. 7.8. b) Surface analysis of polypropylene.
c) Surface analysis of polypropylene (around 2000 µm away from the surface).

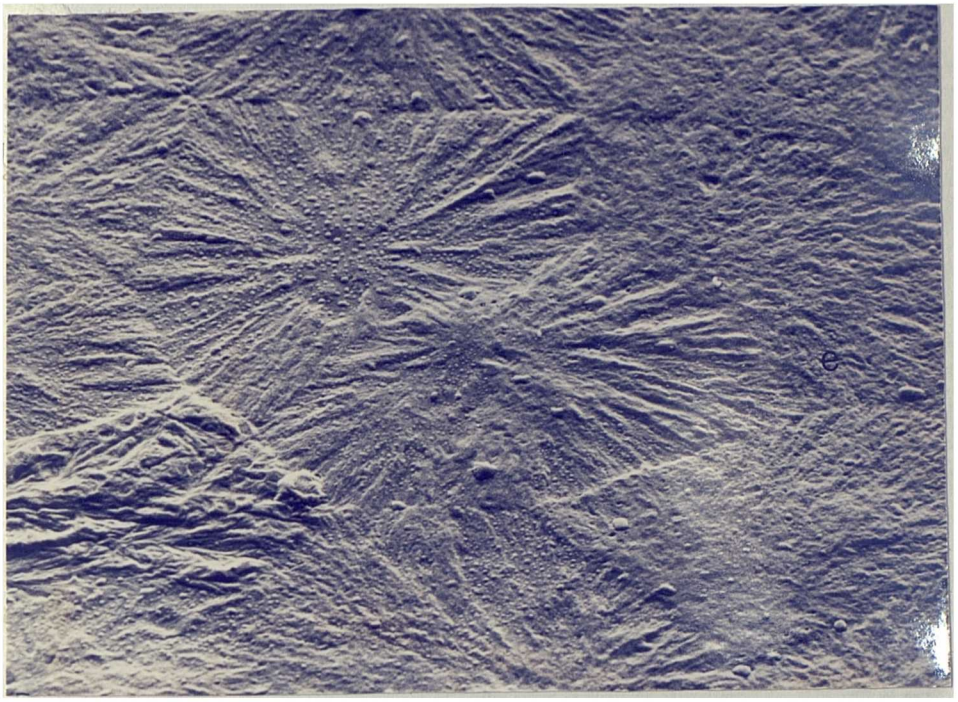

d

10 µm

The observation presented thus far showed that the changed in spherulites size is continuous within each layer and there are changes in type and perfection of spherulites from one layer to another. This phenomenon is due to the temperature gradient existing within the sample upon cooling. Crystallisation of polymer melt cooled by cold media (in this case water with temperature of 60°C) leads to a transient temperature gradient near the surface. This favours a higher nucleation rate at the surface than in the core (163,164). If the gradient is short relative to the induction time for nucleation, the morphology should be composed of crystalline structure of approximately the same spherulite size. This is because development of these growing structures is produced at the same temperature and, therefore, at the same rate. On the other hand, if the extinction time for this gradient was longer than the induction time, the morphology should consist of spherulites having a size gradient with the smallest being near the surface (Compare Figure 7.8.a-7.8.d). Observation supporting this are common in the literature for variety of semi-crystalline polymers (98,161).

7.5. X-ray Diffraction Analysis of Extruded Polypropylene

7.5.1. Introduction

A survey of extruded samples of polypropylene by methods mentioned so far have enabled the identification of two forms of crystalline structure. Since the nucleation of the β form is only few percent as compare to α-phase, therefore it has not been an easy task to assess their concentration or distribution through the cross section. Therefore, an attempt has been made to quantify the concentration and distribution of β-phase by X-ray diffraction technique proposed by Trotingnon et al. (133). The detailed analysis of β-phase concentration, α-phase orientation parallel to the surface and crystallinity index are presented in section 3.11.

7.5.2. X-ray Diffraction Analysis Through the Thickness of Extruded Polypropylene

The same samples (same areas) which were prepared for the TEM and DSC analysis were used for X-ray diffraction investigation. Layers of 500 μm thick were cut parallel to the flow direction then their surface were exposed to the X-ray beam in order to determine the variation of crystallinity index and direction of β-phase and α-phase orientation through the thickness (skin to core layer) of the

extruded rod samples.

Figure 7.9 shows a typical diffractogram for extruded polypropylene. The calculated results obtained from these figures are presented in Table 7.4. The following points can be deduced from analysis of these diffractograms;

i) The diffractogram of skin layer shows a weak β-phase of (300) plane and beyond this layer there is no indication of any β *crystalline* structure.

ii) For isotropic samples, such as powder or granules the values of A =0.57 (133), therefore a slight degree of orientation of c-axis with respect to the flow direction was only observed up to depth of 2000 μm, and the values of A dropped and reaches 0.57 as the thickness approaches the core layer. The variation of orientation of the α-phase with respect to the thickness is shown in Figure 7.10.

iii) The crystallinity index C increases from skin to core layer. The variation of C with respect to the thickness is shown in Figure 7.11. One should bear in mind that C can not directly be related with overall crystalline fracture, but it has been chosen for comparability with A and B indices and suitably for manual routine

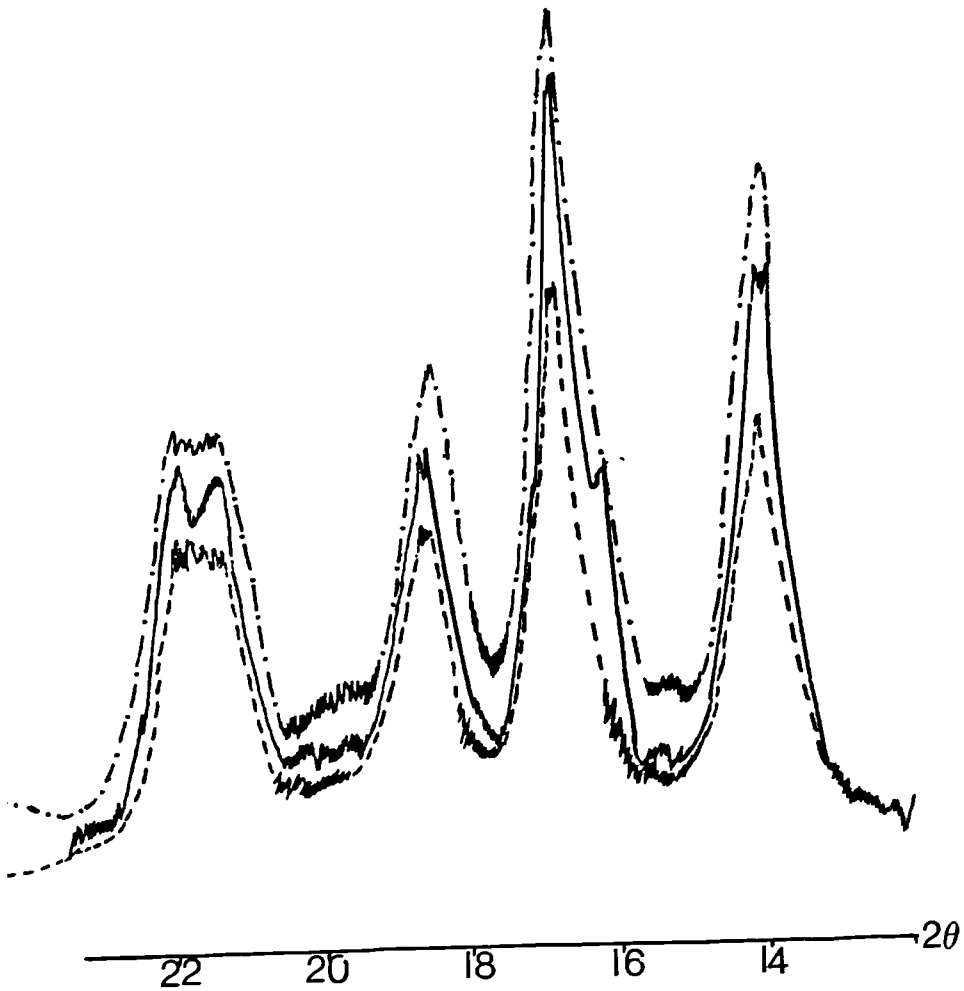

Figure 7.9. X-ray diffraction analysis through the cross section of an extruded sample of PP by layer removal. Skin layer 10-500 μm from the surface (———), 2nd layer 500-1000 μm from the surface (—.—.—), core layer 2500-3000 μm from the surface (- - - -).

Table 7.4 X-ray differaction analysis of cross sectional area of extruded polypropylene by layer removal.

Thickness from the surface (μm)	Peak Hight(mm)						α-phase Index A	β-phase Index B	Crys. Index C
	hα1	hα2	hα3	hα4	hβ	ha			
10-500	95	117	47	49	52	35	0.659	0.169	2.04
500-1000	107	122	58	54	0	32	0.664	0	2.13
1020-1500	75	87	63	47.5	0	26	0.612	0	2.09
2000-2500	61	73	43	39	0	22	0.610	0	1.96
2500-3000	69	79.5	46	49	0	25	0.595	0	1.94

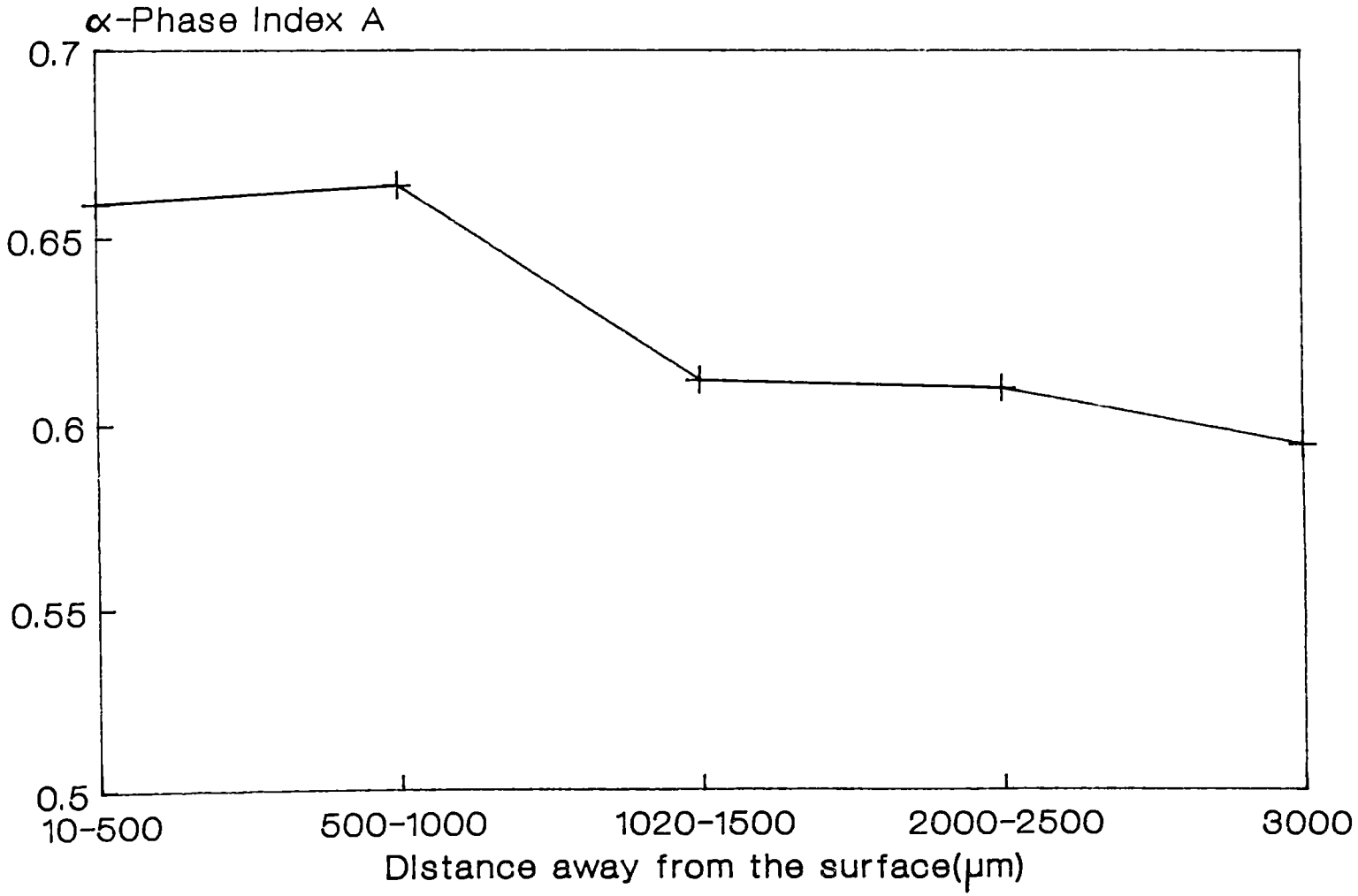

Figure 7.10. Distribution of A values through the cross section of an extruded PP sample by layer removal.

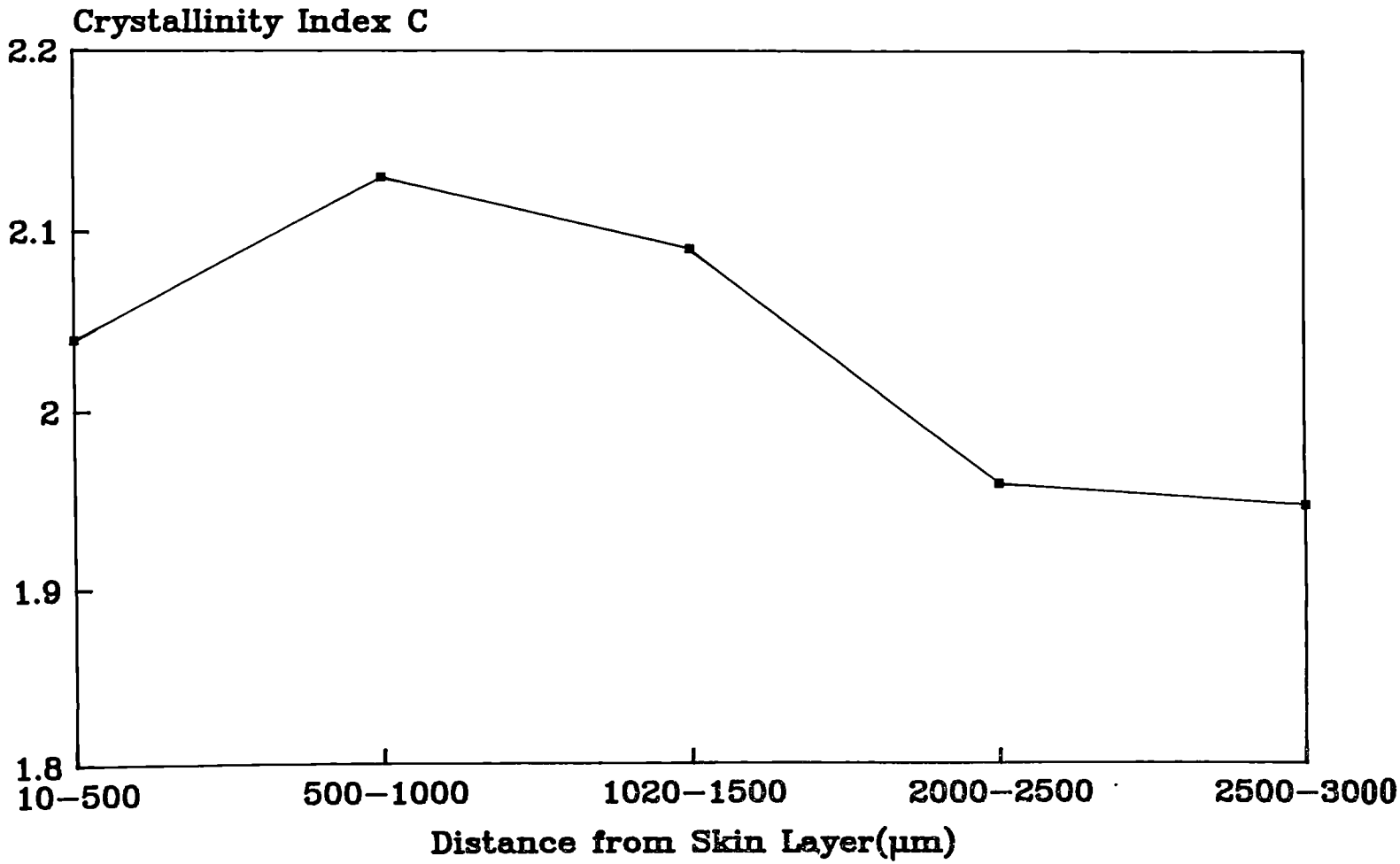

Fig. 7.11 Crystallinity index of extruded PP across the surface

measurements. For instance, for some representative samples the crystalline fracture measured by DSC are Xc =34.14 % for C =2.04 and Xc =33.03 % for C =1.948.

7.6. Microstructural Analysis of Extruded High Density Polyethylene (Solid)

7.6.1. Introduction

In view of establishing an understanding of the microstructure of extruded high density polyethylene several techniques were employed.

In chapter 4, the analysis of melt viscosity showed, due to high entanglement of the molecular chains, the high density polyethylene possess higher melt viscosity than polypropylene resins. The high molecular entanglement favours the fast nucleation (80), and as it has been stated in chapter 2 this phenomenon will lead to a profusion of spherulites which may will be immaturely developed.

Due to foregoing reasons it was found the polarised light microscopy was not suitable for studying the microstructure of the high density polyethylene, therefore, only differential scanning calorimetry, transmission electron microscopy and X-ray analysis results were found to be fruitful as discussed below.

7.6.2. TEM Analysis of Extruded High Density Polyethylene

The surface of the extrudate was microtomed to a thickness of 500 μm parallel to the flow direction. As it has been mentioned previously the molecular weight itself is important factor in crystallisation of the polymer. This is related to the ease with which the crystallisation units can be brought to the lamellae face, complete growth stops, and eventually advances the growth front. Crystal growth is usually governed by diffusion, either of heat or matter, the coefficient of diffusion is inversely proportional to the square of molecular weight, the rate of advance become progressively related, particularly to the initiation rate for new lamellae (165,166). Thus, it is both expected, and observed, that the lateral extension of the lamellae will be significantly reduced with increasing molecular weight at low crystallisation temperatures.

The morphology of skin layer of high density polyethylene is illustrated in Figure 7.12. Spherulites as small as 300 nm in diameter can be distinguished (arrows) in this figure, which is an etched cross section parallel to the extrusion direction.

In order to verify the effect of molecular weight on

the crystallography of high density polyethylene, the microstructure of a lower molecular weight grade of high density polyethylene (Natene 54180 Mw = 2.14* 10^5) was analysed as it is displayed in Figure 7.13. This figure exhibits the top view of pyramidal structure of spherulites with lamellae oriented in the flow direction. It is interesting to point out, that the diameter of these spherulites are almost twenty times larger than the spherulites of high density polyethylene (Rigidex H11042 grade).

Microstructural analysis of the second layer of (Rigidex H11042 grade) has shown curved shape (S shape) lamellae as it is presented in Figure 7.14. Here dominant lamellae, running top to bottom (in the flow direction), are connected by subsidiary rod like platelets. The material in the space between the lamellae web crystallises upon cooling into proliferous S-shaped sheets. Similar findings have been reported by Basset et al.(167,168) for melt crystallised polyethylene at temperature of 128°C (for 1 hour).

7.6.3. Thermal Analysis of Extruded High Density Polyethylene

Samples at the surface of the extrudate were removed by microtomy and the melting behaviour of these

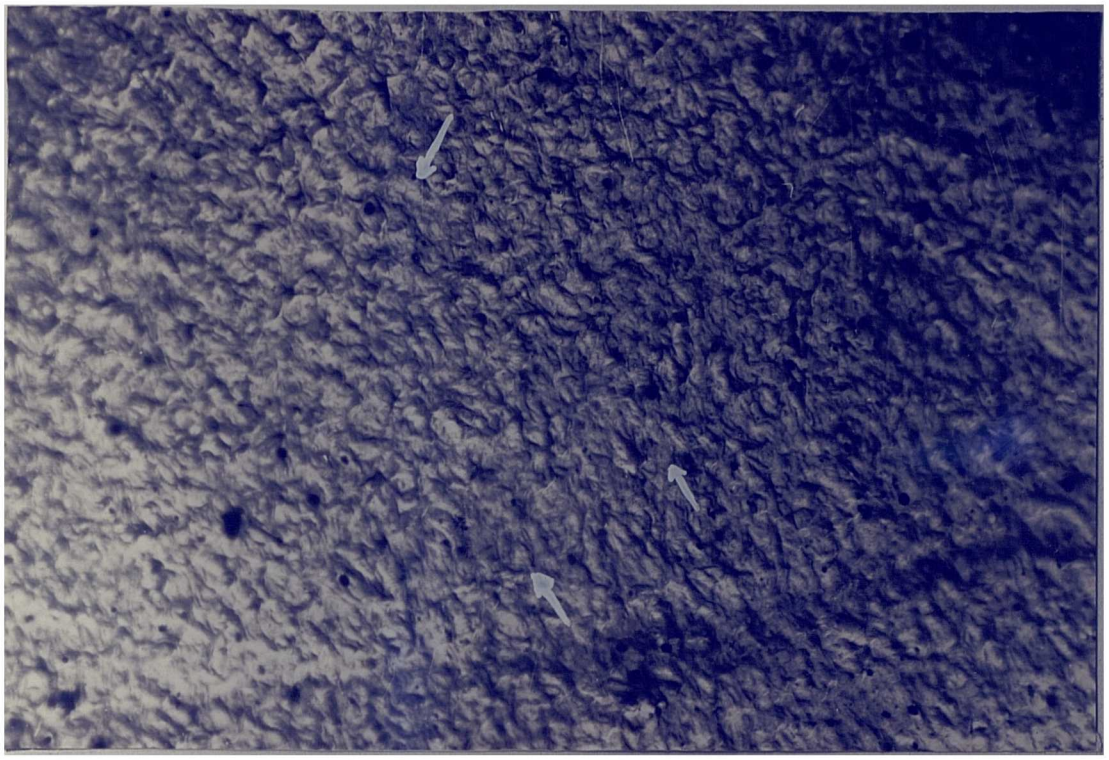

7 12 Skin layer analysis of high density polyethylene(Rigidex H11042) by TEM.

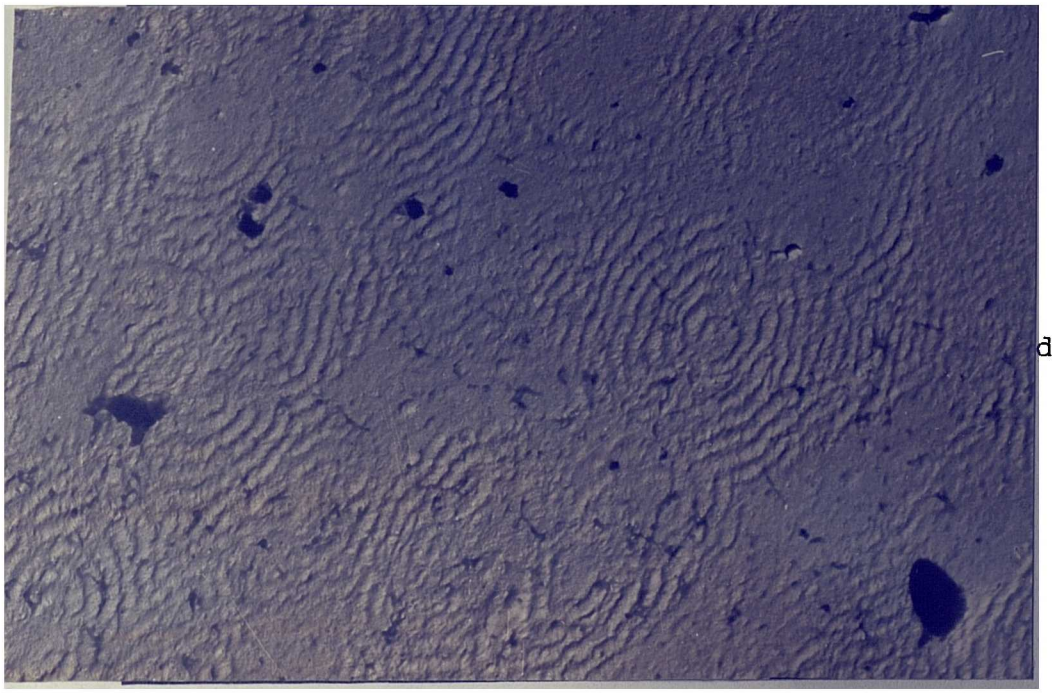

Fig. 7.13 a) Skin layer analysis of high density polyethylene (Natene 54180) by TEM.

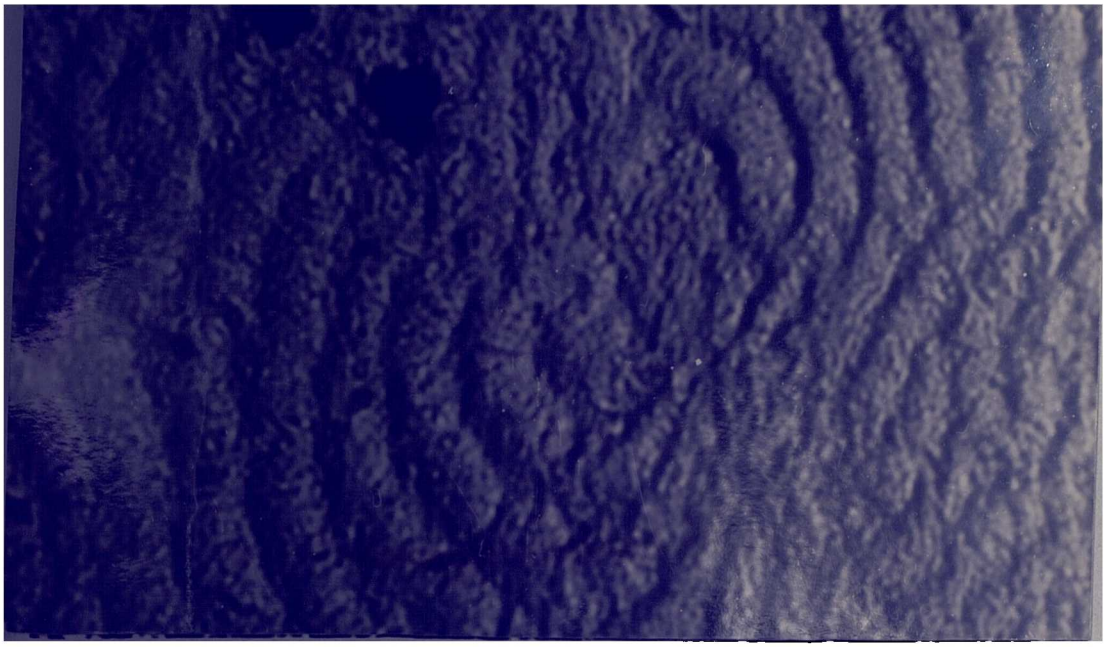

Figure 7.13. b) Higher magnification of Figure 7.13.a

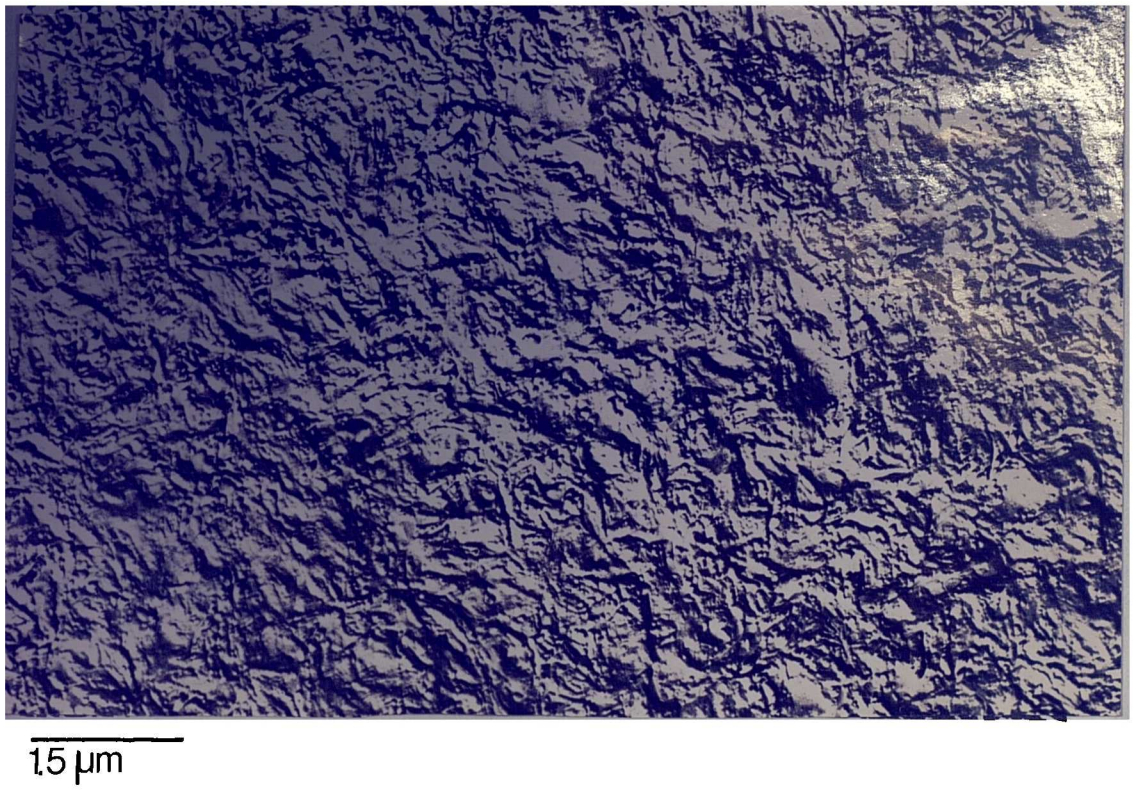

Figure 7.14 Core layer analysis of high density polyethylene (Rigidex H11042) by TEM.

specimens investigated using a Perkin-Elmer differential scanning calorimeter. As with the polypropylene, 500 μm thick layers were cut and tested.

The melting behaviour of the skin layer showed a broad and low melting temperature (402 °K) as it is shown in Figure 7.15.a. The summary of melting behaviour of high density polyethylene is listed in Table 7.5. The broad endotherm and a lower melting peak of the skin layer at 402°K (the accuracy of these peaks are within ±1°K, as three different samples were tested and the results were fairly reproducible), appear to be due to result of the melting of crystallites within the lamellae, which differ in size and perfection. The greater the perfection of crystallites being, thermodynamically are more stable and therefore it will melt at higher temperature as it is witnessed from melting peak of the third layer (around 1000 μm away from the surface) as it is shown in Figure 7.15.b.

Due to slower cooling of the material associated with the core region, chains can relax and coil back to their original structure. This phenomenon will result in lower melting temperature as compare to the second layer. The melting behaviour of this region is shown in Figure 7.15.c.

From the foregoing results one can conclude that

Table 7.5 DSC analysis of extruded high density polyethylene. Screw speed 30 rpm, tempearture of cooling media 60°C.

Thickness of layers from the surface (μm)	meltins temperature (°K)	* Degree of crystallinity %
10-500	402.06	54.90
500-1000	405.11	58.93
1020-1500	406.3	60.80
1500-2000	404.22	57.72
3000-3500	403.23	54.53

* The heat of fusion for 100% crystalline polyehtylene was taken as 276 J g^{-1} (169).

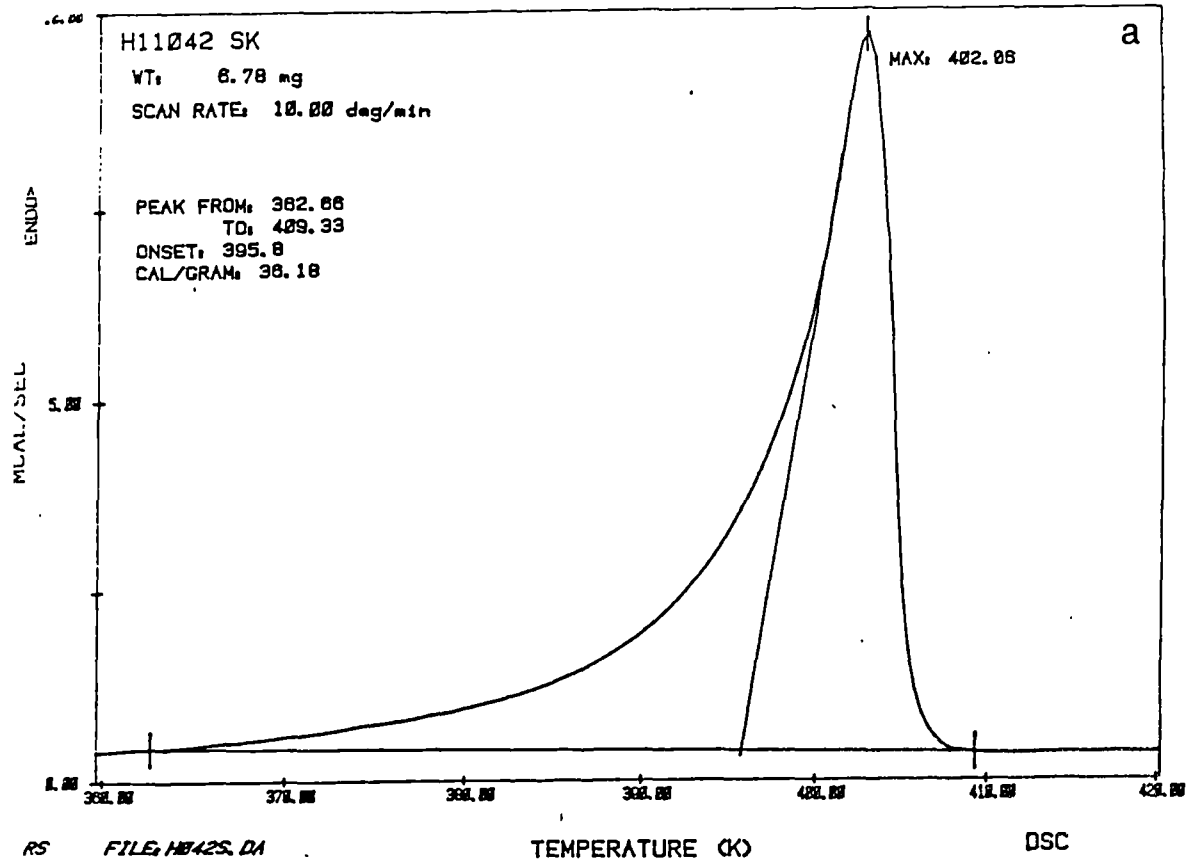

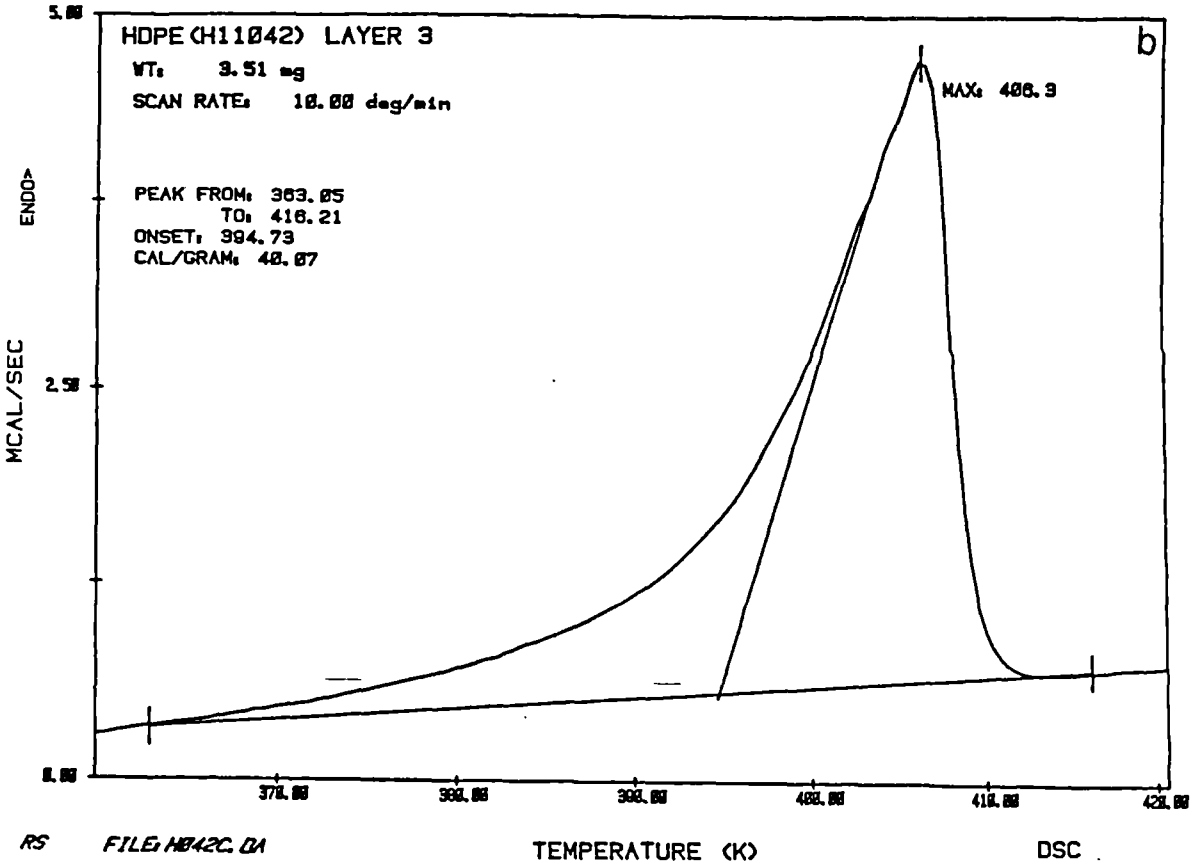

g. 7.15 a) Melting behaviour of skin layer of high density polyethylene (Rigidex-H11042).
b) Melting behaviour of transition layer (around 1000 µm away from the surface) of high density polyethylene (Rigidex- H11042).

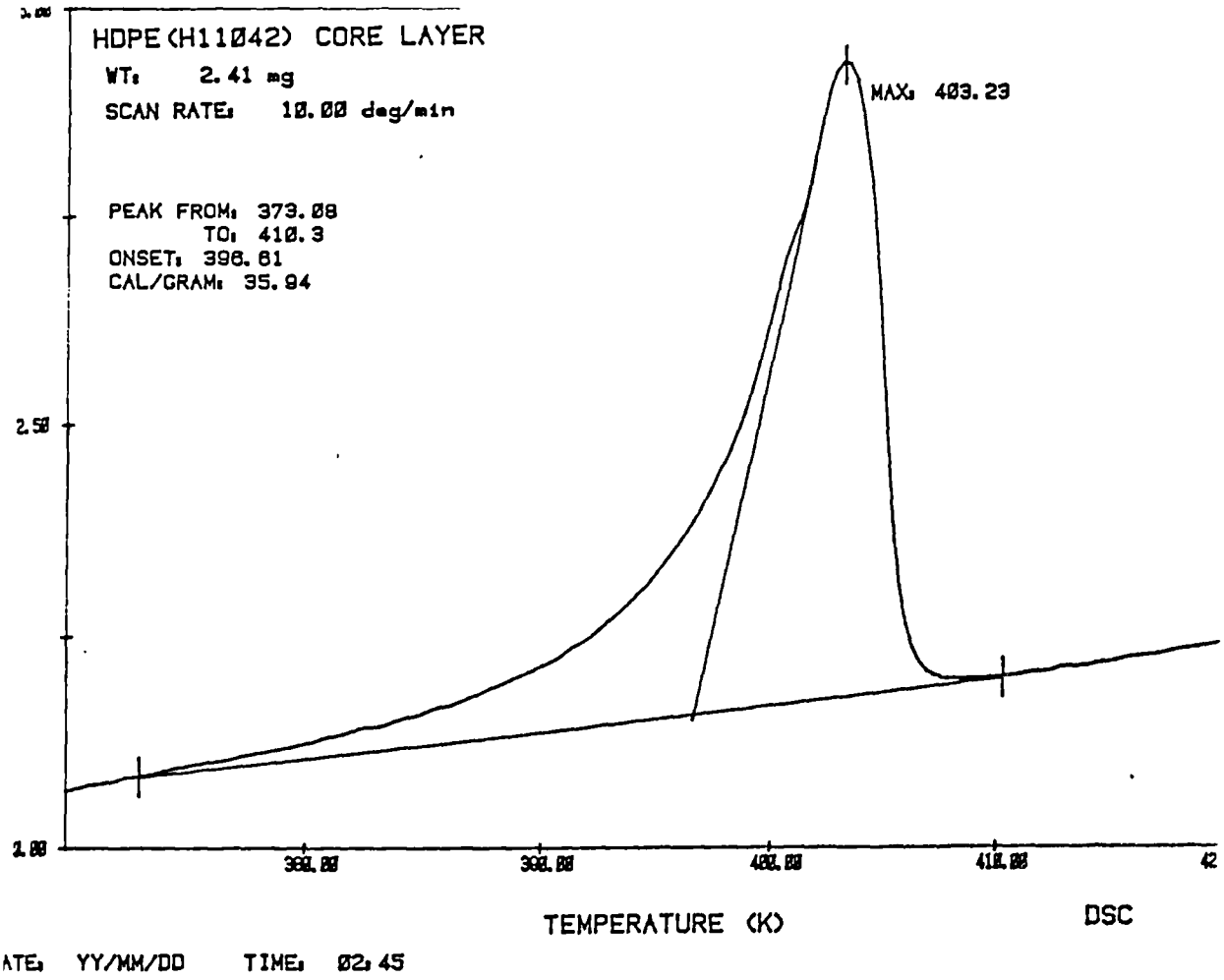

Fig. 7.15 c) Melting behaviour of core layer of high density polyethylene(Rigidex-H11042).

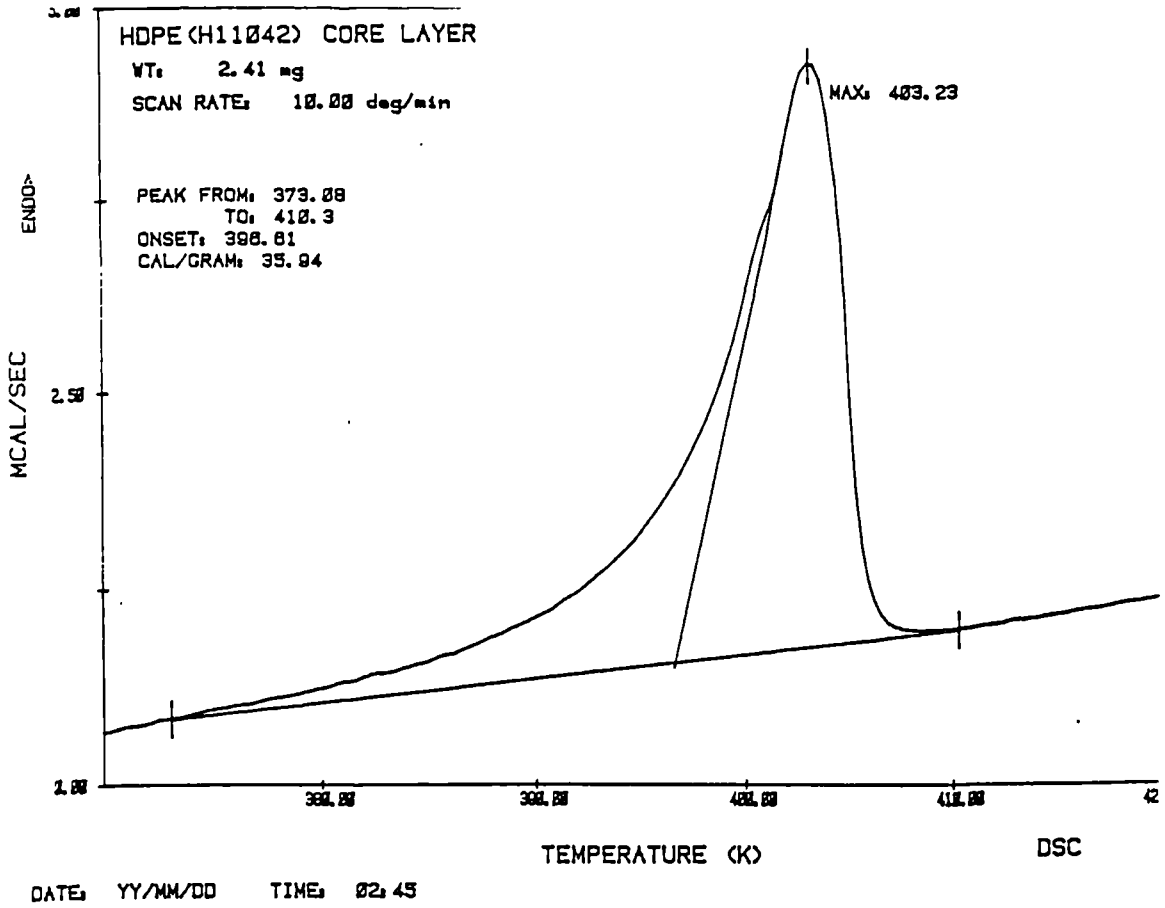

Fig. 7.15 c) Melting behaviour of core layer of high density polyethylene(Rigidex-H11042).

three distinct layers exist in extruded high density polyethylene rod, which second layer shows more chain alignment, hence, more perfect crystalline structure.

7.6.4. X-ray Analysis of Extruded High Density Polyethylene

In this section the X-ray analysis of longitudinal surface of extrudate (parallel to the flow direction) of high density polyethylene has been considered. Similar to polypropylene samples of 500 μm thick were tested and their results are listed below.

Analysis of the surface layer revealed two peaks corresponding to hkl planes of 110 and 200. The position and intensity of these reflection were used as a measure of orientation distribution of crystallites within each sample. Some investigators have revealed that three maxima with hkl planes of 020, 200, and 110, and they found their intensities are in ratio of 1:10:40 (115). Therefore with the knowledge of intrinsic intensities for these planes, comparatively the orientation distribution of skin to core layer can be identified. The summary of these results are presented in Figure 7.16. The results show chain orientation occurs in layer around 1000-2000 μm away from the surface. Calculated inter-planar spacing for hkl plane of 110 and 200 are 4.2 Å and 3.78 Å respectively, which represent the poly-

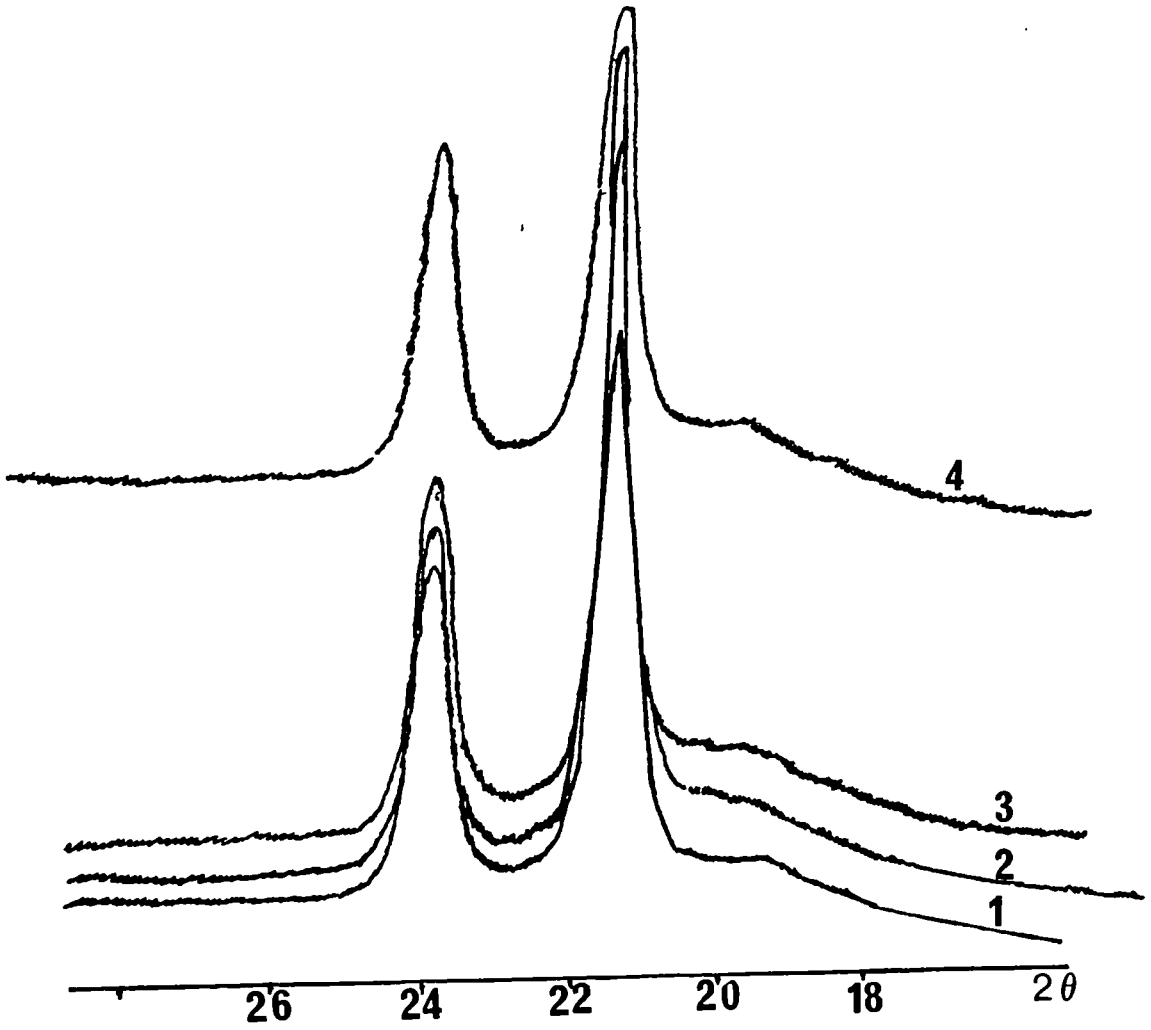

Fig. 7.16. X-ray diffraction analysis through the cross section of an extruded HDPE sample by layer removal. (1) skin layer, (2) 1020-1500 μm away from the surface, (3) 1500-2000 μm away from the surface, (4) centre of the extrudate, 2500-3000 μm away from the surface.

ethylene orthorhombic phase.

7.7 Microstructural Analysis of Binary Blend of High Density Polyethylene and Polypropylene

7.7.1. Introduction

Polyblends of high density polyethylene and polypropylene have been used commercially due to synergistic effect on various properties such as modulus, strength, and elongation (170,171). These effects might be caused by morphological changes such as nucleation of crystallisation of polypropylene by presence of high density polyethylene and/or formation of interpeneterating networks in the blend (171). As it has been mentioned earlier on, blends of these polymers were chosen in order to modify the melt strength and melt crystallisation to stabilise the cell walls within the foam.

Also as it been mentioned in the previous chapter, only blend of 20/80 ratio of high density polyethylene and polypropylene showed best effect in stabilisation of cell walls as well as achievement of lowest density with high open cell fraction in the final product. For these reasons the microstructure of this blend was examined in order to establish a good understanding of co-crystallisation and/or segregation effects and their effect on the recrystallisation behaviour of the blend. In the first part, the surface of

extrudate was analysed by transmission and scanning electron microscopy and the melting behaviour was examined by DSC. X-ray analysis was ignored since the positions of the peaks were difficult to identify each crystalline phase and exact miller indices.

7.7.2. Microstructural Analysis of Binary Blend of Extruded High Density Polyethylene and Polypropylene by SEM and TEM

The skin layer morphology of extruded sample examined by SEM, revealed the expected decrease in spherulite diameter (mainly polypropylene), since at low magnification, the spherulites of high density polyethylene cannot be observed as it has been mentioned in the previous section (see Figure 7.17). The diameter of the spherulites varies from 15-20 μm, which have dropped as much as four times compared to Polypropylene Homopolymer.

Investigation of the core layer by TEM revealed mainly two separate areas designated by A and B. At higher magnification area A shows sheaves of radii lamellae have been formed as shown in Figure 7.18. Still at higher magnification it has been revealed that the radial formation of lamellae at the edge lath show various orientation about their length.

Area B has different texture from area A which it

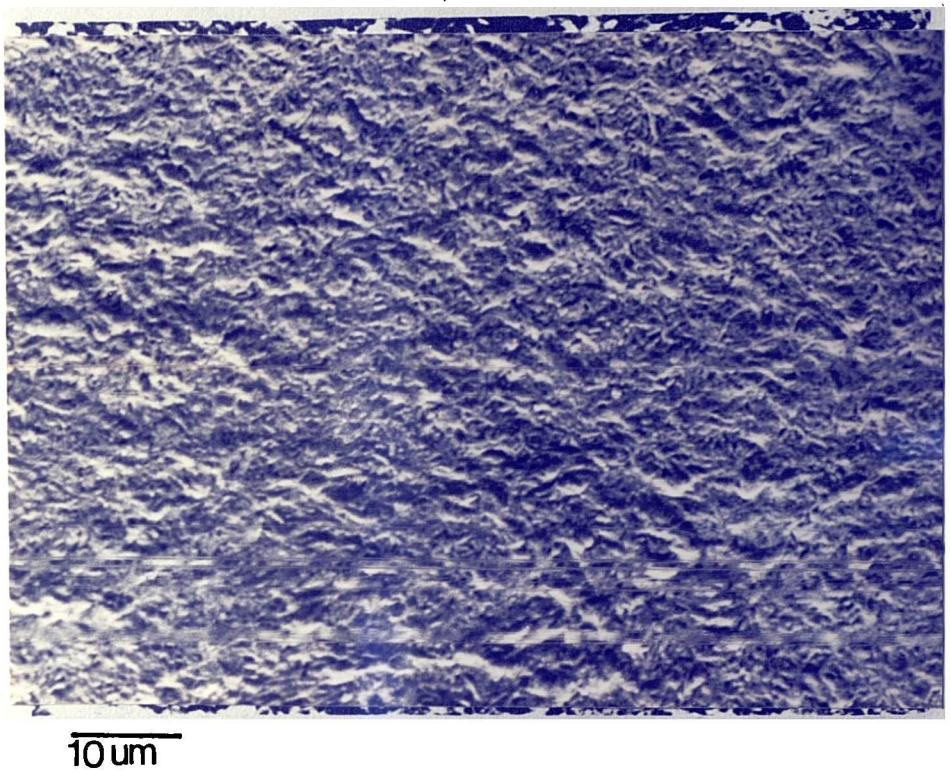

Fig. 7.17 Low magnification of skin layer of blend of PP and HDPE.

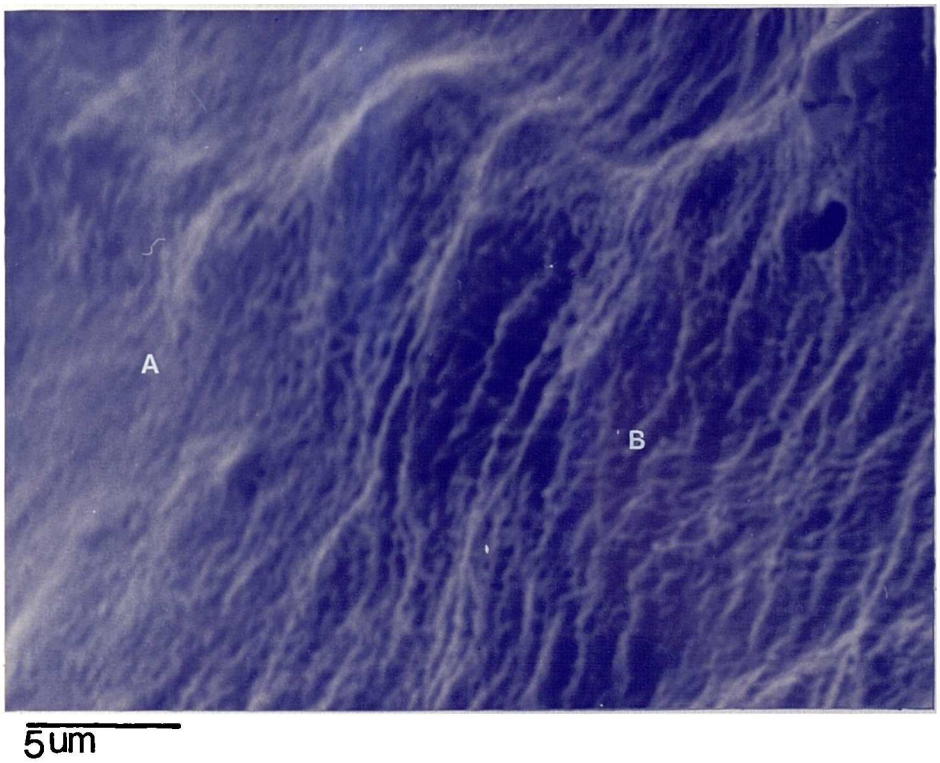

Fig. 7.18 a) Core layer analysis of extruded PP/HDPE blend, revealing two different textures.

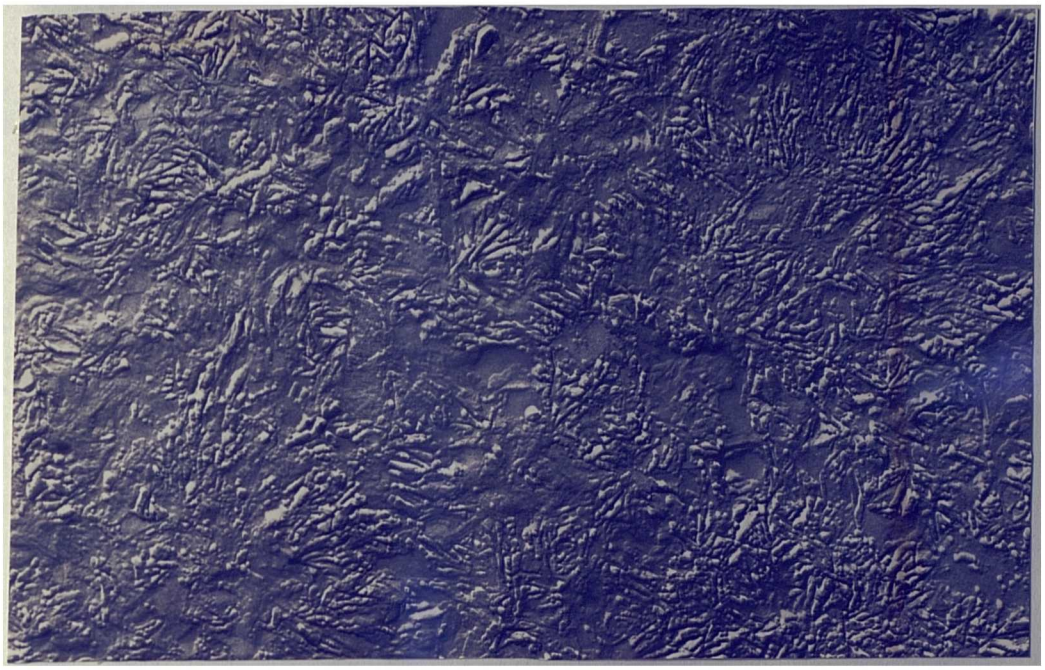

b

1 μm

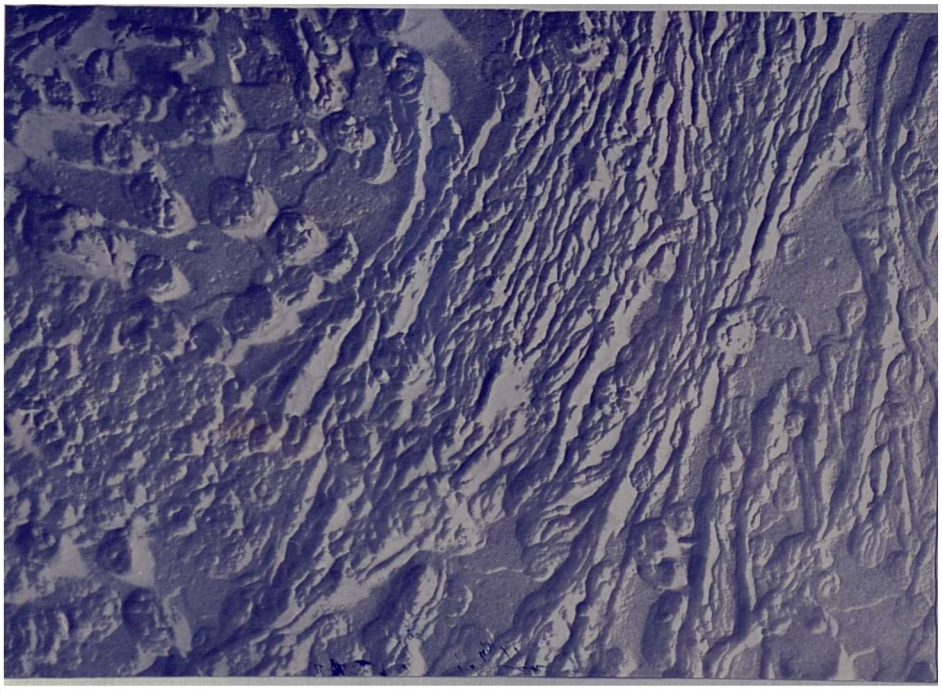

c

1 μm

Fig. 7.18 b and c) Higher magnification of Figure 7.18 a, part A

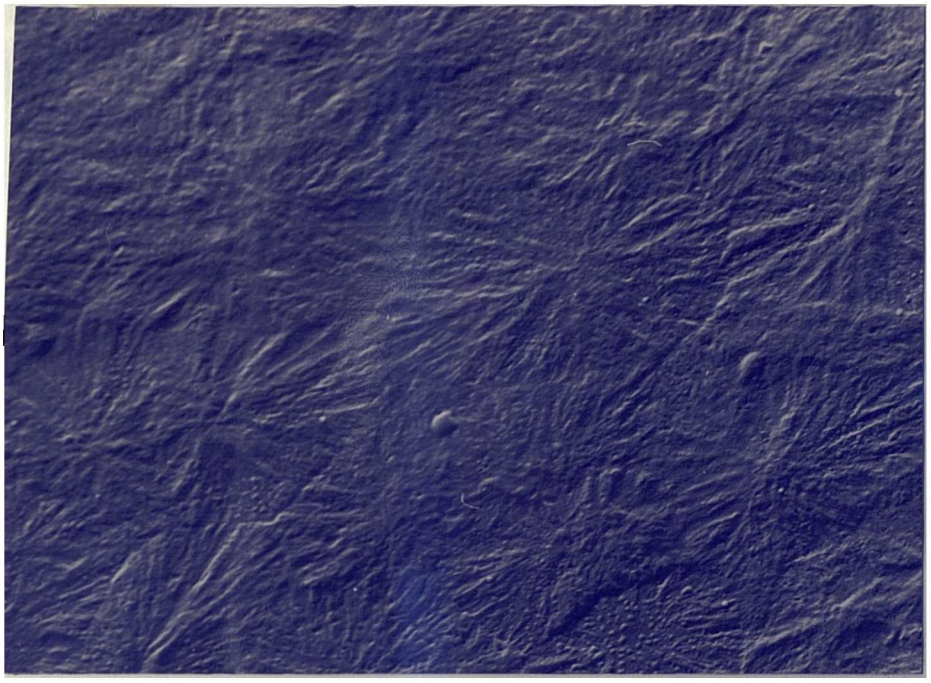

Fig. 7.18. d) Higher magnification of Figure 7.18 a, part B.

proves no co-crystallisation has taken place and upon solidification two different phases are formed. Also it should be pointed out that the spherulitic size has decreased (as compare to polypropylene homopolymer) as a consequence of nucleating effect.

7.7.3. DSC Analysis of Binary Blend of High Density Polyethylene and Polypropylene

The specimens were prepared similar to the previous section and their thermal behaviour was examined according to the procedure described in section 3.10.

By characterising using thermal analysis, it was intended to assess the segregation and nucleating effect of the constituents during the processing. If segregation occurs, by whatever cause, a double or multi-peaked endotherm would be expected to appear on subsequent heating during DSC analysis, owing to the greatly different melting behaviours of the blend components (see Figure 7.19). Comparison of melting behaviour of the sections cut from skin to core layer taken from the blend, and those of polypropylene and high density polyethylene homopolymer, reveals the following points;

i) The skin layer has shown multi-endothermic peaks at 400.27, 421.7, 435.6, and 451.06°K. The first peak correspond to melting temperature of high

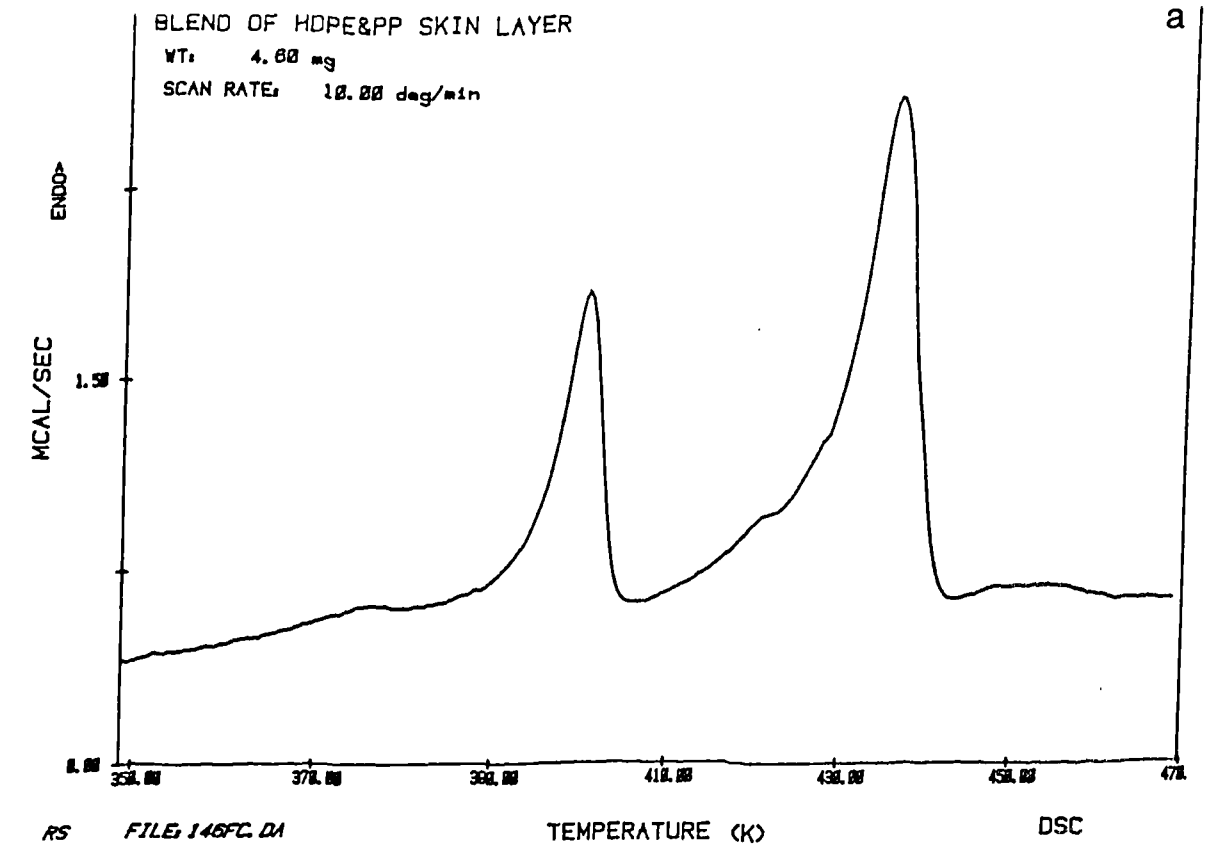

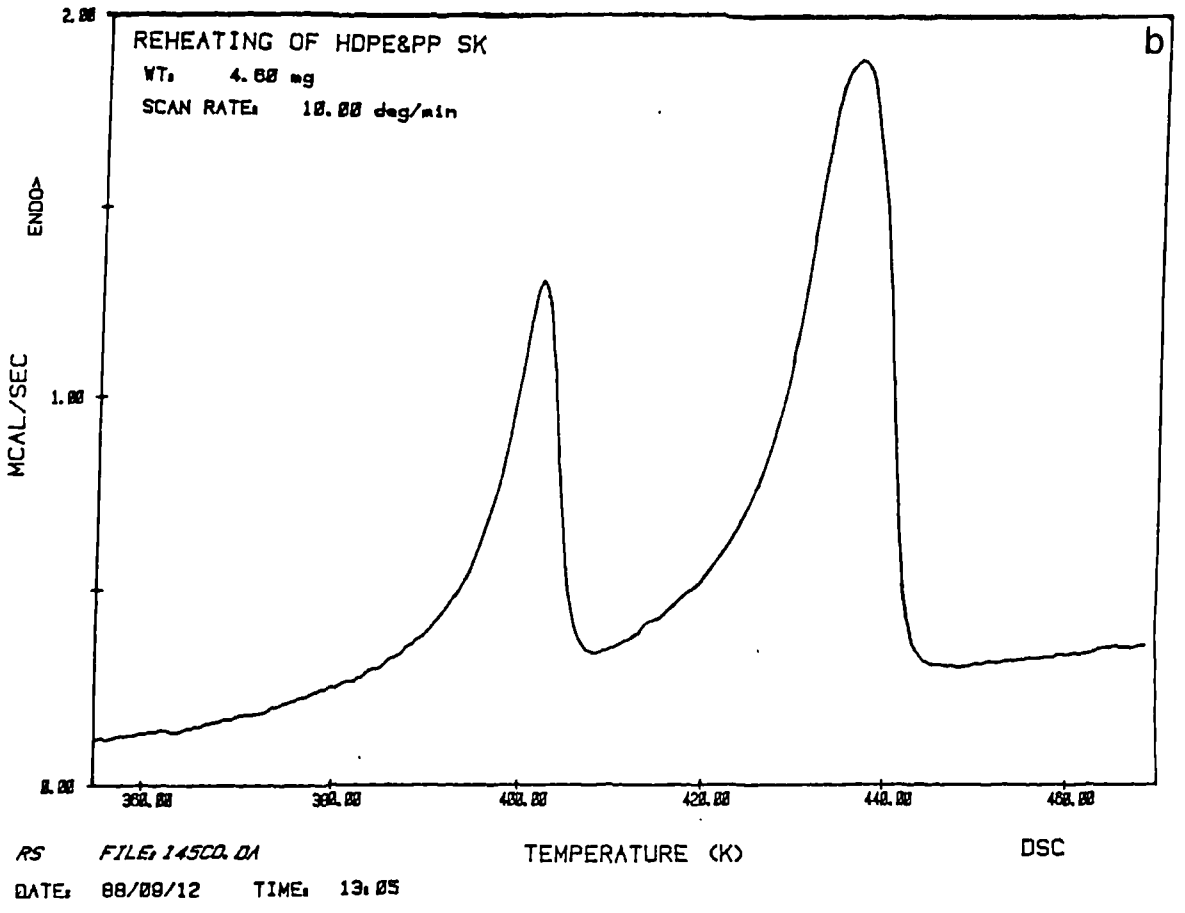

Fig. 7.19 a) Melting behaviour of skin layer of extruded PP/HDPE blend.
b) Melting behaviour of same layer as above, cooled at slow rate ($5\,^{o}K\ min.^{-1}$)

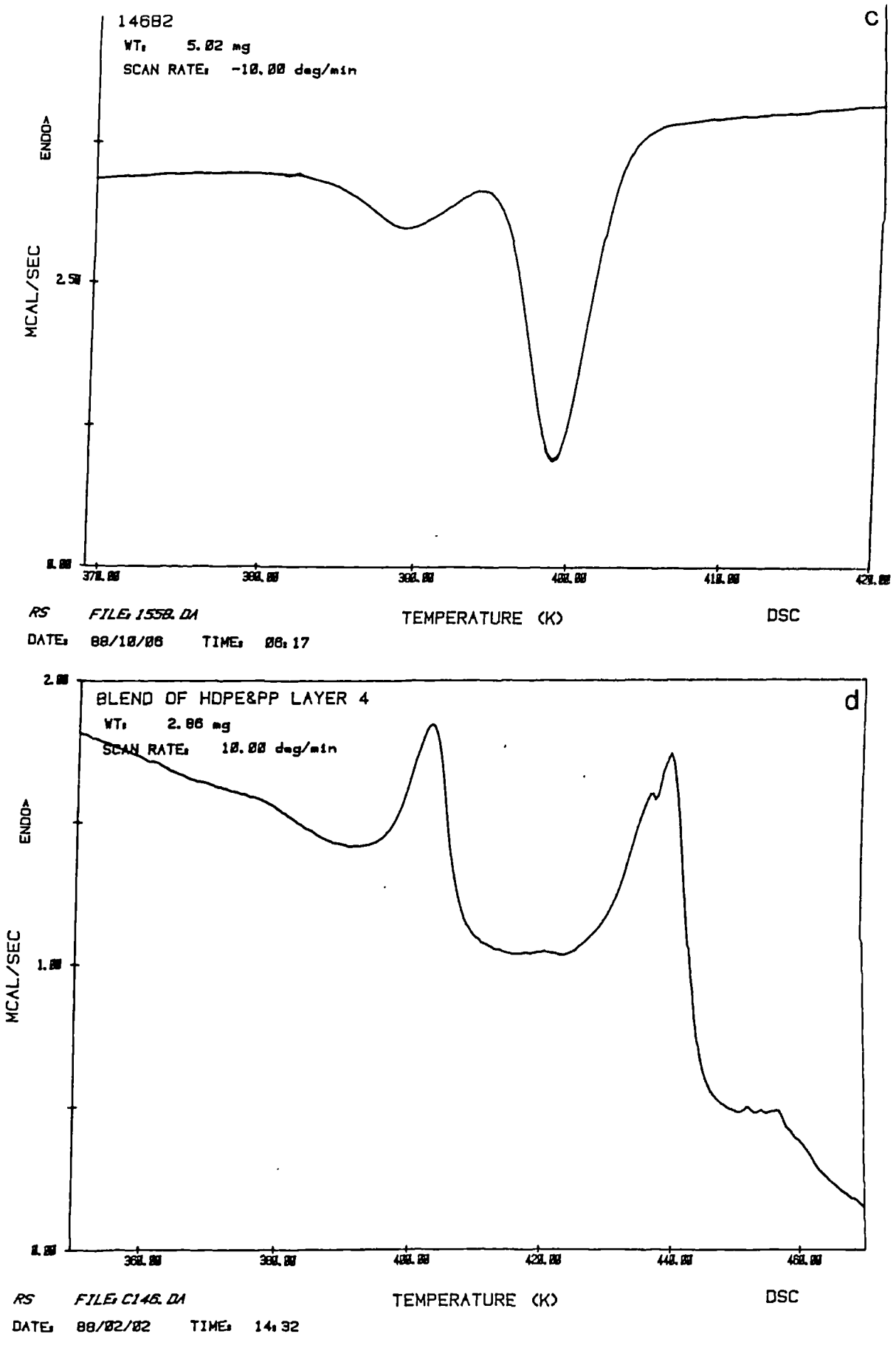

Fig. 7.19 c) Recrystalisation behaviour of PP/HDPE blend.
d) Melting behaviour of extruded PP/HDPE blend (around 2000 μm away from the skin surface).

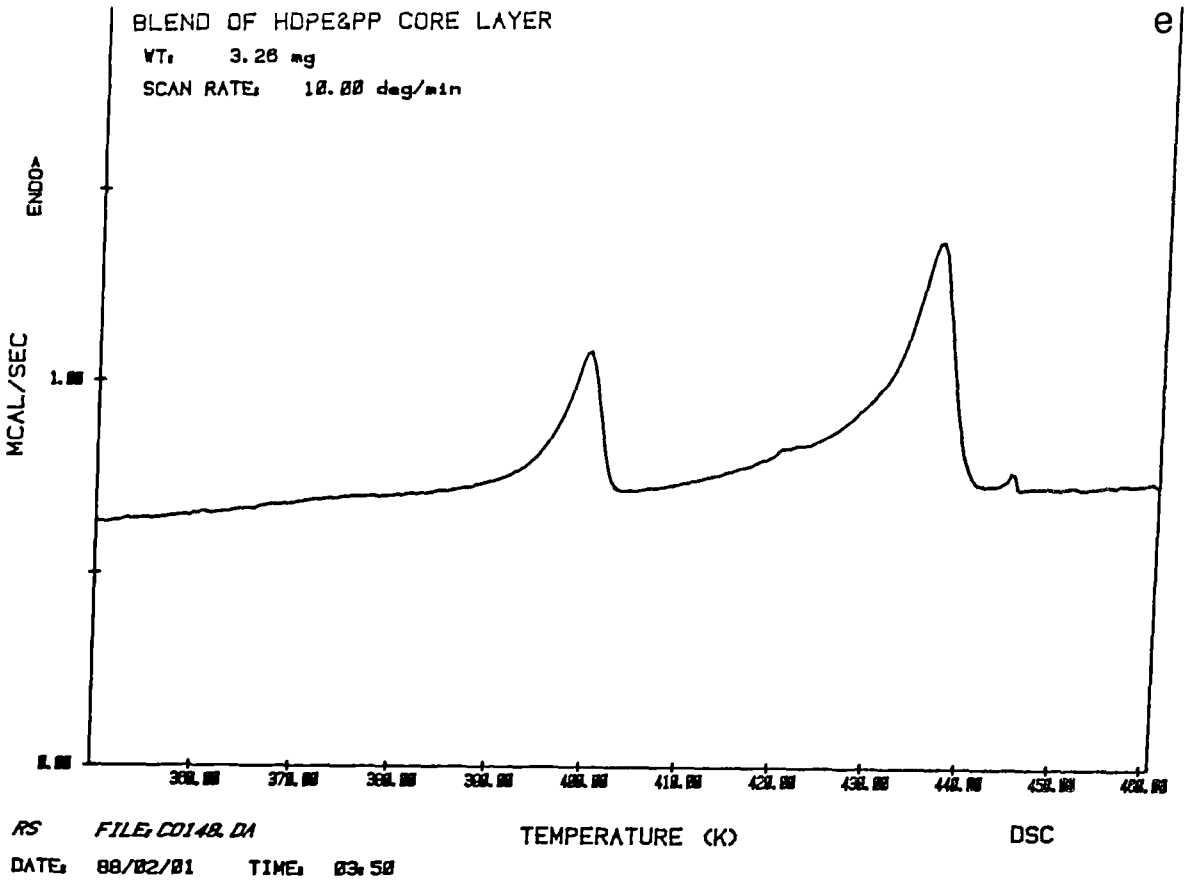

Fig. 7.19 e) Melting behaviour of core layer of PP/HDPE blend.

density polyethylene, which its melting temperature did not change significantly as compared to its homopolymer. On the other hand the melting behaviour of polypropylene have shown up to four peaks, one major and one minor peak corresponding to α-phase melting endotherm at 435.6°K and 451°K respectively, and two minor peaks on the shoulder of the major peak at 422.4°K. As has been mentioned earlier, the peak of 422.4°K agrees with β-phase melting endotherm reported by Lovinger (101).

ii) In the transition layer (around 2000 μm away from skin layer), firstly the melting curve of high density polyethylene appeared at 404°K (2°K higher than endothermic melting peak of this polymer in the skin region). Secondly polypropylene showed up to three peaks. One major peak at 440.2°K and two minor peaks at 437.2 and 456.6°K, which corresponds to α-phase (101).

iii) In the core region (around 3000 μm away from the surface and where a change was noticed in the melting behaviour), the thermal analysis of polypropylene, showed one major peak at 436.5°K and two minor peaks at 421.7 and 445.2°K. The melting peak produced by β-phase was less intense as compare to that of and in the skin layer.

iv) The overall degree of crystallinity measured

across the cross section shows higher crystallinity was appeared in the transition zone. A summary of the melting peak position and degree of crystallinity for extruded specimen of binary blend of polypropylene and high density polyethylene at different layers are shown in Table 7.6.

v) Most important of all, as it is noticed from Figure 7.19.c and Table 7.6, the degree of supercooling temperature of polypropylene has been effected by the presence of high density polyethylene and has dropped as much as 8.36°K (in skin layer) and 9.84°K (in the core region).

From the above results firstly one can conclude that the blend of high density polyethylene and polypropylene is not a single phase system. Secondly high density polyethylene to some extent has effected the crystallisation of polypropylene and provided a nucleating site for crystallisation of polypropylene. This phenomenon supports the idea that better cell stability (in polymer foam) could be achieved with blends of these polymers. Furthermore it can be seen that, due to nucleating effect the diameter of polypropylene spherulites have decreased as much as of four times.

Table 7.6 DSC analysis of extruded PP/HDPE blend. Screw speed 40 rpm, temperature of cooling media 60°C.

Thickness of layer from the surface (μm)	Melting temperature(°K) HDPE	PP				Degree of super cooling of PP (°K)
		β	α1	α2	α3	
10-500	400.27	421.7	427.5	436.5	-	37.92
500-1000	401.71	422.4	428.1	436.1	-	36.98
1020-1500	403.11	422.7	429.1	437.3	-	35.45
1500-2000	404.1	418.4	437.2	440.2	456.6	35.28
2500-3000	400.1	421.7	436.5	445.2	-	35.54

7.8. Microstructural Analysis of Extruded Polypropylene Foam

7.8.1. Surface Analysis by SEM and TEM

The surface of extruded polypropylene foam normal and parallel to direction flow were prepared according to procedure of section 3.9.1 and 3.9.3 for SEM and TEM analysis respectively.

The spherulitic structure of polypropylene foam can be seen at even low magnification as it is displayed in Figure 7.20. At higher magnification (see Figure 7.21) the micro structural analysis of polypropylene revealed several interesting points which are described below.

i) Comparison of spherulitic structure of polypropylene homopolymer and polypropylene foam shows that the spherulites of the foam sample have flat tops. This phenomenon have been explained in detail by Hornsby et al. (61,62), where they have studied spherulitic morphology of injection moulded polypropylene in structural foam. They have suggested the spherulites which have been developed close to a cell, form a concave side where they are in contact with the melt cell interface. Due to surface tension effects the cohesive force between the crystallites and the

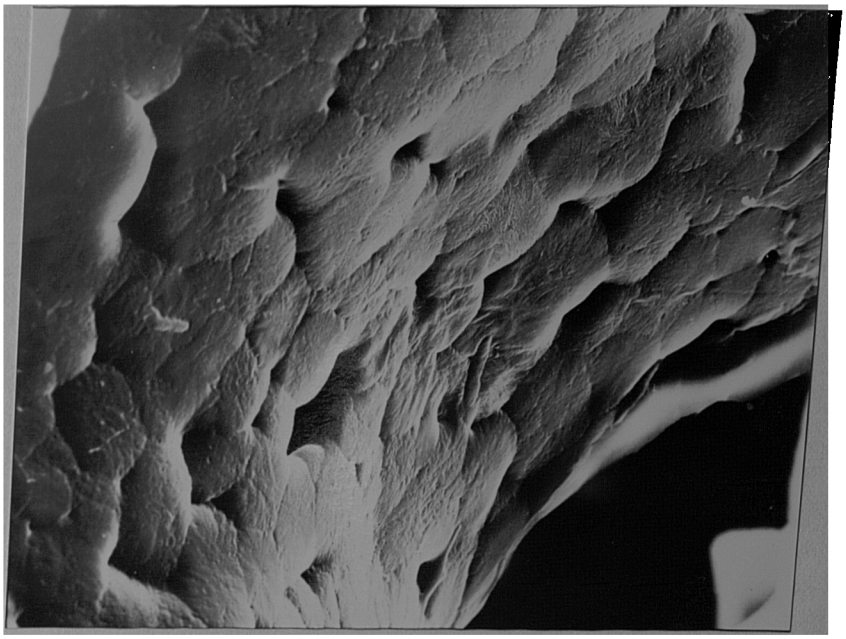

Fig. 7.20. Low magnification of polypropylene foam spherulites.

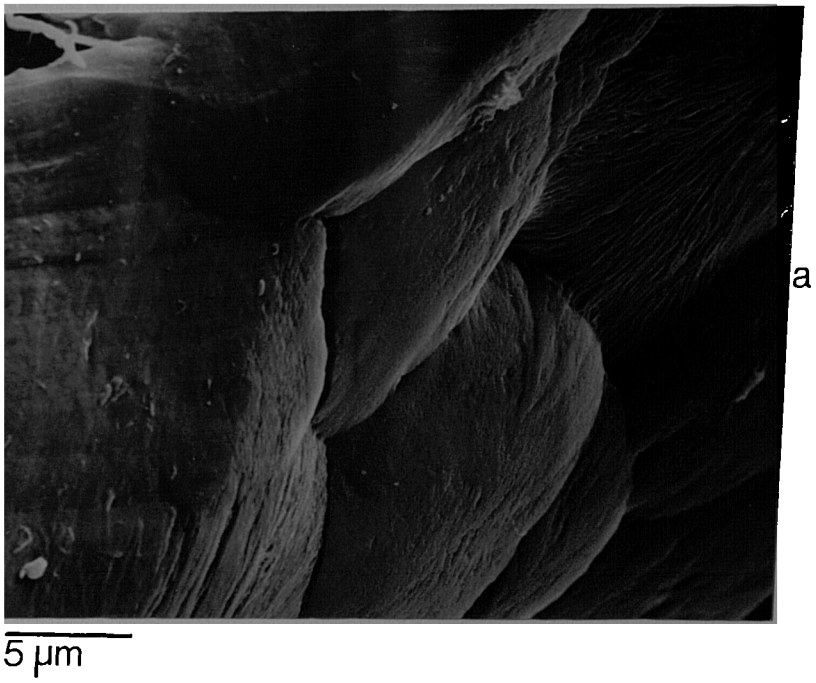

Fig. 7.21. a) higher magnification of above Figure.

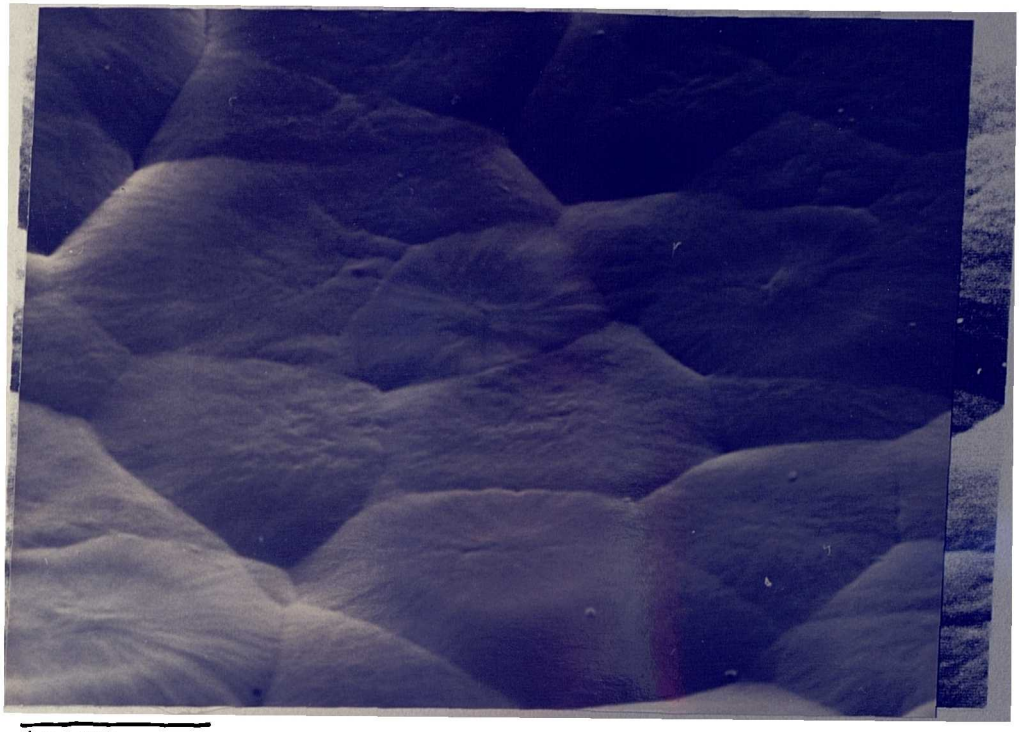

Fig. 7.21. b) Skin layer analysis of extruded polypropylene foam.

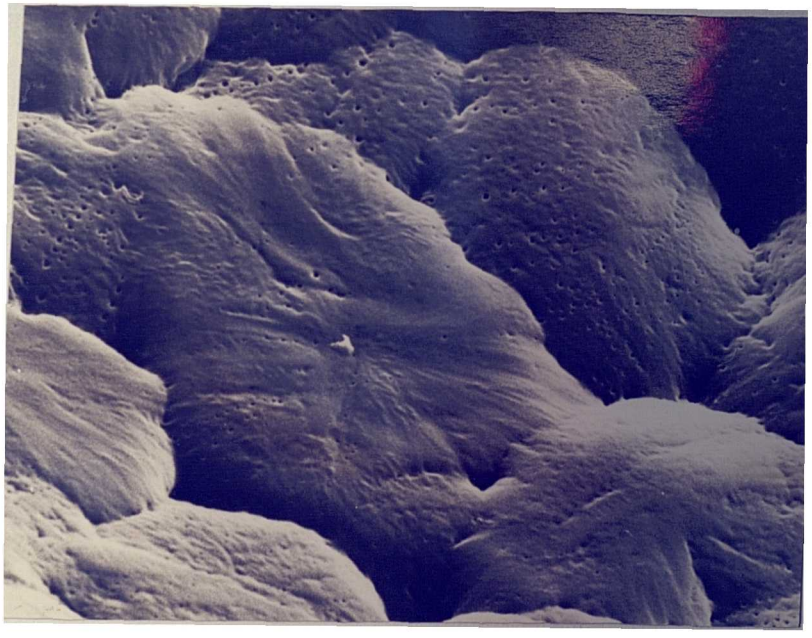

Fig 7.22. Core layer analysis of extruded polypropylene foam by SEM.

melt, and molecular entanglement, these spherulites will remain in the melt and also will be pushed along by the expanding cell. Therefore, upon further expansion it will reach a point where their movement will be restricted and if the cell continues to expand further the spherulites will leave flat topped structure.

ii) At higher magnification it has been found that the gas bubbles have penetrated through the spherulites. It is interesting to add that the position of microbubbles are either in the region of interspherulitic or on the lamellae boundaries (see Figures 7.22-23). In order to verify these voids are not the artefact of bumbarment of electron, by SEM, similar areas have been tested by TEM and also porosimetry. The results obtained from these analysis agrees with the above finding (see Figures 7.23 and 7.24). The size of these voids vary through the spherulites and also through the cross sectional areas of the extrudate foam. The largest microbubbles are formed in the region, where the rate of cooling is much slower than the skin layer.

iii) Due to low thermal conductivity associated with the foamed sample, therefore upon cooling the degree of crystallinity would be greater in the core region. The consequence of this phenomenon will be greater shrinkage within the sample. The shrinkage of the material between the already

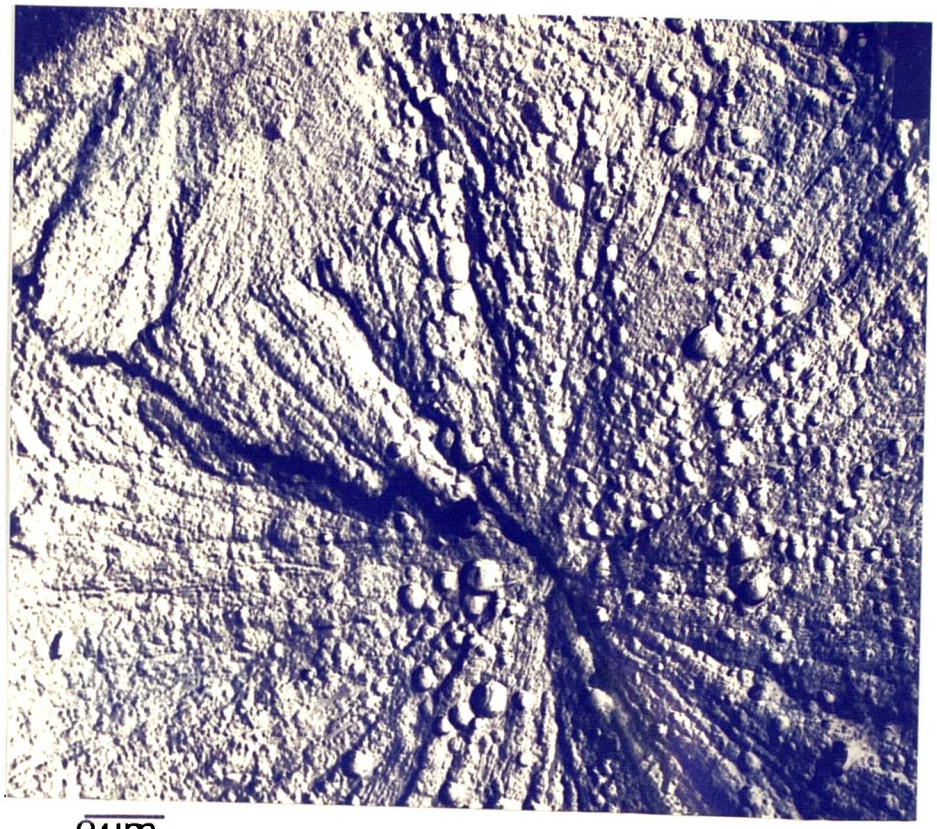

Fig. 7.23. Skin layer analysis of extruded polypropylene foam by TEM.

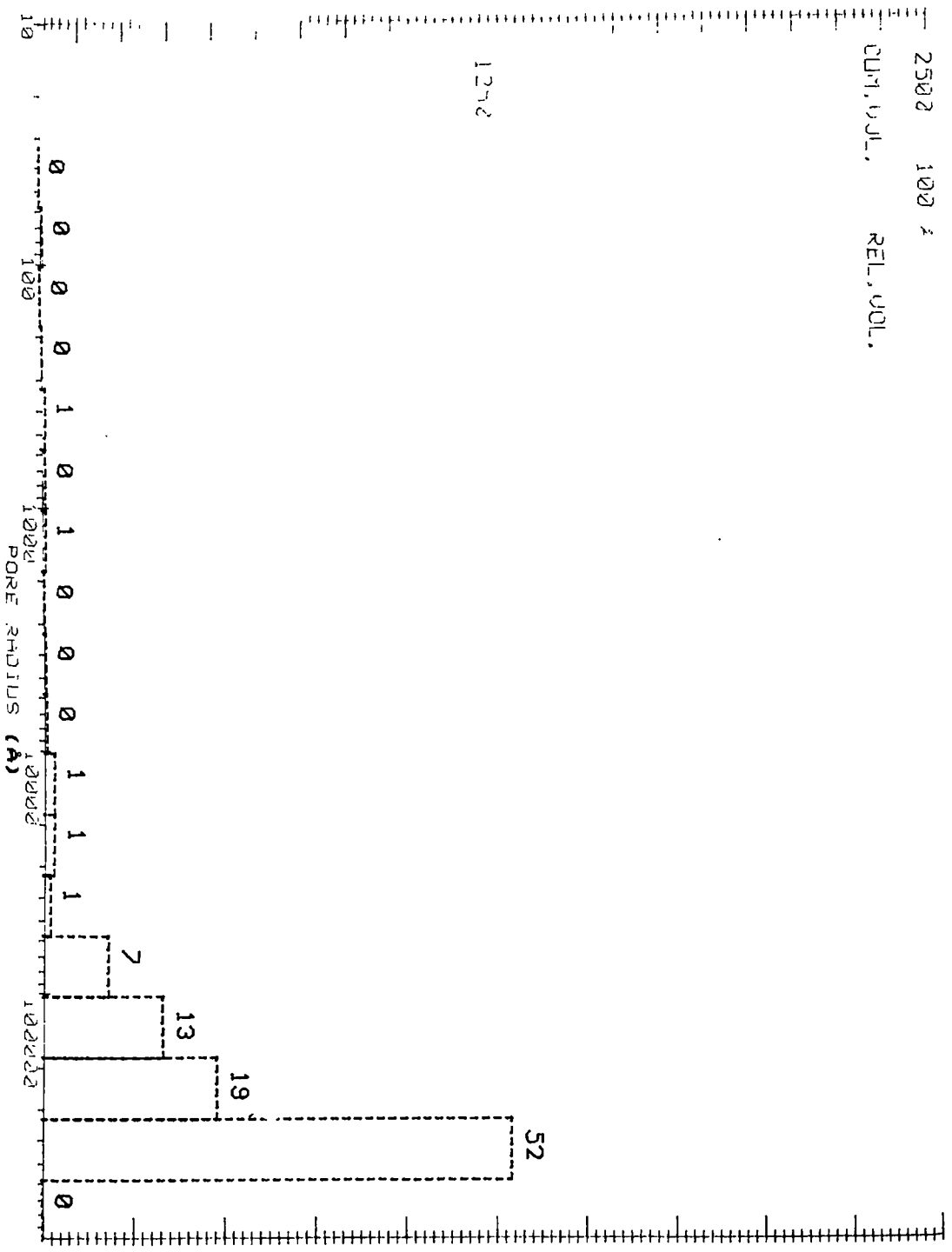

Fig. 7.24. Pore size analysis of extruded polypropylene foam by porosimetery.

formed spherulites has resulted in the funnel-shaped holes which has been observed at spherulites boundaries. Hornsby et al. (62) also found similar results in the morphology of injection moulded of isotactic polypropylene structural foam.

iv) Spherulites diameter varied from skin to core and were to be around 15 and 30 μm respectively.

From further examination of the core layer by TEM (see Figure 7.25), it was found the extremity of a sheaf, showing a very important feature, namely that in these regions one has assembly of more or less equally spaced individual dominant lamellae. From this figure, the central a splaying object can be seen which has almost developed the well known feature of " eye " or Popoff (172) leaves by encirclement from opposite ends. The point which is interesting to raise here is at the edges, laths show various orientation about their lengths. For an ideal axialite, they would all be identical. It is believed that such variation facilitates the attainment of a three dimensional envelope appropriate to a mature spherulite.

7.8.2. Thermal Analysis of Extruded Polypropylene Foam

Similar procedure as those of polypropylene (solid)

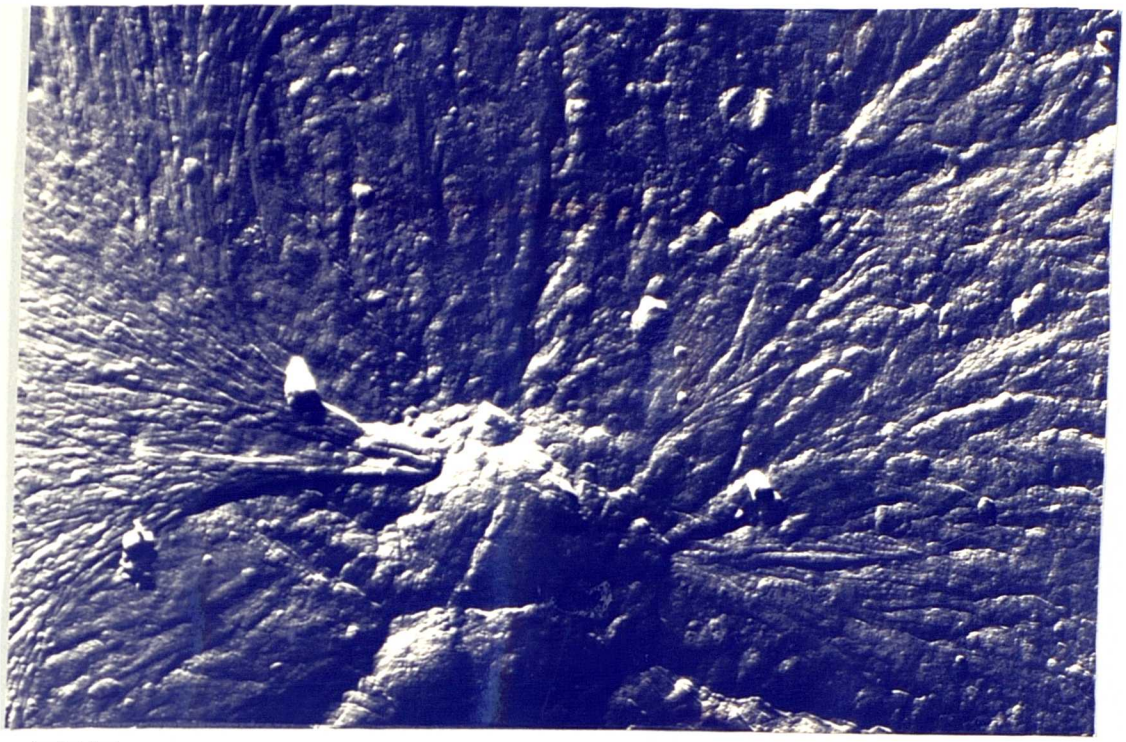

Fig. 7.25. Sheaf-like or "eyes" appearance in mono-clinic spherulite of extruded polypropylene foam (core layer).

was employed to study the thermal behaviour of polypropylene foam.

The melting behaviour of polypropylene foam from skin to core layer is presented in Figure 7.26. As it is noticed since the polymer has strong memory, the different cooling rate has effected its melting history. The skin layer shows one major peak around 437.8°K corresponding to α-phase melting endotherm, and one minor peak at 421.9°K on the shoulder of the major peak which agrees with the β-phase endothermic melting peak reported by Lovinger (101). In order to verify the presence of the β-phase is either due to the cooling rate or nucleating effect the chemical blowing agent, a sample from the same layer was melted and then cooled at slower rate (5°K $min.^{-1}$) and again reheated, which the results received are presented in Figure 7.26.b. As it is noticed again too endothermic peaks appeared at 422.5°K and 438.87°K. The comparison of these results and the results obtained for polypropylene homopolymer brings one to a conclusion that the chemical blowing agent used has nucleating effect on the polypropylene. Evidence of this phenomenon is more clear when a sample from the same layer melted and its recrystallisation behaviour showed a reduction in degree of supercooling as compare to polypropylene homopolymer (compare Figure 7.7.c and 7.26.c). Beck et al. (173)

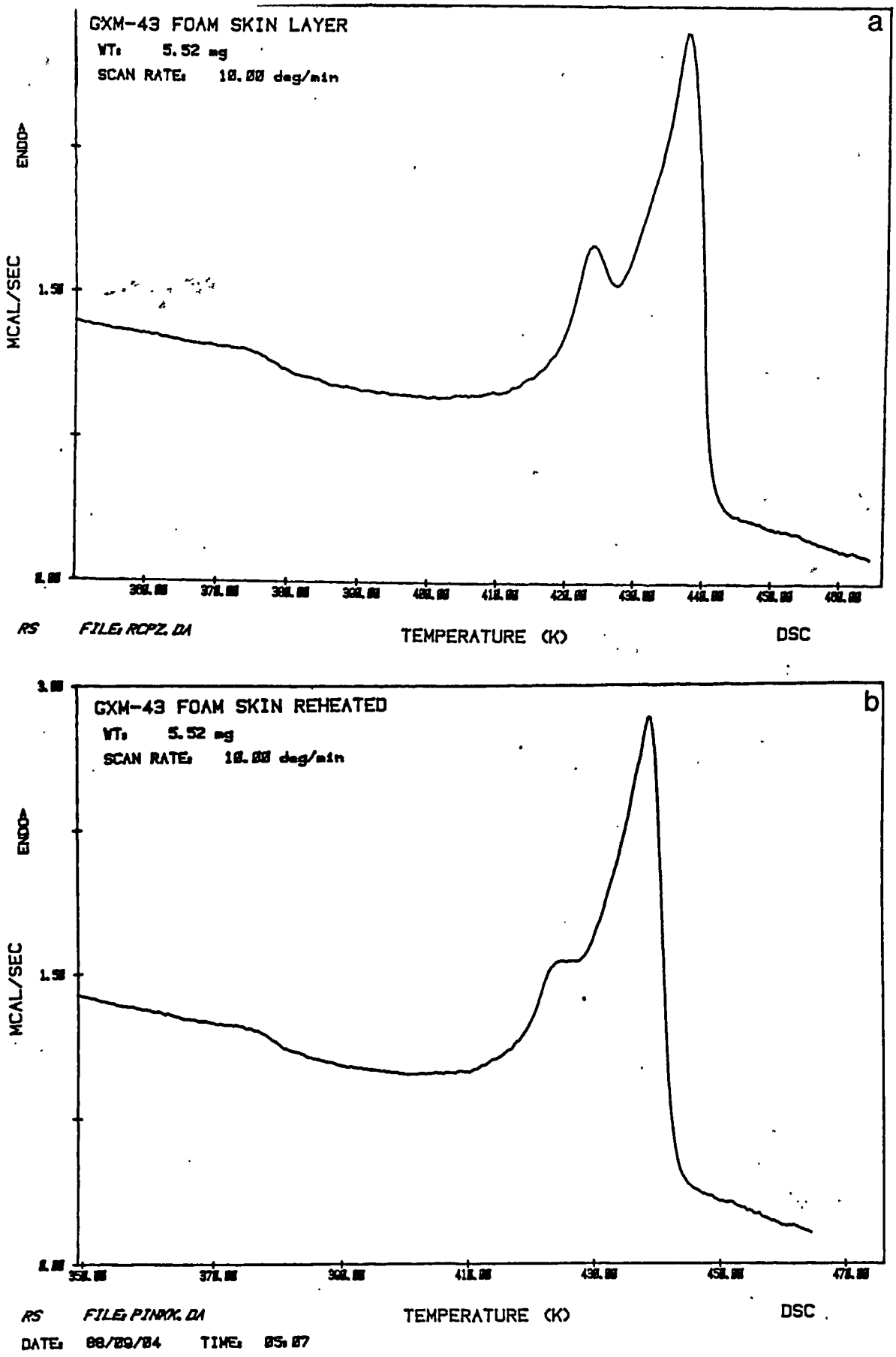

Fig. 7.26. a) Melting behaviour skin layer of extruded polypropylene foam.
b) Melting behaviour of same layer as above, cooled at slow rate($5\ ^{o}K\ min.^{-1}$).

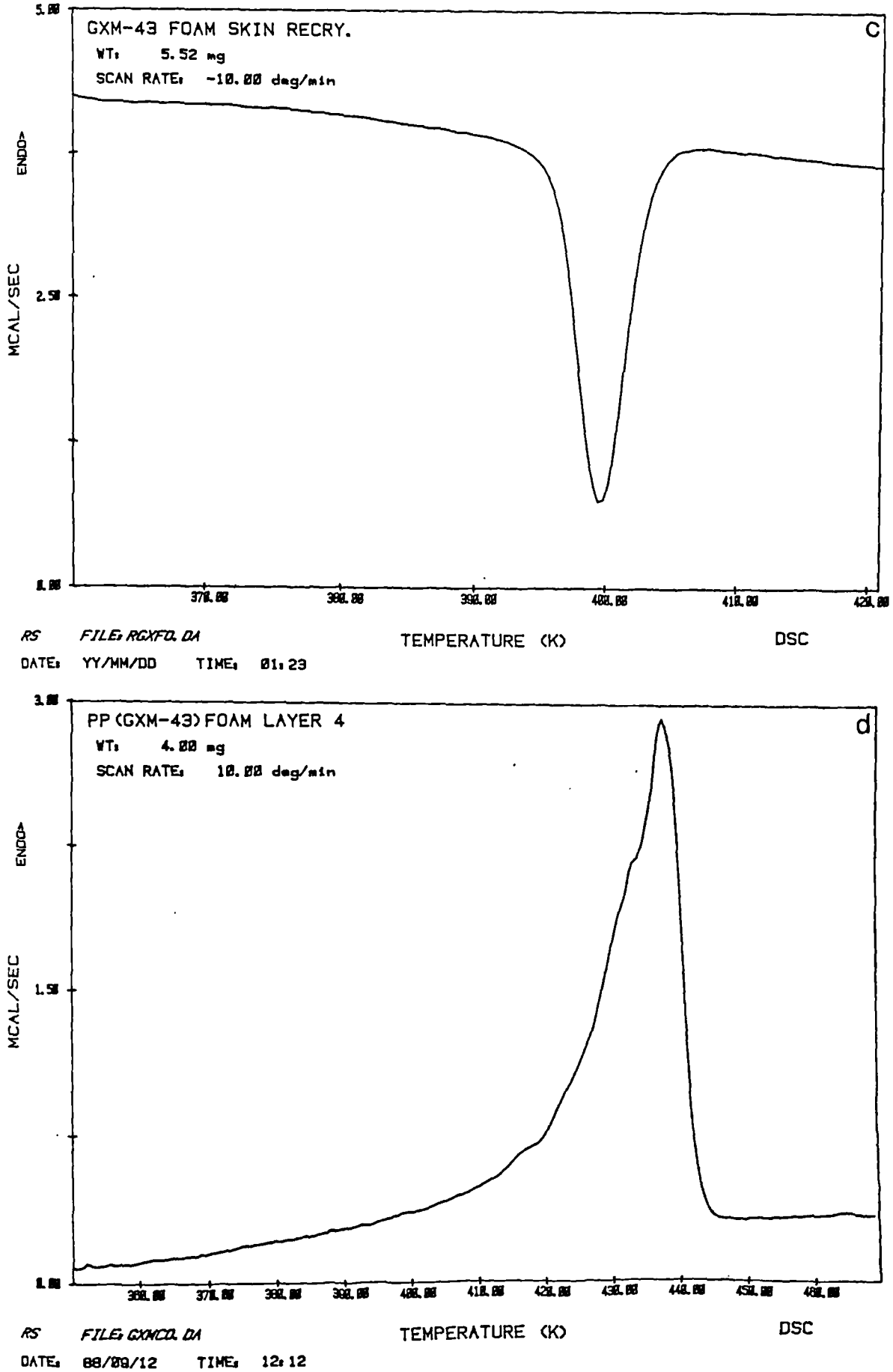

Fig. 7.26. c) Recrystalisation behaviour of polypropylene foam.
d) Melting behaviour of extruded polypropylene foam (around 2000 μm away from the surface).

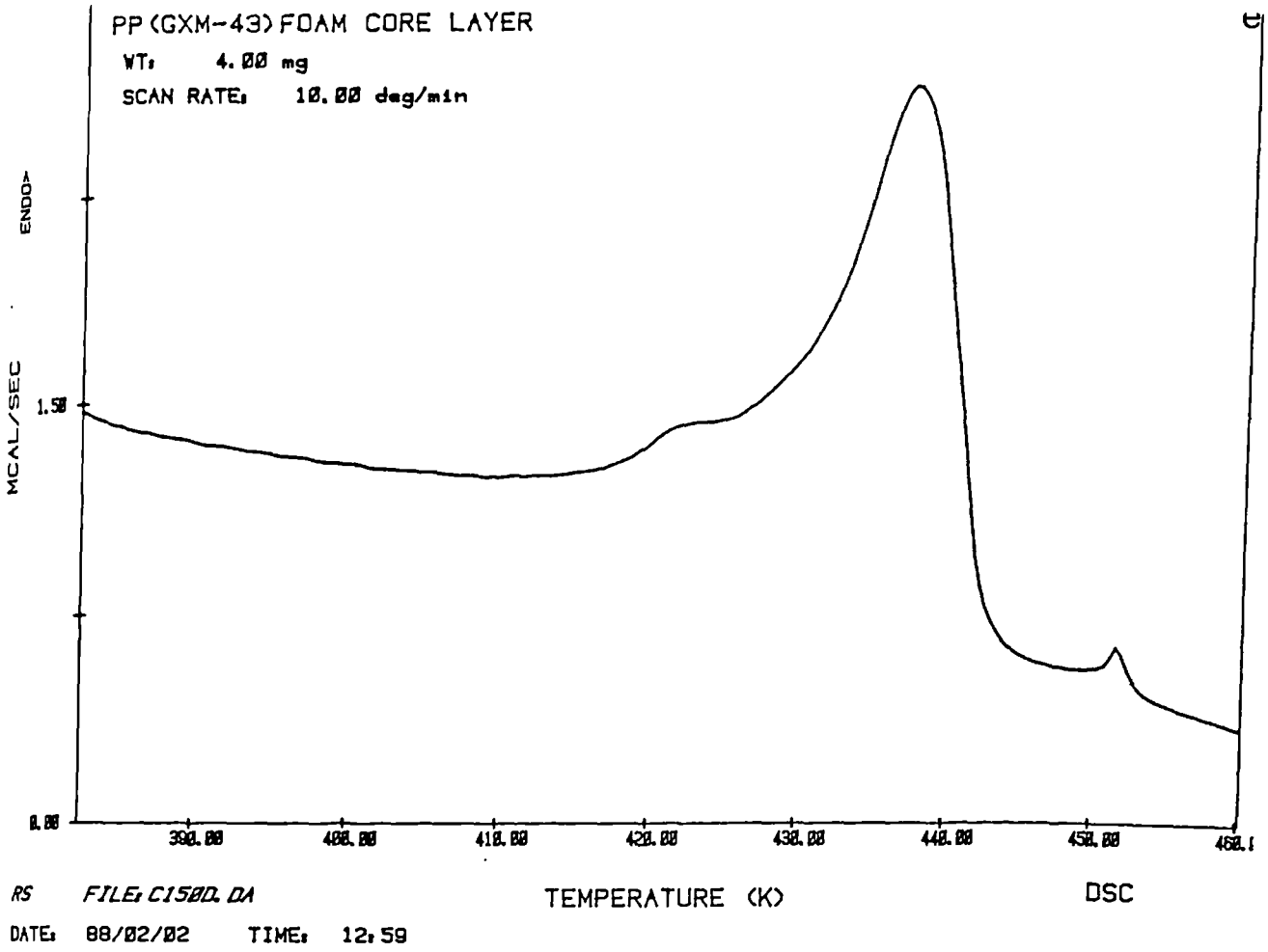

Fig. 7.26. e) Melting behaviour of core layer extruded polypropylene foam.

and Ronca (93) have studied the effect of nucleating agent on the crystallisation of isotactic polypropylene and they have shown that nucleating agent can decrease the degree of supercooling and increase the concentration of β-phase in polypropylene.

When the melting behaviour of material in the core layer was studied, it was revealed that the intensity of the β-phase as compare to the skin layer was reduced, but still significantly present, as shown in Figure 7.26.d and Table 7.7.

Calculated results of degree of crystallinity of foam extrudate as compared to its homopolymer shows it has not been altered significantly as it is shown in Table 7.7.

7.8.3. X-ray Diffraction Analysis of Extruded Polypropylene Foam

For the sake of comparison the foam specimens were prepared for the X-ray analysis similar to those of polypropylene homopolymer.

The X-ray diffraction analysis of skin to core layer are presented in Figure 7.27 and Table 7.8. The following points can be drawn from these analysis.

i) The analysis of skin layer revealed a strong β-phase at plane of 300 and 221. It is interesting to

Table 7.7. DSC analysis of extruded polypropylene foam. Screw speed 60 rpm, temperature cooling media 60°C.

Thickness of layer from the surface (μm)	Melting peak temp.(°K) β	α1	α2	Degree of super cooling (°K)	Degree* of cryst. %
10-500	421.9	437.82	-	37.82	31.18
500-1000	422.1	437.65	-	36.28	32.23
1000-1500	422.9	438.3	428.1	38.29	36.36
1500-2000	421.75	457.33	451.78	36.78	37.1
3000-3500	422.2	436.4	452.76	36.42	34.49
4000-4500	416.5	432.91	437.38	37.77	32.37

* The heat of fusion for 100 % crystalline polypropylene was taken as 247 J g^{-1} (163).

Table 7.8 X-ray analysis of cross sectional area of extruded polypropylene foam by layer removal. Screw speed 60 rpm. The temperature of cooling media 60°C.

Thickness of layers from the surface (μm)	Peak Hight(mm) β-phase hα1	hα2	hα3	α-phase hα4	hβ1	hβ2	ha	α-phase Index A	β-phase Index B	Cryst. Index C
10-500	81	152	44	39	64	23	43	0.675	0.239	1.87
500-1000	92	169	56	40	42	0	41	0.693	0.117	1.95
1500-2000	90	75	36	47	36	0	29	0.656	0.152	1.92
2000-2500	87	75	45	56	22	0	32	0.608	0.096	1.78
3000-3500	61	99	42	46	24	0	35	0.570	0.106	1.55
4000-4500	54	68	32	46	15	0	32	0.540	0.089	1.34

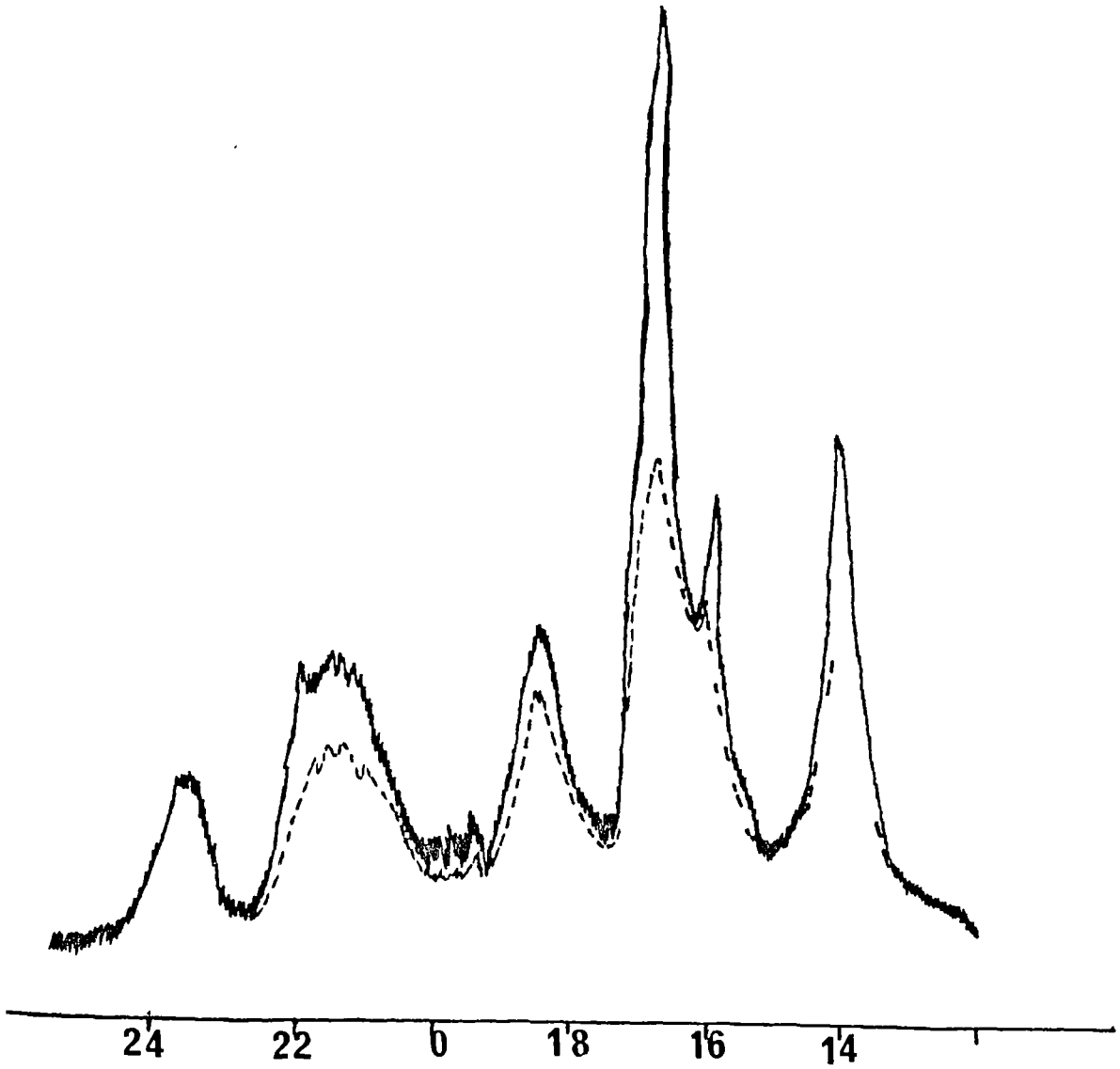

Fig. 7.27. X- ay diffraction through th c os s
extruded PP foam by layer rem v)
layer, (----) centre of xtru
away from the surface).

compare the intensity of these peaks with those of polypropylene homopolymer shown in Figure 7.9. Clearly foamed samples which suggested that the nucleation of polypropylene by chemical blowing agent in responsible for this behaviour. It should be also added that β-spherulites appeared to be stronger in the skin region as compared to core layer.

ii) The α-phase orientation of the c-axis with respect to the flow direction is not significantly changed as compared to those of homopolymers. But still higher order of orientation was observed in layers 500-2000 μm away from skin.

iii) Crystallinity index C also was not drastically changed as compare with the polypropylene homopolymer. These findings are also in a good agreement with results obtained from DSC analysis.

7.9. Microstructural Analysis of Extruded High Density Polyethylene Foam

7.9.1. Surface Analysis of High Density Polyethylene Foam by TEM

As it was mentioned earlier, due to fast nucleation, the skin layer up to thickness of 1500 μm did not show any spherulitic structure. Below this layer at very high magnification the spherulitic structure was more clear as it has been shown in Figure 7.28. Several points can be concluded from this figure.

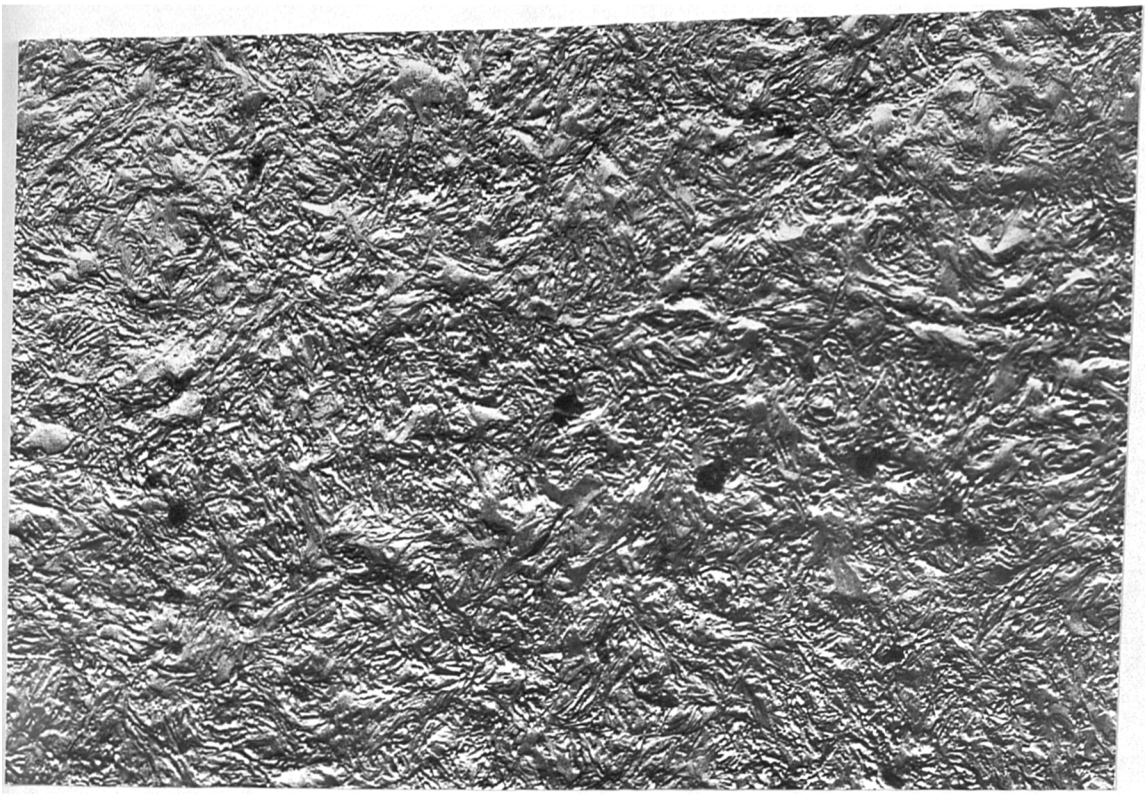

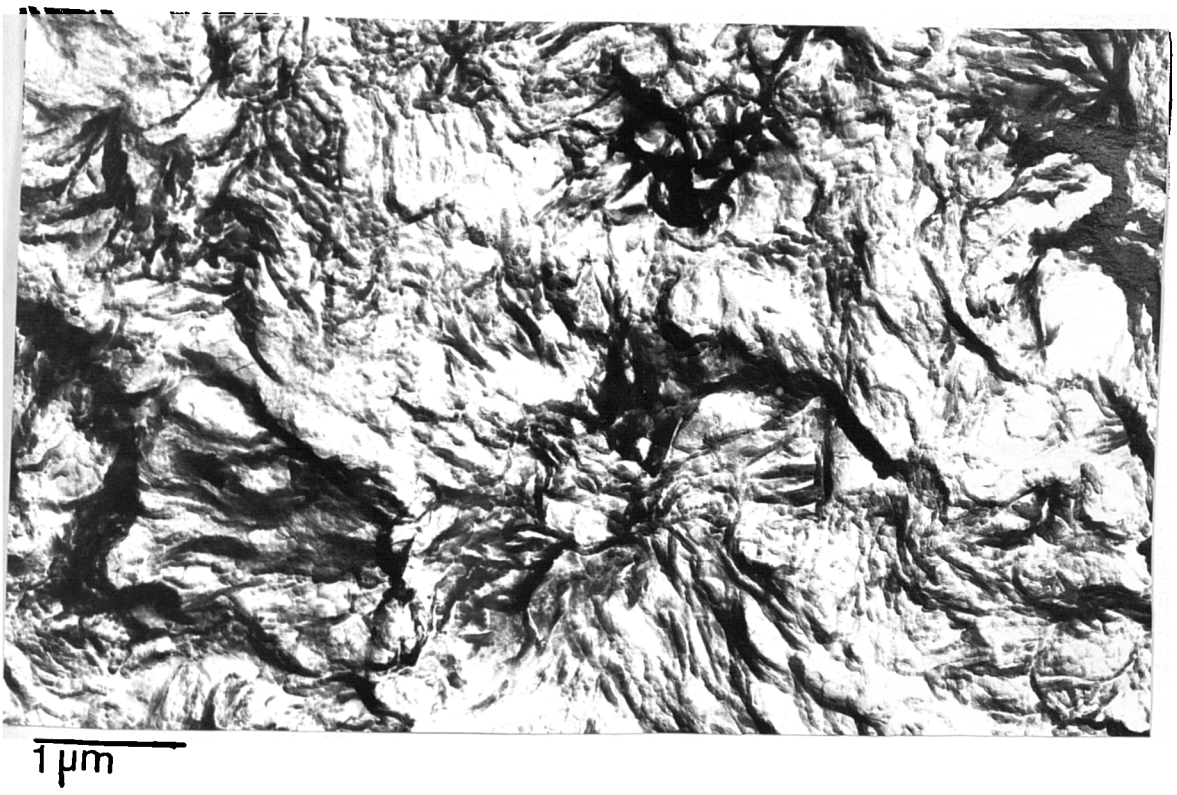

Fig. 7.28. a) Skin layer analysis of extruded high density polyethylene foam(Rigidex H11042) by TEM.
b) Core layer analysis of extruded high density polyethylene foam(Rigidex H11042) by TEM.

Firstly, the chemical blowing agent did not induce significant change in the size of spherulites. Secondly, the dominant lamellae are composed of regular arrays of the connected well defined curved shapes. Thirdly the spherulitic structure to some extent look flatten, which suggest the gas generated from blowing agent has the same effect on the morphology of high density polyethylene as compared to polypropylene.

The effect of chemical blowing agent on the spherulitic structure of high density polyethylene (Natene 54180) is more clear as it has been shown in Figure 7.29. It is interesting to note that the spherulites in the core region (Figure 7.29.b) have flatten top similar to those noticed in PP foam. Also funnel shape holes are observed on the spherulites boundaries. Due to differential cooling and difference in the degree of crystallinity the interspherulite shrinkage is greater in the core region as compared to skin layer (compare Figure 7.29.a and 7.29.b). It should be pointed out, the black spot appearing on the Figure 7.29.b is due to electron beam damage. The fact that the spherulitic structure of polyethylene under study has pyramidal shape, therefore, the top part is more susceptible to electron beam damage than other areas.

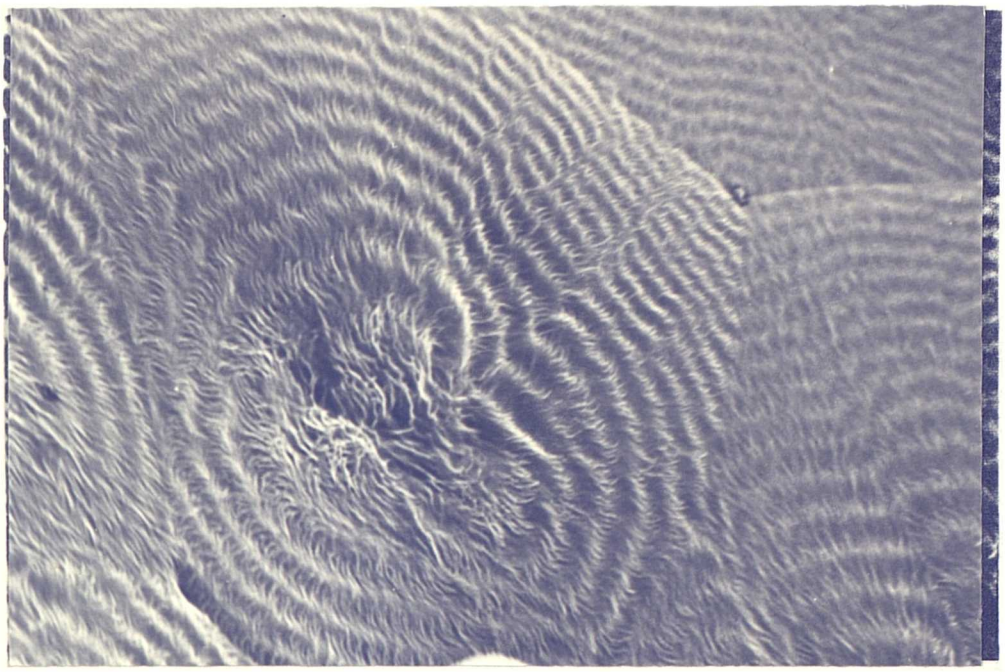

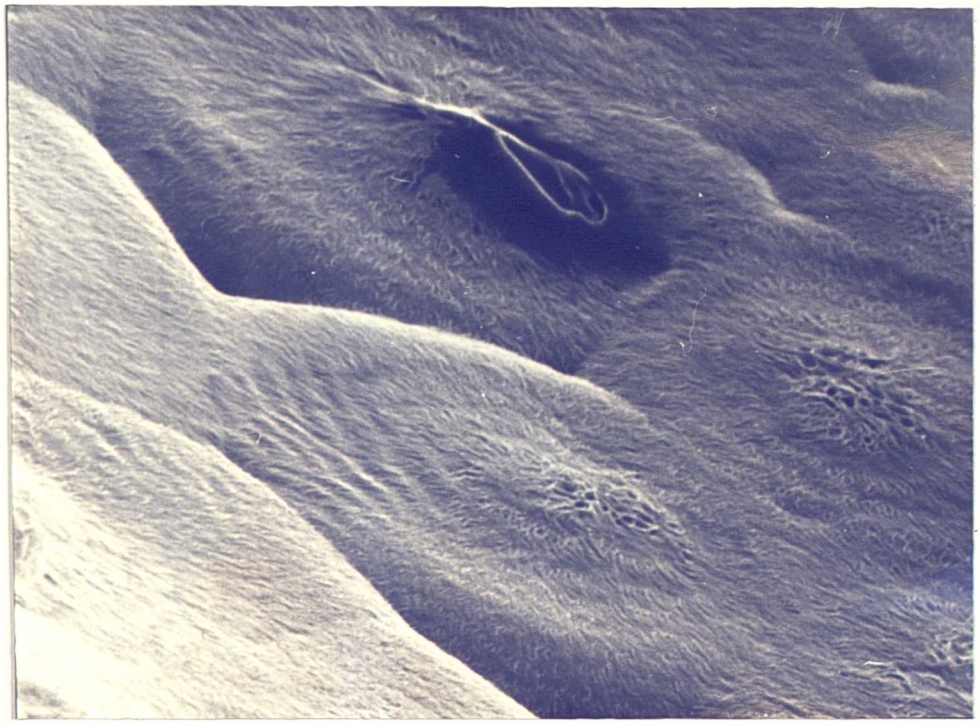

Fig. 7.29. a) Skin layer analysis of extruded high density polyethylene foam (Natene 54180).
b) Core layer analysis of extuded high density polyethylene foam (Natene 54180).

7.9.2. DSC Analysis of Extruded High Density polyethylene Foam

Similar to the previous sections specimens of 500 μm thick were prepared and examined for their melting behaviours.

The endothermic melting peak for each layer was analysed and summary of their results are given in Table 7.9. Similar to its homopolymer the extruded foam also consist of three layers, skin, transition, and core. The thickness of transition zone (where the melting point was found to be higher) was less than the high density polyethylene homopolymer. This could be due to the expansion of the polymer melt, where it will decrease the rate of heat loss and the melt can cool at lower rate, therefore, the extended chains due to shearing action can go back to unperturb state. Also from Figure 7.30 and Table 7.9 it is noticed that the melting temperature as well as the degree of crystallinity has decreased in the foamed sample as compared to its homopolymer. This could be due to faster rate of nucleation of polymer as a results of addition of chemical blowing agent. Also due to this phenomenon and differential cooling two phase system are present in the skin layer crystal structure. The first melting peak which appeared at 385°K most likely is due to imperfect crystal structure and second

Table 7.9 DSC analysis of extruded high density polyethylene foam. Screw speed of 40 rpm, temp. of cooling media 60°C.

Thickness of layer from the surface (μm)	Melting peak (°K)		Degree of Cryst. %
10-500	384.8	400.98	50.96
500-1000	-	402.75	57.02
1020-1500	-	405.75	57.97
2000-2500	-	404.12	56.53
3000-3500	-	403.33	53.92
4000-4500	-	403.85	52.70

* The hae fusion for 100% crystalline polyethylene was taken as 276 J g^{-1} (169).

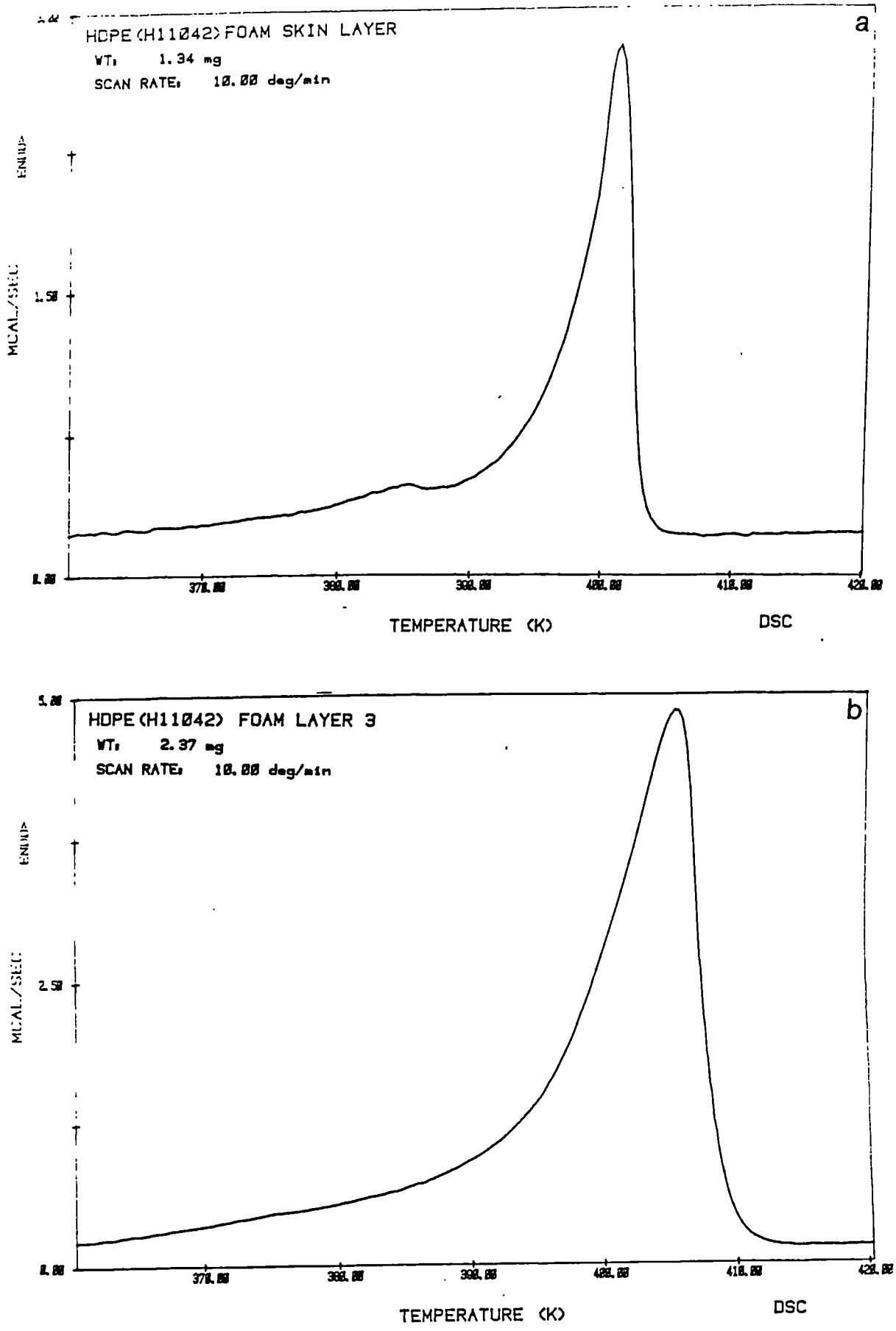

Fig. 7.30. a) Melting behaviour of skin layer of extruded high density polyethylene foam(Rigidex H11042).
b) Melting behaviour of transition layer of high density polyethylene foam (Rigidex H11042).

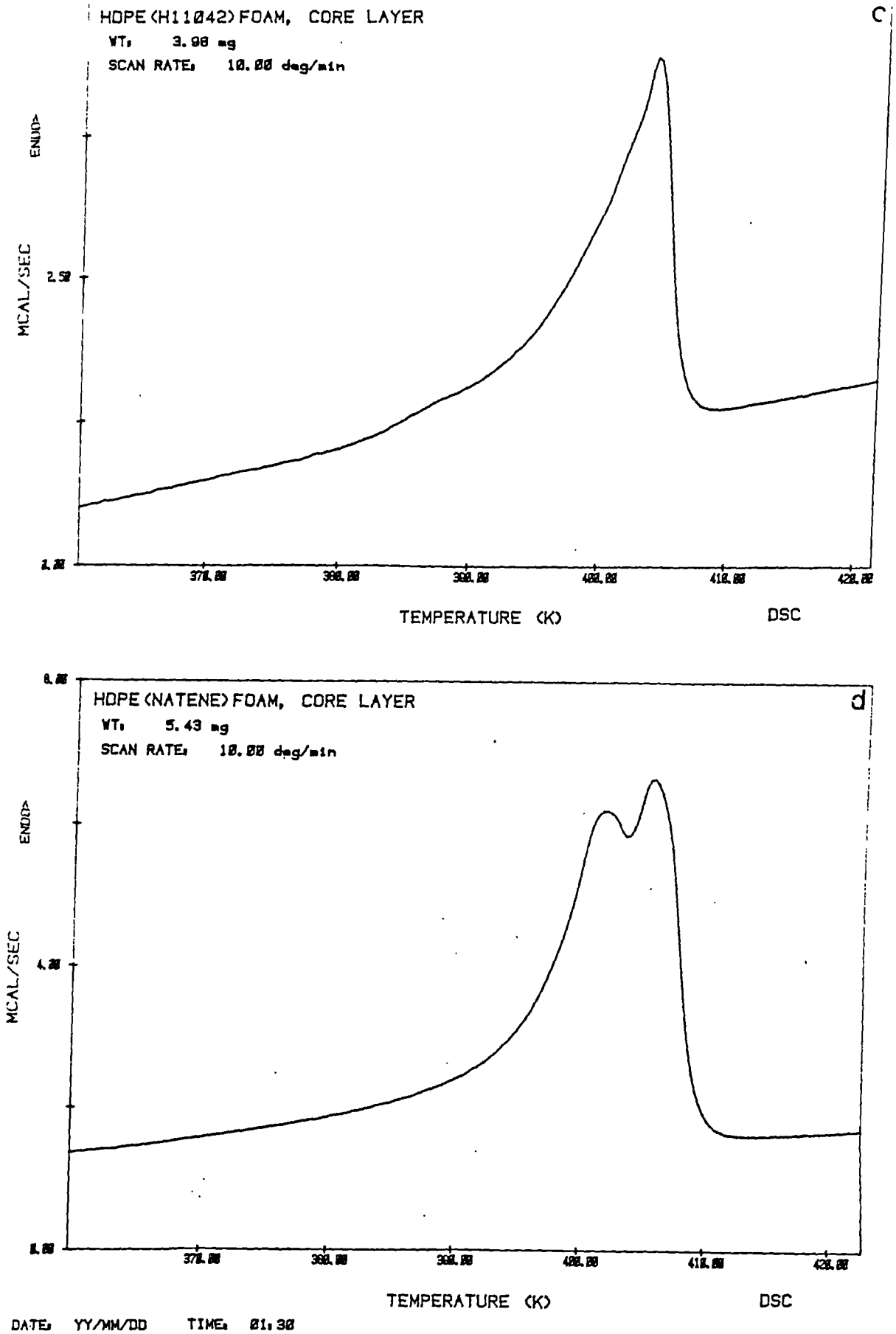

Fig. 7.30. c) Melting behaviour of core layer of extruded high density polyethylene foam(Rigidex H11042).
d) Melting behaviour of core layer of extruded high density polyethylene foam (Natene 54180).

endothermic peak around 401°K (128°C) is due to crystals that form under slower cooling rate, and is typical of melting behaviour of high density polyethylene (116). As the results of slower cooling in the core region (same effect if one would anneal the sample), the first melting peak disappears and the second peak appears at slightly higher temperature (see Figure 7.30.a&b).

For all intensive purposes the melting behaviour of high density polyethylene (Natene 54180) is also shown in Figure 7.30. As it is expected two melting peaks appeared at 402°K (129°K) and 405.5°K (132.5°C) respectively. This could be due to the two different crystal structure present in the crystalline morphology of this polymer noticed in Figure 7.29. These secondary crystallisation most likely are due to differential cooling caused by foaming process of the melt.

7.9.3. X-ray Analysis of Extruded High Density Polyethylene Foam

The X-ray diffraction was used to determine the orientation distribution of crystallites within the cross section of extruded foamed samples.

The diffractograms of skin to core layers are

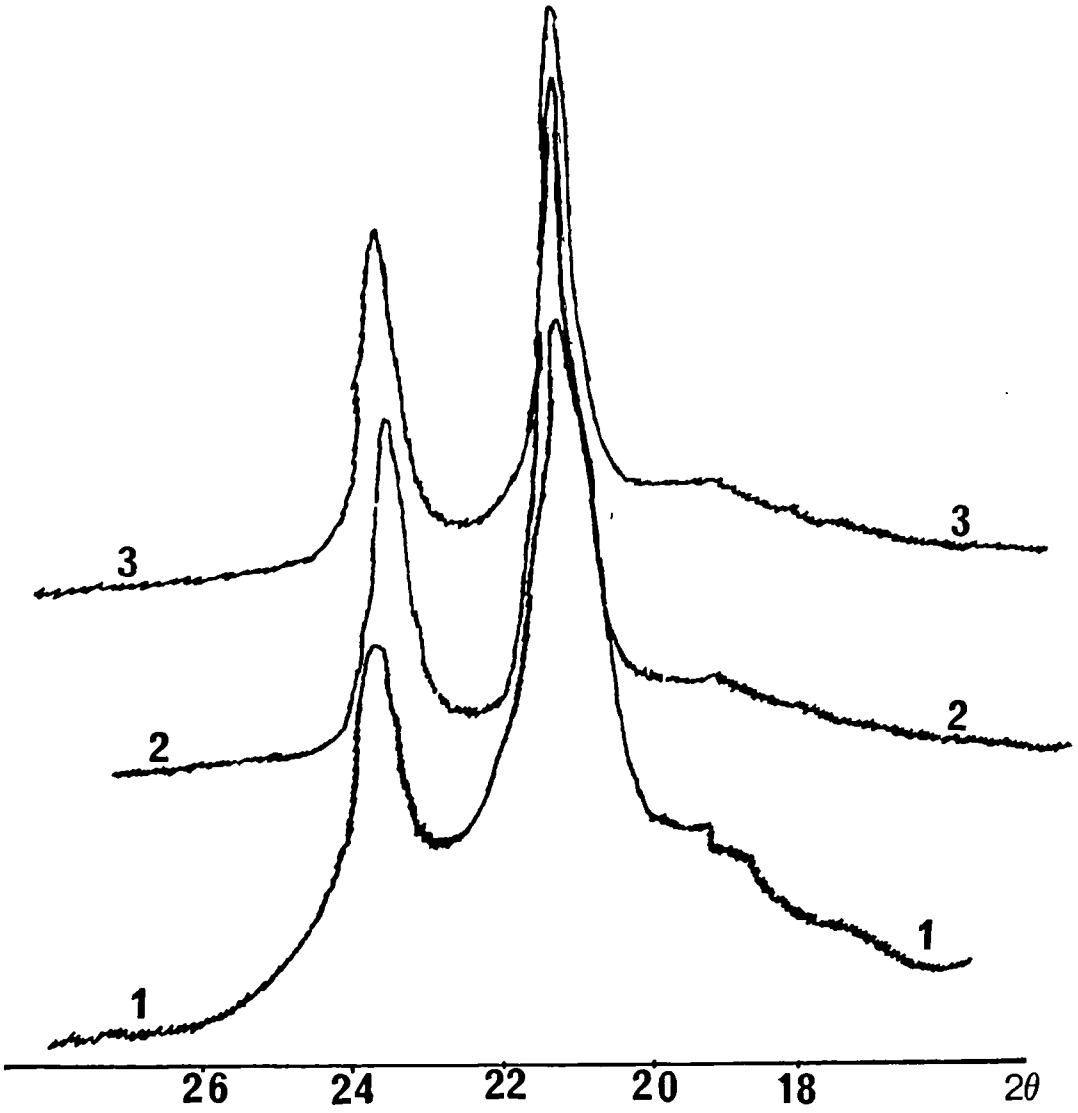

Fig. 7.31 X-ray analysis of cross section of extruded high density polyethylene by layer removal. (1) Skin layer, (2) 1020-1500 μm away from the skin, (3) centre of extrudate 4000-4500 μm away from the skin.

presented in Figure 7.31. As it was expected the intensity of the peaks for skin and core layer is similar to those of homopolymer. The only difference lies in the thickness of these layers. As it is noticed the transition thickness decreased and core layer increased. This phenomenon was previously explained and it was stated that the differential cooling is the main factor for this behaviour.

The Miller indices of these peaks were identified as 200, and 110 planes, with interplanar spacing of 3.78 Å, and 4.2 Å respectively. As mentioned previously this represent the orthorhombic structure of the polyethylene unit cell.

7.10. Microstructural Analysis of Binary Blend of Polypropylene and High Density Polyethylene Foam

7.10.1 Surface Analysis by SEM

Microstructure of skin and core layer was analysed and their results are presented in Figure 7.32. The microstructure of skin layer was found to be different from core region.

From the microstructural analysis of homopolymer it is believed the row nucleated spherulites presence here can be identified as those of polypropylene. As one can notice the diameter of these spherulites decreased as compared to polypropylene homopolymer. This is

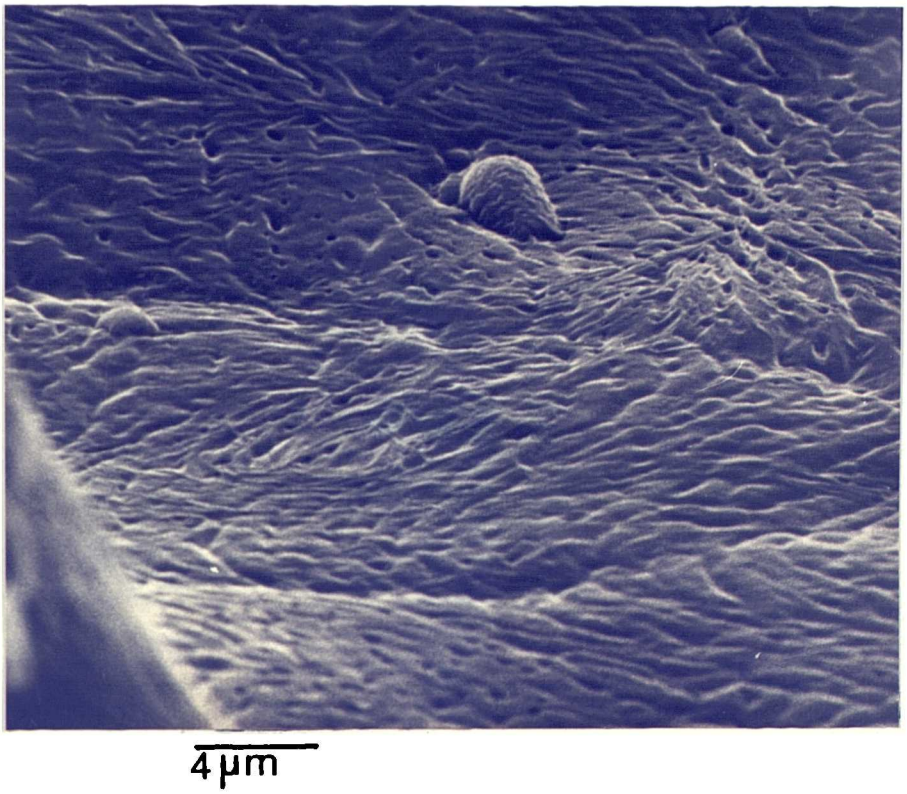

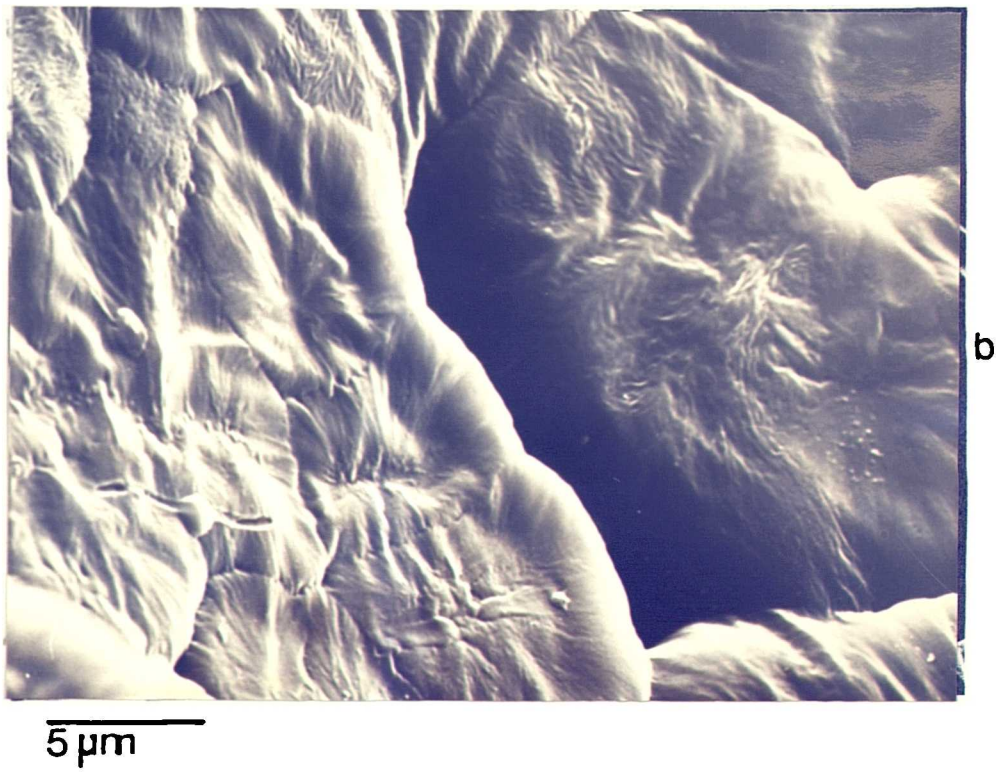

Fig. 7.32. a) Skin layer analysis of extruded PP/HDPE foam by SEM.
b) Core layer analysis of extruded PP/HDPE foam by SEM.

believed is due to nucleation by foreign matters such as chemical blowing agent and presence of high density polyethylene. As it will be shown later, due to this phenomenon the crystallisation temperature (Tc) increased and as a consequence the degree of supercooling has decreased.

It should be added that due to the interspherulite shrinkage, funnel shaped holes are also formed as it can be seen from Figure 7.32. Also make a note that the presence of gas bubbles in the melt caused formation of microvoids in the spherulites as it was explained in previous sections.

The microstructure of core layer shows a different structure with fibrilated lamellae toward the centre of the spherulites. Two interesting points one can raise here. Firstly due to higher concentration and slower rate of nucleation of polypropylene no spherulite of high density polyethylene can be identified in this figure. Secondly the gap between the spherulites due to higher shrinkage associated with this region is increased as it is noticed in Figure 7.32.b.

7.10.2. Thermal Analysis of Extruded Binary Blend of High Density Polyethylene and Polypropylene Foam

The extruded foams were sectioned through their thickness for DSC analysis. As with the thermal study of binary blend of unfoamed polymer, multiple peaks associated with different crystalline structures were observed. As it was expected analysis of skin through core layer resulted in different melting behaviour. Figure 7.33.a display the melting behaviour of skin layer. As it is noticed one major peak appeared at 400.5°K and in addition a peak appeared on the shoulder of major peak at around 399°K as a result of endothermic melting point of high density polyethylene. In general, the melting peak of a semi-crystalline polymer is higher as the thickness of lamellae, l, is larger. Therefore, even though it was not observed from microstructural analysis by SEM two crystalline phase must be present in the crystalline structure.

The melting peaks which associate with thermal behaviour of polypropylene display very interesting results. Four peaks appeared at 414°, 421.5°, 431°, and 437.5°K. The first two and last two peaks associate with melting of and spherulites respectively. The crystallisation temperature (Tc) measured for all the layers were found to be higher than the Tc of

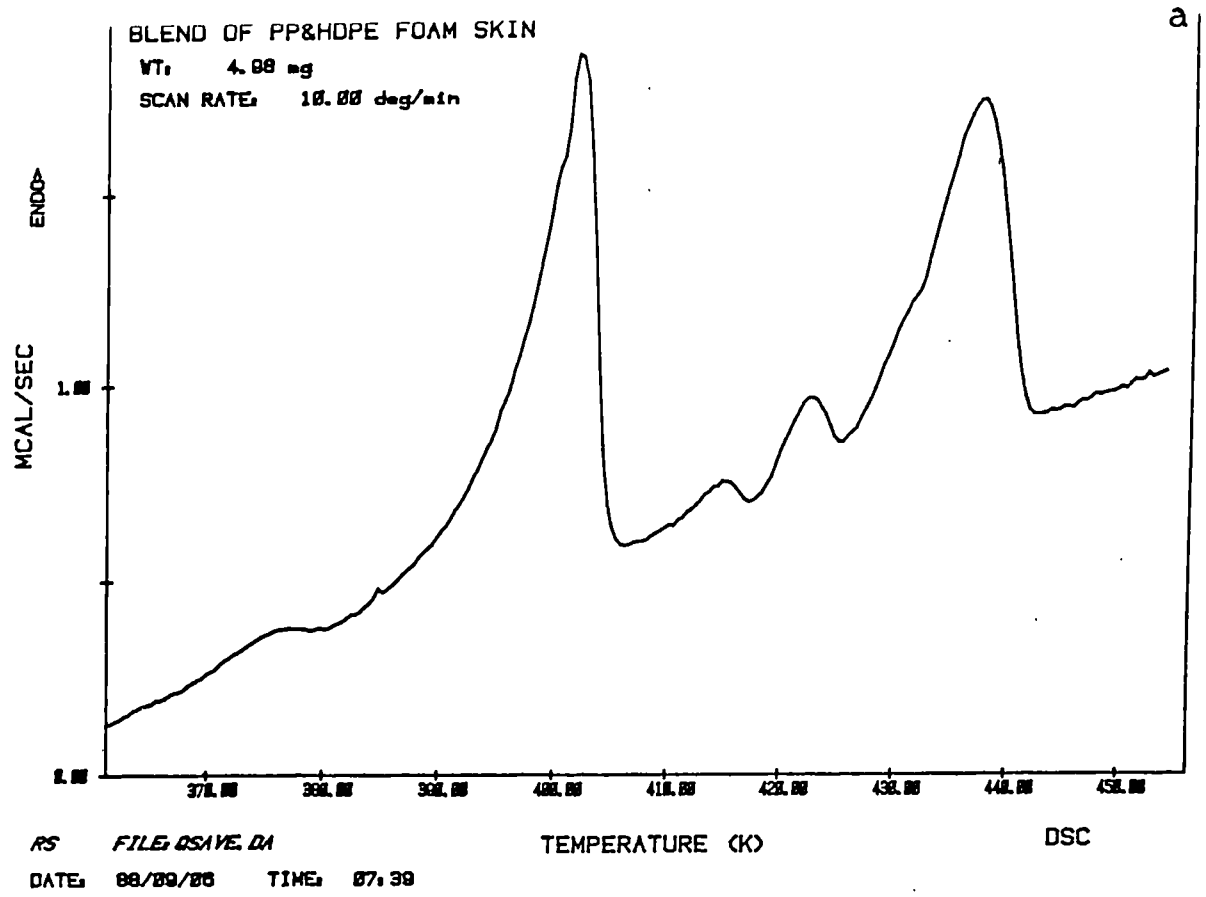

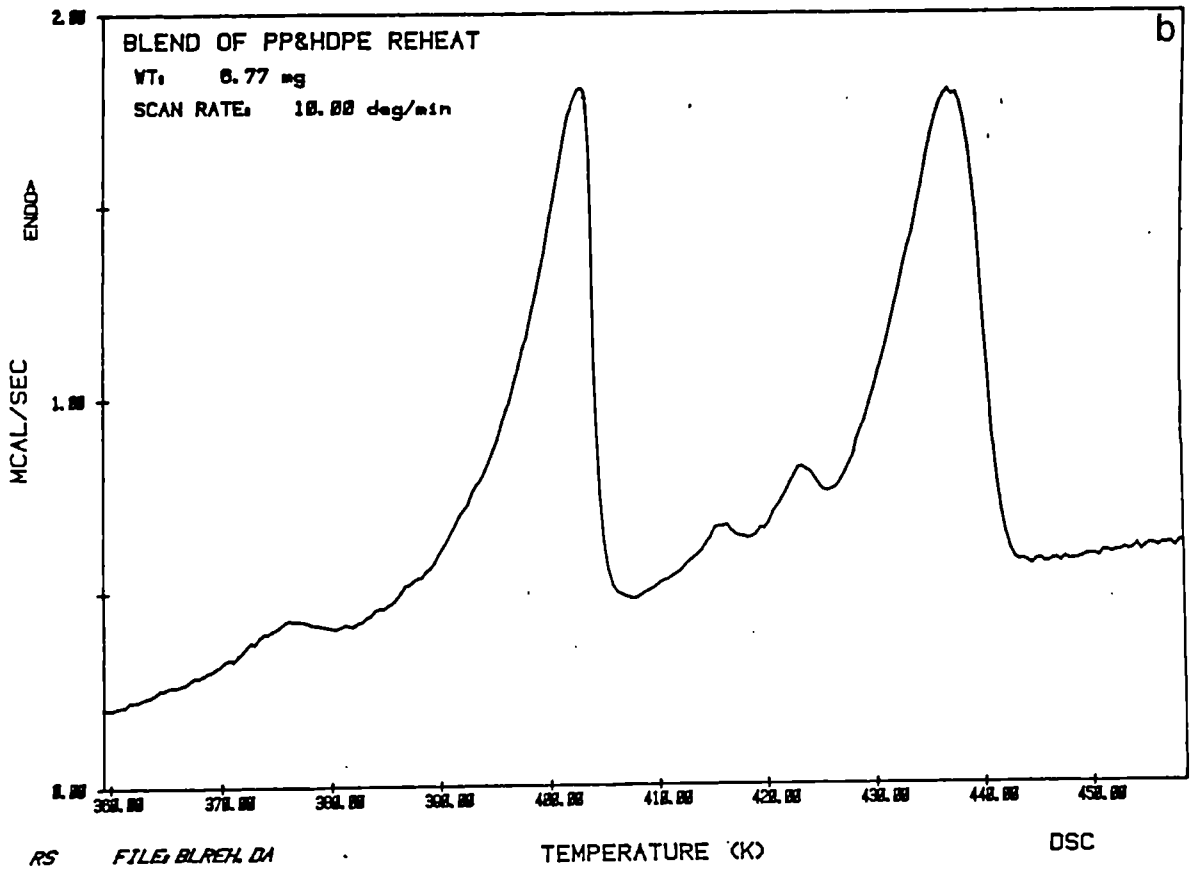

Fig. 7.33 a) Melting behaviour of skin layer of extruded PP/HDPE foam.
b) Melting behaviour of same layer as above cooled at slow rate ($5\ ^{o}K\ min.^{-1}$).

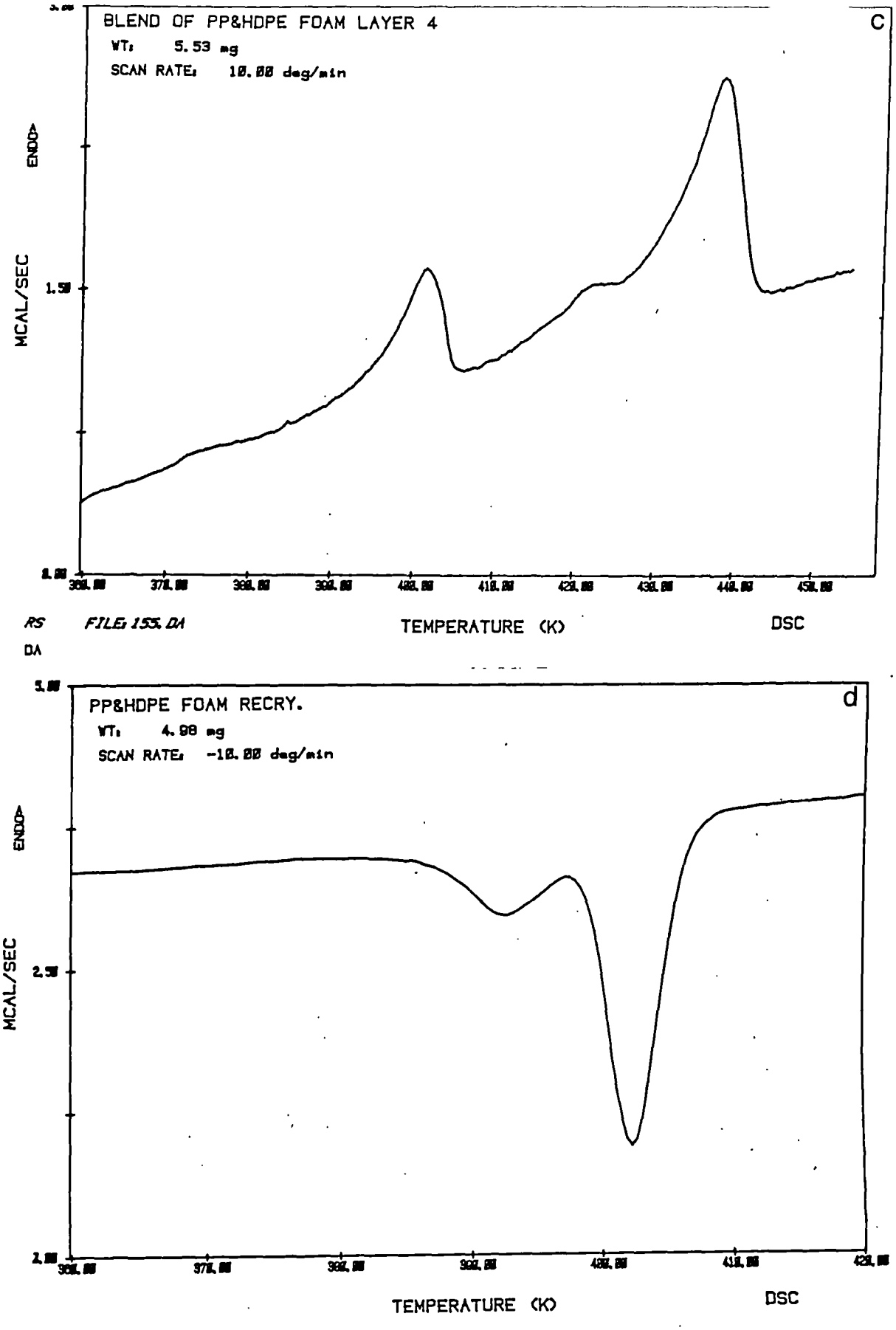

Fig. 7.33. c) Melting behaviour of transition of layer of PP/HDPE foam.
d) Recrystalisation behaviour of PP/HDPE foam.

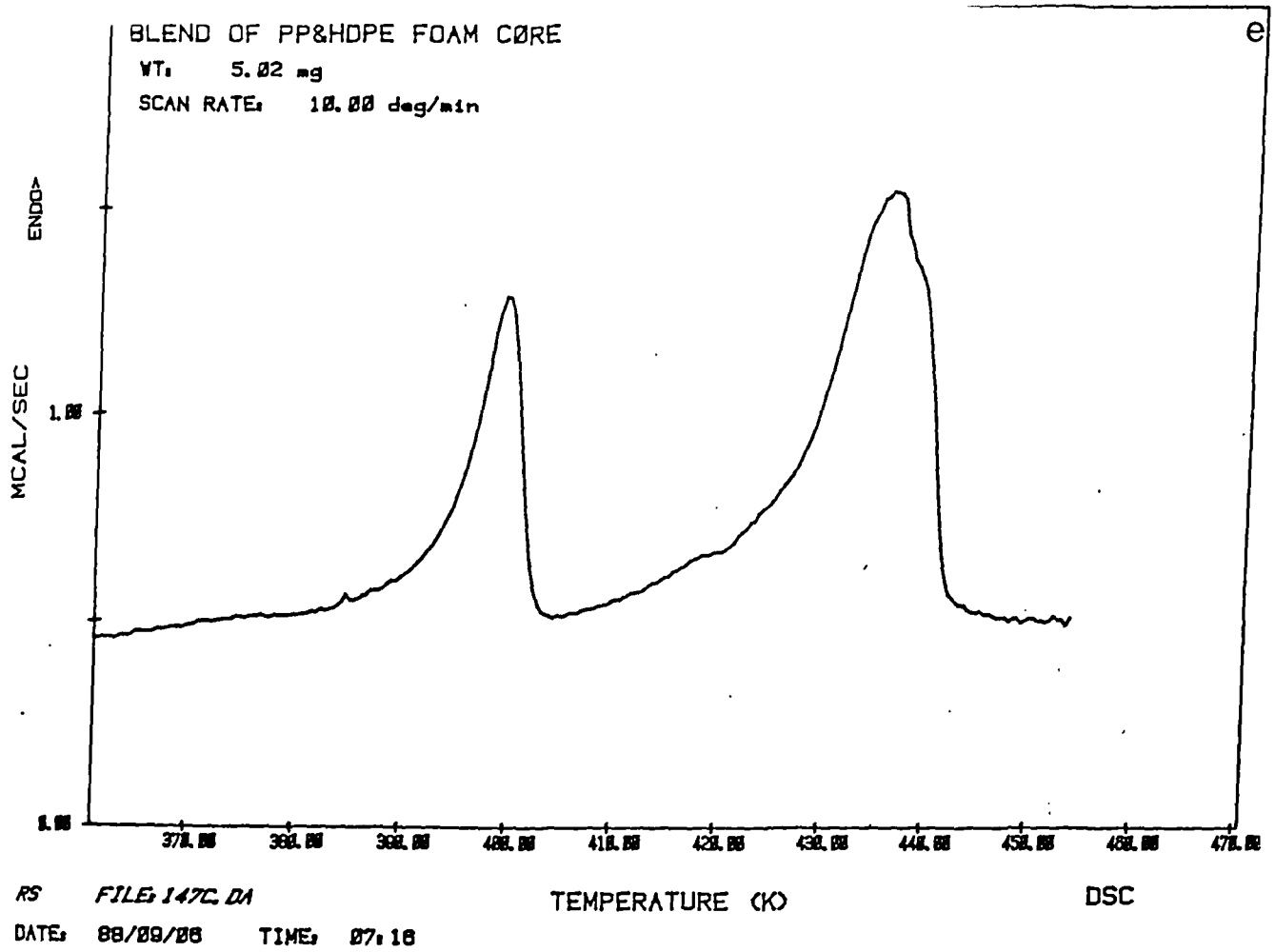

Fig. 7.33 e) Melting behaviour of core layer of extruded PP/HDPE foam.

polypropylene homopolymer, as it is noticed from Table 7.10. Also due to the same phenomenon the degree of supercooling was decreased.

When a sample from the skin layer was first heated to above the melting temperature of polypropylene and then slowly cooled (5°K min^{-1}), the analysis of its melting behaviour gave following results;

i) Only one endothermic peak was observed for high density polyethylene at 402°K. The minor peak at 399°K previously observed in Figure 7.33.a, as the consequence of slow cooling has disappeared.

ii) The peaks corresponding to the melting behaviour of polypropylene (the peaks associated with β-phase) were lower in intensity. This behaviour proves the point that slow cooling diminishes the formation of β-spherulites, but due to nucleating effect of chemical blowing agent and high density polyethylene, the β-phase still is present as it can be seen from Figure 7.33.c.

From the foregoing results one can clearly see that, the addition of high density polyethylene to the blend, can result to better stability of cell formation in the extrusion of polyolefin foam.

Table 7.10 DSC analysis of extruded PP/HDPE (80/20) foam. Screw speed 60 rpm.

Thickness of layer from surface (μm)	Melting temp. (°K)						Temp. of. crys. T_c (°K)
	HDPE		PP				
			β1	β2	α1	α2	
10–500	399.2	400.5	414.2	421.5	430.5	435.95	402.26
500–1000	–	400.95	–	421.5	436.85	–	401.81
1020–1500	–	400.86	–	421.3	437.47	–	402.26
1500–2000	–	401.36	–	421.8	437.87	–	402.75
2000–2500	–	400.73	–	423.4	437.36	–	400.85
3000–3500	–	400.12	–	422.7	436.67	–	400.35
4000–4500	–	398.6	–	420.7	435.45	440.1	399.63

CHAPTER 8

CONCLUSIONS AND RECOMMENDATIONS FOR FUTURE WORK

8. Conclusions and Recommendations for Future Work

A systematic and comprehensive study was carried out to investigate the effect of processing conditions, molecular weight, and concentration of chemical blowing agent upon rheological properties, macro and micro-morphology of PP, HDPE, and blends of PP/HDPE foam. The following conclusions have been made from the results of this research;

i) The viscosity of polymer/gas mixture is strongly affected by the melt temperature and the melt pressure inside the die. It has been found at high processing pressure (pressure greater than 4.14 MPa), the pressure drop inside the die follows a linear relationships with respect to axial distance (dp/dz is constant), whereas at lower pressure the pressure is function of position which clearly indicates formation of two phase system and premature foaming inside the die.

ii) Due to chain branching of high density polyethylene, the processing pressure for this polymer is much higher than polypropylene. Therefore, the reduction in melt viscosity of HDPE/gas mixture is much less as compared to melt viscosity of PP/gas solution.

iii) Addition of chemical blowing agent to polymer melt has resulted in reduction of melt viscosity. The extent of reduction is function of concentration of chemical blowing agent, polymer molecular structure,

and processing temperature and pressure. Addition of 5 wt.% Hydrocerol CF-20 to polypropylene has resulted in reduction of melt viscosity as much as 38% at melt pressure of 1.72 MPa, whereas at melt pressure of 5.5 MPa the reduction in melt viscosity is around 16% as compare to their unfoamed polymer.

iv) Melt fracture is strongly affected by addition of gas in polymer. For polymer gas mixture the melt fracture occurs at higher shear rate as compared to its unfoamed state.

v) The density in both solid and melt states and porosity of extruded polyolefin foam are affected by die entry angle, L/D ratio, processing conditions and blowing agent concentration. It has been found with low entry angle dies (15° and 30°) considerable pressure drop has taken place inside the die, which resulted in premature foaming, hence, bubble collapse prior to cooling. On the other hand, die with entry angle of 60° showed considerable melt fracture at lower shear stress and shear rate. It has been suggested that die with entry angle of 45° is most suitable for processing of polypropylene foam, where, due to higher processing pressure of high density polyethylene, die with entry angle of 30° was found to be more suitable for processing of this polymer.

vi) Over the range of L/D ratios studied, it was found that L/D ratio of 0 and 2 are more appropriate for

achievement of low density and high open cell fraction in high density polyethylene and polypropylene foam respectively.

vii) To achieve low density foam with high open cell fraction, the gas/nucleant ratio should be at its optimum condition. It was found that melt temperatures of 185°C and 255°C are more suitable for processing of polypropylene and high density foam respectively. Addition of foreign nucleanting agent has been shown can affect the cell size and cell size distribution. Therefore it is suggested that an in depth investigation of effect of nucleating agent type and concentration on the cell size and cell size distribution is required.

viii) Melt viscosity also strongly influence foam density and open cell fraction. Grades of polymer with high melt viscosity have higher resistance to expansion, hence, the bubble growth will be suppressed. On the other hand polymers with low melt viscosity, have resulted in premature foaming inside the die, thereby resulting in foam specimen with high density and low open cell fracture. From the six different grades of PP and four different grades of HDPE used in this research, the grades PP with MFI of 9 and HDPE with MFI of 11 g(10 min.)$^{-1}$ were found to give maximum reduction in density and higher fraction of open cell porosity, as compared to other grades of these polymers. To explore the relationship between

melt viscosity and foam density it is would be interesting to extend this work by evaluating the melt strength of each resin in foamed and unfoamed state and correlate it to expansion ratio and density of the foamed specimens.

ix) The melt viscosity was optimised by melt blending PP (GXM-43 MFI = 9 g(10 min.)$^{-1}$) and HDPE (H11042 MFI = 11 g(10 min.)$^{-1}$) at various ratios. Results of this investigation showed that the blend ratio of 80/20 PP/HDPE, was more suitable for achieving maximum reduction in foam density and at the same time obtaining higher percentage of open cell porosity as compare to other blend ratios of these polymers.

x) Cell size and cell size distribution were found to be function of processing condition and melt viscosity of polymeric material. Due to variation of shear rate across the cross sectional area of extrudated foam, the cell geometry varies from circular to elliptical shape, from core to skin layer (where the shear rate is at its maximum). The uniformity of cell size increases with increasing the MFI of polymer, and it goes through a maximum at MFI of 9 and 11 g(10 min.)$^{-1}$ for PP and HDPE foam, respectively. The cell size distribution was found to be more uniform when the concentration of PP was increased in the binary blend of PP/HDPE. It has been shown that the uniformity of the cell size distribution is optimised when the blend ratio of

PP/HDPE foam is 80/20.

xi) In extruded unfoamed specimens of PP, just in skin layer β-phase spherulites were noticed, whereas with addition of blowing agent, distribution of β-phase spherulite was noticed through the whole cross section. Addition of gas in polypropylene resulted in network of troughs and funnel-shaped holes covering the cell walls and circumscribing what were identified as flattened spherulites. Also formation of micro-voids was noticed within the spherulites and in inter-spherulites boundaries. The size of these voids varies through the cross section of extruded specimen. The largest micro-voids are found in core region where the rate of cooling is slowest. It should be added that the size of spherulite is found to be smaller for foamed samples than for unfoamed specimens. In future work it is suggested that the effect of different types of polymorphs structure such as α and β spherulites on the foaming properties of polyolefin foam should be investigated.

xii) Due to differential cooling, the microstructure of high density polyethylene foam (in the core region) shows two distinct structures. The characterisation of these specimen by DSC complements the results obtained by TEM, and shows two different melting peaks.

xiii) The presence of high density polyethylene in the blend of PP/HDPE has a nucleating effect on polypropylene.

It has been shown the degree of super cooling of polypropylene in PP/HDPE foam specimen has been dropped as much as 10.2°K. This phenomenon has resulted in stability of the the cell walls and to some extent preventing bubble collapse prior to entering the cooling tank.

xiv) Microstructural analysis of PP/HDPE shows these two polymers are not compatible, and two distinct regions were found in extruded specimens when they were studied by TEM. DSC results also confirm these findings, were several peaks appeared as result of melting of different crystalline structures.

References

1. N.C. Hilyard " Mechanics of Cellular Plastics", Ed., Applied Science Publishers Ltd, 1982.
2. R.E. Skochdopole and L.C. Rubens, J. Cell. Plat. 1, 91 (1965).
3. R.K. Senn and D.G. Shenefiel, Mod. Plast., 48(4), 66 (1971).
4. C.J. Wacehter, Plast. Des. Process., 10(2), 9(1970).
5. V.L. Gliniescki, Proc. Annu. Conf. Cell. Plast. Div., Soc. Plast. Ind., Sec. 2-I, New York, April 1964.
6. F.H. Collins and F.P. Brown, Plast. Technol., 19 (2), 37(1973).
7. D.A. Knaus and F.H. Collins, Plast. Eng., 30(2), 34 (1974).
8. J.G. Burt, J. Cell. Plast., 15, 158(1979).
9. J.G. Burt, J. Cell. Plast., 14, 341(1978).
10. L.M. Zwolinsk, paper presented at Int. Conf. Polymer Processing, MIT, Cambridge, MA, August 1977.
11. E.A. Meinecke and R.C. Clark, Mechanical Properties of Polymeric Foam, Technomic, Westport, CT, 1973.
12. B.S. Mehta and E.A. Colombo, J. Cell. Plast., 12, 1 (1976).
13. E.A. Colombo, "in Science and Technology of Polymer Processing", N.P. Suh and N.H. Sung, Eds., MIT Press, Cambridge, MA, 1976, p. 394.
14. A. David and S.S. Marsen Jr., Soc. Pet. Eng. J., No. 2544, 1969.
15. H.G. Wenzel, R.J. Brungraber and T.E. Stelson, ASCE: EM6, 153 (1967).
16. J.T. Patton, M. Kuntamukkula and S. Holbrook., Polymer Preprints, ACS, 22 (1), 1981.
17. H.G. Wenzel, R.J. Brungraber, and T.E. Stelson, J. Matl. 5, (2), 396 (1970).
18. A. H. Beyer, R. S. Millhone and R.W. Foote, Soc. Pet. Eng. J., No. 3986, 1972.
19. S.A. Khan and R.C. Armstrong, J. Non-Newtonian Fluid Mech., 22, 1 (1986).
20. L.L. Blyler and T.K. Kwei, J. Polym. Sci., part C No. 35, 165 (1976).
21. D.M. Bigg, J.R. Preston, and D. Brenner, Polm. Eng. Sci., 16, 706 (1976).
22. Y. Oyanagi and J.L. White, J. Appl. Polym. Sci., 23, 1013 (1976).
23. C.D. Han and C.A. Villiamizar, Polym. Eng. Sci., 18, 687 (1978).
24. C.D. Han, Y.W. Kim, and K.D. Malhorta, J. Appl. Polym. Sci., 20 1583 (1976).
25. C. D. Han and C.Y. Ma, J. Appl. Polym. Sci., 28, 831 (1983).
26. H.M. Princen, J. Coll. Int. Sci. 71, (1), 55 (1979).
27. H.M. Princen and J.C. Moser, M.P. Aronson, J. Coll. Int. Sci., 75 (1), 246 (1980).
28. J.L. Throne, J. Cell. Plast., 12, 161(1976).

29. R.T. Fenner, "Principles of Polymer Processing", McMillan press, London, 1979, p.26.
30. J.A. Brydson, "Flow Properties of Polymer Melts", George Goodwin, London, 1981, p.24.
31. C.D. Han " Rheology in Polymer Processing", Academic Press, New York, 1976, ch.5.
32. S. Middleman,"Fundamentals of Polymer Processing", McGraw-Hill, New York, 1977.
33. P. L. Clegg, " The Rheology of Elastomers", Pergamon press, London, 1958 p.174.
34. J.P. Tordella, J. Appl. Phys., 27, 454 (1956).
35. J.L. Den Otter, Plastics Polymer, 155 (1970).
36. R.S. Spencer and R.E. Dillon, J. Coll. Sci., 4, 241 (1949).
37. J. J. Benbow and P. Lamb, S.P.E.,Trans, 3, 1(1963).
38. S.C. Einhorn and S.B. Turetzky, J. Appl. Polym. Sci., 8, 1257 (1964).
39. J.P. Tordella, Rheologica Acta 1, 216 (1958).
40. W.S. Overdiep and D.W. Van Krevelen,J. appl.Polym. Sci., 9, 2779 (1965).
41. G.V. Viinogradov and L.J. Invanova, Rheologica, Acta, 7, 243 (1968).
42. J.M. Lupton and J.W. Regeater, Polym. Eng. Sci., 5, 235 (1965).
43. T. Katoaka and S. Ueda, J. polym. Sci., A1, 4, 1326 (1966).
44. O. Bartos, J. Appl. Phys. 35, 2767 (1964).
45. D.R. Mills, G.E. Moore, and D.W. Pugh, S.P.E. Trans., 1, 40 (1961).
46. E.B. Bagley and A.M. Brikes, J. Appl. Phys., 31, 556 (1960).
47. E.B. Bagley and H.P. Schreiber, Trans. Soc. Rheology, 5, 341 (1961).
48. J.P. Tordella, Rheologica acta, 1, 116 (1958).
49. A.B. Metzner, E.L. Carley and I.K. Park, Mod. Plast., 37, 11, 133 (1960).
50. Foamed Plastics, Modern Plastics Encyclopedia, 50, No. 10A, McGraw-Hill, 1973, p.125.
51. C.Y. Ma and C.D. Han, J. Appl. Polym. Sci., 28, 2983 (1983).
52. C.D. Han and C.A. Villiamizer, SPE, 36th ANTEC Washington April 1978, p.654.
53. H.H. Yang and C.D. Han, J. Appl. Polym. Sci., 30, 3297(1985).
54. N.R. Schott and C. Weininger, SPE, 35th, ANTEC Montreal, 1977, p.549.
55. P.L. Durill and R.G. Griskey, AICHE J., 12, 1147(1966).
56. P.L. Durill and R.G. Griskey, AICHE j., 15, 106(1969).
57. L.I. Stiel and D.F. Harnish, AICHE J., 22, 117(1976).
58. S. Wu, J. Phy. Chem., 74, 632(1970).
59. British Patent, 1,341400 (19 Dec. 1973).
60. A.A. Ahmadi, PhD thesis, Brunel University, 1983.
61. R.H. Burton and P.R. Hornsby, J. Mat. Sci., Lett., 2, 195(1983).
62. P.R. Hornsby and D.A.M. Russell, J. Mat. Sci., Lett., 3, 1061(1984).

63. K.C. Frisch and J.H. Saunder, "Plastic Foams", Ed., Marcel Dekker, New York, 1973, ch.2.
64. C.J. Benning, "Plastic Foams", John Wiley and Sons, Vol. 1, 1969, p. 262.
65. S.Y. Hobbs, Polym. Eng. Sci., 16, 270(1976).
66. G. Pearson and S. MiddleMan, AICHE J., 23, 714(1977).
67. M.S. Plesset and S.A. Zwick, J. Appl. Phys. 23, 95 (1952).
68. M. Amon and C.D. Denson, Polm. Eng. Sci., 24, No.13, 1026(1984).
69. F.W. Billmeyer Jr., "Text Book of Polymer Science", Wiley Interscience, 1971, ch. 5.
70. C.W. Bunn and T.C. Alcock, Trans. Faraday Soc., 41, 317(1945).
71. W.M.D. Bryant, J. Polym. Sci., 2, 547(1947).
72. A. Keller, J. Polym. Sci., 17,291(1955).
73. O.C. Oppenlander, Science, 159, 1311(1968).
74. R.S. Stein, SPE Trans., 178(1964).
75. B. Wunderlich, Macromol. Phys., 1, 69(1973).
76. H.D. Keith and F.J. Padden, J. Polym. Sci., 39, 101 (1959).
77. ibid p. 123.
78. F.P. Price, J. polym. SCI., 39, 139(1959).
79. A. Keller, J. Polym. Sci., 39, 151(1959).
80. D.C. Bassett, "Principles of Polymer Morphology", Cambridge University Press, 1981, ch.2.
81. H.D. Keith and F.J. Padden, J. Appl. Phys. 35, 1286 (1964).
82. H.D. Keith and F.J. Padden, J. Appl. Phy., 34, 2409 (1963).
83. G. Natta, P. Corradini, Nuovo. Cim. Supp., 15, 1(1960).
84. H.D.Keith, F.J. Padden, N.M. Walter, and M.W. Wycoff, J Appl. Phys.30, 1485(1959).
85. A. Turner-Jones, J.M. Aizlewood, and D.R. Beckett, Makromol. Chem. 75, 134(1964).
86. A. Turner-Jones and A.J. Cobbold, J. Polym. SCi., 6, 539(1968).
87. R.J. Samuels and R.Y. Yee, J. Poly. Sci., A-2, 10, 385(1972).
88. H. Dragaun, H. Hubeny and H. Muschil, J. Polym. Sci., Polym. Phys., 15, 1779(1977).
89. A. J. Lovinger, T.O. Chua, C.C. Gryte, J. Polym. Sci., 15, 641 (1977).
90. H.J. Leugering, Die Makromol. Chem., 109, 204(1967).
91. A.A. Duswalt and W.W. Cox, ACS Polym. Preprints, 11, (2), 1154(1970).
92. H.J. Leugering and G. Kirsch, Die. Ang. Makromol. Chem. 33, 17(1973).
93. G. Ronca, PhD thesis, Brunel University, 1985.
94. E. J. Addinck and J. Beintema, Polmer,2,185(1961).
95. J.L. Kardas, A.W. Christinsen and E. Baer, J. Polym. Sci., A-2 4, 777(1966).
96. F.J. Padden and H.D. Keith, J. Appl. Phys., 30, 1479 (1959).
97. M. Fujiyama, S. Kimura and K. Ronbunshu, 32, 10, 581 (1975).

98. F.J. Khoury, Res. Natl. Bur. Stand., A70, 29(1966).
99. F.J. Padden and H.D. Keith, J. Appl. Phys.44, 1217 (1973).
100. F.J. Padden and H.D. Keith, J. Appl. Phy., 37, 4013 (1966).
101. A.J. Lovinger, J. Polym. Sci., Polym. Phys. Ed.,21, 97(1983).
102. D.R. Norton and A. Keller, Polmer, 26, 704(1985).
103. D.C. Bassett, F.R. Dammont and R. Salovey, Polymer, 5, 579(1964).
104. A.A. Duswalt and W.W. Cox, Poly. Character., Interdisciplinary Approaches, Prac. Symp., 147(1970).
105. Y. Fujiwara, Colloid Polym. Sci., 253, 273(1975).
106. W. Ullman and J.H. Wendroff, Progr. colloid Polym. Sci.,66, 25(1979).
107. B. Heise, H.G. Killan, G. Lupke, P. Schultz, and W. Woebeken, Kolloid-2, 250, 120(1972).
108. B. Heise, Colloid Polym. Sci., 279(1976).
109. M. Kamal and F.H. Moy, Poly. Eng. Review, 2, 4, 381 (1983).
110. V. Tan and M. Kamal, J. Appl. Polym. Sci., 22, 2341 (1978).
111. W. Heckmann and U. Johsen, Colloid Polym. Sci., 252, 826(1974).
112. R.A. Chivers, P.J. Barham, J. Martinez-Salazar, and A. Keller,J. Polym. Sci., Polym. Ed., 20, 1717(1982).
113. G.C. Barry, Polym. Prepr. Am. Chem. Soc. Div. Polym. Chem., 20 (2), 168(1979).
114. M. Kronstadt, P.L. Dubin and J.A. Tyburczy, Macromolecules, 11, 37(1978).
115. L. Hay and A. Keller, J. Mat. Sci., 1, 41(1966).
116. T.W. Haas and B. Maxwell, Polym. Eng. Sci., 9, 4, 225(1969).
117. T.W. Haas snd B. Maxwell, J. Appl. Polym. Sci., 14, 2407(1970).
118. M.R.Shishesaz, MSc. Thesis, Lowell University, Lowell Mass., 1979.
119. N.K. Datta and A.W. Birley, Plast. Rubb. Proc. Appl., 2, 3, 237(1982).
120. C.W. Bun, Trans. Faraday Soc., 35, 482(1939).
121. H. Kiho, A. Peterlin, and P.H. Geil, J. Appl. Phy., 35, 1599(1964).
122. Z.W. Wilchinsky, J. polym. Sci. A-2, 6, 281(1968).
123. F.H. Moy and M.R. Kamal, Polym. Eng. Sci., 20, 14, 957(1980).
124. Y. Takahashi and T. Ishida, J. Polym. Sci., Polym. Phys., 26, 2267(1988).
125. W. Woebcken and B. Heise, Kunststoffe, 68, 99(1978).
126. Boehringer Ingelheim leaflet on Hydrocerol compounds.
127. S.J. Gregg and K.S.W. Sing, " Adsorption, Surface Area and Porosity", Academic Press, New york, 1967, p.182.
128. E.E. Underwood, " Quantitative Stereology', Addison-Wesley Publishing Co., 1970, ch.5.
129. R.M. Olley, A.M. Hodge, and D.C.Bassett, J. Polym. Sci., Polym. Phys. Ed., 17, 627(1979).

130. D.R. Norton, PhD Thesis, Bristol University, 1984.
131. R.J. Samuels, J. Polym. Sci., Polym. Phys. Ed., 13, 1417(1975).
132. H. Uejo, S. Hoshino, J. Appl. Polym. Sci., 14, 317 (1970).
133. J.P. Trotigann, J.L. Lebrun, J. Verdu, Plast. Rubb. Proc. App. 2, 247(1982).
134. C.W. Bunn, "Polythene", A. Renfrew and P. Morgan Eds., Iliffe and Sons Ltd, London, 1957, p.99.
135. J.J. Bickerman, " Foams ", Spring-Veriag, New York, 1973.
136. D.J. Shaw, "Introduction to Colloid and Surface Chemistry", 2nd ed., Butterworth and Co. Ltd., 1970.
137. S. Ross, J. Coll. Sci., 95 (1), 97 (1983).
138. J.A. Kitchener, "Recent Progress in Surface Science", Vol. 1, eds. J.F.Danielli and K.G.A. Pankhurst, AP, New York, 1964.
139. R. Lemlich, Ind. Eng. Chem. Fundam., 17 (2), 89 (1978).
140. S. Ross and G. Nishioka, J. Coll. Int. Sci., 81, (1), 1 (1981).
141. S. Hartland and A.D. Barber, Trans. Inst. Chem. Eng., 52, 43 (1974).
142. J.E. Guillet, R.L. Combs, D.F. Slonaker, D.A. Weemes and H.W. Coover Jr., J. Appl. Polym. Sci., 8, 757 (1965).
143. R.L. Ballman and R.H. Simon, J. Polym. Sci. A, 2, 3557 (1964).
144. F.N. Cogswell, "Polymer Melt Rheology", John Wiley and sons, 1981, p.77.
145. J.P. Tordella, " In Rheology", Ed. F.R. Eirich, vol. 5, Academic Press, New York, 1969, ch.2.
146. J.P. Tordella, J. Appl. Polym. Sci., 7, 215(1963).
147. O. Bartas, J. Polym. Sci., B, 3, 1025(1965).
148. J.L. Den Otter, Rheol. Acta, 10, 200(1971).
149. J.L. Den Otter, J.L. Wales and J. Schijf, Rheol. Acta,6, 205(1967).
150. L.L. Blyler, Jr. and A.C. Hart, Polym. Eng. Sci., 10, 193(1970).
151. J.R.A. Pearson, Plast. Polym., 37, 285(1969).
152. R.F. Westover, Polym. Eng. Sci., 6, 83(1966).
153. N.E. Nikolaeva, O.Y. Sabsai, A.Y. Malkin, and M.L. Fridman, Int. Polym. Sci. Tech. 12, n 12, T/51(1985).
154. F.N. Cogswell, "Polymer Melt Rheology", George Goodwin Ltd. London, 1981, p.61.
155. Plastic Engineering Handbook (SPI), Reinhold Publishing Co. 1960.
156. H.R. Lasman, SPE J.,18, 1184(1962).
157. G.M. Fehn, J. Cell. Plast., 3, 10, 456(1967).
158. C.D. Han and C.Y. Ma, Proc. Pac., Chem. Eng. Cong., 3rd, 2, 110(1963).
160. D.R. Fitchumun, S. Newman, and R. Wiggle, J. Appl. Polym. Sci., 14, 2457(1970).
161. D.R. Fitchmun and Z. Mencik, J. Polym. Sci., Polym. Phys. Ed., 11, 951(1973).
162. D.C. Bassett ang R.H. Olley, Polymer, 25, 935(1984).
163. I. Kirshenbaum, Z.W. Wilchinsky, and B. Grtoen, J.

Appl. POlym. Sci., 8, 2723(1964).
164. D.R. Fitchumun and S. Newman, J. Polym. Sci., A-2 8, 1545(1970).
165. R.K. Eby, J. Appl. Phys., 35, 2720(1964).
166. J. Klein and B.J. Briscoe, Proc. R. Soc. Lond., Ser. A, 365, 53(1979).
167. D.C. Bassett and A.M. Hodge, Proc. R. Soc. Lond., Ser. A, 377, 25(1981).
168. D.C. Bassett, A.M. Hodge, and R.H. Olley, Proc. R. Soc. Lond., Ser. A, 377, 39(1981).
169. J. Runt, I.R. Harrison, and S. Dobson, J. Macrmol. Sci.-Phy., B17, 99(1980).
170. R.D. Deanin and M.F. Samsone, Polym. Preprint, 19, (1), 211(1978).
171. R.D. Deanin and G.E.D. Isidoro, ACS Org. Coatings, Plast. Chem. Prepr., 43, Aug. 24-29, 19(1980).
172. A. Keller, "Growth and Perfection of Crystals", Eds. R.H. Duremus, B.W. Roberts and D. Turnball, Wiley, New York, 1958, p.499.
173. H.N. Beck and H.D. Ledbetter, J. Appl. Polym. Sci., 9, 2131(1965).